WHOI-94-05

Woods Hole Oceanographic Institution

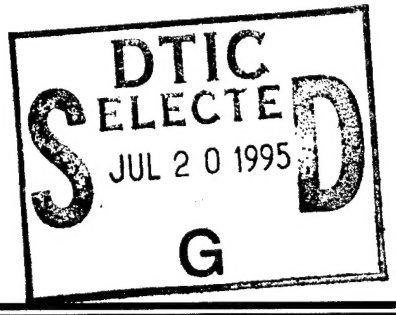

Abstracts of Manuscripts Submitted in 1993 for Publication

Technical Report WHOI-94-05

WHOI-94-05

Research In Progress

Abstracts of Manuscripts

Submitted in 1993 for Publication

Woods Hole Oceanographic Institution

Woods Hole, Massachusetts

Editor: Alora K. Paul

Approved for Distribution: _____

James R. Luyten
Associate Director for Research

When citing this report, it should be referenced as:

Woods Hole Oceanographic Institution
Technical Report No. WHOI-94-05

PREFACE

This volume contains the abstracts of manuscripts submitted for publication during calendar year 1993 by the staff and students of the Woods Hole Oceanographic Institution. We identify the journal of those manuscripts which are in press, have been submitted for publication or have been published. The volume is intended to be informative, but not a bibliography.

The abstracts are listed by title in the Table of Contents and are grouped into one of our five departments, Marine Policy Center, Coastal Research Center, or the student category. An author index is presented in the back to facilitate locating specific papers.

Acknowledgements

Special thanks to Suzanne B. Volkmann, Research Associate; Staff Assistants Shirley Bowman, Applied Ocean Physics and Engineering; Ethel LeFave, Biology; Pamela Foster, Geology and Geophysics; Molly Lumping, Marine Chemistry and Geochemistry; Debbie Taylor, Physical Oceanography; Gretchen McManamin, Marine Policy Center; Olimpia McCall, Coastal Research Center; Pamela Goulart, Education; and Maureen O'Donnell, Library Assistant.

TABLE OF CONTENTS

DEPARTMENT OF APPLIED OCEAN PHYSICS AND ENGINEERING

Simulating the Dynamics of Underwater Vehicles with Low-Tension Tethers
M. A. Grosenbaugh, C. T. Howell, and S. Moxnes AOPE-1

The Frontomandibular Stay of Balaenopteridae: A Mechanism for Momentum Recapture During Feeding
Richard Lambertsen, Nathan Ulrich, and Janice Straley AOPE-1

Evidence for Slow Mixing Across the Pycnocline from an Open-Ocean Tracer-Release Experiment
James R. Ledwell, Andrew J. Watson, and Clifford S. Law AOPE-1

Ocean Acoustic Tomography at 1000-km Range Using Wavefronts Measured with a Large-Aperture Vertical Array
Bruce D. Cornuelle, Peter F. Worcester, John A. Hildebrand, William S. Hodgkiss, Jr., Timothy F. Duda, Janice Boyd, Bruce M. Howe, James A. Mercer, and Robert C. Spindel . AOPE-1

Vertical Array Receptions of the Heard Island Transmissions
Arthur B. Baggeroer, Khosrow Lashkari, Ching-sang Chiu, James H. Miller, Peter Mikhalevsky, and Keith von der Heydt AOPE-2

Robust Maximum Energy Adaptive Matched Field Processing
James C. Preisig AOPE-2

Bottom Boundary Layer Spectral Dissipation Estimates in the Presence of Wave Motions
T. F. Gross, A. J. Williams III, and E. A. Terray AOPE-3

A New Distributed Real-Time Control System for the JASON Underwater Robot
Louis L. Whitcomb and Dana R. Yoerger AOPE-3

Evidence for Enhanced Boundary Mixing in Santa Monica Basin
James R. Ledwell and Barbara M. Hickey AOPE-3

Observations of Currents and Water Properties in the Amazon Frontal Zone
W. Rockwell Geyer and Gail C. Kineke AOPE-3

Spray Droplet Modeling, I: Lagrangian Model Simulation of The Turbulent Transport of Evaporating Droplets
J. B. Edson and C. W. Fairall AOPE-4

Design and Testing of the Autonomous Benthic Explorer
Albert M. Bradley and Dana R. Yoerger AOPE-4

Adaptive Multichannel Combining and Equalization for Underwater Acoustic Communications
M. Stojanovic, J. Catipovic, and J. G. Proakis AOPE-4

Adaptive Receivers for Underwater Acoustic Communications: Their Relation to Beamforming and Diversity Combining
M. Stojanovic, J. Catipovic, and J. G. Proakis AOPE-5

A Comparison of Measured and Predicted Broadband Acoustic Arrival Patterns in Travel Time-Depth Coordinates at 1000-km Range
Peter F. Worcester, Bruce D. Cornuelle, John A. Hildebrand, William S. Hodgkiss, Jr., Timothy F. Duda, Janice Boyd, Bruce M. Howe, James A. Mercer, and Robert C. Spindel . AOPE-5

Adaptive Equalization Techniques for Interference Suppression in Shallow Water Acoustic Telemetry Channels
Zoran Zvonar, David Brady, and Josko Catipovic AOPE-6

A Soft-Decision-Directed Multiuser Receiver for Underwater Acoustical Channels
David Brady and Josko A. Catipovic AOPE-6

Acoustic Scattering Losses in the Greenland Sea Marginal Ice Zone during the 1988-89 Tomography Experiment
Guoliang Jin, James F. Lynch, Richard Pawlowicz, and Peter Worcester AOPE-6

Phase-Coherent Digital Communications for Underwater Acoustic Channels
M. Stojanovic, J. Catipovic, and J. G. Proakis AOPE-7

Analysis of the Impact of Channel Estimation Errors on the Performance of a Decision Feedback Equalizer in Fading Multipath Channels
Milica Stojanovic, John G. Proakis, and Josko Catipovic AOPE-7

Directional Wave Spectra from a Swath Ship at Sea
W. M. Drennan, M. A. Donelan, N. Madsen, K. B. Katsaros, E. A. Terray, and C. N. Flagg AOPE-7

Co-positivity and the Minimization of Quadratic Functions with Non-negativity and Quadratic Equality Constraints
James C. Preisig AOPE-8

Multi-Season Acoustic Tomography Experiment in the Arctic
Kenneth R. Peal, Subramaniam D. Rajan, and George V. Frisk AOPE-8

The Dependence of Microwave Backscatter from the Sea on Illuminated Area: Correlation Times and Lengths
William J. Plant, Eugene A. Terray, Robert A. Petitt, Jr., and William C. Keller AOPE-8

Analysis of the Performance of a Decision Feedback Equalizer in Fading Multipath Channels in the Presence of Channel Estimation Errors
Milica Stojanovic, John G. Proakis, and Josko Catipovic AOPE-9

Microwave Backscatter from the Sea: The Modulation of Received Power and Doppler Bandwidth by Long Waves
Williams J. Plant, William C. Keller, Eugene A. Terray, and Robert A. Petitt, Jr. AOPE-9

Segmentation of Seafloor Sidescan Imagery Using Markov Random Fields and Neural Networks
Min Jiang, W. K. Stewart, and M. Marra AOPE-9

Inductive Telemetry on a Deep Ocean Surface Mooring
Daniel Frye, Alessandro Bocconcelli, Stephen Liberatore, and Edward Hobart AOPE-10

Distribution of Fluid Muds on the Amazon Continental Shelf
G. C. Kineke and R. W. Sternberg AOPE-10

Determination of the Hydrodynamic Parameters of an Underwater Vehicle During Small Scale, Nonuniform, 1-Dimensional Translation
Archie T. Morrison III and Dana R. Yoerger AOPE-10

Optical Measurements of Capillary-Gravity Wave Spectra Using a Scanning Laser Slope Gauge
Erik J. Bock, Tetsu Hara, and Robert J. Martinsen AOPE-11

Calibration of the BASS Acoustic Current Meter With Carrageenan Agar
Archie T. Morrison III, Albert J. Williams 3rd, and Marinna Martini AOPE-11

A Free-Drifting Measurement of Mid-Water Mixing by an Acoustic Current Meter Array in NATRE
Albert J. Williams 3rd AOPE-11

Dynamic Testing of the Autonomous Benthic Explorer
Dana R. Yoerger, Albert M. Bradley, and Barrie Walden AOPE-11

Instrumentation to Measure Electromagnetic Fields on Continental Shelves
R. A. Petitt, Jr., J. H. Filloux, H. H. Moeller, and A. D. Chave AOPE-12

Feedback Error Learning Control of an Underwater Vehicle and Its Comparison with Adaptive Sliding Control
He Huang and Dana Yoerger AOPE-12

Determining Suspended Sediment Particle Size Information from Acoustical and Optical Backscatter Measurements
James F. Lynch, James D. Irish, Christopher R. Sherwood, and Yogesh C. Agrawal AOPE-12

Structure and Dynamics of Fluid Muds over the Amazon Continental Shelf
J. H. Trowbridge and G. C. Kineke AOPE-13

In Situ Measurements of Capillary-Gravity Wave Spectra Using a Scanning Laser Slope Gauge and Microwave Radars
Tetsu Hara, Erik J. Bock, and David Lyzenga AOPE-13

Acoustic Characterization and Discrimination of Marine Zooplankton and Turbulence
Timothy Stanton, Peter H. Wiebe, Dezhang Chu, and Louis Goodman AOPE-14

CoOP: Coastal Ocean Processes Study – Interdisciplinary Approach, New Techology to Determine Coupled Biological, Physical, Geological Processes Affecting Larval Transport on the Inner Shelf
Cheryl Ann Butman AOPE-14

Estimates of Kinetic Energy Dissipation Under Breaking Waves
E. A. Terray, M. A. Donelan, Y. C. Agrawal, W. M. Drennan, K. K. Kahma, P. A. Hwang, A. J. Williams III, and S. A. Kitaigorodskii AOPE-14

A Note On Seasonal Cycles of Temperature and Salinity in the Upper Waters of the Greenland Sea Gyre from Historical Data
Richard Pawlowicz AOPE-15

Thermal Evolution of the Greenland Sea Gyre in 1988-89
R. Pawlowicz, J. F. Lynch, W. B. Owens, P. F. Worcester, W. M. L. Morawitz, and P. J. Sutton AOPE-15

Sound Scattering by Cylinders of Noncircular Cross Section
Daniel T. DiPerna and Timothy K. Stanton AOPE-15

What Accuracy of Measurements and Calculations is Required in Underwater Acoustics: A View from a Position of Wavefield Predictability
Yu A. Kravtsov and James F. Lynch AOPE-16

Particle Bioturbation in Massachusetts Bay: Preliminary Results Using a New Deliberate Tracer Technique
Robert A. Wheatcroft, Ilhan Olmez, and Francis X. Pink AOPE-16

Ray-Acoustic Caustic Formation and Timing Effects from Ocean Sound-Speed Relative Curvature
Timothy F. Duda and James B. Bowlin AOPE-17

Vortex-Induced Vibrations in a Shared Flow: A New Predictive Method
M. S. Triantafyllou, M. A. Grosenbaugh, and R. Gopalkrishnan AOPE-17

A Mechanism for the Formation and Maintenance of Shore-Oblique Sand Ridges on Storm-Dominated Continental Shelves
J. H. Trowbridge AOPE-17

Development of Underwater Acoustic Modems and Networks
Josko Catipovic, David Brady, and Steven Etchemendy AOPE-17

Autonomous Oceanographic Sampling Networks
Thomas B. Curtin, James G. Bellingham, Josko Catipovic, and Doug Webb AOPE-17

Measurements in the Bottom Boundary Layer on the Amazon Prodelta: Analysis of a Sedimentation Event
D. A. Cacchione, D. E. Drake, R. W. Kayen, R. W. Sternberg, G. C. Kineke, and G. B. Tate AOPE-18

On Acoustic Estimates of Zooplankton Biomass
Timothy K. Stanton, Peter H. Wiebe, Dezhang Chu, Mark Benfield, Lori Scanlon, Linda Martin, and Robert L. Eastwood AOPE-18

DEPARTMENT OF BIOLOGY

Cross Reactivity of Five Monoclonal Antibodies to Various Isolates of *Alexandrium* from the United States, Japan, Spain and Thailand as Determined by an Indirect Immunofluorescent Method
M. Adachi, Y. Sako, Y. Ishida, D. M. Anderson, M. Kodama, T. Ogata, and B. Reguera B-1

Identification of Harmful Algal Species Using Molecular Probes: An Emerging Technology
Donald M. Anderson B-1

Subtidal Benthic Community Respiration & Production Near the Heavily Oiled Coast of Saudi Arabia
Kathryn A. Burns, Manfred G. Ehrhardt, Brian L. Howes and Craig D. Taylor B-2

Microbial Food Webs in Oceanic Plankton Communities: The Protozoan Link
David A. Caron B-2

Use of Tritiated Thymidine (TdR) to Estimate Rates of Bacterivory: Implications of Label Retention and Release by Bacterivores
David A. Caron, Evelyn J. Lessard, Mary Voytek and Mark R. Dennett B-3

Characterization of a Periplasmic 3′:5′-Cyclic Nucleotide Phosphodiesterase Gene, *cpdP*, from the Marine Symbiotic Bacterium *Vibrio fischeri* †
Paul V. Dunlap and Sean M. Callahan B-3

Polychlorinated Biphenyl Congener Distributions in Winter Flounder as Related to Gender, Spawning Site, and Congener Metabolism
Adria E. Elskus, John J. Stegeman, Jay W. Gooch, Dianne E. Black and Richard J. Pruell B-4

Biological Effects of Gulf Stream Meandering
Glenn R. Flierl and Cabell S. Davis B-4

Regulation of Cytochrome P4501A1 in Teleosts: Sustained Induction of CYP1A1 mRNA, Protein, and Catalytic Activity by 2,3,7,8-Tetrachlorodibenzofuran in the Marine Fish *Stenotomus chrysops*
Mark E. Hahn and John J. Stegeman B-4

Photoaffinity Labeling of the Ah Receptor: Phylogenetic Survey of Diverse Vertebrate and Invertebrate Species
Mark E. Hahn, Alan Poland, Edward Glover and John J. Stegeman B-5

Form and Feeding Mechanism of a Living *Planctosphaera pelagica* (Phylum Hemichordata)
Michael W. Hart, Richard L. Miller, and Laurence P. Madin B-5

Dimethylsulfoniopropionate in Hawaiian Reef Corals
Richard W. Hill, John W. H. Dacey, and David A. Krupp B-6

Amino Acid Requirements of Two Hyperthermophilic Archaeal Isolates from Deep-Sea Vents: *Desulfurococcus* Strain SY and *Pyrococcus* Strain GB-D
Toshihiro Hoaki, Carl O. Wirsen, Satoshi Hanzawa, Tadashi Maruyama and Holger W. Jannasch B-6

Monitoring Underwater Ambient Sound Levels for Marine Animal Acoustics
Terrance Howald B-6

The Ecology of Buzzards Bay: An Estuarine Profile
Brian L. Howes and Dale D. Goehringer B-6

Oxygen Loss from *Spartina alterniflora* and its Relationship to Salt Marsh Oxygen Balance
Brian L. Howes and John M. Teal B-7

Predator-Mediated Coexistence of Epiphytic Grass Shrimp that Compete for Refuges
Tayasu Ichiro, Nanako Shigesada, Hiroshi Mukai and Hal Caswell B-7

Growth and Grazing Rates of *Protoperidinium hirobis* Abé, A Thecate Heterotrophic Dinoflagellate
Dean M. Jacobson and Donald M. Anderson B-8

Die Mikroben der heissen Tiefseequellen
Holger W. Jannasch B-8

Isolation and Cultivation of Heterotrophic Hyperthermophiles from Deep-Sea Hydrothermal Vents
Holger W. Jannasch, Carl O. Wirsen, Toshihiro Hoaki B-8

Larval Dispersal via Entrainment Into Hydrothermal Vent Plumes
Stacy L. Kim, Lauren S. Mullineaux, and Karl R. Helfrich B-9

Dimethylsulfide Production from Dimethylsulfoniopropionate By A Marine Bacterium
Kathleen M. Ledyard and John W. H. Dacey B-9

Characterization of a DMSP-Degrading Bacterial Isolate from the Sargasso Sea
Kathleen M. Ledyard, Edward F. DeLong and John W. H. Dacey B-9

Application of rRNA-Based Probes for Observing Marine Nanoplanktonic Protists
E. L. Lim, L. A. Amaral, D. A. Caron and E. F. DeLong B-10

Uptake of Waterborne 3,3',4,4'-Tetrachlorobiphenyl and Cytochrome P4501A Induction in the Fathead Minnow *Pimephales promelas*
Pirjo Lindstrom-Seppa, Peter J. Korytko, Mark E. Hahn, and John J. Stegeman B-10

Patterns of Occurrence of Salps (*Tunicata, Thaliacea*) near Bermuda
L. P. Madin, P. Kremer and S. Hacker B-11

Implementing *i*-State Configuration Models for Population Dynamics: An Object-Oriented Programming Approach
Carlo C. Maley and Hal Caswell B-11

In situ Observations of Foraging, Feeding, and Escape Behavior in Three Orders of Oceanic Ctenophores: *Lobata, Cestida* and *Beroida*
G. I. Mastumoto and G. R. Harbison B-11

Patterns of Groundwater
Newton P. Millham and Brian L. Howes B-12

Freshwater Flow Into A Coastal Embayment: Groundwater and Surface Water Inputs
Newton P. Millham and Brian L. Howes B-12

A Comparison of Methods to Determine K in a Shallow Coastal Aquifer
Newton P. Millham and Brian L. Howes B-13

Pathobiology of Chemical-Associated Neoplasia in Fish
Michael J. Moore and Mark S. Myers B-13

Periodic Response to Periodic Forcing of the Droop Equations for Phytoplankton Growth
Mercedes Pascual B-14

Transport of Juvenile Gem Clams (*Gemma gemma*) in a Headland Wake
Kelly L. Rankin, Lauren S. Mullineaux and W. Rockwell Geyer B-14

Descriptive Oceanography of the Indian Ocean
T. S. S. Rao B-14

How Fish Power Swimming
Lawrence C. Rome, Doug Swank and David Corda B-14

Natural History of A Solengaster Mollusc from Papua New Guinea, *Epimenia australis* (Thiele) (= *Dinomenia verrucosa* Nierstrasz) With A Redescription of the Species (Aplacophora, Neomeniomorpha)
Amélie H. Scheltema, Matthew Jebb B-15

Passive Dispersal of Planktonic Larvae: Relevance for the Biogeography of Caribbean Mollusks
Rudolf S. Scheltema B-15

Experiments on Variation in Length of Planktonic Life Among Veliger Larvae of *Ilyanassa obsoleta* (Gastropoda: Prosobranchiata): Delay in Metamorphosis and the Prolongation of Larval Life.
Rudolf S. Scheltema and Michael Chin B-16

Identification of Group- and Strain-Specific Genetic Markers for Globally Distributed *Alexandrium* (Dinophyceae) Species. I. Restriction Fragment Length Polymorphisms Analysis of Small-Subunit Ribosomal RNA Genes
Christopher A. Scholin and Donald M. Anderson B-16

Identification of Group- and Strain-Specific Genetic Markers for Globally Distributed *Alexandrium* (Dinophyceae) Specifics. II. Sequence Analysis of a Fragment the Large Subunit Ribosomal RNA Gene
Christopher A. Scholin, Michel Herzog, Mitchell Sogin and Donald M. Anderson B-17

Hydrodynamic Enhancement of Invertebrate Larval Settlement in Microdepositional Environments: Colonization Tray Experiments in a Muddy Habitat
Paul V. R. Snelgrove B-17

Potential Flow Artifacts Associated With Benthic Experimental Gear: Deep-Sea Mudbox Examples
Paul V. R. Snelgrove, Cheryl Ann Butman and J. Frederick Grassle B-18

Macrofaunal Response to Artificial Enrichments and Depressions in a Deep-Sea Habitat
Paul V. R. Snelgrove, J. F. Grassle and R. F. Petrecca B-19

Biochemistry and Molecular Biology of Monooxygenases: Current Directions in Forms, Functions, and Regulation of Cytochrome P450 in Aquatic Species
J. J. Stegeman and M. E. Hahn B-19

Automated Instrumentation for Time Series Measurement of Primary Production and Nutrient Status in Production Platform-Accessible Environments
Craig D. Taylor, Brian L. Howes, and Kenneth W. Doherty B-20

Grazing Rates for Three Life History Stages of the Doliolid *Dolioletta gegenbauri* Uljanin (Tunicata, Thaliacea)
Christopher M. Tebeau and Laurence P. Madin B-20

Unusual Whale Sound Tracked by Navy SOSUS
William A. Watkins, Mary Ann Daher, Joseph George, Velma Ronquille, and Amy Stanley . . . B-20

Nitrogen Incorporation Into Decomposing Litter of *Spartina alterniflora*
David S. White and Brian L. Howes B-21

Long-Term ^{15}N-Nitrogen Retention in the Vegetated Sediments of a New England Salt Marsh
David S. White and Brian L. Howes B-21

Translocation, Remineralization and Turnover of Nitrogen in Roots and Rhizomes of *Spartina alterniflora*
David S. White and Brian L. Howes B-22

Catalytic and Immunochemical Characterization of Hepatic Microsomal Cytochromes P450 in Beluga Whale (*Delphinapterus leucas*)
Renee D. White, Mark E. Hahn, W. Lyle Lockhart and John J. Stegeman B-22

The Use of High Frequency Acoustics in the Study of Zooplankton Spatial and Temporal Patterns
Peter H. Wiebe and Charles H. Greene B-22

Long Range Needs for Deep-Sea Platforms: The Deep-Sea Observatory Concept
Peter H. Wiebe, David D. Moran, Robert Knox, Charles B. Miller and John A. McGowan . . . B-23

P450 Induction and Histopathology in Pre-Emergent Pink Salmon From Oiled Streams In Prince William Sound, Alaska
Michael Wiedmer, Mark J. Fink, John J. Stegeman, Roxanna Smolowitz, Gary D. Marty and David E. Hinton B-23

DEPARTMENT OF GEOLOGY & GEOPHYSICS

ACCELERATOR MASS SPECTROMETRY

Varve calibrated records of carbonate and organic carbon accumulation over the last 2000 years in the Black Sea
M. A. Arthur, W. E. Dean, E. D. Neff, B. J. Hay, J. King and G. A. Jones GG-1

Automated sample processing at the National Ocean Sciences AMS Facility
G. J. Cohen, D. L. Hutton, K. F. von Reden, E. A. Osborne, A. P. McNichol and G. A. Jones GG-1

Lake-Level history of Lake Michigan for the past 12,000 years: The record from deep Lacustrine sediments
S. M. Colman, R. M. Forester, R. L. Reynolds, D. S. Sweetkind, J. W. King, P. Gangemi, G. A. Jones, L. D. Keigwin and D. S. Foster GG-1

Radiocarbon dating of Lake Baikal Sediments – A progress report
S. M. Colman, V. M. Kuptsov, G. A. Jones, and S. J. Carter GG-2

Holocene climate and deep ocean circulation changes: Evidence from AMS radiocarbon-dated sediment drifts of the Argentine Basin (SW Atlantic)
G. A. Jones GG-2

A New Hypothesis for the Holocene Appearance of Coccolithophores in the Black Sea
Glenn A. Jones GG-3

Timing of the Holocene repopulation of the Atlantic Ocean by *G. menardii* and *G. tumida* and implications for surface watermass Paleoceanography
G. A. Jones GG-3

High-precision AMS radiocarbon measurements of central Arctic Ocean seawaters
G. A. Jones, A. R. Gagnon, R. J. Schneider, K. F. von Reden and A. P. McNichol GG-4

Western North Atlantic evidence for millennial-scale changes in ocean circulation and climate
L. D. Keigwin and G. A. Jones GG-4

Comparative study of AMS target performance using the NOSAMS recombinator ion source
D. B. Klinedinst, A. P. McNichol, L. A. Currie, R. J. Schneider, G. A. Klouda, K. F. von Reden, R. M. Verkouteren and G. A. Jones GG-4

Rapid analysis of seawater samples at the National Ocean Sciences Accelerator Mass Spectrometry Facility, Woods Hole, MA
A. P. McNichol, G. A. Jones, D. L. Hutton, A. R. Gagnon and R. M. Key GG-5

TIC, TOC, DIC, DOC, PIC, POC - Unique aspects in the preparation of oceanographic samples for ^{14}C-AMS
A. P. McNichol, E. A. Osborne, A. R. Gagnon, B. Fry and G. A. Jones GG-5

Electric Dissociation of Negative Ions-II
M-J. Nadeau, A. E. Litherland, M. A. Garwan and X-L. Zhao GG-5

Internal and external checks in the NOSAMS Facility Sample Preparation Laboratory for target quality and homogeneity
E. A. Osborne, A. P. McNichol, A. R. Gagnon, D. L. Hutton and G. A. Jones GG-6

Methods for data screening, flagging, and error analysis at the National Ocean Sciences AMS Facility
R. J. Schneider, G. A. Jones, A. P. McNichol, K. F. von Reden, K. L. Elder, K. Huang and E. D. Kessel GG-6

Optimized data analysis for AMS radiocarbon dating
F. H. Séguin, R. J. Schneider, G. A. Jones and K. F. von Reden GG-6

Performance characteristics of the 3 MV Tandetron AMS system at the National Ocean Sciences AMS Facility
K. F. von Reden, R. J. Schneider, G. J. Cohen and G. A. Jones GG-7

Radiocarbon ages from two submerged strandline features in the Western Gulf of Maine and a sea-level curve for the Northeastern Massachusetts coastal region
R. N. Oldale, S. M. Colman and G. A. Jones GG-7

A new high-temporal resolution Paleoceanographic tool for the northern North Atlantic: the mollusc *Arctica islandica*
C. R. Weidman and G. A. Jones GG-7

Development of the mollusc Arctica islandica as a Paleoceanographic tool for reconstructing annual and seasonal records of $\Delta^{14}C$ and $\delta^{18}O$ in the mid-to high-latitude North Atlantic Ocean
C. R. Weidman and G. A. Jones GG-8

The long-lived mollusc; *Arctica islandica*: A new paleoceanographic tool for the reconstruction of maximum bottom temperatures for the continental shelves of the northern North Atlantic Ocean
C. R. Weidman and G. A. Jones GG-8

GEOCHEMISTRY

The Geochemistry of McMurdo Group Volcanic Rocks
Stanley R. Hart and Philip R. Kyle GG-8

Orphan Strontium-87 in Abyssal Peridotites: Daddy was a Granite
Jonathan E. Snow, Stanley R. Hart and Henry J. B. Dick GG-9

GEOLOGY

Effects of Multiple Inlet Morphology on Tidal Exchange: Waquoit Bay, Massachusetts
David G. Aubrey, Thomas M. McSherry and Pierre P. Eliet GG-9

Production of Small Volcanoes in the Superswell Region of the South Pacific
Karen G. Bemis and Deborah K. Smith GG-9

Comparative Volcanology of Small Axial Eruptive Centers in the MARK Area
Wilfred B. Bryan, Susan E. Humphris, Geoffrey Thompson and John F. Casey GG-10

Crustal Structure of North Atlantic Fracture Zones
R. S. Detrick, R. S. White and G. M. Purdy GG-10

Hydrodynamical Modeling of a Multiple-Inlet Estuary/Barrier System: Insight into Tidal Inlet Formation and Stability
Carl T. Friedrichs, David G. Aubrey, Graham S. Giese and Paul E. Speer GG-11

Equilibration During Mantle Melting: A Fractal Tree Model
Stanley R. Hart GG-11

Mesozoic-Cenozoic Sedimentation in the Kane Fracture Zone, Western North Atlantic, and Uplift History of the Bermuda Rise
Gary E. Jaroslow and Brian E. Tucholke GG-11

Tidal Residual Currents and Sediment Transport through Multiple Tidal Inlets
James T. Liu and David G. Aubrey GG-12

Morphodynamic Evolution of a Newly Formed Tidal Inlet
James T. Liu, Donald K. Stauble, Graham S. Giese and David G. Aubrey GG-12

Chaotic Deposition by a Giant Wave, Molokai, Hawaii
J. G. Moore, W. B. Bryan and K. R. Ludwig GG-13

Pressure-Temperature-Time Paths from Two-Dimensional Thermal Models: Prograde, Retrograde, and Inverted Metamorphism
C. Ruppel and K. V. Hodges GG-13

Building the Crust at the Mid-Atlantic Ridge
Deborah K. Smith and Johnson R. Cann GG-14

Spring Sapping Origin of the Enigmatic Relict Valleys of Cape Cod and Martha's Vineyard and Nantucket Islands
Elazar Uchupi and Robert N. Oldale GG-14

Cyclic Spit Morphology in a Developing Inlet System
Christopher R. Weidman and James R. Ebert GG-14

GEOPHYSICS

The Magma Body at Kilauea Iki Lava Lake: Potential Insights into Mid-Ocean Ridge Magma Chambers
G. A. Barth, M. C. Kleinrock and R. T. Helz GG-15

Mantle-Plume-Head Instabilities and Venus Coronae
David Bercovici and Jian Lin GG-15

Deep Structure of the Earth: Constraints Provided by Spatial Variability of the Gravity Potential Field and Its Vertical Derivatives
Carl Bowin GG-16

On Electric and Magnetic Galvanic Distortion Tensor Decompositions
Alan D. Chave and J. Torquil Smith GG-16

Seismic Constraints on Shallow Emplacement Processes at the Fast-Spreading East Pacific Rise
G. L. Christeson, G. M. Purdy and G. J. Fryer GG-17

The Shallow Attenuation Structure of the Fast-Spreading East Pacific Rise Near 9°30'N
G. L. Christeson, W. S. D. Wilcock and G. M. Purdy GG-17

Flow Structure and Dispersion Within Algal Mats
J. Escartin Guiral and David G. Aubrey GG-17

Terrestrial Heat Flow in Lake Superior
S. R. Hart, J. S. Steinhart and T. J. Smith GG-18

Suppression of Previous Shot Noise on Marine Wide-Angle Seismic Data
W. Steven Holbrook and Edmund C. Reiter GG-18

Deep Structure of the U.S. Atlantic Continental Margin, offshore South Carolina, from Coincident Ocean-Bottom and Multichannel Seismic Data
W. S. Holbrook, E. C. Reiter, G. M. Purdy, D. Sawyer, P. L. Stoffa, J. A. Austin, Jr. , J. Oh and J. Makris GG-18

Mantle Temperatures Along the Present and Paleo-axes of the Galapagos Spreading Center as Inferred from Residual Gravity Analyses
Garrett T. Ito and Jian Lin GG-19

The Uniform Accretion of Oceanic Crust South of the Garrett Transform at 14°15'S on the East Pacific Rise
Graham M. Kent, Alistair J. Harding, John A. Orcutt, Robert S. Detrick, John C. Mutter and Peter Buhl GG-19

Static Stress Changes and the Triggering of Earthquakes
Geoffrey C. P. King, Ross S. Stein and Jian Lin GG-20

The Southeastern Boundary of the Juan Fernandez Microplate: Braking Microplate Rotation and Deforming the Antarctic Plate
Martin C. Kleinrock and Robert T. Bird GG-20

Construction and Destruction of Volcanic Knobs at the Cocos-Nazca Spreading System near 95°W
Martin C. Kleinrock and Benjamin A. Brooks GG-21

Large-Scale Electric Field Measurements on the Earth's Surface: A Review
L. J. Lanzerotti, A. D. Chave, C. H. Sayres, L. V. Medford and C. G. Maclennan GG-21

Surface and Subsurface Tectonic Loading on the Oceanic Lithosphere at the Mid-Atlantic Ridge
Jian Lin and Y. John Chen GG-22

Wavelet Analysis of a Bathymetric Profile Reveals Anomalous Crust
Sarah A. Little, Patricia Carter and Deborah Smith GG-22

Crustal Structure Across the Brunswick Magnetic Anomaly, Offshore Georgia, from Coincident Ocean-Bottom and Multichannel Seismic Data
Daniel Lizarralde and W. Steven Holbrook GG-22

Estimation of the Spatial Variability of Transmission Losses at Low Frequency in Shallow Water Using Multichannel Seismic Reflection Data
G. M. Purdy, D. L. DuBois and J. I. Ewing GG-23

Implications of New Gravity Data for Baikal Rift Zone Structure
C. Ruppel, M. G. Kogan and M. K. Mcnutt GG-23

An Estimate of Late Pleistocene Geomagnetic Intensity Variation from Sulu Sea Sediments
David A. Schneider GG-23

Paleomagnetism of Some Leg 138 Sediments: Detailing Miocene Magnetostratigraphy
David A. Schneider GG-23

Edge-Driven Microplate Kinematics
Hans Schouten, Kim D. Klitgord and David G. Gallo GG-24

Conductivity Discontinuities in the Upper Mantle Beneath a Stable Craton
A. Schultz, R. D. Kurtz, A. D. Chave and A. G. Jones GG-24

Segmentation and Morphotectonic Variations Along a Slow-Spreading Center: The Mid-Atlantic Ridge (24°00'N - 30°40'N
Jean-Christophe Sempere, Jian Lin, Holly S. Brown, Hans Schouten and G. M. Purdy GG-24

Age Variations of Oceanic Crust Poisson's Ratio: Inversion and a Crustal Evolution Model
Peter R. Shaw GG-25

Causes and Consequences of Variations in Faulting Style at the Mid-Atlantic Ridge
Peter R. Shaw and Jian Lin GG-26

The Seafloor Borehole Array Seismic System (SEABASS) and VLF Ambient Noise
R. A. Stephen, D. E. Koelsch, H. Berteaux, A. Bocconcelli, S. Bolmer, J. Cretin, N. Etourmy, A. Fabre, R. Goldsborough, M. Gould, S. Kery, J. Laurent, G. Omnes, K. Peal, S. Swift, R. Turpening and C. Zani GG-26

Finite Difference Modeling of Geoacoustic Interaction at Anelastic Seafloors
Ralph A. Stephen and Stephen A. Swift GG-27

Fine-Scale Magnetic Anomaly Field over the Southern Juan de Fuca Ridge: The Axial Magnetization Low and Implications for Crustal Structure
Maurice A. Tivey GG-27

High-Resolution Magnetic Surveys Over the Middle Valley Mounds, Northern Juan de Fuca Ridge
Maurice A. Tivey GG-28

Variations in Oceanic Crustal Structure and Implications for the Fine-Scale Magnetic Anomaly Signal
Maurice A. Tivey and H. Paul Johnson GG-28

Reduced Crustal Magnetization beneath the Active Sulfide Mound, TAG Hydrothermal Field, Mid-Atlantic Ridge 26°N
Maurice A. Tivey, Peter A. Rona and Hans Schouten GG-28

A Note on the Seafloor Coupling Characteristics of the New ONR OBS
Anne Trehu and George H. Sutton GG-29

A Geological Model for the Structure of Ridge Segments in Slow-Spreading Ocean Crust
Brian E. Tucholke and Jian Lin GG-29

Evidence from Earthquakes for Bookshelf Faulting at Large Non-transform Ridge Offsets
Laura Reiser Wetzel, Douglas A. Wiens and Martin C. Kleinrock GG-30

Morphology and Crustal Structure of the Atlantis Transform, Mid-Atlantic Ridge
Christopher E. Zervas, Jean-Christophe Sempere and Jian Lin GG-30

HYDRODYNAMICS

Uniform Bottom Shear Stress and Equilibrium Hypsometry of Intertidal Flats
Carl T. Friedrichs and David G. Aubrey GG-31

Tidal Propagation in Strongly Convergent Channels
Carl T. Friedrichs and David G. Aubrey GG-31

ISOTOPE GEOCHEMISTRY

Variations of the $^{187}Os/^{186}Os$ Ratio of Seawater Over the Past 28 Million Years as Inferred from Metalliferous Carbonates
Greg Ravizza GG-31

The Geochemical Cycle of Rhenium: A Reconnaissance
Debra Colodner, Julian Sachs, Gregory Ravizza, Karl Turekian, John Edmond and Edward Boyle GG-32

A Possible Link Between the Sea Water Osmium Isotope Record and Weathering of Ancient Sedimentary Organic Matter
Greg Ravizza and B. K. Esser GG-32

Osmium Isotopic Variations in Metalliferous Sediments from the East Pacific Rise and the Bauer Basin
Greg Ravizza and Gary M. McMurtry GG-32

OCEANOGRAPHY

The Western Black Sea Rim Current
T. Oguz, S. Besiktepe, D. G. Aubrey, V. Diaconu, L. Ivanov and U. Unluata GG-33

PALEOCEANOGRAPHY

A Model for Variation in the Chemistry of Planktonic Foraminifera Due to Secondary Calcification and Selective Dissolution
G. P. Lohmann GG-33

Vertical $\delta\ ^{13}C$ Gradient in the South Atlantic Ocean During the Last Glacial Maximum
G. P. Lohmann and K. C. Lohmann GG-34

Reassessment of the Influence of Temperature on the Distribution of ^{13}C in the Upper Ocean
G. P. Lohmann, D. W. Oppo and W. B. Curry GG-34

Depth Profiles of $\delta^{13}C$ in Bottom Water and Core-Top *C. wuellerstorfi* on the Ontong-Java Plateau and Emperor Seamounts
Daniel C. McCorkle and Lloyd D. Keigwin GG-35

Glacial-Holocene Paleoproductivity Off Western Australia: A Comparison of Proxy Records
D. C. McCorkle, H. H. Veeh and D. T. Heggie GG-35

Cd/Ca Changes in a Deep Cape Basin Core Over the Past 388,000 Years: Response of Circumpolar Deep Water Variability to Northern Hemisphere Ice Sheet Melting?
Delia W. Oppo GG-36

PALEOCLIMATOLOGY

Deep Circulation Change Linked to HEINRICH Event 1 and Younger Dryas in a Middepth North Atlantic Core
Lloyd D. Keigwin and Scott J. Lehman GG-36

Variability of Atlantic Circulation on Sub-Millennial Timescales
Scott J. Lehman GG-36

Transport of Freshwater into the Deep Ocean by the Conveyor
Scott J. Lehman, Daniel G. Wright and Thomas F. Stocker GG-36

PALEONTOLOGY

Evolution of Depth Ecology in the Planktic Foraminifera Lineage *Globorotalia (Fohsella)*
R. D. Norris, R. M. Corfield and J. E. Cartlidge GG-38

PETROLOGY

The Influence of Water on the Petrogenesis of Subduction-Related Igneous Rocks
Glenn A. Gaetani, Timothy L. Grove and Wilfred B. Bryan GG-38

Evidence for Hotspot-Related Carbonatite Metasomatism in the Oceanic Upper Mantle
Erik H. Hauri, Nobu Shimizu, Julie J. Dieu and Stanley R. Hart GG-38

SEDIMENTOLOGY

Automated Ice-Ocean Environmental Buoys (IOEBs) for the Telemetry of Air, Ice and Ocean Data from the Polar Oceans
R. Krishfield, S. Honjo, W. B. Tucker III, T. Nakanishi and T. Takizawae GG-38

Production and Accumulation of Calcium Carbonate in the Ocean: Budget of a Non-Steady State
John D. Milliman GG-39

DEPARTMENT OF MARINE CHEMISTRY AND GEOCHEMISTRY

BIOGEOCHEMISTRY

Tracing the Downward Flux of Nitrogen and Carbon into the Deep Ocean During the JGOFS N. Atlantic Bloom Experiment
Mark A. Altabet MCG-1

Spectroscopic Characterization and Remote Sensing of Non-Living Organic Matter
Neil V. Blough and S. A. Green MCG-1

Reactions of Oxygen Species in Natural Waters
Neil V. Blough and Richard G. Zepp MCG-1

Seasonal Variations in the Nitrogen Isotopic Composition of Sediment Trap materials Collected in Lake Malawi
R. Francois, C. H. Pilskaln, and Mark A. Altabet MCG-2

Variations of Marine Plankton $\delta^{13}C$ with Latitude Temperature and Dissolved CO_2 in the World Ocean
Ralf Goericke and Brian Fry MCG-2

Chlorophylls *a* and *b* and Divinyl Chlorophylls *a* and *b* in the Open Subtropical North Atlantic Ocean
Ralf Goericke and Daniel J. Repeta MCG-2

A High Resolution Historical Record of Holocene Anoxygenic Primary Production in the Black Sea
Daniel J. Repeta MCG-2

Reassessment of the Oceanic Residence Time of Phosphorus
K. C. Ruttenberg MCG-3

The Role of Bottom Sediments in the Aquatic Phosphorus Cycle
K. C. Ruttenberg MCG-3

Transport of Sludge-Derived Organic Pollutants to Deep-Sea Sediments at Deep Water Dump Site 106
Hideshige Takada, John W. Farrington, Michael H. Bothner, Carl G. Johnson, and Bruce W. Tripp MCG-3

An Experimental Model of the Chromophoric Dissolved Organic Matter Solar-Stimulated Fluorescence Spectrum
Anthony Vodacek, Sarah A. Green, and Neil V. Blough MCG-4

ORGANIC GEOCHEMISTRY

EPR Study of Kerogens from Three Alaskan North Slope Wells
Trudy A. Dickneider, Jean K. Whelan, and Neil V. Blough MCG-4

Carbon Isotopic Evidence for the Origin of Macromolecular Aliphatic Structures in Kerogen
Timothy I. Eglinton MCG-4

Relation of Shale Compaction to Deep Overpressures and Hydrocarbon Expulsion in the Gulf Coast
John M. Hunt, Jean K. Whelan, Lorraine Buxton Eglinton, and Lawrence M. Cathles III. . . MCG-5

Thermal Evolution of Sediments from Leg 139, Middle Valley, Juan De Fuca Ridge: An Organic Petrological Study
Shaozhi Mao, Lorraine Buxton Eglinton, Jean Whelan, and Li Liu MCG-5

Metastable Equilibrium as a Control on the Abundance of Low Molecular Weight Hydrocarbons
Jeffrey S. Seewald MCG-6

Organic Geochemical Indicators of Dynamic Fluid Flow Processes in Petroleum Basins
Jean K. Whelan, Mahlon C. Kennicutt, James M. Brooks, Dietmar Schumacher, and Lorraine B. Eglinton MCG-6

Time-Temperature Histories of Kerogen and Mineral Ammonia from ODP Leg 139 (Middle Valley) Sediments
Jean K. Whelan, Jeffrey Seewald, Lorraine Eglinton, and Fran Miknis MCG-7

GEOCHEMISTRY—INORGANIC, ISOTOPIC

A View of the Lower Crustal Component of Hydrothermal Systems at the Mid-Atlantic Ridge
Kathryn M. Gillis, Geoffrey Thompson, and Deborah S. Kelley MCG-7

Fluid Evolution in Submarine Magma-Hydrothermal Systems at the Mid-Atlantic Ridge
Deborah S. Kelley, Kathryn M. Gillis, and Geoff Thompson MCG-8

Active and Relict Sea-floor Hydrothermal Mineralization at the TAG Hydrothermal Field, Mid-Atlantic Ridge
Peter A. Rona, Mark D. Hannington, C. V. Raman, Geoffrey Thompson, Margaret K. Tivey, Susan E. Humphris, Claude Lalou, and Sven Petersen MCG-8

Rare Earth Element Composition of Precipitation, Precipitation Particles and Aerosols
Edward R. Sholkovitz, Thomas M. Church, and Richard Arimoto MCG-9

Heinrich Events in the North Atlantic: Radiochemical Evidence
Roger Francois and Michael P. Bacon MCG-9

Size-Fractionated ^{234}Th in Continental Shelf Waters off New England: Implications for the role of Colloids in Oceanic Trace Metal Scavenging
S. Bradley Moran and Ken O. Buesseler MCG-10

Variations in the Chemical and Stable Isotope Composition of Carbon and Sulfur Species During Organic-Rich Sediment Alteration: An Experimental and Theoretical Study of Hydrothermal Activity at Guaymas Basin, Gulf of California
Jeffrey S. Seewald, William E. Seyfried, Jr., and Wayne C. Shanks III MCG-10

The Use of Nitrogen Isotopic Ratio for Reconstruction of Past Changes in Surface Ocean Nutrient Utilization
Mark A. Altabet and Roger Francois MCG-11

Introduction to Atlantic Hydrothermal Activity
Peter A. Rona and Geoffrey Thompson MCG-11

Relict Hydrothermal Zones in the TAG Hydrothermal Field, Mid-Atlantic Ridge 26°N, 45°W
P. A. Rona, Y. A. Bogdanov, E. G. Gurvich, N. A. Rimski-Korsakov, A. M. Sagalevitch, M. D. Hannington, and G. Thompson MCG-12

MARINE CHEMISTRY

pH of the North Atlantic Ocean: Improvement to the Global Model for sound Absorption in Sea Water
Peter G. Brewer, David M. Glover, Catherine Goyet, and Deborah K. Shafer MCG-13

Stability of the Oxic/Anoxic Interface in the Black Sea
K. O. Buesseler, H. D. Livingston, L. Ivanov, and A. Romanov MCG-13

Long-Term Variability of Particle Flux in the Deep Sargasso Sea
W. G. Deuser MCG-13

Optical Absorption and Fluorescence Properties of Chromophoric Dissolved Organic Matter in Natural Waters
Sarah A. Green and Neil V. Blough MCG-14

Ocean Particle Chemistry: The Fractionation of Rare Earth Elements Between Suspended Particles and Seawater
Edward R. Sholkovitz, William M. Landing, and Brent L. Lewis MCG-14

INSTRUMENTS AND METHODS

Mooring Line Motions and Sediment Trap Hydromechanics: In-Situ Intercomparison of Three Common Deployment Designs
G. Gust, A. F. Michaels, R. Johnson, W. G. Deuser, and W. Bowles MCG-15

Analyses of Dissolved Organic Carbon in Seawater: The JGOFS EqPac Methods Comparison
Jonathan H. Sharp, Ronald Benner, Lenore Bennett, Craig A. Carlson, Steve E. Fitzwater, Edward T. Peltzer, and Luis M. Tupas MCG-15

DEPARTMENT OF PHYSICAL OCEANOGRAPHY

OCEAN CIRCULATION & LOW FREQUENCY VARIABILITY

A Closer Look at Particle Exchange in the Gulf Stream
Amy S. Bower and M. Susan Lozier PO-1

Exchange Through the Strait of Gilbraltar
Harry L. Bryden, Julio Candela and Thomas H. Kinder PO-1

Salt Flux as a Mechanism of Large-Scale Circulation in the Black Sea
S. N. Bulgakov, G. K. Korotaev and J. A. Whitehead PO-2

Barotropic Response of the Western Mediterranean to Observed Atmospheric Pressure Forcing
Julio Candela and Carlos J. Lozano PO-2

Changes in Antarctic Bottom Water Properties in the Western South Atlantic in the Late 1980's
Victoria J. Coles, Michael S. McCartney, Donald B. Olson and William M. Smethie, Jr. PO-3

Bio-Optical and Physical Variability in the Sub-Arctic North Atlantic Ocean During the Spring of 1989
T. Dickey, J. Marra, M. Stramska, C. Langdon, T. Granata, R. Weller, A. Plueddemann and J. Yoder PO-3

The Influence of Distributed Sources and Upwelling on the Baroclinic Structure of the Abyssal Circulation
Christopher A. Edwards and Joseph Pedlosky PO-3

Deep Circulation in the Tropical North Atlantic
Marjorie A. M. Friedrichs and Melinda M. Hall PO-4

Hemispheric Asymmetry of Deep Water Transport Modes in the Atlantic
Marjorie A. M. Friedrichs, Michael S. McCartney and Melinda M. Hall PO-4

Mean Sea Surface Height of the Antarctic Circumpolar Current from Geosat Data: Method and Application
Sarah T. Gille PO-5

Mean Circulation of the Upper Layers of the Western Equatorial Pacific Ocean
Yves Gouriou and John Toole PO-5

Synthesizing the Gulf Stream Thermal Structure from XBT Data
Melinda M. Hall PO-6

Observations of Gulf Stream Meander Induced Disturbances
Nelson G. Hogg PO-6

The Long-Term Hydrographic Record at Bermuda
Terrence M. Joyce PO-6

Spatial Variability of Subducting Water in the North Atlantic: A Pilot Study
Terrence M. Joyce and William J. Jenkins PO-6

Monitoring Gulf Stream Transport by Radar Altimeter and Inverted Echo Sounders
Kathryn A. Kelly and D. Randolph Watts PO-7

Anomalous Anomalies in Averaged Hydrographic Data
M. Susan Lozier, Michael S. McCartney and W. Brechner Owens PO-7

Gulf Stream-Generated Topographic Rossby Waves
Robert S. Pickart PO-7

Interaction of Gulf Stream and Deep Western Boundary Current Where They Cross
Robert S. Pickart PO-8

Determining the Mean Gulf Stream and its Recirculations Through Combining Hydrographic and Altimetric Data
Bo Qiu PO-8

Upper Ocean Heat Balance in the Kuroshio Extension Region
Bo Qiu and Kathryn A. Kelly PO-8

North Brazil Current Retroflection Eddies
P. L. Richardson, G. Hufford, R. Limeburner and W. S. Brown PO-9

Observations of Super-Inertial and Near Inertial Wind-Driven Flow
Daniel L. Rudnick and Robert A. Weller PO-9

Wave-Induced Abyssal Recirculations
Michael A. Spall PO-9

Advection and Eddy Mixing in the Mediterranean Salt Tongue
Michael A. Spall, Phillip L. Richardson and James Price PO-10

A Hydrographic Section Across the Subtropical South Indian Ocean
John M. Toole and Bruce A. Warren PO-10

A Western Atlantic Section from South Georgia Island (54° S) Northward Across the Equator
Mizuki Tsuchiya, Lynne D. Talley and Michael S. McCartney PO-11

A Homogeneous Model of the Wind-Driven Overturning Cell in the Southern Ocean
Liping Wang and Rui Xin Huang PO-12

A Simple Model of Abyssal Circulation in a Circumpolar Ocean
Liping Wang and Rui Xin Huang PO-12

Topographic Control of the Antarctic Circumpolar Current. Part I: A Linear Homogeneous Channel Model
Liping Wang and Rui Xin Huang PO-12

Driving the Meridional Overturning in the Indian Ocean
Bruce A. Warren PO-13

Slight Northwestward Inflow to the Deep South Fiji Basin
Bruce A. Warren, Thomas Whitworth, III., Mike I. Moore and Worth D. Nowlin, Jr. PO-13

Direct Observations of the Ekman Balance at 10° N in the Pacific
Susan Wijffels, Eric Firing and Harry Bryden PO-13

THEORETICAL AND LABORATORY MODELS

Thermals with Background Rotation and Stratification
Karl R. Helfrich PO-13

Time-Dependent Two-Layer Hydraulic Exchange Flows
Karl R. Helfrich PO-14

Thermohaline Circulation: Intermediate Water Formation and Energetics of Halocline Catastrophe
Rui Xin Huang PO-14

Three-Dimensional Structure of the Wind-Driven Circulation in the Subtropical North Pacific
Rui Xin Huang and Bo Qiu PO-14

Rotating Hydraulic Models of Continental Shelf and Circular Eddy Fonts
Ryuji Kimura and J. A. Whitehead PO-15

Thermocline Forced by Annual and Decadal Surface Temperature Variation
Z. Liu and J. Pedlosky PO-15

Stratified Abyssal Flow in the Presence of Fractured Ridges
Joseph Pedlosky PO-16

Predicting Eddy Detachment for an Equivalent Barotopic Thin Jet
Elise A. Ralph and Larry Pratt PO-16

Does Stommel's Mixed-Layer 'Demon' Work?
Richard G. Williams, Michael A. Spall and John C. Marshall PO-16

COASTAL CIRCULATION & DYNAMICS

The Semi-Diurnal Tides on the Amazon Shelf
Robert C. Beardsley, Julio Candela, Richard Limeburner, W. Rockwell Geyer, Steven J. Lentz, Belmiro Castro, David Cacchione and Nelson Carneiro PO-17

The Effect of Short-Scale Wind Variations on Shelf Currents
K. H. Brink, J. H. LaCasce and J. D. Irish PO-17

An Update on the Formation and Maintenance of Shelfbreak Fronts
David C. Chapman and Glen Gawarkiewicz PO-18

Variability of Water Properties and Currents in Late Spring in the Northern Great South Channel. Part I. Water Properties
Changsheng Chen, Robert C. Beardsley and Richard Limeburner PO-18

Variability of Water Properties and Currents in Late Spring in the Northern Great South Channel. Part II. Currents
Changsheng Chen, Robert C. Beardsley and Richard Limeburner PO-19

Quantifying the Effect of Discrete Contaminant Discharge on the Marine Environment
James H. Churchill PO-19

Transport of South Atlantic Bight Shelf Water to the Shelf Edge of the Middle Atlantic Bight
James H. Churchill, Jonathan A. Hare, Robert K. Cowen, Paul Dragos, Scott M. Glenn and Peter C. Cornillon PO-20

Heat and Salt Balances over the Northern California Shelf in Winter and Spring
E. P. Dever and S. J. Lentz PO-20

A Numerical Study of Dense Water Formation and Transport on a Shallow, Sloping Continental Shelf
Glen Gawarkiewicz and David C. Chapman PO-20

Summertime synoptic variability of frontal systems in the Northern Bering Sea
Glen Gawarkiewicz, J. Christopher Haney and Michael Caruso PO-21

Current Dynamics Over the Northern California Inner-Shelf
Steven J. Lentz PO-21

Seasonal Variations in the Amazon Plume Structure Inferred from Historical Hydrographic Data
Steven J. Lentz PO-22

Sensitivity of the Inner-Shelf Circulation to the Form of the Eddy Viscosity Profile
Steven J. Lentz PO-22

The Amazon River Plume During AMASSEDS: Subtidal Current Variability and the Importance of Wind Forcing
Steven J. Lentz PO-22

The Amazon River Plume During AMASSEDS: Spatial Characteristics and Salinity Variability
Steven J. Lentz and Richard Limeburner PO-23

Langrangian Flow Observations of the Amazon River Discharge in the North Atlantic
Richard Limeburner, Robert C. Beardsley, Ivan D. Soares and Steven J. Lentz PO-23

INSTRUMENTATION & EXPERIMENTAL NUMERICAL METHODOLOGY

Determination of Longwave Heat Flux at the Air-Sea Interface Using Measurements From Buoy Platforms
T. D. Dickey, D. V. Manov, D. A. Siegel and R. A. Weller PO-24

Discussion of the NRC Report "Statistics in Oceanography"
Anand Gnanadesikan PO-24

The IMET (Improved METeorology) Ship and Buoy Systems
D. S. Hosom, R. A. Weller, R. E. Payne and K. E. Prada PO-24

A Comparison of Some Barometric Pressure Sensors
Richard E. Payne PO-25

OTHER

Investigation of Ferroelectric Effects in Two Sulfide Deposits
Charles E. Corry PO-25

Reply to Discussion of "Geology of the Solitario" GSA Special Paper 250 by Henry and others
Charles E. Corry PO-25

A Laramide Age Push-Up Block: The Structures and Formation of the Terlingua-Solitario Structural Block, Big Bend Region, Texas
Charles E. Corry, James B. Stevens and Eugene Herrin PO-26

Wind Forced Biological-Physical Interactions on an Isolated Offshore Bank
Craig V. W. Lewis, Cabell S. Davis and Glen Gawarkiewicz PO-26

Finescale Parameterizations of Turbulent Dissipation
K. Polzin, J. Toole and R. Schmitt PO-26

Double Diffusion in Oceanography
Raymond W. Schmitt PO-27

The Distribution of Lanternfish Ceratoscopelus Maderensis (Lowe 1839) Off Northwest-Africa and its Relation to Water Masses
Clementine Zelck and Birgit Klein PO-27

MARINE POLICY CENTER

Climate Changes and Socio-Economic Impacts
Anders Alm, Erik Blommestein, and James M. Broadus MPC-1

Flat Organizations for Earth Science
Jesse H. Ausubel and John H. Steele MPC-1

Report on the Marine Policy Center of the Woods Hole Oceanographic Institution (WHOI), Woods Hole, Massachusetts
James M. Broadus MPC-1

Marine Pollution Gets International Attention
James Broadus, Yoshiaki Kaoru, Sarah Repetto, and Suzanne Demisch MPC-1

Problems in the Meso-Scale Interpretation of Satellite Chlorophyll Data
E. W. Henderson and J. H. Steele MPC-2

Manganese nodule price trends: Dim Prospects for the Commercialization of Deep Seabed Mining
Porter Hoagland MPC-2

Planning vs. Reality: Political and Scientific Determinants of Outer Continental Shelf Lease Sales
Porter Hoagland and Scott Farrow MPC-2

Technology Transfer and Scientific Relevance
Porter Hoagland and Hauke Kite-Powell MPC-3

Multimedia Waste Disposal Optimization Under Uncertainty with an Ocean Option
Di Jin MPC-3

Environmental Compliance and Optimal Oil and Gas Exploitation
Di Jin and Thomas A. Grigalunas MPC-3

Monitoring Marine Resources: Ecological and Policy Implications Affecting the Scientific Collecting and Commercial Value of New England Conch *(Busycon)*
Ilene M. Kaplan and Barbara C. Boyer MPC-3

Discrete-Choice Contingent Valuation of Beach Recreation Benefits for Tourists and Local Residents
Yoskiaki Kaoru MPC-4

The Value of Historic Shipwrecks: Conflicts and Management
Yoshiaki Kaoru and Porter Hoagland MPC-4

Using Random Utility Models to Estimate Recreational Value of Estuarine Resources
Yoshiaki Kaoru, V. Kerry Smith, and Jin Long Liu MPC-4

Economics of Standards, System Analysis, and Sea Trials: Toward an Assessment of the Proposed IMO Performance Standard for ECDIS
Hauke Kite-Powell MPC-5

Electronic Chart Systems in the Ship Control Process: The Role of Operators and Instruments in Safety of Navigation
Hauke Kite-Powell MPC-5

Preliminary Operational and User Survey Results from U.S. ECDIS Test Bed Project Sea Trials
Hauke Kite-Powell MPC-5

Book Review: *Oceanography in the Next Decade*
James C. Kraska MPC-6

Gatekeeper of the Gulf: The Iranian Navy and Persian Gulf Security Toward the 21st Century
James C. Kraska MPC-6

Oceanographic and Naval Deployments of Expendable Marine Instruments Under U.S. and International Law
James C. Kraska MPC-6

The US Navy and No Cure, No Pay Salvage Law
James C. Kraska MPC-6

The U.S. Navy and the Marine Pollution Convention
James C. Kraska MPC-7

Development of the United States Electronic Chart Display and Information System (ECDIS)
David J. Scott and Arthur G. Gaines, Jr. MPC-7

An Exploratory Analysis of a Record of El Niño Events, 1800-1987
Andrew R. Solow MPC-7

A Test of Independence Between a Time Series and a Markov Chain
Andrew R. Solow MPC-7

Comment (On NRC Report on Statistics and Physical Oceanography)
Andrew R. Solow MPC-8

Detecting Change in the Composition of a Multi-Species Community
Andrew R. Solow MPC-8

Inferring Extinction in a Declining Population
Andrew R. Solow MPC-8

On the Association Between Snow Accumulation and El Niño Events in the Quelccaya Ice Cap, Peru
Andrew S. Solow MPC-8

On the Use of Cross-Correlation in Seismology
Andrew R. Solow MPC-8

Saturday Effects in Tanker Oil Spills: Comment
Andrew R. Solow MPC-9

Statistical Methods for Bout Analysis
Andrew R. Solow MPC-9

Estimating the Rate of Synonymy
Andrew R. Solow, Laurence A. Mound, and Kevin J. Gaston MPC-9

On the Measurement of Biological Diversity
Andrew Solow, Stephen Polasky, and James Broadus MPC-9

Conditional Simulation and the Value of Information: A Bayesian Approach
Andrew R. Solow and Samuel J. Ratick MPC-9

Coupling Between Physical and Biological Scales
John H. Steele and Eric W. Henderson MPC-10

The Significance of Interannual Variability
John H. Steele and Eric W. Henderson MPC-10

COASTAL RESEARCH CENTER

A Model for the Mediterranean Seas: The Cooperative Marine Science Program for the Black Sea (CoMSBlack)
David G. Aubrey and Frank J. Gable CRC-1

GRADUATE STUDENT

An Experimental Study of Air Entrainment by Breaking Waves
Eric Lamarre GS-1

Hydrodynamics and Morphodynamics of Shallow Tidal Channels and Intertidal Flats
Carl Takeo Friedrichs GS-1

Late Cretaceous (Maestrichtian) Calcareous Nannoplankton Biogeography with Emphasis on Events Immediately Preceding the Cretaceous/Paleocene Boundary
Thomas Wolfgang Ehrendorfer GS-2

The Behavioral Physiology of Labroid Fishes
Mary Carla Curran GS-3

Chlorophyll Diagenesis in the Water Column and Sediments of the Black Sea
Linda L. King GS-4

Marine Microbial Production of Dimethylsulfide from Dissolved Dimethylsulfoniopropionate
Kathleen M. Ledyard GS-5

Analysis of Toxic and Non-Toxic *Alexandrium* (Dinophyceae) Species Using Ribosomal RNA Gene Sequences
Christopher Alan Scholin GS-5

Vortex-Induced Forces on Oscillating Bluff Cylinders
Ramnarayan Gopalkrishnan GS-6

Cosmogenic ^{32}P and ^{33}P in the Atmosphere and Oligotrophic Ocean and Applications to the Study of Phosphorus Cycling
Nathalie Waser GS-7

Acoustic Tomography in the Straits of Florida
David Brian Chester GS-7

Structural Characterization and Bacterial Degradation of Marine Carbohydrates
Carol Arnosti GS-8

Analysis of Modal Evolution Caused by a Weakly Range-Dependent Seabed in Shallow Water and its Application to Inversion for Geoacoustic Properties
Kazuhiko Ohta GS-8

Design of a Controllable Pitch Underwater Thruster System
Robert W. Keefe GS-9

Ambient Noise and Surface Wave Dissipation in the Ocean
Francis C. Felizardo GS-9

The Importance of Fine-Scale Flow Processes and Food Availability in the Maintenance of Soft-Sediment Communities
Paul V.R. Snelgrove GS-10

Exchanges between Hemispheres and Gyres: A Direct Approach to the Mean Circulation of the Equatorial Pacific
Susan Elizabeth Wijffels GS-11

Acoustic Travel Time Perturbations due to an Internal Tide and Internal Wave Field in the Barents Sea
Douglas Scott Ray GS-12

Orientation Dependence of the Acoustic Backscatter for Elongated Zooplankton
Matthew Lloyd Johnson GS-12

Forward Scattering of a Pulsed Continuous Wave Signal Through Laminar and Turbulent Thermal Plumes
Stephen Gerard Bowen GS-13

Dispersion of Fine Particles by Wave-Induced Mass Transport
Carole A. Womeldorf GS-13

Time-Dependent Assimilation of CTD Data to an Open Ocean Rossby Wave Model
James Reginald Gunson GS-13

Passive Localization of Underwater Acoustic Beacons
Dennis Michael Wojcik GS-13

The Dynamic Role of Ridges in a β-Plane Channel Towards Understanding the Dynamics of Large Scale Circulation in the Southern Ocean
Liping Wang GS-14

A Tomographic Ocean Sound Speed Profile from a Long Vertical Acoustic Array
James Murwanthanje Njeru GS-15

Deeply-Towed Underwater Vehicle Systems: A Verified Analytical Procedure for Creating Parameterized Dynamic Models
Franz S. Hover GS-15

Turbulent Mixing in Stratified Fluids - Layer Formation and Energetics
Young-Gyu Park GS-15

Assimilation of Altimeter Data in a Quasi-Geostrophic Model of the Gulf Stream System: A Dynamical Perspective
Antonietta Capotondi GS-16

The Isotope Geochemistry of Abyssal Peridotites and Related Rocks
Jonathan E. Snow GS-17

DEPARTMENT OF APPLIED OCEAN PHYSICS & ENGINEERING

George V. Frisk, Chairman

SIMULATING THE DYNAMICS OF UNDERWATER VEHICLES WITH LOW-TENSION TETHERS

M. A. Grosenbaugh, C. T. Howell, and S. Moxnes

A numerical technique for calculating the two-dimensional motions of a tethered underwater vehicle is presented. The method is unique because of its ability to simulate accurately the dynamics of cables that are under low tensions. This is accomplished by incorporating bending stiffness into the cable equations and thus removing the singularity that occurs when the cable tension becomes zero. Numerical results for several tether-vehicle maneuvers are presented.

Published in: *International Journal of Offshore Polar Engineering*, September, 3(3):213-218, 1993.

Supported by: ONR grant N00014-89-J-3061 (MIT) and ONT contract N00014-89-C-0179.

WHOI Contribution No. 8266.

THE FRONTOMANDIBULAR STAY OF BALAENOPTERIDAE: A MECHANISM FOR MOMENTUM RECAPTURE DURING FEEDING

Richard Lambertsen, Nathan Ulrich, and Janice Straley

The feeding process of Balaenopteridae (rorquals) is characterized by a highly energetic event in which a large volume of seawater is engulfed and filtered. Here observations are reported which identify a major structural component of a stay apparatus which exists in the rorqual craniomandibular system. This fibrous appendage of the temporalis muscle introduces a continuous mechanical linkage between the supraorbital process of the frontal bone and the coronoid process of the mandible. It is named the frontomandibular stay. Anatomic relationships and biomechanical findings indicate that this structure would control and assist a process of continuous change in position of the jaws during engulfment events. The dynamic form of mandibular kinesis produced would function to increase the power of feeding. Owing to the stay's nonmuscular construction its adaptive action necessarily is driven by the kinetic mass of the moving whale.

WHOI Contribution No. 8267.

EVIDENCE FOR SLOW MIXING ACROSS THE PYCNOCLINE FROM AN OPEN-OCEAN TRACER-RELEASE EXPERIMENT

James R. Ledwell, Andrew J. Watson, and Clifford S. Law

The distributions of heat, salt and trace substances in the ocean thermocline depend on mixing along and across surfaces of equal density (isopycnal and diapycnal mixing, respectively). Measurements of the invasion of anthropogenic tracers, such as bomb tritium and ^{3}He (see, for example, refs 1 and 2), have indicated that isopycnal processes dominate diapycnal mixing, and turbulence measurements have suggested that diapycnal mixing is small[3, 4), but it has not been possible to measure accurately the diapycnal diffusivity. Here we report such a measurement, obtained from the vertical dispersal of a patch of the inert compound SF_6 released in the open ocean. The diapycnal diffusivity, averaged over hundreds of kilometers and five months, was 0.11 $\pm$ 0.02 cm^2 s^{-1}, confirming previous estimates[1-4]. Such a low diffusivity can support only a rather small diapycnal flux of nitrate into the euphotic zone; it justifies the neglect of diapycnal mixing in dynamic models of the thermocline[25-27], and implies that heat, salt and tracers must penetrate the thermocline mostly by transport along, rather than across density surfaces.

Published in: *Nature*, 364(6439):701-703, 1993.

Supported by: NSF contract OCE-9020492.

WHOI Contribution No. 8269.

OCEAN ACOUSTIC TOMOGRAPHY AT 1000-KM RANGE USING WAVEFRONTS MEASURED WITH A LARGE-APERTURE VERTICAL ARRAY

Bruce D. Cornuelle, Peter F. Worcester, John A. Hildebrand, William S. Hodgkiss, Jr., Timothy F. Duda, Janice Boyd, Bruce M. Howe, James A. Mercer, and Robert C. Spindel

Broadband acoustic signals transmitted from a moored 250-Hz source to a 3-km long vertical line array of hydrophones 1000 km distant in the Northcentral Pacific Ocean were used to determine the amount of information available from tomographic techniques in the vertical plane connecting a source-receiver pair. A range-independent, pure-acoustic inverse to obtain the sound speed field using travel-time data from the array is shown to be possible by iterating from climatological data, without using any information

from concurrent environmental measurements. Range-dependent inversions indicate resolution of components of oceanic variability with horizontal wavelength shorter than 50 km, although the limited spatial resolution of concurrent direct measurements does not provide a strong cross-validation, since the typical cast spacing of 20-25 km gives a Nyquist wavelength of 40- 50 km. The small travel time signals associated with high wavenumber ocean variability place stringent, but achievable, requirements on travel time measurement precision. The forward problem for the high-wavenumber components of the model is found to be subject to relatively large linearization errors, however, unless the sound speed field at wavelengths greater than about 50 km is known from other measurements or from a 2-D tomographic array. The high-ocean-wavenumber resolution that is in principle available from tomographic measurements is therefore achievable only under restricted conditions.

Published in: *Journal of Geophysical Research*, 98(C9):16,365-16,377, 1993.

Supported by: ONT N00014-87-0670, N00014-89-K-0120, ONR N00014-87-K-0120, N00014-87-K-0445, N00014-88-K-0263, N00014-90-J-1022, N00014-91-J-4055, Duda was partially supported by Woods Hole Oceanographic Institution.

WHOI Contribution No. 8312.

VERTICAL ARRAY RECEPTIONS OF THE HEARD ISLAND TRANSMISSIONS

Arthur B. Baggeroer, Khosrow Lashkari, Ching-sang Chiu, James H. Miller, Peter Mikhalevsky, and Keith von der Heydt

The Heard Island Feasibility Test (HIFT) demonstrated that coded acoustic signals could be detected at ranges up to 18,000 km with currently available source technology. This paper describes one component of the HIFT where a large aperture vertical line array was deployed to record the signals transmitted from Heard Island.

One may pose the question: why use a vertical line array (VLA)? There are several responses to this. The first simply involves the signal to noise ratios (SNR). The transmissions to both coasts of the United States were nearly antipodal. While explosive signals have been detected at these ranges, transmission loss measurements did not exist.[10] In fact, one of the major challenges prior to HIFT was predicting the received signal amplitudes; estimates differed by more than ± 30 dB depending upon the assumptions made about the propagation! This scale of prediction error is indicative of our uncertainty about transglobal acoustic propagation. In its simplest use the VLA provides some array gain to improve SNR's.

A second response concerns long range acoustic propagation. Signals must propagate axially in the SOFAR duct to be detected at these long ranges. At the 57 Hz center frequency of the HIFT these axial, or ducted, paths are efficiently described using a modal representation. The modal distribution is critical to understanding the acoustic propagation. The spatial distribution of the signals across the VLA provided information which is not available from a time series.

Supported by: Department of Energy grant De-FG02-91ER61100.

WHOI Contribution No. 8328.

ROBUST MAXIMUM ENERGY ADAPTIVE MATCHED FIELD PROCESSING

James C. Preisig

While adaptive array processing algorithms are effective at rejecting unwanted signals (i.e., controlling sidelobe levels) and have good resolution (.e., have narrow mainlobes), they also usually suffer a significant degradation in performance in the presence of environmental mismatch. A Maximum Energy Minimum Variance (MEMV) Matched Field Processor is formulated which "tunes" the replica vector used by a Minimum Variance Distortionless Response (MVDR) Matched Field Processor to adjust for fluctuations in the environment. The resulting processor has the same structure as the two-stage MVDR processor interpretation of the Adaptive Minmax Matched Field Processor proposed previously. However, the criterion which the two processors use to "tune" the replica vector differ. The result is that the MEMV processor can accommodate a wider range of environmental uncertainty than can be accommodated by the Adaptive Minmax processor while at the same time achieving level of sidelobe suppression and mainlobe resolution that are close to those of traditional adaptive processors.

In Press: *IEEE Transactions on Signal Processing.*

Supported by: ONR grant N00014-91-J-1246.

WHOI Contribution No. 8360.

BOTTOM BOUNDARY LAYER SPECTRAL DISSIPATION ESTIMATES IN THE PRESENCE OF WAVE MOTIONS

T. F. Gross, A. J. Williams III, and E. A. Terray

Turbulence measurements are an essential element of the Sediment TRansport Events on Shelves and Slopes experiment (STRESS). Sediment transport under waves is initiated within the wave boundary layer at the seabed, at most a few tens of centimeters deep. The suspended load is carried by turbulent diffusion above the wave boundary layer. Quantification of the turbulent diffusion active above the wave boundary layer requires estimates of shear stress or energy dissipation in the presence of oscillating flows. When the wave orbital velocity is of similar magnitude to the mean flow, kinematic effects on the estimation techniques of stress and dissipation must be accounted. Lumley and Terray (1984) presented the theory describing the effect of orbital motions on kinetic energy spectra. Their model is used here with observations of spectra taken within a turbulent boundary layer which is affected by wave motion. The necessity of accounting for wave orbital motion is demonstrated, but variability within the field setting made it difficult to discern what improvement in accuracy the corrections afforded.

In Press: *Continental Shelf Research.*

Supported by: ONR grant N00014-90-J-1046.

WHOI Contribution No. 8362.

A NEW DISTRIBUTED REAL-TIME CONTROL SYSTEM FOR THE JASON UNDERWATER ROBOT

Louis L. Whitcomb and Dana R. Yoerger

This paper articulates design principals for the rapid development of large scale robot systems. Points are illustrated with examples from a new computer system for closed loop control of the underwater robot JASON at full ocean depth as follows: (*i*) The use of subsystems with differing computer architectures is shown to permit effective matching of capability to function. (*ii*) A two-part system design is described which partitions safety-critical from non safety-critical subsystems for cost-effective implementation and enhancement. (*iii*) JasonTalk, a machine-independent message-passing communication protocol which enables integration of disparate computer architectures into a unified system is described. Results from a recent JASON deployment in the Pacific Ocean are presented.

Published in: *International Workshop on Robotics and Systems (IEEE Presentation). IROS 93 Conference Proceedings*, Yokahama, Japan, 1993.

Supported by: Internal support from the Woods Hole Oceanographic Institution.

WHOI Contribution No. 8370.

EVIDENCE FOR ENHANCED BOUNDARY MIXING IN SANTA MONICA BASIN

James R. Ledwell and Barbara M. Hickey

Transients in the heat content in Santa Monic and San Pedro Basins imply a basin-wide diapycnal eddy diffusinvity greater than 1. cm^2/s. This is significantly larger than the value of SF_6 of 0.25 ± 0.08 cm^2/s determined for the interior of Santa Monica Baisn for September 1985 to February 1986 by Ledwell and Watson [1991]. However, the exodus of SF_6 from Santa Monic Basin after February 1986, by which time the tracer had mixed to the boundaries of the basin, was fast enough to be consistent with a greatly enhanced vertical flux. Since the kinetic energy in the basin had not changed significantly, it is unlikely that a temperoal increase in forcing resulted in enhanced fluxeds in the interior of the basin. The most likely interpretation is that diapycnal fluxes in the basin are dominated by processes in the boundary regions. Temperature and SF_6 profiles from near the edges of the basin do not give conclusive evidence either for or against such enhanced mixing.

Supported by: NSF grants OCE-8401658, OCE-8614635, and OCE-9013299; Dept. of Energy grant DE-FGOS-85-91-ER60333; and NSF grant OCE-8918175.

WHOI Contribution No. 8371.

OBSERVATIONS OF CURRENTS AND WATER PROPERTIES IN THE AMAZON FRONTAL ZONE

W. Rockwell Geyer and Gail C. Kineke

Measurements of currents and water properties were obtained at various locations in the frontal zone of the Amazon River outflow plume during four cruises in 1989-1991 as part of A Multidisciplinary Amazon Shelf Sediment Study (AMASSedS). A salinity front resembling a salt wedge is found approximately 100 km seaward of the river mouth. It continues northwestward more than 400 km along the shelf close to the 10-m isobath. The salinity stratification within the frontal zone varies by a factor of four through the

spring-neap cycle due to variations of tidal mixing. Tidal currents, which are oriented principally in the cross-shelf direction, reach 200 cm s^{-1} during spring tides and drop to less than 80 cm s^{-1} during neaps in the vicinity of the river mouth. The non-tidal flow is strongly sheared, with near-surface speeds of up to 100 cm s^{-1}. The direction of the near-surface flow is consistent with the trajectory of the plume, with a generally northwestward orientation except near the river mouth, where there is a significant offshore component of flow. Near-bottom flows are weak, with some suggestion of onshore flow beneath the plume as it progresses up the shelf. The strong velocity shears are stabilized by strong stratification by salinity in the middle of the water column and by highly concentrated suspended sediment (i.e., fluid mud) near the seabed.

In Press: *Journal of Geophysical Research.*

Supported by: NSF grants OCE-8812917, OCE-9115712 and OCE-8813399.

WHOI Contribution No. 8382.

SPRAY DROPLET MODELING, I: LAGRANGIAN MODEL SIMULATION OF THE TURBULENT TRANSPORT OF EVAPORATING DROPLETS

J. B. Edson and C. W. Fairall

The investigation of aerosol production and transport over the worlds' oceans is of importance in studies concerning cloud physics, air pollution, atmospheric optics, and air-sea interaction in general. However, the contribution of sea spray droplets to the transfer of moisture and latent heat from the sea to the atmospheric is not well known. IN light of this, the HEXIST and CLUSE programs were designed to investigate the generation, turbulent transport, and evaporation of droplets ejected by bursting bubbles within the air-sea simulation tunnel at IMST, Luminy, France. This first part describes the Lagrangian model developed as part of these programs to simulate the turbulent transport of evaporating droplets. The model relies on a form of the Langevin equation, which has been modified to account for the effects of gravity and the inertia of the droplets. the comparisons between the model and measurements show good agreement, particularly within the surface layer at IMST. Part II describes the coupling of the model with an Eulerian $e - \epsilon$ model, which allows for improved simulation of the velocity and scalar field, as well as a means for interaction between the droplets and these fields. The model is designed to provide a better understanding of the influence of these droplets on the near surface energy budget.

Supported by: ONR contract N00015-86-K-250, NSF grants INT-8907676 and OCE- 9115227.

WHOI Contribution No. 8397.

DESIGN AND TESTING OF THE AUTONOMOUS BENTHIC EXPLORER

Albert M. Bradley and Dana R. Yoerger

The Autonomous Benthic Explorer (ABE) is an autonomous underwater vehicle designed to perform long-term repeated surveys in the deep ocean. We designed ABE in response to the needs of biologists and geologists who study hydrothermal vents [1]. These deep water hot springs are very dynamic, and a comprehensive understanding of their long-term variability requires time-series observations that cannot be achieved solely from the limited time windows offered by manned submersibles and remotely operated vehicles. Likewise, the mobility of a vehicle can significantly enhance data from moored and bottom-mounted instruments.

These needs dictated the basic design of ABE. ABE will be able to descend to a prepared site on the bottom, dock to a mooring, and place itself in a very low power "sleep" state. Then, at preplanned intervals, ABE will undock, perform a grid survey, then redock to the mooring. ABE's principal data will be monochrome and color video stills of the bottom and basic CTD measurements.

Figure 1 shows several views of ABE, highlighting the components that will be discussed in this paper. While ABE was designed with a particular type of mission in mind, we have designed the subsystems to be applicable to a wide range of AUV applications. In this paper, we give an overview of several of the most important ABE subsystems, illustrated by our initial dockside and deep-water test data.

Published in: *Proceedings AUV-93 Conference*, June 28-30, Washington, DC, :1,044-1,049, 1993.

Supported by: NSF grant OCE-8820227 and NSF grant OCE-9216775.

WHOI Contribution No. 8408.

ADAPTIVE MULTICHANNEL COMBINING AND EQUALIZATION FOR UNDERWATER ACOUSTIC COMMUNICATIONS

M. Stojanovic, J. Catipovic, and J. G. Proakis

A theoretically optimal multichannel receiver for intersymbol interference communication channels is derived, and its suboptimal versions with linear and decision feedback equalizer are

presented. A practical receiver based on any of these structures encounters difficulties in the underwater acoustic channels in which the extended time varying multipath is accompanied by phase instabilities. A receiver which overcomes these problems by jointly performing adaptive mean squared error diversity combining, multichannel carrier phase synchronization and decision feedback equalization is proposed. Its performance is demonstrated on the experimental telemetry data from deep and shallow water long range acoustic channels. Presented results indicate superior quality of coherent PSK and QAM reception obtained through joint equalization of very few channels.

Published in: *Journal of the Acoustical Society of America*, 94(3):1621-1631, 1993.

Supported by: DARPA grant MDA 972-91-J-1004.

WHOI Contribution No. 8412.

ADAPTIVE RECEIVERS FOR UNDERWATER ACOUSTIC COMMUNICATIONS: THEIR RELATION TO BEAMFORMING AND DIVERSITY COMBINING

M. Stojanovic, J. Catipovic, and J. G. Proakis

A major difficulty encountered in the underwater acoustic (UWA) channels is the extended and dynamic multipath propagation. At the same time, relative simplicity of building a hydrophone array, and relatively low data rates used, offer advantages of both multichannel combining and powerful equalization methods for UWA communications.

In order to select a suitable combining method, we derive the optimal multichannel receiver for a general ISI communication channel. When there exists a certain spatial distribution of the signals across the array, the optimal combiner can be identified as a 'beamformer' and a bank of filters matched to the individual path responses. This beamformer differs from a conventional one in that it does not null-out the multiple signal reflections, but makes use of them.

The optimal receiver structure gives rise to two classes of adaptive implementations. The first class makes no assumptions about the spatial signal distribution, and corresponds to pure diversity combining. The second class explicitly uses knowledge of the angles of signal arrivals. For the receiver of the second class, we present an algorithm for joint adaptive equalization and tracking of the angles of arrival. While the receiver of the first class has an advantage of not being sensitive to any propagation-model mismatch, its computational complexity may become very high when a large array is used together with long equalizers. To reduce the receiver complexity, but make no explicit assumptions about the relationship between the array signals, we combine the two approaches considered. The resulting beamformer and reduced-complexity equalizer are optimized jointly, to provide the same mean-squared-error performance as that of the full-complexity multichannel equalizer.

To compare the approaches considered, we derive the condition for equality between the full-complexity multichannel combiner and an arbitrary fixed beamformer followed by a smaller adaptive combiner. We use this condition to check the equivalence for several interesting beamforming strategies, whose performance, together with that of the fully adaptive combining methods, is demonstrated in simulation.

Published in: *Proceedings of Comcon 4 Conference*, Greece, June 1993.

Supported by: DARPA grant MDA 972-91-J-1004.

WHOI Contribution No. 8413.

A COMPARISON OF MEASURED AND PREDICTED BROADBAND ACOUSTIC ARRIVAL PATTERNS IN TRAVEL TIME-DEPTH COORDINATES AT 1000-KM RANGE

Peter F. Worcester, Bruce D. Cornuelle, John A. Hildebrand, William S. Hodgkiss, Jr., Timothy F. Duda, Janice Boyd, Bruce M. Howe, James A. Mercer, and Robert C. Spindel

Broadband acoustic signals were transmitted from a moored 250-Hz source to a 3-km long vertical line array of hydrophones 1000 km distant in the eastern North Pacific Ocean during July 1989. The sound-speed field along the great circle path connecting the source and receiver was measured directly by nearly 300 XBT, CTD, and AXBT casts while the transmissions were in progress. This experiment is unique in combining a vertical receiving array that extends over much of the water column, extensive concurrent environmental measurements, and broadband signals designed to measure acoustic travel times with 1 ms precision. The time-mean travel times of the early ray-like arrivals, which are evident as wavefronts sweeping across the receiving array, are consistent with predictions based on the direct measurements of temperature and salinity, within measurement uncertainty. The comparisons show that sub-inertial oceanic variability with horizontal wavelengths shorter than 50 km, which is not resolved by the direct measurements, significantly (25 ms peak-to-peak) affects the time-mean ray travel times. the times at which the acoustic

reception ends (the final cut-offs) occur significantly later than predicted using ray theory for hydorphones more than 100-200 m off the sound channel axis. Non-geometric effects, such as diffraction at caustics, partially account for the observations.

In Press: *Journal of the Acoustical Society of America.*

Supported by: ONT Contracts N00014-87-J-K-0670 and N00014-89-K-0120; ONR contracts N00014-87-K-0120, N00014-87-K-0445, N00014-90-J-1022 and N00014-91-J-4055 and ONR grant N00014-92-J-1162.

WHOI Contribution No. 8414.

ADAPTIVE EQUALIZATION TECHNIQUES FOR INTERFERENCE SUPPRESSION IN SHALLOW WATER ACOUSTIC TELEMETRY CHANNELS

Zoran Zvonar, David Brady, and Josko Catipovic

Despite the severe propagation conditions in shallow water acoustic telemetry channels, coherent high-speed data transmission may be established using adaptive receivers based on a decision feedback equalizer (DFE) structure. The performance of DFE in shallow water acoustic networks is affected by substantial cochannel interference from acoustic modems, in addition to extended, time-varying ISI and large Doppler fluctuations.

In this paper we address the interference suppression ability of a DFE by evaluating a channel-specific structure for reliable interference suppression and dynamic channel tracking. The DFE performance is compared to adaptive multiuser receiver which jointly performs adaptive equalization and multiple-access interference cancellation.

Published in: *Proceedings of the Twenty-Seventh Annual Asilomar Conference on Signals, Systems and Computers*, Pacific Grove, California, November 1993.

Supported by: ARPA grant MDA 972-91-J-1004.

WHOI Contribution No. 8415.

A SOFT-DECISION-DIRECTED MULTIUSER RECEIVER FOR UNDERWATER ACOUSTICAL CHANNELS

David Brady and Josko A. Catipovic

An underwater acoustic local area network (ALAN) is being tested which permits multipoint-to-point telemetry between many high-rate, ocean-bottom sensors and a central, surface-deployed receiver in the 10-30kHz vertical acoustical channel. Ocean-bottom modems initiate the transmission process by requesting data channel time slots via a common narrowband request channel. Request packets overlap in time and frequency in this channel, and the throughput and average transmission delay rely heavily on the successful resolution of the request packet collisions. This paper describes the design and performance of a request channel receiver capable of resolving collisions between several asynchronous and cochannel packets. The receiver algorithm differs from: standard capture schemes (by demodulating the data from both strong and weak transmitters), conventional spread-spectrum receivers (by overcoming the near-far problem), and existing multiple-access demodulation techniques (by adapting to the number of interfering signals, and the unknown phase, Doppler, amplitude and timing of each signal in the collision). The receiver demodulates the collided packets by decision-directed techniques, and it differs from existing decision-directed multiple-access receivers [1] [2] [3] through a novel method of estimating the interference for each user which minimizes error propagation due to inaccurate tentative decisions [4] [5]. An in-water experiment illustrates that this technique is extremely desirable for collision resolution in underwater acoustic local area networks, and also for underwater autonomous vehicles with both sidescan sonar as well as acoustic telemetry links.

In Press: *Journal of Ocean Engineering.*

Supported by: DARPA grant MDA 972-91-J-1004 and NSF grant OCE-9201191.

WHOI Contribution No. 8416.

ACOUSTIC SCATTERING LOSSES IN THE GREENLAND SEA MARGINAL ICE ZONE DURING THE 1988-89 TOMOGRAPHY EXPERIMENT

Guoliang Jin, James F. Lynch, Richard Pawlowicz, and Peter Worcester

Using arrival amplitude data from the 1988-89 Greenland Sea tomography experiment, the effects of ice scattering at 250 Hz in the Marginal Ice Zone (MIZ) are estimated. The resolution of the arrivals is examined first, showing that arrivals are resolved as rays from about 8° to 10° launch angle and as nominal modes for low angles, below about 4° launch angle. The under-ice reflection losses of resolved rays and modes are then considered using two methods. First, the ratio of arrival amplitudes during ice free and ice covered periods is

estimated. Second, the ratio of members of a ray group with different reflection numbers is used, showing similar results to the first method. For higher grazing angle reflections, fast field calculations using the program SAFARI are seen to model the data reasonably, using a combination of measured and historical ice parameter values. For the low angle arrivals, the amplitudes of the arrivals are seen to depend strongly upon both the details of the surface mixed layer and the ice cover itself. Using reasonable mixed layer estimates from both data and model inputs, it is seen that part of the amplitude reduction seen in the data is indeed due to ice, though the exact amount is sensitive to the details of the mixed layer.

Supported by: ONR grant N00014-91-J-1138.

WHOI Contribution No. 8418.

PHASE-COHERENT DIGITAL COMMUNICATIONS FOR UNDERWATER ACOUSTIC CHANNELS

M. Stojanovic, J. Catipovic, and J. G. Proakis

High-speed phase coherent communications in the ocean channel are made difficult by the combined effects of large Doppler fluctuations and extended, time varying multipath. In order to account for these effects, we consider a receiver which performs optimal jointly phase synchronization and channel equalization. Since the intersymbol interference in some underwater acoustic channels spans several tens of symbol intervals, making the optimal maximum-likelihood receiver unacceptably complex, we use a suboptimal, but low complexity, decision feedback equalizer. The mean squared error multiparameter optimization results in an adaptive algorithm which is a combination of recursive least squares and second-order digital phase and delay locked loops. The use of fractionally spaced equalizer eliminates the need for explicit symbol delay tracking.

The proposed algorithm is applied to experimental data from three types of UWA channels: long-range deep water, long-range shallow water, and short-range shallow water channels. The modulation techniques used are 4- and 8-PSK. The results indicate the feasibility of achieving power-efficient communications in these channels and demonstrate the ability to coherently combine multiple arrivals, thus exploiting diversity inherent in multipath propagation.

In Press: *IEEE Journal of Oceanic Engineering.*

Supported by: DARPA grant MDA 972-91-J-1004.

WHOI Contribution No. 8424.

ANALYSIS OF THE IMPACT OF CHANNEL ESTIMATION ERRORS ON THE PERFORMANCE OF A DECISION FEEDBACK EQUALIZER IN FADING MULTIPATH CHANNELS

Milica Stojanovic, John G. Proakis, and Josko Catipovic

A coherent receiver with a decision feedback equalizer (DFE) operating on a Rayleigh fading channel under a suitable adaptive algorithm is considered. In the analysis of a DFE, a common assumption is that the receiver has perfect knowledge of the channel impulse response. However, this is not the case in practice, and for a rapidly fading channel, errors in channel tracking can become significant. We analyze theoretically the impact of these errors on the performance of a multichannel DFE. The expressions obtained for the achievable average MPSK bit error probabilities depend on the estimation error covariance. In order to specify this matrix, we focus on a special case when a Kalman filter is used as an optimal channel estimator. In this case, the probability of bit error can be assessed directly in terms of channel fading model parameters, the most interesting of which is the fading rate. Our results show the penalty imposed by imperfect channel estimation, as well as the fading induced irreducible error rates.

In Press: *IEEE Transactions on Communications.*

Supported by: DARPA grant MDA 972-91-J-1004.

WHOI Contribution No. 8425.

DIRECTIONAL WAVE SPECTRA FROM A SWATH SHIP AT SEA

W. M. Drennan, M. A. Donelan, N. Madsen, K. B. Katsaros, E. A. Terray, and C. N. Flagg

During the Surface Wave Dynamics Experiment (SWADE), the Swath ship *Frederick G. Creed* was equipped with an array of wave staffs for the estimation of wave directional spectra. This paper reports on what are believed to be the first such estimates taken from a ship at sea. An algorithm for removing the effects of the ship motion, including those resulting from the Doppler shifting of observed frequencies, is presented along with some results from the SWADE experiment. A comparison with directional wave spectra taken from a nearby buoy shows the fidelity of the method.

In Press: *Journal of Atmospheric and Oceanic Technology.*

Supported by: ONR grant N00014-88-J-1028; National Water Research Institute grant N00014-89-1785.

WHOI Contribution No. 8426.

CO-POSITIVITY AND THE MINIMIZATION OF QUADRATIC FUNCTIONS WITH NON-NEGATIVITY AND QUADRATIC EQUALITY CONSTRAINTS

James C. Preisig

The problem of finding the minimum value of a quadratic function on a set defined by non-negativity and quadratic equality constraints is analyzed. The difficulty in finding the solution to this problem is primarily due to the fact that the feasible region in non-convex. An algorithm, requiring only strict co-positivity of the Hessian of the quadratic constraint function is developed for finding the minimal value of the quadratic objective function. It is shown that problem of finding this global minima can be mapped into the problem of determining whether or not a particular matrix is co-positive and is therefore NP-complete. A more efficient algorithm for finding solutions which satisfy the Kuhn-Tucker necessary conditions is developed and its convergence behavior is analyzed. This algorithm requires that the Hessians of the quadratic constraint and objective functions be both positive semi-definite and strictly co-positive.

Supported by: DARPA grant N00014-89-J-1489 and ONR grant N00014-90-J-1452.

WHOI Contribution No. 8427.

MULTI-SEASON ACOUSTIC TOMOGRAPHY EXPERIMENT IN THE ARCTIC

Kenneth R. Peal, Subramaniam D. Rajan, and George V. Frisk

Acoustic properties of sea ice are important parameters which affect the propagation of sound both within the ice and in the water column under the ice. These properties are functions of space and time. We present details of a crosshole tomography experiment conducted in the Arctic to estimate two important acoustic parameters (compressional and shear wave speeds) of multi-year sea ice in three dimensions and to monitor their evolution with season. Some preliminary results of the data analysis are also presented.

Published in: *IEEE Oceans '93 Proceedings*, II:41-46, 1993.

Supported by: ONR grant N00014-90-J-1517.

WHOI Contribution No. 8430.

THE DEPENDENCE OF MICROWAVE BACKSCATTER FROM THE SEA ON ILLUMINATED AREA: CORRELATION TIMES AND LENGTHS

William J. Plant, Eugene A. Terray, Robert A. Petitt, Jr., and William C. Keller

During the SAXON-FPN experiment we mounted two CW microwave systems on an elevator on the German Research Platform Nordsee for the purpose of investigating the dependence of microwave backscatter from the sea surface on illuminated area. The two systems operated at X- and Ka-bands (10 and 35 GHz) and collected HH and VV polarized backscattered signals simultaneously. The elevator system allowed us to vary the altitude of the two microwave systems above the sea surface from 7.5 to 27 m, always in the far field of the antennas. Most data were collected at a 45° incidence angle which implied that the Ka-band system illuminated areas from 0.4 to 6.0 m^2 while the X-band system viewed spots between 2.0 and 41.3 m^2. We examined the dependence of the normalized radar cross section (σ_o), its variance, and the bandwidth of the Doppler spectrum on illuminated area. We were unable to detect any dependence of σ_o on area but found a definite decrease in its variance as area increased. At X-band, the variance divided by the square of σ_o, the normalized variance, decreased from values near 12 for small areas to values near 2 for large areas. At Ka-band, corresponding values were 40 and 2. The normalized variance was always slightly larger for HH polarization. By fitting the area dependence of the normalized variance to available theory, we deduce that correlation lengths are on the order of 10 times the microwavelength at both X and Ka-band. Values for the normalized variance of an elementary scattering facet were also inferred and are presented in the paper. From the Doppler bandwidths, we obtained radial velocity spreads over the illuminated areas and found that they agreed well at X and Ka-band. These velocity spreads, which are inversely proportional to the correlation time of the backscatter, increased rapidly with illuminated area for small areas but tended to level off to values of about 0.5 m s^{-1} at large areas. This implies a decorrelation time for large illuminated areas of about 10 ms at X-band and 3 ms at Ka-band but somewhat larger values for small areas. The dependence of the velocity spread was found to be well explained by theory if an intrinsic velocity spread of 0.07 m s^{-1} was used to represent scatterer lifetime effects.

Supported by: ONR grant N00014-89-J-3224.

WHOI Contribution No. 8431.

ANALYSIS OF THE PERFORMANCE OF A DECISION FEEDBACK EQUALIZER IN FADING MULTIPATH CHANNELS IN THE PRESENCE OF CHANNEL ESTIMATION ERRORS

Milica Stojanovic, John G. Proakis, and Josko Catipovic

A coherent receiver with an adaptive decision feedback equalizer (DFE) operating on a Rayleigh fading channel is considered. A common assumption in the analyses of a DFE is that the receiver has perfect knowledge of the channel impulse response. However, for a rapidly fading channel, errors in channel tracking can become significant. We analyze theoretically the impact of these errors on the performance of a multichannel DFE. The expression obtained for the achievable average PSK bit error probability depends on the estimation error covariance. To specify this matrix, we focus on a special case when the Kalman filter is used as an optimal channel estimator. Conveniently, the bit error probability can be assessed directly in terms of the channel fading model parameters, the most interesting of which is the fading rate. Our results show the penalty imposed by imperfect channel estimation, as well as the fading induced irreducible error rates.

Published in: *Proceedings of Conference on Information, Sciences and Systems*, Baltimore, MD, March, :139-144, 1993.

Supported by: DARPA MDA972-91-J-1004.

WHOI Contribution No. 8432.

MICROWAVE BACKSCATTER FROM THE SEA: THE MODULATION OF RECEIVED POWER AND DOPPLER BANDWIDTH BY LONG WAVES

Williams J. Plant, William C. Keller, Eugene A. Terray, and Robert A. Petitt, Jr.

Two CW microwave systems were mounted on an elevator on the German Research Platform NORDSEE during the SAXON-FPN experiment. Here we report on measurements of long wave effects in the power received by these systems and in the Doppler bandwidths recorded from the systems. The two systems operated at X and Ka-band (10 and 35 GHz) and collected HH and VV polarized backscatter signals simultaneously. The elevator system allowed us to vary the altitude of the microwave antennas above the sea surface from 7.5 to 27 m, always in the far field of the antennas. Most data were collected at 45° incidence angle which implied that the Ka-band system illuminated areas from 0.4 to 6.0 m^2 while the X-band system viewed spots between 2.9 and 41.3 m^2. We have attempted to characterize the modulation of both received power and Doppler bandwidth in terms of the standard modulation transfer function (MTF) concept. We find that our measurements of the MTF for received power agree well with previous measurements at X-band but that the phase of the MTF for VV polarization is different from that previously reported for Ka-band at a 60° incidence angle. We show how the amplitude and phase of the MTF as well as the coherence function vary with wind speed, long wave frequency, long wave propagation direction, and antenna height. In the case of the first three parameters, our results agree with previous work except as noted above for Ka-band. The dependence of the MTF on antenna height has not bene investigated previously. Our results show that this dependence is small and well explained by the height variations induced as long waves propagate through the footprint on the surface. When we apply the MTF concept to the Doppler bandwidth, we find that the MTF of the bandwidth is small except at very low wind speeds. In view of the association of this bandwidth with velocities of sub-resolution-scale, or intermediate, waves which are themselves modulated by the long waves, we find these small MTFs associated with Doppler bandwidths to be somewhat surprising. We present a simple model to attempt to draw inferences about the amplitude modulation of intermediate scale waves from our results. We also conclude from the small MTFs for Doppler bandwidths that the assumption of a constant correlation time in theories of synthetic aperture radar imagery of the ocean is well justified.

Supported by: ONR grant N00014-89-J-3224.

WHOI Contribution No. 8433.

SEGMENTATION OF SEAFLOOR SIDESCAN IMAGERY USING MARKOV RANDOM FIELDS AND NEURAL NETWORKS

Min Jiang, W. K. Stewart, and M. Marra

Segmentation of seafloor acoustic imagery is of great importance in a wide range of applications. Although considerable successes have been achieved, a critical issue in this domain is the lack of reliable 2-D image models from which segmentation and related processing can consistently proceed. In this paper we describe a nonparametric algorithm for the segmentation of

seafloor sidescan imagery (SSI) based on a combination of Markov random fields and multiple layer perceptrons (MLP). SSI, which is considerably noisy and textured, is embodied by a hierarchy of Gibbs distributions. Segmentation of SSI is then considered as a maximum *a posteriori* estimation. To obtain better estimates of local likelihood, an MLP is adopted for learning the distribution of observations from training data. Experimental results using data from a Pacific mid-ocean ridge area are demonstrated.

Published in: *Oceans '93*, III:456-461, 1993.

Supported by: ONR grants N00014-90-K-0070 and N00014-90-J-1848.

WHOI Contribution No. 8436.

INDUCTIVE TELEMETRY ON A DEEP OCEAN SURFACE MOORING

Daniel Frye, Alessandro Bocconcelli, Stephen Liberatore, and Edward Hobart

A long term engineering test of ocean data telemetry using inductive coupling is being performed offshore Bermuda as a part of the ONR-sponsored Atlantic Long Term Oceanographic Mooring (ALTOMOOR) program. Inductive modems are general purpose telemetry devices which can be used with standard, plastic-jacketed steel mooring lines to transmit data between instruments in the water column and a receiver in the surface buoy.

The advantage of inductive coupling over electrically connected instrumentation is that expensive and unreliable electro-mechanical cables and terminations are not needed to accomplish real time data telemetry. The modems send and receive data via toroids clamped around the wire which act as single turn transformers. Data telemetered up the wire are sent at a rate of 1200 b/s; commands are sent down the wire at 300 b/s.

In Press: *Proceedings MTS '93*, Long Beach, CA, September 22-24, 1993.

Supported by: ONR grant N00014-90-J-1719.

WHOI Contribution No. 8441.

DISTRIBUTION OF FLUID MUDS ON THE AMAZON CONTINENTAL SHELF

G. C. Kineke and R. W. Sternberg

A comprehensive study of suspended sediment transport on the Amazon shelf was conducted as part of the AmasSeds project (A Multidisciplinary Amazon Shelf SEDiment Study) to understand the link between physical processes and the fate of Amazon River sediment. A small instrumented tripod was used to measure the fluid, flow, and suspended-sediment characteristics throughout the water column on varying time scales (e.g. semidiurnal, fortnightly, seasonal). Dense nearbed suspensions, or fluid muds (suspended sediment concentration $> 10g\ 1^{-1}$), on the order of a few meters in thickness were found on the inner and middle shelf covering an area ranging from ~5,700 km^2 during falling and low river discharge to ~10,000 km^2 during rising and high discharge. Fluid muds generally were observed in the region of bottom salinity fronts and extend across the topset beds to the foreset beds during rising and high discharge. Salinity and temperature anomalies frequently observed in fluid muds imply that the muds often are not the result of erosion and resuspension from the seabed, but the result of trapping processes at the bottom salinity front, and then transport cross-shelf. The vertical structure of fluid mud varies in space and time. Variability close to the river mouth is predominantly fortnightly, related to the location and structure of the salt wedge; on the Open Shelf, the variability appears to be related to seasonal differences in river and sediment discharge and the location of the bottom salinity front. The total suspended sediment inventory on the shelf during the season of high discharge is approximately equal to the annual sediment discharge from the river (1.2×10^9 tons yr^{-1}) and >90% of that inventory is within fluid mud. Suspended sediment out of the shelf system, suspended-sediment transport on the shelf is dominated by fluid mud.

In Press: *Marine Geology.*

Supported by: NSF grant OCE-8813399 and OCE-9115712.

WHOI Contribution No. 8444.

DETERMINATION OF THE HYDRODYNAMIC PARAMETERS OF AN UNDERWATER VEHICLE DURING SMALL SCALE, NONUNIFORM, 1-DIMENSIONAL TRANSLATION

Archie T. Morrison III and Dana R. Yoerger

The hover and tight maneuvering regime of an underwater vehicle is difficult to characterize hydrodynamically. Characterization in a reliable model is necessary for successful control of the vehicle during task performance. A 1-dimensional system identification procedure for this regime is described. The experimental set up is simple and noncritical. The analysis is performed by minimizing the error between the trajectories of the vehicle and several numerical models during a free decay. Minimization is controlled by the

Nelder-Meade simplex algorithm. Agreement with the work of other researchers is strong. The procedure is flexible and may be extended to coupled models with 4 degrees of freedom.

Published in: *IEEE Oceans '93 Proceedings*, II:277-282, 1993.

Supported by: ONR contract N00014-90-J-1912 and NSF grant OCE-8820227.

WHOI Contribution No. 8446.

OPTICAL MEASUREMENTS OF CAPILLARY-GRAVITY WAVE SPECTRA USING A SCANNING LASER SLOPE GAUGE

Erik J. Bock, Tetsu Hara, and Robert J. Martinsen

A description of a new scanning laser slope gauge (SLSG) is given and the preliminary results obtained from laboratory wave tank measurements are presented. The device relies on the measurements of two components of surface slope to compute spatial and temporal lags that are used to estimate the full three-dimensional slope spectrum. The device is capable of resolving frequencies in the range between zero and 31.5 Hertz (in practice up to 63 Hz), and wavelengths in the range between 0.625 and 20 centimeters. The technique makes use of a two-dimensional laser scanner that samples the perimeter of a 10 centimeter square (an unfilled aperture). The laboratory results show mechanically generated waves propagating on both distilled water and a 1 M solution of Triton X-100 in distilled water. Results indicate the device is well suited to measure the full three dimensional spectra of capillary-gravity waves and is capable of providing ground-truthing measurements for the verification of remotely sensed ocean surface features.

Supported by: ONR grant N00014-91-J-1770.

WHOI Contribution No. 8448.

CALIBRATION OF THE BASS ACOUSTIC CURRENT METER WITH CARRAGEENAN AGAR

Archie T. Morrison III, Albert J. Williams 3rd, and Marinna Martini

The BASS current meter can measure currents down to the millimeter per second range. Due to the dependence of zero offset on pressure, determining a sensor referenced velocity requires accurate in situ zeroing of the meter. Previously, flow was restricted during the calibration by placing plastic bags around the acoustic volume. In this paper, bacterial grade and carrageenan agars are used in the laboratory to create a zero flow condition during calibration and are shown to be acoustically transparent. Additionally, the results of open ocean and dockside carrageenan and plastic bag comparisons are presented. Carrageenan is shown to reliably provide a low noise, zero mean flow environment that is largely independent of ambient conditions. The improved zeros make millimeter per second accuracy possible under field conditions.

Published in: *IEEE Oceans '93 Proceedings*, II:143-148, 1993.

Supported by: NSF and ONR through NSF grant OCE-9018623.

WHOI Contribution No. 8449.

A FREE-DRIFTING MEASUREMENT OF MID-WATER MIXING BY AN ACOUSTIC CURRENT METER ARRAY IN NATRE

Albert J. Williams 3rd

A five meter tall array of acoustic travel-time current meters was deployed in the North Atlantic Tracer Release Experiment in May, 1992, to measure shear and internal wave mixing. Preliminary results from a four-day test deployment at the start of the experiment show shear of 2 cm/s over the 5 meter length of the array with much variability.

Published in: *IEEE Oceans '93 Proceedings*, II:131-136, 1993.

Supported by: NSF and ONR through NSF grant OCE-9018623.

WHOI Contribution No. 8453.

DYNAMIC TESTING OF THE AUTONOMOUS BENTHIC EXPLORER

Dana R. Yoerger, Albert M. Bradley, and Barrie Walden

This paper describes results of shallow water dynamic testing of the Autonomous Benthic Explorer (ABE), and AUV designed to perform long-term surveys of the deep see floor. In a typical ABE mission lasting several months to a year, the vehicle will spend most of its time "sleeping" in a low power configuration, but will periodically undock from its mooring, perform a survey along precisely controlled track lines, and redock with its mooring before returning to the sleep mode. Early objectives of our in-water testing of the vehicle were to determine the precise

amount of power consumed by the vehicle during hover and transit, as well as to examine the vehicle's over controllability.

We gathered data in a set of tethered tests, to verify our projections of the vehicle's power consumption and controllability. To determine the vehicle's required propulsive power and to evaluate our propeller design and placements, we examined the steady state power consumption in each axis as a function of thrust. For controllability tests, we examined the longitudinal coupling between pitch and vertical displacement, yaw dynamics at hover and while transiting, and vertical excursions while hovering. Together with our laboratory measurements of various hotel load elements, these data will allow us to accurately project the total power consumption of a given survey profile.

Published in: *Proceedings of the 8th International Symposium on Unmanned Untethered Submersible Technology*, University of New Hampshire, September 27-29, 1993.

Supported by: NSF grant OCE-8820227 and OCE-9216775.

WHOI Contribution No. 8454.

INSTRUMENTATION TO MEASURE ELECTROMAGNETIC FIELDS ON CONTINENTAL SHELVES

R. A. Petitt, Jr., J. H. Filloux, H. H. Moeller, and A. D. Chave

We have constructed a set of instruments designed explicitly for shallow water (up to 1000 m) electromagnetic measurements. These units record (with sixteen bit accuracy on EPROM memory cards) the vector horizontal electric field, the vector variations of the magnetic field, pressure, temperature and two components of tilt at a nominal sample rate of 2 Hz for a month. This could be extended to 10 Hz for short experiments as the sensors are easily capable of operation to this point.

Published in: *IEEE Oceans '93 Proceedings*, I:164-168, 1993.

Supported by: NSF grant EAR-9206820.

WHOI Contribution No. 8457.

FEEDBACK ERROR LEARNING CONTROL OF AN UNDERWATER VEHICLE AND ITS COMPARISON WITH ADAPTIVE SLIDING CONTROL

He Huang and Dana Yoerger

Underwater vehicles are important tools for exploration of the oceans. They are widely used in seafloor survey, sampling, inspection and reconstruction. However, precise control of underwater vehicles is very difficult to realize due to the nonlinearity and uncertainties of the dynamics model of the vehicles. Traditional linear control, which is a well developed control technique, performs poorly on the vehicles because the vehicle dynamics model has to be linearized. Nonlinear control design techniques like adaptive controls have been successfully used on the vehicles. Yet the dynamics structure of vehicles has to be understood beforehand. This paper introduces integration of a neural networks scheme called feedback error learning into the trajectory control of the underwater vehicles. No a priori information about the vehicle is required, the network will gradually learn the inverse dynamics model from error signals feedbacked by a conventional PD controller. It simultaneously controls the motion of the vehicle while it learns. After a movement pattern is learned, the network has the ability to generalize and control a different and fast movement. The performance of the neural network control is compared with adaptive sliding control, and their advantages and disadvantages are discussed.

Published in: *Proceedings of Workshop on Integration Technology for Real-Time Intelligent Control Systems*, October 5-7, Madrid, Spain, :16-1–16-8, 1993.

Supported by: Mitre Corporation N-87331.

WHOI Contribution No. 8466.

DETERMINING SUSPENDED SEDIMENT PARTICLE SIZE INFORMATION FROM ACOUSTICAL AND OPTICAL BACKSCATTER MEASUREMENTS

James F. Lynch, James D. Irish, Christopher R. Sherwood, and Yogesh C. Agrawal

During the winter of 1990-91 an Acoustic BackScatter System (ABSS), five Optical Backscatter Sensors (OBSs) and a Laser *In-Situ* Settling Tube (LISST) were deployed in 90 meters of water off the California coast for three months as part os the Sediment Transport Events on Shelves and Slopes (STRESS) experiment. By looking at sediment transport events with both optical (OBS) and acoustic (ABSS) sensors, one obtains information about the size of the particles transported as well as their concentration. Specifically, we employ two different methods of estimating "average particle size". First, we use vertical scattering intensity profile slopes (acoustical and optical) to infer average particle size using a Rouse profile model of the boundary

layer and a Stokes law fall velocity assumption. Secondly, we use a combination of optics and acoustics to form a multifrequency (two frequency) inverse for the average particle size. These results are compared to independent observations from the LISST instrument, which measure the particle size spectrum *in-situ* using laser diffraction techniques. Rouse profile based inversions for particle size are found to be in good agreement with the LISST results except during periods of transport event initiation, when the Rouse profile is not expected to be valid. The two frequency inverse, which is boundary layer model independent, worked reasonably during all periods, with average particle sizes correlating well with the LISST estimates.

In order to further corroborate the particle size inverses from the acoustical and optical instruments, we also examined size spectra obtained from *in-situ* sediment grab samples and water column samples (suspended sediments), as well as laboratory tank experiments using STRESS sediments. Again, good agreement is noted.

The laboratory tank experiment also allowed us to study the acoustical and optical scattering law characteristics of the STRESS sediments. It is seen that, for optics, using the cross sectional area of an equivalent sphere is a very good first approximation whereas for acoustics, which is most sensitive in the $ka \sim 1$, the particle volume itself is best sensed.

In concluding, we briefly interpret the history of some STRESS transport events in light of the size distribution and other information available. For one of the events "anomalous" suspended particle size distributions are noted, i.e. larger particles are seen suspended before finer ones. Speculative hypotheses for why this signature is observed are presented.

In Press: *Continental Shelf Research.*

Supported by: ONR grant N00014-89-J-1049.

WHOI Contribution No. 8488.

STRUCTURE AND DYNAMICS OF FLUID MUDS OVER THE AMAZON CONTINENTAL SHELF

J. H. Trowbridge and G. C. Kineke

Thick layers of fluid mud occur in strong tidal flows over the inner portion of the Amazon continental shelf, in regions of strong salinity fronts associated with the plume discharged from the Amazon River. Detailed shipboard profile measurements obtained in this region during A Multidisciplinary Amazon Shelf Sediment Study (AMASSEDS) provide an unprecedented opportunity to examine the structure and dynamics of fluid muds under natural conditions. The analysis focuses on flows in which the motion is fully turbulent and suspended sediment dominates the stratification. Under these conditions, a comparison of measurements and one-dimensional model calculations indicates that vertical transport is controlled by suppression of turbulent mixing at gradient Richardson numbers near 1/4. This constraint produces a distinctive vertical structure and leads to an upper bound on the total amount of suspended sediment that may be carried in a turbulent suspension by a tidal flow.

Published in: *Journal of Geophysical Research,* 99(C1):865-875, 1994.

Supported by: NSF grants OCE-8912917 and OCE-9115712 and NSF grant OCE-8813399.

WHOI Contribution No. 8495.

IN SITU MEASUREMENTS OF CAPILLARY-GRAVITY WAVE SPECTRA USING A SCANNING LASER SLOPE GAUGE AND MICROWAVE RADARS

Tetsu Hara, Erik J. Bock, and David Lyzenga

Capillary-gravity wave spectra are measured using a scanning laser slope gauge (SLSG), and simultaneously by X and K-band Doppler radars off the Chemotaxis Dock at the Quissett campus of the Woods Hole Oceanographic Institution at Woods Hole, Massachusetts. Radar cross section and the wavenumber spectra measured using thee SLSG at the Bragg wavenumber are within a few dB of each other, a fact suggesting that Bragg scattering theory is appropriate for the estimate of the radar cross section at intermediate incidence angle in field environment, provided long waves are not too significant. The observed degree of saturation of capillary-gravity waves is in reasonable agreements with the measurements by Jähne and Riemer [1990] obtained from measurements in a large wind-wave flume at intermediate wind speeds, but our data indicate a higher degree of saturation at very low wind speeds. The rate at which the slope-frequency spectrum falls off, however, is much lower in the field than in laboratories - even at moderate winds, suggesting long waves are responsible for a large Doppler shift of capillary-gravity waves. Close examination of combined wavenumber-frequency slope spectra also reveals significant smearing of the spectra in the frequency domain due to long waves. These observations confirm that spatial measurements (wavenumber spectra measurements) are essential for characterizing short capillary-gravity waves since this strong Doppler shift will dramatically change apparent frequency spectra.

In Press: *Journal of Geophysical Research - Oceans.*

Supported by: ONR grant N00014-91-J-1770.

WHOI Contribution No. 8496.

ACOUSTIC CHARACTERIZATION AND DISCRIMINATION OF MARINE ZOOPLANKTON AND TURBULENCE

Timothy Stanton, Peter H. Wiebe, Dezhang Chu, and Louis Goodman

The use of high frequency acoustic scattering techniques has become central to the study of biological and physical oceanography, yet the importance of discriminating between sound scattered by zooplankton and turbulence only recently has been recognized. We have performed laboratory measurements of the acoustic scattering properties of a small patch of turbulence and a 2-cm long decapod shrimp over a frequency range of 300 kHz - 800 kHz. The data were used to emulate echoes that one might expect in the ocean environment. The spectrum of the new turbulence emulated echo was relatively flat which is in contrast to the spectrum of the echo from the individual animals which contained major peaks and nulls. These results indicate the potential for discriminating between large turbulent fields and single animals.

Supported by: ONR grants N00014-89-J-1729 and N00014-93-WX24131.

WHOI Contribution No. 8497.

COOP: COASTAL OCEAN PROCESSES STUDY – INTERDISCIPLINARY APPROACH, NEW TECHOLOGY TO DETERMINE COUPLED BIOLOGICAL, PHYSICAL, GEOLOGICAL PROCESSES AFFECTING LARVAL TRANSPORT ON THE INNER SHELF

Cheryl Ann Butman

In temperate latitudes, most coastal invertebrates living on or in the sediment (i.e., "benthic" organisms), such as clams, worms and snails, spawn their gametes or larvae in the water column where they drift for hours to months before settling back down onto the seafloor, metamorphosing, and assuming an entirely benthic existence. The planktonic larval stage is critical in the life histories and population dynamics of benthic organisms because it is the primary dispersal stage, and thus is responsible for colonizing new habitat or replenishing established populations. Understanding and predicting natural variability in benthic populations is a fundamental problem in biological oceanography and fisheries management, and the extent to which variation in larval settlement may determine population dynamics is one of the least understood aspects of the problem. Studies of it require a highly interdisciplinary approach because larvae are vulnerable to physical transport, changing water properties, predation, competition and patchiness in resources (food, habitat, etc.) while they are in the water column and when they settle onto the seafloor.

The research program focuses on benthic invertebrates which live as adults in sandy, nearshore sediments and whose planktonic larvae disperse for approximately one month across waters of the inner continental shelf as the region roughly from just off the beach to several kilometers offshore, typically depths of less than 30 meters.) The basic hypothesis guiding the research is that planktonic larvae of nearshore dwelling organisms exploit the vertical variation of inner shelf circulation to control their cross-shelf transport. This control is expected to be species-specific, depending on the extent of acceptable adult habitat. Thus, invertebrates confined as adults to the sandy beach-face (because they must return to the beach at the end of their larval period) may exert more active control over their vertical distributions in the water column than larvae of sandy, subtidal species for which their is a broader band of acceptable adult habitat across the inner shelf.

Published in: *Sea Technology*, 35(1):44-49, 1994.

Supported by: NSF grant OCE-9123514.

WHOI Contribution No. 8508.

ESTIMATES OF KINETIC ENERGY DISSIPATION UNDER BREAKING WAVES

E. A. Terray, M. A. Donelan, Y. C. Agrawal, W. M. Drennan, K. K. Kahma, P. A. Hwang, A. J. Williams III, and S. A. Kitaigorodskii

The dissipation of kinetic energy at the surface of natural water bodies has important consequences for many physical and biochemical processes including wave dynamics, gas transfer, mixing of nutrients and pollutants and photosynthetic efficiency of plankton. Much attention has been focussed on the measurement of kinetic energy dissipation in the upper mixed layer but relatively little reliable information is available in the near surface wave zone. Most experimental results are in general agreement with dissipation rates following wall layer theory. Our results clearly indicate a near surface zone of enhanced dissipation - well above that predicted by wall layer theory. Here we provide a scaling law for the

rate of dissipation based on wind and wave parameters, and conclude that the dissipation rate under breaking waves depends on the depth , to varying degrees, in three stages. In the near surface layer - depths of one to ten significant heights - the observed dissipation rate is high and varies rapidly (z^{-2}). At greater depths, this merges into a zone that is in general agreement with wall layer theory (z^{-1}). Very near the surface, within one significant height, the dissipation rate is high and roughly constant.

Supported by: NSF grants OCE-9218711 and OCE-9301440; ONR grant N00014-87-K-0007; Panel for Energy Research and Development and Quest Integrated.

WHOI Contribution No. 8509.

A NOTE ON SEASONAL CYCLES OF TEMPERATURE AND SALINITY IN THE UPPER WATERS OF THE GREENLAND SEA GYRE FROM HISTORICAL DATA

Richard Pawlowicz

Monthly climatologies of temperature and salinity for two regions in the Greenland Sea are created by combining historical archives of hydrographic stations with observations from recent cruises. The first region corresponds to the gyre center, where deep water formation occurs and a large bay forms in the winter ice pack ("*nordbukta*"), and the second region lies directly to the south, in the area usually covered by an ice tongue ("*odden*") in February and March. Surface temperature responds primarily to local surface heat fluxes, consistently warming in the summer to about 4.°C and cooling in the fall to the freezing point. The salinity climatology is affected more by interannual variability; however in July and August surface salinity in both regions decreases drastically, with freshening being more pronounced (and beginning slightly earlier) in the southern region. In the fall, this mixed-layer fresh anomaly is removed, probably by brine rejection due to the local formation of ice and its removal by northerly winds. Eventually ice formation causes the surface waters to overturn and entrain the warmer water below, inhibiting further ice formation. In the gyre center the fresh anomaly is smaller than in the odden region so that ice formation will end there earlier, resulting in the appearance of an ice tongue. Since entrainment of deeper and warmer water is a necessary precursor to mixing deeper than about 100m, this suggests that large areal changes in ice cover may be used as a proxy for identifying the onset of deep convection.

Supported by: ONR grant N00014-92-J-1291.

WHOI Contribution No. 8514.

THERMAL EVOLUTION OF THE GREENLAND SEA GYRE IN 1988-89

R. Pawlowicz, J. F. Lynch, W. B. Owens, P. F. Worcester, W. M. L. Morawitz, and P. J. Sutton

Slice inverses of temperature and heat content from the 1988-89 Greenland Sea Tomography experiment and other observations including standard CTD stations, moored thermistors, surface meteorological variables, and surface ice cover are combined to better understand the thermodynamics of the Greenland Sea Gyre. Thermal evolution of the gyre center seems to divide naturally into three periods: a preconditioning phase (November-January), during which surface salinity is increased by brine rejection from ice formation and by entrainment but in which the mixed-layer deepens only slowly to depth of some 150-200m, a deep mixing phase (February-March) during which the surface mixed-layer deepens rapidly to approximately 1500m in the gyre center purely under the influence of local surface cooling, and a restratification phase during which the products of deep mixing are replaced by Arctic Intermediate Water flowing in from the gyre edges. The onset of the deep mixing phase occurs after ice formation in the gyre center stops, resulting in an area of open water where large heat fluxes can occur. In surrounding regions, including the odden region to the south, ice is still being formed. To the north and west, closer to the steep topography of the continental shelf, the inverse results show significant variability due to advection, and large temperature and heat content fluctuations with a period of about 50 days are seen.

Supported by: ONR grant N00014-92-J-1291.

WHOI Contribution No. 8515.

SOUND SCATTERING BY CYLINDERS OF NONCIRCULAR CROSS SECTION

Daniel T. DiPerna and Timothy K. Stanton

A new method for predicting the farfield scattered pressure due to a plane wave incident upon an infinitely long cylinder of non-circular cross section is presented. The method, referred to herein as the Fourier Matching Method (FMM), involves conformally mapping the exterior and interior of a closed surface to a semi-infinite strip. The resultant formulation is numerically efficient (much more so than the T-Matrix method, for example) and works well for both small and large deviations from a circular cross section, as well as penetrable and impenetrable materials.

Furthermore, the basis functions generated in the calculation can also improve the efficiency of other methods such as the T-Matrix method. Example calculations are presented for elliptic, square, and three-leaf clover cross sections for several types of boundary conditions. In all cases, the results compare extremely well with exact or high frequency asymptotic results.

In Press: *Journal of the Acoustical Society of America.*

Supported by: ONR grant N00014-89-J-1729 and MIT/WHOI Joint Program.

WHOI Contribution No. 8538.

WHAT ACCURACY OF MEASUREMENTS AND CALCULATIONS IS REQUIRED IN UNDERWATER ACOUSTICS: A VIEW FROM A POSITION OF WAVEFIELD PREDICTABILITY

Yu A. Kravtsov and James F. Lynch

The question: "to what accuracy should one calculate acoustic fields in the ocean" is considered from a position of wavefield predictability, based on incomplete information about ocean parameters. The concept "degree of predictability" is introduced in the form of a normalized scalar product (correlation) of observed and computed values. With good matching of observed and computed values the degree of predictability approaches unity, and conversely, it decreases to zero with poor matching.

Three characteristics zones of prediction are singled out in which one can make reliable calculations of: first, the total field including the phase; second, the intensity pattern only; and third, the mean intensity and statistical field characteristics (variance, correlation function) only. The scales of the zones, which are enclosed in one another, are estimated for low frequency sound fields (f = 100 to 500 Hz) in shallow seas. The first one stretches from hundreds of meters to several kilometers; the second, from several kilometers to several dozens of kilometers; and the third zone, until loss of the signal.

We also briefly examine the predictability of various quantities based on the decomposition of the total field into rays and modes. Ray and mode travel times and phases, which are useful data in many applications of ocean acoustics, are of particular interest.

Some examples are given for solutions of underwater acoustic problems for which the concept of predictability order seems to be useful: characterization of ocean regions; the inverse problem solution; detection of random inhomogeneities in the ocean; predictability of pulse forms in shallow seas; estimation of the quality of tomographic inverses; medium efforts in matched field signal processing; etc.

Supported by: ONR grant N00014-91-J-1246.

WHOI Contribution No. 8544.

PARTICLE BIOTURBATION IN MASSACHUSETTS BAY: PRELIMINARY RESULTS USING A NEW DELIBERATE TRACER TECHNIQUE

Robert A. Wheatcroft, Ilhan Olmez, and Francis X. Pink

To better understand temporal and particle size-dependent bioturbation processes, we conducted an *in situ* study of sediment mixing in Massachusetts Bay using a newly developed deliberate tracer technique. Sediments from a 32-m, fine-grained site were collected and the 38-62 ("silt") and 63-125 ("sand") μm fractions isolated. These particle-size fractions were labeled with two different noble metals (Au: silt & Ag: sand) using a thermal diffusion technique. Mixtures of the tracers were spread onto the seafloor surface in April and July 1992 by divers and were tube-cored (3 replicates) ~80 d later in each case. Vertical concentrations of the tracers were measured at μg/g (Ag) and ng/g (Au) levels by instrumental neutron activation analysis. During the spring experiment, Au (silt) was mixed to depths >15 cm and displayed multiple subsurface maxima, whereas Ag (sand) was confined to the upper 5 cm of the bed and showed a near monotonic decrease in concentration with depth. In the fall experiment, the tracers displayed more coherent patterns consisting of local surface minima followed by decreasing concentrations with depth. At least three distinct bioturbation modes are required to explain the tracer data: reverse conveyor-belt transport, head-down deposit feeding or excavation and biodiffusion. A particle caching strategy by an unidentified macrofaunal species(s) in response to the spring phytoplankton bloom is postulated to explain the subsurface peaks in the spring gold profiles, but remains conjectural without better process-level natural history information regarding bioturbation.

Supported by: U.S. Geological Survey

WHOI Contribution No. 8545.

RAY-ACOUSTIC CAUSTIC FORMATION AND TIMING EFFECTS FROM OCEAN SOUND-SPEED RELATIVE CURVATURE

Timothy F. Duda and James B. Bowlin

Using deterministic ray-acoustic modeling of 1000-km propagation in the North Pacific, a depth dependent parameter of ocean sound channels has been found to strongly influence geometrical ray propagation. This parameter is the second vertical derivative of sound speed divided by the square of the first derivative. Ray and wavefront timing and intensity can be influenced within realistic ocean sound channels because of unpredictable wavefront triplications and caustics. These triplications are associated with large values of the parameter at ray turning points. The parameter, a relative curvature, behaves as a random variable because of ocean finestructure, causing the unpredictability. The relative curvature has a higher rms value near the sound-speed minimum for both an internal-wave model and actual data, and is a plausible explanation of poor multipath resolution and identifiability late in North Pacific pulse trains.

Supported by: ONR grant N00014-92-J-1162 and ONT contract N00014-90-C-0098.

WHOI Contribution No. 8546.

VORTEX-INDUCED VIBRATIONS IN A SHARED FLOW: A NEW PREDICTIVE METHOD

M. S. Triantafyllou, M. A. Grosenbaugh, and R. Gopalkrishnan

It is shown that a linear hydrodynamic damping term is an intrinsic feature of the vortex-induced vibrations of slender cylinders in the lock-in regime. The damping coefficient can be directly evaluated from experimental measurements of the force acting on a section of the cylinder forced to move in a uniform flow.

Supported by: ONR grant N00014-92-J-1269.

WHOI Contribution No. 8553.

A MECHANISM FOR THE FORMATION AND MAINTENANCE OF SHORE-OBLIQUE SAND RIDGES ON STORM-DOMINATED CONTINENTAL SHELVES

J. H. Trowbridge

Shore-oblique sand ridges occupy the inner continental shelf in many storm-dominated coastal environments. A mechanism for present-day formation and maintenance of these distinctive geological features follows from a linearized analysis based on a depth-averaged fluid dynamical model. The analysis indicated ridge growth as a result of offshore deflection of storm-driven alongshore flows at the ridge crests, which leads to sediment deposition because the increase in ambient depth slows the flow, and possibly because a cross-shore gradient of wave energy reduces the carrying capacity of the flow. Model computations of topographical perturbations are strikingly similar to the observed sand ridges.

Supported by: SeaGrant Program administered by the National Oceanic and Atmospheric Administration under grant NA90-AA-D-SG480.

WHOI Contribution No. 8574.

DEVELOPMENT OF UNDERWATER ACOUSTIC MODEMS AND NETWORKS

Josko Catipovic, David Brady, and Steven Etchemendy

Recent development in underwater acoustic communications enable digital communication with underwater sensors, vehicles and other instruments, offering novel ocean observational capabilities which may change future oceanographic operations. This article summarizes the current state of the art in underwater acoustic communications and telemetry equipment. Several currently deployed observational systems illustrating the potential of the new technology are presented.

In Press: *Oceanography.*

Supported by: NSF grant OCE-9201191.

WHOI Contribution No. 8585.

AUTONOMOUS OCEANOGRAPHIC SAMPLING NETWORKS

Thomas B. Curtin, James G. Bellingham, Josko Catipovic, and Doug Webb

With current trends, advances in a significant class of ocean science problems will be increasingly platform limited. An approach to this problem is the Autonomous Oceanographic Sampling Network (AOSN). Each network node consists of a base buoy and a selectable number of small Autonomous Underwater Vehicles (AUV's). Network configuration is driven by the science or application addressed. A relevant oceanic volume is defined, based on modeling or data voids. Acceptable gradient error bounds are estimated.

Appropriate sensors, nodal distribution and initial sampling strategy are then determined with allowance for adaptive adjustment. Design is based on many, low-cost, lightweight vehicles with simple, reliable, navigational skills. Implementation capitalizes on state-of-the-art technology and proceeds systematically in a series of well-defined, manageable steps toward progressively more complex scientific questions. Use of an AOSN entails a fundamentally different approach to ocean sampling in which hypothesis testing using interactive experiment design and execution plays a major role.

In Press: *Oceanography.*

Supported by: ARPA contract MDA 972-91-J-1004 and MDA 972-93-1-1019; NSF contract OCE-9201191; ONR contract N00014-93-1-0098 and NOAA support through MIT.

WHOI Contribution No. 8586.

MEASUREMENTS IN THE BOTTOM BOUNDARY LAYER ON THE AMAZON PRODELTA: ANALYSIS OF A SEDIMENTATION EVENT

D. A. Cacchione, D. E. Drake, R. W. Kayen, R. W. Sternberg, G. C. Kineke, and G. B. Tate

An instrumented bottom tripod(GEOPROBE) recorded flow and suspended sediment data in the bottom boundary layer above the lower foresets of the Amazon prodelta in 65 m mean water depth in February, 1990. After about two weeks of operation the apparent seafloor at the tripod site rapidly elevated over a 14 hour period by about 44 cm. This sudden change which was detected by an acoustic altimeter and which caused the loss of signals from the lowermost GEOPROBE current and optical sensors is thought to have been caused by the incursion of a dense bottom layer of fluid mud which migrated downslope from shallower sections of the foresets. The fluid mud migration across the outer part of the foresets, if a repetitive and occasional process in this region, could be a major mechanism for expanded seaward growth of the prodelta. Current velocity profiles are used to estimate shear velocities, u_*, and roughness lengths z_0, during the first two weeks of measurements. The extremely energetic semi-diurnal tidal motion required correction of the estimates of u_* and z_0 for acceleration. Average values of u_* and z_0 for the two week period were 1.7 cm/s and 0.3 cm, respectively. The effects of strong stratification due to flocculated, near-bottom suspended sediment on the estimates of u_* are significant for the lower values of u_* ($u_* <$ about 1 cm/s).

In Press: *Marine Geology.*

Supported by: NSF grant OCE-9115712.

WHOI Contribution No. 8604.

ON ACOUSTIC ESTIMATES OF ZOOPLANKTON BIOMASS

Timothy K. Stanton, Peter H. Wiebe, Dezhang Chu, Mark Benfield, Lori Scanlon, Linda Martin, and Robert L. Eastwood

Acoustic echo sounders have been used relatively successfully for several decades in the detection and possible classification of simple populations (i.e. single size, single species) of fish. One assumption used in these studies is that the energy of the acoustic echo from a school of fish is related to the biomass of the animals via a simple linear regression curve. However, as a result of the natural species diversity within zooplankton aggregations, use of acoustic methods to quantify the populations of zooplankton represents a challenge because the acoustic scattering properties of each gross zooplankton anatomical class are quite unique. As a result, large errors can occur if one relies on a simple regression curve to describe the echo energy/biomass relationship. Because of the great importance of understanding variability of echo levels due to changes in anatomical features of these animals, we embarked on an experimental investigation in which ship-board laboratory measurements of echo levels were made of freshly caught zooplankton. Our results indicate an average variation of a factor of about 19,000 to 1 in the relative echo energy per unit biomass due to animals ranging from fluid-like (salps) to elastic shelled (gastropods).

Supported by: NSF grant OCE-9201264 and ONR grant N00014-89-J-1729.

WHOI Contribution No. 8605.

DEPARTMENT OF BIOLOGY

Joel C. Goldman, Chairman

CROSS REACTIVITY OF FIVE MONOCLONAL ANTIBODIES TO VARIOUS ISOLATES OF *ALEXANDRIUM* FROM THE UNITED STATES, JAPAN, SPAIN AND THAILAND AS DETERMINED BY AN INDIRECT IMMUNOFLUORESCENT METHOD

M. Adachi, Y. Sako, Y. Ishida, D. M. Anderson, M. Kodama, T. Ogata, and B. Reguera

Species within the marine dinoflagellate genus *Alexandrium* have typically been identified on the basis of the morphological features of thecal plates. Some of these features change with environmental conditions or growth stage, and others are very small and difficult to resolve for all but taxonomic experts. It has thus become difficult to distinguish closely related species from each other. Within the genus *Alexandrium*, morphological criteria have been especially inconclusive and controversial.

Antibody M8751-1 was reactive to two strains of *A. tamarense*, one strain of *A. catenella* one strain of *A. fundyense*, one strain of *A. excavatum*. A similar labelling pattern was observed for antibody M22-1, although it did react to a moderate degree (30-50% of cells tested) with *A. tamarense* from Thailand. Antibody MT15-1 was highly reactive to all of the strains tested, including *A. tamarense* from Thailand. In contrast, antibody MT15-2 only labelled the Thai strain of *A. tamarense*. MT15-4 behaved similarly, although it also showed slight positive reactivity (10-30%) with *A. excavatum* and *A. catenella*. Antibody MT15-1 thus has potential to be genus-specific, and possibly to be specific for only the *tamarensis/catenella/fundyense* species complex, though further testing is clearly needed. Antibodies M22-1, M8751-1, MT15-2 and MT15-4 together provide resolution within this species complex, whereas MT15-2 and MT15-4 are highly specific for only *A. tamarense* from Thailand.

These data show clearly that antibodies raised against Japanese strains of *A. tamarense* and *A. catenella* cross react to a significant degree with not only strains of these same species from other countries, but to strains of closely related species as well. They thus have utility as general "tags" or probes for toxic *Alexandrium* species. Furthermore, these immunological results lend support to the contention that *A. tamarense, A. catenella*, and *A. fundyense* should not be separate species, but rather varieties of a single species. Designation of strain or variety names might be better based on biochemical, physiological, or molecular characteristics than on geographic origin or morphology. Antibody reactivity may well provide such a distinction in the future.

Published in: *Nippon Suisan Gakkaishi*, 59:(10)1807, 1993.

Supported by: National Sea Grant College Program Office, Grant No. NA90-AA-D-SG480 (WHOI Sea Grant Project No. R/B-112.

WHOI Contribution No. 8301.

IDENTIFICATION OF HARMFUL ALGAL SPECIES USING MOLECULAR PROBES: AN EMERGING TECHNOLOGY

Donald M. Anderson

A major constraint to research and monitoring programs for marine biotoxins and harmful algae stems from the need to identify and enumerate cells of potentially dangerous species within a mixed plankton assemblage. An alternative to microscope identification is the use of "molecular" probes that bind to proteins, nucleic acids, or other molecules located inside or on the cell surface of the species of interest and that are detected using fluorescence or other visualization techniques. This technology is used extensively by microbiologists to detect pathogenic bacteria, for example, but it is only now being applied to harmful algal species. To date, the most common probes of this type for harmful algae are antibodies (both polyclonal and monoclonal) that bind to cell surface proteins. These are now being used to identify species such as *Aureococcus anophagefferens, Alexandrium tamarense, A. catenella, Gyrodinium aureolum, Gymnodinium nagasakiense, Chatonella marina, C. antiqua*, and *Pseudonitzschia pungens*, and even to distinguish between strains or varieties of single species within these groups. A second type of probe targets nucleic acid sequences inside cells. These target sequences are short segments of DNA or RNA in which particular series of nucleotide bases occur which are unique to the species of interest. Nucleic acid-based probes for harmful algae are not as advanced as is the case for antibodies, but results thus far offer excellent promise with respect to specificity and ease of use. Work has focused on two harmful species complexes – dinoflagellates within the *Alexandrium* genus and diatoms in *Pseudonitzschia*. Short segments of DNA have been synthesized (oligonucleotides) which bind to target sequences of ribosomal RNA (rRNA) or rRNA genes (rDNA) of these two species. The rRNA probes are readily introduced into the cytoplasm of the cells, and are detected using fluorescence. Alternatively, extracted nucleic acids from a culture or from field samples can be immobilized on filters or other solid surfaces and probed.

This paper will review the general concepts of molecular probe development for harmful algae, and will highlight areas where methods have been

applied or where development and refinement are still needed.

Submitted to: *Toxic Marine Phytoplankton.*

Supported by: NSF Grant OCE89-11226, NOAA Office of Sea Grant NA 90-AA-D-SG480.

WHOI Contribution No. 8492.

SUBTIDAL BENTHIC COMMUNITY RESPIRATION & PRODUCTION NEAR THE HEAVILY OILED COAST OF SAUDI ARABIA

Kathryn A. Burns, Manfred G. Ehrhardt, Brian L. Howes and Craig D. Taylor

As part of the NOAA/ROPME/MSRC sponsored assessment of the coast of Saudi Arabia, heavily impacted by the large oil spills of the 1991 Gulf War, we measured benthic community respiration (R) and primary production (P) rates in shallow subtidal basins near heavily oiled coastlines. Study sites were located in zones predicted to be basins of maximum deposition of any oiled sediments likely to wash off the adjacent coast and in reference bays predicted to be clean and unaffected. We measured oxygen exchange using *in situ* benthic respirometers and analyzed petroleum hydrocarbon (PHC) levels in the near surface sediments at five stations. We concentrated our efforts in mud habitats to complement related studies in seagrass habitats. Measured community R rates ranged from a low of 700 $\mu M/m^2$ hr in coarse sand sediments with total organic carbon content (TOC) of only 0.16% of dry wt to the highest rate of 2,184 $\mu M/m^2$ hr in finer mud-sand habitats with 0.39% TOC. All measured rates were in the range of literature values for shallow marine sediments at temperatures of 17 to 19°C. Sediment oil content was 13-540 μ/g dry wt by ultraviolet fluorescence (UVF) analysis and 0.5-103 μ/g by gas chromatography (GC). Benthic P rates, calculated as light minus dark changes in dissolved oxygen, ranged from a low of 1,162 $\mu M/m^2$ hr at the most heavily oiled site to a high of 5,216 $\mu M/m^2$ hr at less oiled sites. While a weak inverse relationship between benthic P and sediment oil content was not significant statistically due to the small number of samples, a significant inverse relationship was found between the ration of production to respiration (P/R) and the total petroleum content of the sediments by UVF. The effect appears to be driven more by differences in production than an effect on respiration which showed little relationship with either oil content or productivity. We conclude that within one year after the oil grounded on the intertidal sands of Saudi Arabia, the levels of oil in subtidal benthic sediments had decreased in most habitats to levels that did not show community stress by our oxygen measurements. Rather, long term damage to benthic subtidal habitats was limited only to enclosed bays adjacent to the most heavily oiled coastlines. Preliminary estimates of yearly P converted to carbon units indicates the shallow mud sediments of the Gulf are at least as productive as most oligotrophic water columns. Since benthic habitats covered by seagrass, algae beds or coral reefs are likely to have even higher production rates, we conclude that benthic processes contribute significantly to the overall carbon flux in the Gulf ecosystem.

In Press: *Effects of Oil Contamination in the Persian Gulf.*

Supported by: NOAA.

WHOI Contribution No. 8344.

MICROBIAL FOOD WEBS IN OCEANIC PLANKTON COMMUNITIES: THE PROTOZOAN LINK

David A. Caron

Oceanic communities typically are areas of low total primary productivity. High solar irradiance and the absence of strong physical forcing result in strong thermal stratification and low nutrient availability. Such oligotrophic oceanic environments are dominated by small phytoplankton species (relative to large species) and large standing stocks of bacteria (relative to total biomass). Because of their small size, these producer assemblages are consumed largely by protozoa. These microbial consumers constitute an important trophic link between small primary and secondary producers and metazoan consumers in oligotrophic environments because their activities "repackage" small prey into particles that can be effectively captured by the metazoa. In contrast, large phytoplankton which often dominate in productive coastal ecosystems can be consumed directly by metazoan zooplankton potentially resulting in relatively short food chains. Based on this reasoning, it is anticipated that the relative importance of the "microbial loop" in the Arabian Sea will differ strongly between monsoonal and non-monsoonal seasons. It is hypothesized that microbial consumers will play a much greater role in total community processes (carbon consumption) during non-monsoonal periods relative to their role during monsoonal periods. These differences should be attributable to changes in the size structure of the phytoplankton assemblage, which in turn should be related to differences in physical forcing between monsoonal and non-monsoonal periods.

Submitted to: U.S.-C.I.S. Workshop on the Biochemical Processes in the Arabian Sea, September 20-26, 1993, Sevastopol, Ukraine.

Supported by: NSF Grants OCE90-0201.

USE OF TRITIATED THYMIDINE (TDR) TO ESTIMATE RATES OF BACTERIVORY: IMPLICATIONS OF LABEL RETENTION AND RELEASE BY BACTERIVORES

David A. Caron, Evelyn J. Lessard, Mary Voytek and Mark R. Dennett

Tritiated thymidine (TdR) has become a common method for the measurement of bacterial productivity. It has also been employed to measure the grazing rates of bacterivorous microorganisms by using labeled bacteria as a tracer to follow the fate of bacterial assemblages. There has been very little work, however, concerning the fate of the radiolabel in bacterivores consuming TdR-labeled bacteria, or the consequences of label retention or release for estimates of grazing rates. We investigated incorporation and retention by cultured protozoa of the ^{3}H in TdR-labeled bacteria during time-course experiments involving bacteria and cultured protozoa. We found, using a uniformly-labeled bacterial population and two species of protozoa, that the ingestion rates of the protozoa were accurately measured by the TdR method during the first 1-2 hr of the experiment. Ingestion was significantly underestimated, however, with incubation periods longer than 2 hr. The retention of the ^{3}H-label in the particulate fraction was considerably less than the gross growth efficiency of the protozoa (based on carbon of biovolume). We conclude that, although TdR is an appropriate tool for these studies, it should be used in relatively short time-course experiments to avoid underestimation of the grazing rate due to release of the label. For experiments lasting longer than the residence time of individual food vacuoles, grazing rates calculated using this method must be assumed to underestimate the actual grazing rates.

In Press: *Marine Microbial Food Webs.*

Supported by: NSF Grants OCE86-00510 and OCE89-01005.

WHOI Contribution No. 8376.

CHARACTERIZATION OF A PERIPLASMIC 3′:5′-CYCLIC NUCLEOTIDE PHOSPHODIESTERASE GENE, *CPDP*, FROM THE MARINE SYMBIOTIC BACTERIUM *VIBRIO FISCHERI* †

Paul V. Dunlap and Sean M. Callahan

Vibrio fischeri, a common marine bacterium, exhibits the unusual attribute of growth on 3′:5′-cAMP (cAMP), apparently through the activity of a 3′:5′-cyclic nucleotide phosphodiesterase (3′:5′-CNP) of exceptionally high activity that is located in the periplasm, a novel cellular location for this enzyme. To gain insight into the physiological function of this enzyme, we cloned the gene (designated *cpdP* encoding it from *V. fischeri* MJ-1. This the first bacterial 3′:5′-CNP gene to be cloned. Sequencing and analysis of the 1.26-kilobase (kb) *cpdP* locus revealed a single open reading frame specifying a protein of 330 amino acid residues, including a 22 amino acid leader peptide. The putative *cpdP* promoter contained a reasonable -10 promoter region (TATTAT) but contained no obvious -35 region; instead a 12-base pair inverted repeat (TTAAATATTTAA) occurred just upstream of this location. A possible rho-independent transcriptional terminator with a calculated free energy of -21.2 kcal-mol^{-1} followed the CpdP protein coding sequence. The predicted subunit MW of 33,636 for the mature CpdP protein (36,087 Da less 2451 Da for the leader peptide) was consistent with the MW of 34,000 estimated by SDS-PAGE. The deduced amino acid sequence of the CpdP protein exhibited 33.6% residue identity with the extracellular 3′:5′-CNP of *Dictyostelium discoideum* and 30.3% identity with the low affinity 3′:5′-CNP (PDE1) of *Saccharomyces cerevisiae*. The residue identities clustered in two regions, residues 100-146 and 238-269, which contained 30 of the 33 amino acids conserved in all three proteins, four of which were histidines. A gene replacement mutant of *V. fischeri* MJ-1 containing a 0.45-kb *Bgl*II deletion within the *cpdP* gene lacked periplasmic 3′:5′-CNP activity and did not grow on cAMP, which confirmed in *V. fischeri* the relationship between *cpdP*, synthesis of the periplasmic 3′:5′- CNP, and growth on cAMP. The mutant exhibited no obvious sensitivity to high extracellular concentrations of cAMP (5 mM and 10 mM), which suggests the enzyme does not play a role in defense against extracellular cAMP.

Published in: *Journal of Bacteriology,* 175(15):4615-4624, 1993.

Supported by: NSF Grant DCB91-04653.

WHOI Contribution No. 8363.

POLYCHLORINATED BIPHENYL CONGENER DISTRIBUTIONS IN WINTER FLOUNDER AS RELATED TO GENDER, SPAWNING SITE, AND CONGENER METABOLISM

Adria E. Elskus, John J. Stegeman, Jay W. Gooch, Dianne E. Black and Richard J. Pruell

Concentrations of 17 polychlorinated biphenyl (PCB) congeners were measured in liver of gonadally mature winter flounder collected from Fox Island and Gaspee Point, RI, and from New Bedford Harbor, MA. These locations represent spawning sites with different degrees and sources of PCB contamination. The results indicate that the PCB concentrations and patterns in these fish reflect those of their spawning grounds, that the content of PCB congeners in winter flounder liver is not influenced by sex or reproductive condition, and that flounder selectivity metabolize PCB congeners with adjacent meta, para-unsubstituted carbon atoms. Based on congener concentrations and 2,3,7,8-tetrachlorodibenzo-p-dioxin equivalency factors, the non-ortho congeners, 77, 162 and 169, contributed more to the potential (mammalian) toxicity of PCB in flounder than more abundant, but less toxic, non-coplanar congeners. PCB concentrations in New Bedford flounder are among the highest measured in fish worldwide.

In Press: *Environmental Science and Technology.*

Supported by: U.S. EPA CR 813155 and the Surdna Foundation.

WHOI Contribution No. 8324.

BIOLOGICAL EFFECTS OF GULF STREAM MEANDERING

Glenn R. Flierl and Cabell S. Davis

A modeling study was conducted to examine the effects of time-dependent mesoscale meandering of a jet on nutrient-phytoplankton-zooplankton (NPZ) dynamics. The jet was represented as a quasi-geostrophic flow using the method of contour dynamics. Two cases for biology were examined: 1) plankton in a mixed layer of fixed depth, and 2) plankton at the base of a mixed layer (i.e., pycnocline) of variable depth. When the mixed layer depth is fixed, nutrient upwelling and dilution of the phytoplankton and zooplankton populations occur along the northward branch of the meander. The additional nutrients and reduced grazing pressure leads to significant enhancement (10-20%) of the phytoplankton production and biomass, while the zooplankton biomass decreases similarly. For plankton on a material surface of variable depth, phytoplankton growth in the pycnocline is increased by the higher light levels encountered during a long-isopycnal upwelling. The nutrients decrease and the zooplankton mass in the pycnocline increases by a small amount downstream of the phytoplankton peak. Although the biological enhancements found are not large, the results suggest that vertical motions resulting from mesoscale oceanographic features such as jet meanders and mid-ocean eddies can be an important source of new nutrients for oceanic plankton production.

Published in: *Journal of Marine Research,* 51:529-560, 1993.

Supported by: ONR Grants N00014-89-J-1358, N00014-92-J-1527, and NSF OCE90-16893.

WHOI Contribution No. 8388.

REGULATION OF CYTOCHROME P4501A1 IN TELEOSTS: SUSTAINED INDUCTION OF CYP1A1 MRNA, PROTEIN, AND CATALYTIC ACTIVITY BY 2,3,7,8-TETRACHLORODIBENZOFURAN IN THE MARINE FISH *STENOTOMUS CHRYSOPS*

Mark E. Hahn and John J. Stegeman

Cytochrome P4501A1 (CYP1A1) is known to play important roles in the activation and detoxification of carcinogens and other toxicants in vertebrate animals, including fish. Although extensively studied in mammalian systems, the regulation of CYP1A forms in other vertebrates is less well understood. We examined the time course and dose-response relationships for induction of CYP1A1 mRNA, protein, and catalytic activity by 2,3,7,8-tetrachlorodibenzofuran (TCDF) in the marine fish *Stenotomus chrysops* (scup). The time course of CYP1A1 induction was determined following a single ip does (10 nmol/kg) of 2,3,7,8-TCDF. Hepatic ethoxyresorufin O-deethylase (EROD) activity and CYP1A1 protein content were increased after one day, reached a maximum after 8 days, and were still elevated 14 days after treatment. CYP1A1 protein content was also strongly induced in heart and gill beginning at two days after treatment and extending through day 14. Hepatic CYP1A1 mRNA was strongly induced by one day after dosing and remained elevated through 14 days. The sustained induction of CYP1A1 mRNA by 2,3,7,8-TCDF contrasts with the transient induction seen previously in fish treated with non-halogenated inducers. Dose-response studies indicated that induction of CYP1A1 mRNA,

protein, and catalytic activity occurred following doses of 2,3,7,8-TCDF as low as 0.4 nmol/kg (120 ng/kg), within the range of whole-body contents of this congener measured in fish from contaminated environments. The estimated dose producing half-maximal CYP1A1 induction in scup was approximately 2-10 nmol/kg, suggesting that the sensitivity of these fish to induction may be as great or greater than that of rats. In contrast to previous results obtained with 3,3',4,4'-TCB and BNF, which appear to inhibit or inactivate CYP1A1 in fish and other vertebrates, there was a good correlation between levels of CYP1A1 mRNA, protein, and catalytic activity achieved following various doses of 2,3,7,8-TCDF. These results illustrate temporal and dose-dependent aspects of CYP1A1 induction in fish that are highly inducer-specific. In additional studies to evaluate structure-activity relationships for CYP1A1 induction by chlorinated dibenzofurans in fish, scup were treated with 2,3,6,8-tetrachlorodibenzofuran (2,3,6,8-TCDF). At 10 or 50 nmol/kg, 2,3,6,8-TCDF was inactive as an inducer of CYP1A1 mRNA, protein, or catalytic activity. Overall, these results indicate that fundamental features of CYP1A1 regulation appear to be conserved in fish and mammals, two widely divergent groups of vertebrates.

Submitted to: *Toxicology and Applied Pharmacology.*

Supported by: Surdna Foundation Postdoctoral Fellowship, NIH Grants ES05479 and ES04220, EPA Grant R817988.

WHOI Contribution No. 8569.

PHOTOAFFINITY LABELING OF THE AH RECEPTOR: PHYLOGENETIC SURVEY OF DIVERSE VERTEBRATE AND INVERTEBRATE SPECIES

Mark E. Hahn, Alan Poland, Edward Glover and John J. Stegeman

The mammalian aromatic hydrocarbon (Ah) receptor is a soluble protein involved in the regulation of gene expression by halogenated aromatic hydrocarbons such as 2,3,7,8-tetrachlorodibenzo-*p*-dioxin (TCDD). Little is known, however, about the presence and properties of this receptor in non-mammalian species. In these studies, we sought evidence for an Ah receptor in the liver or liver-equivalent of diverse species of invertebrate and vertebrate animals. Velocity sedimentation analysis of hepatic cytosol labeled with [^{3}H]TCDD gave equivocal results with three species of marine fish. In subsequent studies, photoaffinity labeling with 2-azido-3-[^{125}I]iodo-7,8-dibromodibenzo-*p*-dioxin was used to identify the Ah receptor. Specific labeling (labeling that could be displaced by an excess of unlabeled ligand) was observed in seven species of teleost and elasmobranch fish, including winter flounder (*Pleuronectes americanus*), killifish (*Fundulus heteroclitus*), scup (*Stenotomus chrysops*), rainbow trout (*Oncorhynchus mykiss*), brown trout (*Salmo trutta*), and dogfish (*Mustelus canis* and *Squalus acanthias*). Specific labeling was also found in cytosolic fractions prepared from PLHC-1 fish hepatoma cells and livers of a turtle (*Chrysemys picta*) and a cetacean, the beluga whale *Delphinapterus leucas*. The fish Ah receptor was sensitive to conditions of tissue preparation; inclusion of proteinase inhibitors in the homogenization buffer stabilized the receptor in some species. There was heterogeneity in the apparent molecular mass of the largest specifically labeled band in each species; these ranged from 105 to 146 kDa, slightly larger on average than mammalian Ah receptors (95-130 kDa). In contrast to the results obtained with teleost and elasmobranch fish, no specifically labeled polypeptides were detectable in cytosol from two agnathan fish species (hagfish *Myxine glutinosa* and sea lamprey *Petromyzon marinus*), the tunicate *Ciona intestinalis*, or any of nine other invertebrate species representing eight classes in four phyla. Overall these results suggest that the Ah receptor evolved at least 450 million years ago, prior to the divergence of bony and cartilaginous fishes. Although the exact relationship between receptor presence and dioxin-responsiveness in these species is uncertain, our data predict that the invertebrate species examined in this study, which appear to lack an Ah receptor protein like that seen in mammals and fish, may be less sensitive than vertebrates to the effects of environmental contaminants that act through this transcriptional regulator.

In Press: *Archives of Biochemistry and Biophysics.*

Supported by: US PHS Grants ES05479, ES06272, ES04220, and ES01886, NCI Center 07175, and the Donaldson Charitable Trust.

WHOI Contribution No. 8478.

FORM AND FEEDING MECHANISM OF A LIVING *PLANCTOSPHAERA PELAGICA* (PHYLUM HEMICHORDATA)

Michael W. Hart, Richard L. Miller, and Laurence P. Madin

We describe aspects of the anatomy and suspension-feeding mechanism of a single *Planctosphaera pelagica* captured from the plankton. This rare larval form, of which the adult is unknown, has not, to our knowledge, been seen alive before. The planctosphaera larva appears to

capture food particles on the upstream side of a band of simple cilia and transports them along convoluted food grooves to the mouth. Although we could not observe cilia directly, the movement of dye streams and food particles and the structure of the ciliated band suggest that particles are probably captured at the ciliated band by the reversal of ciliary beat, as in the pluteus and bipinnaria larvae of echinoderms and the tornaria larva of enteropneust hemichordates. The planctosphaera possesses many prominent mucous glands near the food grooves. This suggests an important role of mucus in the biology of the larva, but we were not able to observe directly any role of mucus in particle capture.

Submitted to: *Marine Biology.*

Supported by: NSF Grant OCE91-15453.

WHOI Contribution No. 8505.

DIMETHYLSULFONIOPROPIONATE IN HAWAIIAN REEF CORALS

Richard W. Hill, John W. H. Dacey, and David A. Krupp

Measures on freshly removed and homogenized polyp tissue indicate that *Montipora verrucosa, Pocillopora damicornis,* and *Porites compressa* contain 100-170 μmol dimethylsulfoniopropionate (DMSP) /mL cellular volume of zooxanthellae. The zooxanthellae of reef corals thus appear to contain relatively high amounts of DMSP, similar to those in free- living dinoflagellates. Direct measures on pieces of coral show that the species studied contain 1-3 mmol DMSP/m^2 of living surface area. DMSP is the principal precursor of dimethylsulfide (DMS), a gas implicated in climate regulation. The levels of DMSP we have measured indicate that releases of DMS from reefs – as during aerial exposure, bleaching events, or other physiological stresses – could potentially be great enough to affect local climate. Our measures indicate also that DMS from zooxanthellae should be investigated as a possible source of off-flavors in polyp-consuming fish or in edible forms like tridacnids that have endogenous zooxanthellae.

Submitted to: *Bulletin of Marine Science.*

Supported by: NSF Grant OCE91-02532, NASA Grants NAGW-2431, NASA NAGW-2783.

WHOI Contribution No. 8468.

AMINO ACID REQUIREMENTS OF TWO HYPERTHERMOPHILIC ARCHAEAL ISOLATES FROM DEEP-SEA VENTS: *DESULFUROCOCCUS* STRAIN SY AND *PYROCOCCUS* STRAIN GB-D

Toshihiro Hoaki, Carl O. Wirsen, Satoshi Hanzawa, Tadashi Maruyama and Holger W. Jannasch

Two sulfur dependent hyperthermophilic archaea, *Desulfurococcus* Strain SY and *Pyrococcus* Strain GB-D, isolated from deep sea hydrothermal vents, utilized free amino acids and peptides from various molecular size fractions of yeast extract. It was found that 11 particular amino acids were essential for growth. Metabolic products were acetate, i-butyrate and i-valerate.

Published in: *Applied and Environmental Microbiology,* 59(2):610-613, 1993.

Supported by: NSF Grants OCE89-22854 and OCE92-00458, ONR Grant N00014-91-J-1751.

WHOI Contribution No. 8197.

MONITORING UNDERWATER AMBIENT SOUND LEVELS FOR MARINE ANIMAL ACOUSTICS

Terrance Howald

A system for monitoring the intensity of underwater ambient sounds is described. This computer-based system measures 1/3-octave bandwidth levels at regular intervals. Data from a field test of this system are presented, and the importance of monitoring the variability of underwater acoustic environments while conducting experiments on the intensity perception of marine mammals is discussed.

Submitted to: *Marine Mammal Science.*

Supported by: ONR Grants N00014-92-J-1843 and N00014-92-J-1816.

WHOI Contribution No. 8481.

THE ECOLOGY OF BUZZARDS BAY: AN ESTUARINE PROFILE

Brian L. Howes and Dale D. Goehringer

Buzzards Bay remains one of the few relatively pristine bays in the metropolitan corridor from Washington to Boston. The Bay and its surrounding marshes and uplands have provided a variety of biotic resources not only to European settlers over the past almost 400 years, but to the

Native Americans who relied on this estuary for thousands of years before them. Today the uplands are divided between 18 communities and while the Bay is still exploited for its biotic resources, its aesthetic and recreational values add to the growing concern to preserve its environmental quality. At the same time, it has become clear that the health of the Buzzards Bay ecosystem, like almost all estuarine systems, is controlled not just by processes within the Bay waters themselves, but by inputs from the surrounding upland as well. Therefore, to properly understand and manage this system, it is important to detail activities and land use patterns within the watershed as well as within the tidal reach of the Bay waters. This combined watershed-bay system is referred to as the Buzzards Bay Ecosystem and is the necessary frame of reference for understanding the biotic structure of the Bay and for managing and conserving its resources.

The purpose of this community profile is to provide an overview of the ecology of the Buzzards Bay ecosystem. It is not intended to represent an all inclusive review of the literature, but instead is an attempt to present key features of the Bay in a readily accessible form and to summarize the dominant ecological processes and parameters which structure the bay environment. Since the current and future environmental health of these types of embayments can be directly influenced by activities within contributing watersheds, understanding the interactions between land and sea is an important component to understanding the ecosystem as a whole. The subjects addressed in this profile, therefore, focus not only on the open bay waters, but also on the ecology of Buzzards Bay within its watershed including management issues and the difficulties in balancing demands for access and development while protecting water quality.

Submitted to: *U. S. Fish and Wildlife Service, National Wetlands Research Center.*

Supported by: U. S. Fish and Wildlife Service, 84110-0269-83.

WHOI Contribution No. 8591.

OXYGEN LOSS FROM *SPARTINA ALTERNIFLORA* AND ITS RELATIONSHIP TO SALT MARSH OXYGEN BALANCE

Brian L. Howes and John M. Teal

Spartina alterniflora has evolved a network of continuous gas spaces (lacunae) for the transport of oxygen from above-ground sources to support aerobic respiration in roots and rhizomes typically growing in anoxic, reducing substrates. Previous study has suggested that oxygen transport in excess of root system respiration may result in a significant loss of oxygen to the rhizosphere where it can play an important role in biogeochemical cycling and influence plant productivity in vegetated salt marsh sediments.

The potential significance of this oxidative pathway was evaluated using laboratory split-chamber experiments to quantify oxygen loss from intact root systems under a wide variety of pre- treatment and incubation conditions including antibiotics to inhibit microbial respiration. The results of previous studies where oxygen transport 1.3 to 2. times higher than respiratory uptake were found when root systems are held in a low oxygen (0-2%) gas phase were confirmed but were not supported by measurements in water. In none of the water phase experiments made under a variety of test conditions was detectable net oxygen loss found from *S. alterniflora* root systems. In contrast, non-respiratory gases (Ar. N2, CH4) were found to be "rhizosphere". It appears that studies employing gas phases to investigate the flux of respiratory gases from roots normally growing in water saturated sediments significantly over-estimate the flux rate due to the removal of physical water-jacket effects. Root system respiration coupled with the slow diffusion of oxygen from lacunae to rhizosphere appear to form the major barrier for oxygen loss. The role of respiration is consistent with the apparent increased potential for root system oxygen loss when respiration was lowered by cooling the root medium or by metabolic poisons. Our results do not conflict with the finding of oxygen loss from individual plant roots or the geochemical evidence from nitrification rates or root oxidative coatings but suggest that the mass amount of oxygen loss from *S. alterniflora* root systems is small relative to the total oxygen balance of vegetated salt marsh sediments.

Submitted to: *Oecologia.*

Supported by: NSF Grants BSR87-17701, BSR85-07356.

WHOI Contribution No. 8386.

PREDATOR-MEDIATED COEXISTENCE OF EPIPHYTIC GRASS SHRIMP THAT COMPETE FOR REFUGES

Tayasu Ichiro, Nanako Shigesada, Hiroshi Mukai and Hal Caswell

If two species in a trophic level compete for the same resource, the inferior one will be excluded from the community (Gause 1934). However, the presence of predator may lead to the coexistence of the prey species, especially if the predator selects

competitively dominant species (Paine, 1966; Dayton, 1971). For instance Paine (1966) showed that removal of the top predator from an intertidal community of marine invertebrates resulted in a decrease in the number of major space-utilizing species. Such an effect is referred to as "predator-mediated coexistence".

Nevertheless, Mukai (1990) reported that several epiphytic grass shrimp coexist in Japanese shallow seas even though they are competing for refuges. These shrimp live on the leaves of eelgrass (*Zostera marina*), which grows on the muddy bottom and provides effective refuges by its complex mechanisms sustaining the coexistence of grass shrimps under predation pressure. Mukai (1990) examined the competitive interaction between *L. acicularis* and *H. geniculatus* in experimental aquaria, both in the presence and absence of a predator. On the basis of that study, this paper presents a mathematical model to explain why the predator enhances the coexistence of the shrimps competing for the same refuge.

Submitted to: *Ecological Modelling.*

Supported by: NSF Grants OCE91-11562, INT91-16334.

WHOI Contribution No. 8450.

GROWTH AND GRAZING RATES OF *PROTOPERIDINIUM HIROBIS* ABÉ, A THECATE HETEROTROPHIC DINOFLAGELLATE

Dean M. Jacobson and Donald M. Anderson

Growth and feeding rates of a laboratory-reared small thecate heterotrophic dinoflagellate, *Protoperidinium hirobis* Abé, grown on the diatom *Leptocylindrus danicus*, were measured in batch cultures. Ingestion rates were determined directly by the enumeration of empty diatom frustules produced by dinoflagellate feeding. Both growth and feeding rates saturated at diatom concentrations of approximately 10^4 cells ml^{-1}, and reached maximum values of 1.7 divisions day^{-1} and 23 diatoms $grazer^{-1}$ day^{-1}, respectively. This rate of cell division is notably high compared to photosynthetic dinoflagellates, which seldom grow faster than 1 division day^{-1}. A maximal clearance rate of 0.5 μl h^{-1} was measured. Mean cell size varied proportionally with food abundance, with food- saturated cells having double the mean volume of food-depleted cells. Timing of cell division and grazing rate patterns were also examined; while mitosis occurred chiefly during the dark period, no diel variations in feeding rate were detected. These rates represent the first direct growth and ingestion measurements to be made for a thecate heterotrophic dinoflagellate. They serve to underscore one function these dinoflagellates perform within the microzooplanktonic food web: that of transforming large diatoms into particles more easily ingested by microzooplankters.

Published in: *Journal of Plankton Research,* 15(7):723-736, 1993.

Supported by: NSF Grants DCB85-20605, OCE89-11226 and NSF Predoc Fellowship.

WHOI Contribution No. 8254.

DIE MIKROBEN DER HEISSEN TIEFSEEQUELLEN

Holger W. Jannasch

In conformance with the general theme of a book on Extremophilic Bacteria (in German, title: "Extremophile - Mikroorganismen in extremen Lebensräumen"), this chapter deals with the typical microorganisms of the hydrothermal vent communities with special reference to their physiological characteristics adaptations to the following environmental factors: low and high temperatures (from 2°- 3°C up to 110°C, *psychrophily* and *hyperthermophily*, hydrostatic pressure (200-400 atm, *barophily*), pH (3.5-8.1, *acido-* and *alkalophily*), oxygen stress (short- and long-term survival of anaerobes in bottom seawater) and high heavy metal concentrations (short- and long-term survival in the presence of Cu, Pb and Zn ions at growth limiting concentrations).

Published in: *Extremophile - Mikroorganismen in ausgefallenen Levensraumen.* K. Hausmann and B. P. Kremer, eds. VCH Publishing Company, Weinheim, :69-86, 1993.

Supported by: NSF Grant OCE93-00458, ONR Grant N00014-91-J-1751.

WHOI Contribution No. 8445.

ISOLATION AND CULTIVATION OF HETEROTROPHIC HYPERTHERMOPHILES FROM DEEP-SEA HYDROTHERMAL VENTS

Holger W. Jannasch, Carl O. Wirsen, Toshihiro Hoaki

Over the last decade a large number of heterotrophic archeaebacteria have been isolated that grow within a temperature range of about 75-110°C. This paper represents a protocol of techniques used for collecting and retrieving samples from deep ocean hydrothermal vents with the aid of the research submersible ALVIN, and for

the subsequent isolation of hyperthermophilic bacteria from these materials. The sample sites were: 11°and 21°N of the East Pacific Rise (depth 2500-2700 m), Guaymas Basin (Gulf of California, depth 2010 m) and 23°and 26°N of the Mid-Atlantic Ridge (depth 3600-3700 m). Since most presently known heterotrophic hyperthermophiles are requiring complex organic media for growth, the composition of free amino acids in years extract, peptone and casamino acids (all Difco) have been analyzed and are presented.

Submitted to: *Archaea: A Laboratory Manual.* F. T. Robb, K. Sowerd, A. A. Place, H. J. Schrier, S. DasSarma and E. Fleischman, eds. Cold Spring Harbor Laboratory Press.

Supported by: NSF Grant OCE92-00458 and ONR Grant N00014-91-J-1751.

WHOI Contribution No. 8265.

LARVAL DISPERSAL VIA ENTRAINMENT INTO HYDROTHERMAL VENT PLUMES

Stacy L. Kim, Lauren S. Mullineaux, and Karl R. Helfrich

One of the most intriguing ecological questions remaining unanswered about hydrothermal vents is how vent organisms disperse and persist. Because vent species are generally endemic and their habitat is patchy and ephemeral on time scales as short as decades, they must disperse frequently, presumably in a planktonic larval stage. We suggest that dispersal occurs not only in near-bottom current, but also several hundred meters above the seafloor, at the level of the laterally spreading hydrothermal plumes. Using a standard buoyant plume model, and observed larval abundances near hydrothermal vents at 9°50′N along the East Pacific Rise, we estimate a mean vertical flux of approximately 100 vent larvae/hr at a single black smoker. Larval abundances were extremely variable near vents, resulting in a range in estimated fluxes of at least an order of magnitude. The suitability of the plume model for these calculations was determined by releasing dyes (fluorescein and rhodamine) as larval mimics into a black smoker plume. The plume model predicted dye fluxes in the plume adequately, given the short averaging times of our measurements and the difficulty of sampling the plume centerline. Our calculations of substantial numbers of vent larvae entrained into the plume support the idea that transport in the lateral plume is an important mechanism of dispersal. Because vertical shear in flows above vents can cause larval dispersal trajectories in the plume to deviate considerably from those along the seafloor, larvae in the plume may access habitats that are unreachable by larvae in near-bottom flows.

Submitted to: *Journal of Geophysical Research.*

Supported by: NSF Grant OCE90-19575.

WHOI Contribution No. 8421.

DIMETHYLSULFIDE PRODUCTION FROM DIMETHYLSULFONIOPROPIONATE BY A MARINE BACTERIUM

Kathleen M. Ledyard and John W. H. Dacey

The processes of dimethylsulfoniopropionate (DMSP) uptake and dimethylsulfide (DMS) production from DMSP were investigated in a marine bacterium isolated from Sargasso Sea water. Uptake of DMSP into the cell preceded cleavage to form DMS< indicating an intracellular or possible periplasmic location for the DMSP lyase. The rate of DMS production accelerated rapidly during the timecourse of DMSP cleavage, independent of cell growth; this increase in rate was suppressed in the presence of 500 μM chloramphenicol, consistent with induction of the DMSP lyase. Additionally, preincubation with acrylic acid, the putative by-product of the cleavage, as well as with DMSP, was found to stimulate the initial rate of DMS production from DMSP. The K_m and V_{max} of DMSP uptake were 192 $\pm$ 50 nM (mean $\pm$ standard error, n=3) and 2.1 $\pm$ 0.6 fmol cell^{-1} hr^{-1}, respectively. The rate of DMS production from DMSP exhibited a concave-upward dependence on extracellular DMSP at low concentrations, but at higher concentrations appeared to follow saturation kinetics. The high half-saturation value observed for DMSP uptake (relative to bulk concentrations in the Sargasso Sea) may reflect small-scale patchiness in the distribution of this compound in seawater.

Submitted to: *Marine Ecology Progress Series.*

Supported by: NASA Grants NGT-50456, NAGW 2783, NAGW 2431, NSF OCE91-02532.

WHOI Contribution No. 8504.

CHARACTERIZATION OF A DMSP-DEGRADING BACTERIAL ISOLATE FROM THE SARGASSO SEA

Kathleen M. Ledyard, Edward F. DeLong and John W. H. Dacey

A bacterium which cleaves dimethylsulfoniopropionate (DMSP) to form dimethylsulfide (DMS) was isolated from surface

Sargasso Sea water by a DMSP enrichment technique. The isolate, here designated LFR, is a Gram-negative, obligately aerobic, rod-shaped, carotenoid- containing bacterium with a DNA G + C content of 70%. Sequencing and comparison of its 16S ribosomal ribonucleic acid (rRNA) with that of known eubacteria revealed highest similarity (91% unrestricted sequence similarity) to *Roseobacter denitrificans* (formerly *Erythrobacter* species strain OCh114), an aerobic, bacteriochlorophyll-containing marine representative of the *α-Proteobacteria*. However, physiological differences between the two bacteria, and the current lack of other characterized close relatives, preclude assignment of strain LFR to the *Roseobacter* genus. Screening of fifteen characterized marine bacteria revealed only one, *Pseudomonas doudoroffii*, capable of degrading DMSP to DMS. Strain LFR is deposited with the American Type Culture Collection (ATCC 51258) and 16S rRNA sequence data are available under GenBank accession number 15345.

Published in: *Archives of Microbiology*, 160:312-318, 1993.

Supported by: NASA, Grants NGT-50456, NAGW2783, NSF Grant OCE91-02532 and the BBS Gift to MIT/WHOI Joint Program.

WHOI Contribution No. 8337.

APPLICATION OF RRNA-BASED PROBES FOR OBSERVING MARINE NANOPLANKTONIC PROTISTS

E. L. Lim, L. A. Amaral, D. A. Caron and E. F. DeLong

The use of small-subunit rRNA-based oligonucleotides as probes for detecting marine nanoplanktonic protists was examined with a ciliate (an *Uronema* sp.), a flagellate (a *Cafeteria* sp.), and mixed assemblages of protists from enrichment cultures and natural seawater samples. Flow cytometry and epifluorescence microscopy analyses demonstrated that hybridizations employing fluorescein-labeled, eukaryote-specific probes intensely stained logarithmically growing protists, whereas these same protist strains in late stations growth were barely detectable. The fluorescence intensity due to probe binding was significantly enhanced by the use of probes end labeled with biotin, which were detected by fluorescein-labeled avidin. The degree of signal amplification ranged from two- to fivefold for cultured protists in both logarithmic and stationary growth phases. Mixed assemblages of heterotrophic protists from enrichment cultures were otherwise undetectable when hybridized with fluorescein-labeled probes were easily visualized by this approach. In the latter samples, hybridization with multiple, biotin-labeled probes was necessary for detection of naturally occurring marine protists by epifluorescence microscopy. The signal amplification obtained with the biotin-avidin system should increase the utility of rRNA-targeted probes for identifying protists and facilitate characterization of the population structure and distribution of protists in aquatic environments.

Published in: *Applied and Environmental Microbiology*, 59(5):1647-1655, 1993.

Supported by: NOAA Sea Grant No. NA90-AA-D-SG480, WHOI Sea Grant Project No. R/B-114-PD, WHOI Education Program, ONR Young Investigator Award N00014-90-J-1917, NSF Grant OCE92-16270.

WHOI Contribution No. 8325.

UPTAKE OF WATERBORNE 3,3',4,4'-TETRACHLOROBIPHENYL AND CYTOCHROME P4501A INDUCTION IN THE FATHEAD MINNOW *PIMEPHALES PROMELAS*

Pirjo Lindstrom-Seppa, Peter J. Korytko, Mark E. Hahn, and John J. Stegeman

Chemical uptake and cytochrome P450 induction were measured in female fathead minnows, *Pimephales promelas*, exposed to water-borne [^{14}C]-3,3',4,4'- tetrachlorobiphenyl (TCB). Four groups of fish were dosed on days 0 and 5, for 24 hours each time, in water with 0, 0.29, 2.9 or 29 mg TCB/kg total fish mass. Between treatments the fish were kept in clean water with normal feeding and light conditions. Liver, ovary and skeletal muscle were collected at 2 hours, on day 5 prior to the second dosing and on day 12. TCB uptake was initially greatest in the liver, but after 5 days TCB concentrations in the ovaries (ca. 5 ug TCB/g wet weight) were similar to or slightly greater than those in the liver (ca. 4 ug/g wet weight). TCB concentrations in muscle were about 10% of the concentration (per gram of tissue) in the liver or ovary. TCB concentrations were similar at 5 days after the first dose and 6 days after the second dose. Immunoblot analysis using monoclonal antibody 1-12-3, specific for CYP1A proteins, showed no detectable CYP1A in liver homogenates of control samples. In treated fish CYP1A content in liver homogenates increased with increasing content of TCB in the liver, to about 5 pmol scup CYP1A equivalents at 1.8 ug TCB/g liver. Between 1.8 and 4 ug/g liver, the CYP1A content increased another 10-fold. Ethoxyresorufin O-deethylase (EROD) activity in liver homogenates also increased with increasing

content of TCB in the liver. At TCB concentrations greater than 1.8 ug TCB/g liver, the catalytic activity was suppressed, consistent with results in other species showing that higher dose of 3,3',4,4'-TCB can inhibit or inactivate CYP1A. Immunohistochemical staining with the anti-scup CYP1A1 monoclonal antibody 1-12-3 showed induction in liver and in multiple extrahepatic organs; analysis with a second anti-scup CYP1A1 MAb (1-71-3) confirmed the induction. The induction was strongly detectable only in fish in the highest dose group at either sampling, and was prominent in the endothelium but weak at best in epithelial cells of each organ. The CYP1A seen in immunoblots of liver homogenates at lower doses was likely due to endothelial cell P450. There was also mild staining indicating CYP1A induction in the embryos hatched from exposed fish. The results provide a foundation for employing CYP1A induction as a marker in fathead minnows, relevant to evaluating chemicals that may be activated or detoxified by CYP1A enzymes.

In Press: *Aquatic Toxicology*

Supported by: Proctor & Gamble, EPA R81-7988, WHOI Education Program, Academy of Finland, Research Council for Environmental Science.

WHOI Contribution No. 8367.

PATTERNS OF OCCURRENCE OF SALPS (*TUNICATA, THALIACEA*) NEAR BERMUDA

L. P. Madin, P. Kremer and S. Hacker

Salps sampled near Bermuda by trawling and SCUBA diving were present in low numerical abundances and constituted only a small fraction of the total zooplankton biomass in August 1989 and March-April, 1990. Occurrence of a total of 16 species at the same site varied between and within the two sampling periods. Several species were found in the surface waters only at particular times of day, suggesting diel vertical migrations on different schedules. The possible role of these migrations in the life history of the salps is discussed.

Submitted to: *Journal of Plankton Research.*

Supported by: NSF Grants OCE88-18503 and OCE88-18502.

WHOI Contribution No. 8510.

IMPLEMENTING *I*-STATE CONFIGURATION MODELS FOR POPULATION DYNAMICS: AN OBJECT-ORIENTED PROGRAMMING APPROACH

Carlo C. Maley and Hal Caswell

Demographic models describe population dynamics in terms of the distribution of individuals among categories (e.g., age or size classes); such models are called *i-state distribution models.* In contrast, *i-state configuration models* describe population dynamics by simulating the birth, development, and eventual death of each individual in the population. Such models (also referred to, less precisely, as *individual-based models*) are necessary when interactions among individuals make the assumption of *i*-state distribution models untenable. The basic components of an *i*-state, configuration model are a set of individuals (each characterized by its *i*-state, an interaction structure, and an environment. Each of these components changes dynamically as a function of the others. The implementation of *i*-state distribution models is familiar; here we present a general framework, based on object-oriented programming (OOP), for the numerical implementation of *i*-state configuration models. The individuals, interaction structure, and environment are all defined as objects. A special object called the simulator transfers information among these objects as needed. The properties of OOP (data protection, inheritance, polymorphism, modularity) lend themselves naturally to *i*-state configuration simulations.

Published in: *Ecological Modelling*, 68:75-89, 1993.

Supported by: Grants OCE89-00231 and DOE DE-FG02-89ER60882.

WHOI Contribution No. 8332.

IN SITU OBSERVATIONS OF FORAGING, FEEDING, AND ESCAPE BEHAVIOR IN THREE ORDERS OF OCEANIC CTENOPHORES: *LOBATA, CESTIDA* AND *BEROIDA*

G. I. Mastumoto and G. R. Harbison

The foraging, feeding, and escape behaviors of members of four genera of oceanic ctenophores were studied by direct observation in the field. Patterns of water movement around these ctenophores were studied using fluorescein dye. *Bolinopsis infundibulum* forages vertically, capturing prey with mucus-covered oral lobes. Species of *Ocyropsis* forage horizontally and produce a reduced wake, due to the extreme

compression of the body and the aboral location of the ctene rows. Prey are trapped by the muscular oral lobes and ingested by the prehensile mouth. In both genera, the auricles are held rigidly, and apparently are used both to reduce the pressure wave as they forage and to startle prey onto the surfaces of the oral lobes. *Cestum veneris* also forages horizontally, but continually reverses direction. Prey startled by the turbulent wake produced in the previous pass are captured by tentilla that stream over the side of the body. All three species of *Beroe* studied swim in a spiral while foraging and produce similar wakes. Prey are ingested by the negative pressure produced by the rapid expansion of the mouth, and with the macrocilia that line the oral portion of the stomodaeum. The escape behavior of species of *Bolinopsis, Ocyropsis*, and *Cestum* appears to function primarily to elude non-visual predators like *Beroe*. Species of *Beroe* bend and swim rapidly during the escape response, and will turn themselves inside-out when repeatedly stimulated. The types of prey captured depend in part on an interplay of foraging and feeding mechanisms.

Submitted to: *Marine Biology.*

Supported by: NSF OCE87-46136, Monterey Bay Aquarium Research Institute and the Woods Hole Oceanographic Institution.

WHOI Contribution No. 8428.

PATTERNS OF GROUNDWATER

Newton P. Millham and Brian L. Howes

The patterns of groundwater flow and discharge in a highly permeable aquifer were investigated relative to determination of nutrient loading to a shallow coastal embayment on Cape Cod, Massachusetts. Both the rate and pattern of groundwater discharge to coastal embayments appears to be very dynamic, being modified by short-term changes in upland hydrologic processes, fluctuations in the hydraulics within the receiving waters, and long term changes due to depositional processes within the tidal basin. The regional and embayment morphology resulting from de-glaciation and subsequent depositional processes within the aquatic system were found to be major factors affecting current patterns of groundwater discharge. Discharge through the embayment bottom based upon measured profiles of interstitial salinity, temperature, and porosity indicated that fine-grained, subtidal sediments (> 1m thick) had low hydraulic conductivities and acted as aquicludes, focusing seepage in the marginal nearshore zone. The hydraulic gradients determining groundwater discharge to embayment waters were coupled to tidal elevations, generating periodic increases or decreases in rates of freshwater inflow. Water table measurements and interstitial salinity profiles indicated that as mean tidal levels increased, groundwater discharge decreased, and conversely at low mean tide levels discharge into the embayment increased. At peak embayment levels the embayment acted like a flow-through lake with groundwater discharging along one shore while saline embayment waters simultaneously infiltrated along the opposite shore. At the same time upland groundwater flow diverged from the embayment, resulting in significant reduction (29%) in the area contributing groundwater to the embayment. Changes in the patterns and rates of groundwater discharge due to seasonal variations in water table elevation or short-term variations in embayment level, underscores the need to integrate upland water table mapping with hydraulic measurements within the zone of discharge in order to determine the input of groundwater and groundwater-borne nutrients to coastal embayments.

Submitted to: *Marine Ecology Progress Series.*

Supported by: NOAA Sea Grant NA86-AA-D-SG090, NA90-AA-D-SG480 and the Town of Falmouth.

WHOI Contribution No. 8406.

FRESHWATER FLOW INTO A COASTAL EMBAYMENT: GROUNDWATER AND SURFACE WATER INPUTS

Newton P. Millham and Brian L. Howes

Groundwater is a principal pathway for transport of dissolved nutrients from terrestrial ecosystems to coastal waters, and in highly permeable aquifers can dominate the freshwater budget. In a two year study, freshwater flow to a shallow coastal embayment was measured by five different methods. Three methods measured water volumes as they move into and out of the embayments: a chloride mass balance of tidal exchange; a volumetric balance of tidal exchange; and a volumetric calculation based upon rates of rise in embayment water levels (inlet blocking). Two upland hydrologic methods measured transfers from the watershed to the embayment: Darcian flow analysis with direct stream discharge measurements, and a water budget. Net freshwater flux from the embayment calculated by the five methods ranged from 4,100 $\pm$700 m^3 d^{-1}, for the Darcian-stream discharge method, to 9,100 $\pm$3,400 m^3 d^{-1}, for the volumetric tidal method. The tidal volumetric approach appeared to inflate freshwater flux during non-uniform tidal conditions. Except for the tidal volumetric method, the approaches yielded similar results, with a mean annual discharge of 4,800 $\pm$670 m^3 d^{-1}.

Groundwater discharge accounted for almost all of total freshwater flow to the embayment, being 54-68% of direct discharge and increasing to >95% of the flux when combined with indirect discharge as streamflow. Daily freshwater discharge varied seasonally from 3,000 $m^3\ d^{-1}$ during low rainfall periods, to 15,000 $m^3\ d^{-1}$ during peak flow periods, the range of discharges is equivalent to 6% and 40% respectively, of the average daily tidal flux in the embayment (37,500 $m^3\ d^{-1}$). The spatial distribution of freshwater discharge was not uniform: 83% of total freshwater discharged to the northern half of the estuary and under maximum flow conditions could lower the salinity by 5 ppt in one day.

Submitted to: *Limnology and Oceanography.*

Supported by: NOAA, Grant NA90-AA-D-SG480.

WHOI Contribution No. 8361.

A COMPARISON OF METHODS TO DETERMINE K IN A SHALLOW COASTAL AQUIFER

Newton P. Millham and Brian L. Howes

Five methods (tidal transmissivity, tracer, slug, permeameter, and grain size) for the determination of hydraulic conductivity (K) were compared in the watershed of a small coastal embayment. Laboratory methods (grain-size and permeameter) were less reliable predictors of K than *in situ* field methods. Permeameters yielded lower K values under all conditions. Grain-size analysis (GSA) using the Hazen method most closely approximated field results obtained by tidal transmissivity, tracer, and slug tests. The equation specific nature of GSA methods indicate that grain-size approaches cannot be used in isolation, in coastal areas but require comparative *in situ* tests other than by permeameters.

Slug test results compared well with tracer test and tidal transmissivity results (mean upland K = 85 m/d). A 7.0 m tracer test measured mean upland K as 109 m/d, and had the best spatial replication (C.V. = 2.0-5.5%). Tidal methods yielded a mean upland K of 106/md over horizontal distances of 30 to 85 m and the full thickness of the aquifer. However, the small tidal signal, large aquifer storativity, shallow wells, and irregular local tidal regime increased the variability of the tidal transmissivity technique, and rendered tidal amplitude method unusable.

Aquifer settings significantly affected the methods selected and the results obtained. Alternations to the aquifer matrix in the zone of discharge affect measured K. All methods indicated lower hydraulic conductivities in near-shore versus upland aquifer areas (nearshore 40-71% of upland eg. slug tests, 30 m/d vs. 71 m/d; GSA, 55 m/d vs. 86 m/d; permeameters, 18 m/d vs. 29 m/d). The systematic decrease in K nearshore to tidal embayments has generally not been addressed, although it is clearly significant to the measurement and modelling of coastal groundwater discharge.

Submitted to: *Ground Water.*

Supported by: NOAA Grants NA90-AA-D-SG480 and NA86-AA-D-SG090 and National Sea Grant College Program Office, Department of Commerce.

WHOI Contribution No. 8336.

PATHOBIOLOGY OF CHEMICAL-ASSOCIATED NEOPLASIA IN FISH

Michael J. Moore and Mark S. Myers

The study of neoplasia in aquatic animals has largely focussed on morphology and epizootiology. Correlations have been sought between prevalences of specific lesion types and significant biological and environmental variables as potential etiological factors. These factors have included age, gender, and exposure to chemical contaminants and infectious agents, as well as predisposing genetic characteristics. Experiments have shown a number of chemicals to be hepatocarcinogens in fish. These include: aflatoxin in rainbow trout, and nitroso-compounds, azo compounds, methylazoxymethanol acetate, polynuclear aromatic hydrocarbons and aromatic amines in trout, medaka, guppy, zebra danio, mangrove rivulus, sheepshead minnow, and top-minnow. Furthermore, the carcinogenicity of extracts derived from chemically contaminated sediments has been demonstrated in the rainbow trout and brown bullhead, and putatively preneoplastic focal hepatic lesions have been induced in English sole by exposure to similar sediment extracts. However, we know less of the significance of PCBs, chlorinated pesticides and other non-geotoxic agents as promoters of the hepatocarcinogenic process in laboratory and feral species of fish. In this context we discuss the mechanisms of chemical carcinogenesis in fish species exposed to environmentally important chemicals, and the application of current and more sophisticated methods to elucidate these mechanisms.

In Press: *Aquatic Toxicology: Molecular, Biochemical, and Cellular Perspectives.* G. Ostrander and D. Malins, eds. CRC Press, Boca Raton.

Supported by: NOAA Grant NA-90-AA-D-SG480.

WHOI Contribution No. 8268.

PERIODIC RESPONSE TO PERIODIC FORCING OF THE DROOP EQUATIONS FOR PHYTOPLANKTON GROWTH

Mercedes Pascual

The dynamics of a phytoplankton population growing in a chemostat under a periodic supply of nutrients is investigated with the model proposed by Droop. This model differs from the well-known Monod equations by incorporating nutrient storage by the cells. In spite of its nonlinearity and the time delays introduced by an internal nutrient pool, the model predicts a simple response to a periodic nutrient supply. The population is shown to oscillate with the same frequency as the forcing. To prove the existence of a periodic solution local and global bifurcation results are used. This work establishes a basis on which to evaluate experimental data against the model as a representation of the nutrient-phytoplankton interaction when nutrients fluctuate.

In Press: *Journal of Mathematical Biology.*

Supported by: NSF Grant OCE89-0231 and ONR Grant N00014-92-J-1527.

WHOI Contribution No. 8502.

TRANSPORT OF JUVENILE GEM CLAMS (*GEMMA GEMMA*) IN A HEADLAND WAKE

Kelly L. Rankin, Lauren S. Mullineaux and W. Rockwell Geyer

Accumulation of bivalve recruits in the bottom convergence at the center of coastal eddies has been suggested as a possible mechanism resulting in locally abundant adult populations. We investigated transport of juvenile gem clams (*Gemma gemma*) in a headland wake to determine whether they accumulated, and where. Velocity measurements during three flood tides showed that a wake consistently formed, but that flow speeds were too slow to transport juvenile clams to the eddy center. Instead, the clams were deposited just inside the wake perimeter, where shear velocities decreased to levels below critical erosion velocities of the clams. This result demonstrated that accumulation in a coastal flow separation can occur even in the absence of a well-defined eddy or a strong bottom convergence. Juvenile gem clams were carried, probably as bedload, to regions in the wake dominated by sediments with similar grain sizes, rather than similar fall velocities, suggesting that bedload transport was particularly dependent on particle diameter in this flow regime. Adult gem clam populations tended to be locally abundant in regions receiving transported juveniles, but clam transport on any specific flood tide was not sufficient to fully predict the adult distributions.

In Press: *Estuaries.*

Supported by: Sea Grant NA90-AA-D-SG48, Project R/B 104; ONR N00014-89-J-1431.

WHOI Contribution No. 8194.

DESCRIPTIVE OCEANOGRAPHY OF THE INDIAN OCEAN

T. S. S. Rao

The subject matter for this book is on the Indian Ocean including its extension up to the Antarctic coast, and examines those processes that control its major features and the life in it. I have attempted to produce a book in which each chapter contributes to the overall theme of describing the multidisciplinary aspects of the Indian Ocean and its adjacent part of the Antarctic (Southern) Ocean.

The history and development of oceanography of the Indian Ocean and its biology are the principal chapters in the book and these two are linked by chapters on geology, hydrography and nutrients, thus presenting a unified picture of this ocean. The book is targeted to a wide range of people, keeping in view that what has been written is understandable to laymen and also of value to specialists world over.

What has fascinated me most, while reviewing the various aspects of the Indian Ocean, is the fact that all basic findings in the different disciplines are closely interlinked and influence one another, thus vindicating the 'Gaia' hypothesis of Lovelock (1979), according to which the physical and chemical conditions of the surface of the earth, of the atmosphere and the oceans has been and is actively made fit by the presence of life itself. Earlier, Alfred Redfield (1958) had come to an almost similar conclusion stating that the chemical composition of the atmosphere and the oceans are biologically controlled. These elegant ideas echo throughout the description of the oceanography of the Indian Ocean.

Supported by: ONR Grant No. N00014-92-J-1517 and the Woods Hole Oceanographic Institution.

WHOI Contribution No. 8482.

HOW FISH POWER SWIMMING

Lawrence C. Rome, Doug Swank and David Corda

It is commonly thought that fish generate the power needed for swimming with their anterior musculature and that the posterior musculature

serves only to transmit forces to the tail and in doing so performs negative work. Detailed muscle mechanics, kinematics, and electromyography on fish swimming with its red muscle show exactly the opposite patterns. By using the new approach of driving isolated muscle bundles through the length changes and stimulation pattern they undergo during steady swimming, we show that most of the power for swimming comes from muscle in the posterior region of the fish and relatively little from the anterior musculature. These experiments also show that there is a significant adaptation in the muscle along the length of the fish which enhances power generation.

Submitted to: *Science.*

Supported by: NIH AR38404, NSF IBN 9205397.

WHOI Contribution No. 8389.

NATURAL HISTORY OF A SOLENGASTER MOLLUSC FROM PAPUA NEW GUINEA, *EPIMENIA AUSTRALIS* (THIELE) (= *DINOMENIA VERRUCOSA* NIERSTRASZ) WITH A REDESCRIPTION OF THE SPECIES (APLACOPHORA, NEOMENIOMORPHA)

Amélie H. Scheltema, Matthew Jebb

Epimenia australis (Thiele) is a large, tropical, shallow-water neomenioid aplacophoran, or solenogaster, of the west Pacific. More than 30 individuals were collected during January and February by diving off Madang, Papua New Guinea, where they occurred in aggregations with their cnidarian prey underneath overturned coral slabs at 15 to 24 m depth in a steeply sloping coral rock area with swift currents. Animals were kept alive for several weeks in large aquaria with running sea water and fed *Scleronephthya.*

Like other species of Epimeniidae, *E. australis* is brightly colored, with iridescent green and blue patches on a reddish-brown background. Madang specimens were up to 11 cm long and 6 mm in width and were in reproductive condition with brooding embryos in the mantle cavity. Some individuals contained embryos in several stages of development. *Epimenia* fed on *Scleronephthya* by clamping onto the soft coral with the hook-shaped radular teeth while sucking in the polyps. They move by ciliary action of the small foot along a mucous strand secreted within the pedal groove; the foot remains within the groove. When not moving, the body can be held rigidly upright. *Epimenia* were active at night but remained hidden during the day, firmly wrapped around each other and the coral rock on which they were found. The anterior end, with its vestibule containing bundles of papillae and with a dorsal protuberance bordered by sensory cirri, was sensitive to touch, and the animals appeared capable of olfaction, able to find their prey and reacting to each other.

The species is redescribed by spicule, radula, and internal morphology. The synonymy of *Dinomenia verrucosa* Nierstrasz is considered.

In Press: *Journal of Natural History.*

Supported by: In part NSF Grant EAR 92 04080.

WHOI Contribution No. 8447.

PASSIVE DISPERSAL OF PLANKTONIC LARVAE: RELEVANCE FOR THE BIOGEOGRAPHY OF CARIBBEAN MOLLUSKS

Rudolf S. Scheltema

Occurrence of teleplanic veliger larvae in major currents of the tropical Atlantic Ocean supports the hypothesis that passive dispersal contributes importantly to the biogeography of molluscan species. Criticisms of the role of passive dispersal as a factor in molluscan biogeography are: (1) that larvae have a fixed life span too short to account for long-distance dispersal: both laboratory and field data show this assertation to be mistaken; (2) that larvae after a time lose their competence to metamorphose: whenever tested teleplanic larvae have been shown to retain their ability to metamorphose; (3) that dispersal is random and cannot explain congruent nonrandom associations among widely differing taxa: dispersal is largely accounted for by advection along major ocean currents which provide quasi-permanent or seasonally reoccurring corridors for the transport of planktonic larvae; therefore various taxa necessarily are dispersed over similar routes, leading to congruent geographic distributions; and (4) that species lacking a planktonic larval stage nevertheless have wide geographic ranges and consequently there is little relationship between mode of reproduction and geographic range of species: those species lacking a planktonic larval stage yet having a wide geographic range are mostly sessile forms that attach to hard substrata, and consequently are preadapted for passive dispersal by rafting.

Geotectonics and sea-floor spreading have been significant in controlling the pattern and extent of passive dispersal by planktonic larvae over geologic time. The closing of the Tethys Seaway during the Oligocene and Early Miocene resulted in the isolation of the southwestern tropical Pacific Ocean from the tropical eastern Atlantic. Similarly the closing of the corridor between North and South America divided the tropical east Pacific from the Caribbean Sea.

Continental drift and sea-floor spreading resulted in the initial formation and subsequent enlargement of the Atlantic Basin and has led subsequently to the "mid-Atlantic barrier" which acts as a filter between the tropical eastern Atlantic Ocean and Caribbean Sea. Both tectonic events and sea-floor spreading have placed important constraints on larval dispersal.

Faunal studies support the hypothesis that both passive dispersal and vicariance events have been important in determining the Carribean molluscan fauna. In particular the amphi-Atlantic and amphi-American geographic distributions illustrate this point. Low endemism of molluscs on oceanic islands suggest that initial colonization must be accomplished largely by teleplanic larvae. The available evidence shows that although no single process can completely explain the present composition of Caribbean molluscan fauna, passive dispersal of planktonic veliger larva must have played important role in colonization and today continues to maintain genetic continuity between widely disjunct regions of the tropical Atlantic Ocean.

In Press: *American Malacological Bulletin.*

Supported by: NSF Grant OCE92-01499 and the Woods Hole Oceanographic Institution.

WHOI Contribution No. 8391.

EXPERIMENTS ON VARIATION IN LENGTH OF PLANKTONIC LIFE AMONG VELIGER LARVAE OF *ILYANASSA OBSOLETA* (GASTROPODA: PROSOBRANCHIATA): DELAY IN METAMORPHOSIS AND THE PROLONGATION OF LARVAL LIFE

Rudolf S. Scheltema and Michael Chin

The interval of time that veliger larvae of *Ilyanassa obsoleta* [= *Nassarius obsoletus*] remain planktonic depends not only upon the ecological conditions under which growth and morphological development occur, but also on the time required to attain competence to metamorphose, and on the ability of larvae to delay metamorphosis until by chance they encounter the appropriate sediment of an intertidal flat. Even among larvae grown under identical laboratory conditions, the time required to attain competence can vary up to 1.5 times. At 22-23°C) some veligers became competent within three weeks; only after *ca.* 35 days were all larvae in the experiments competent when presented with an appropriate cue. When denied such a cue about one-third of all veligers were unable to delay metamorphosis for more than 5 days, but only 5 percent could prolong the duration of their planktonic life beyond 30 days. Variation in the time required to achieve metamorphosis among larvae of the same cohort can vary (between three weeks and >60 days) and results in a widespread dispersion of the post-larval juvenile form. Alternatively, if veligers encounter an appropriate cue, all will settle and metamorphose together. The capacity of *Ilyanassa obsoleta* veligers to delay metamorphosis differs markedly from that of certain opisthobranchs, whose veligers seemingly can delay metamorphosis almost indefinitely (>300 days) when denied their specific cue for metamorphosis.

Supported by: NSF Grants OCE920-1499 and OCE91-00594.

WHOI Contribution No. 8392.

IDENTIFICATION OF GROUP- AND STRAIN-SPECIFIC GENETIC MARKERS FOR GLOBALLY DISTRIBUTED *ALEXANDRIUM* (DINOPHYCEAE) SPECIES. I. RESTRICTION FRAGMENT LENGTH POLYMORPHISMS ANALYSIS OF SMALL-SUBUNIT RIBOSOMAL RNA GENES

Christopher A. Scholin and Donald M. Anderson

Two distinct small-subunit ribosomal RNA genes (SsrDNAs), termed the "A gene" and "B gene," were recently found in the toxic dinoflagellate *Alexandrium fundyense* Balech. A restriction fragment length polymorphism (RFLP) assay was developed to rapidly detect the A and B genetic markers. SsrDNAs from fifty-eight cultures with species designations of *A. tamarense* (Lebour) Balech, *A. catenella* (Whedon et Kofoid) Balech, *A. fundyense, A. affine* (Fukuyo et Inoue) Balech, *A. minutum* Halim, *A. lusitanicum* Balech, and *A. andersoni* Balech were screened. These cultures represent isolates from North America, Western Europe, Thailand, Japan, Australia, and the ballast water of several cargo ships. The RFLP assay revealed five distinct groups among these isolates. Three subdivide the "*A. tamarense/catenella/fundyense* species complex," but do not correlate with morphospecies designations. The fourth group consists of *A. affine* isolates. The fifth group is represented by *A. minutum, A. lusitanicum* and *A. andersoni.*

The B gene was only found in *Alexandrium tamarense, A. catenella* and *A. fundyense,* but not in all members of this closely related group. Thus, there is no strict correlation between the presence of the B sequence and morphospecies designations. The B sequence is not essential for toxin production, but those organisms harboring it are toxic. The B gene is not uniformly distributed among global populations of *Alexandrium.* All *A.*

tamarense, A. catenella and *A. fundyense* isolates from North America harbor this gene, but it has also been found in some *A. tamarense* from scattered locations in Japan, as well as in *A. tamarense* from the ballast waters of one cargo vessel which was on a defined run from Japan to Australia. The B gene may be endemic to North American populations of *A. tamarense, A. catenella* and *A. fundyense*. If so, it is possible that in the recent past North American *A. tamarense* were introduced to Japanese waters, and a subset of these populations subsequently dispersed to Australia. The B sequence may be useful for tracking this particular populations' regional and/or global dispersal.

Isolates which do not harbor the B sequence appear to carry only a single class of small-subunit rRNA genes. However, since the enzymes used in the RFLP assay sample only a small number of bases in the A and B molecules, it is possible that other *Alexandrium* carry "B-like genes" that have not yet been detected. A more thorough search for these molecules is necessary to establish the uniqueness of the B gene and its apparent origin in North America.

Submitted to: *Journal of Phycology.*

Supported by: NSF Grant OCE89-11226 and Ocean Ventures Fund.

WHOI Contribution No. 8258.

IDENTIFICATION OF GROUP- AND STRAIN-SPECIFIC GENETIC MARKERS FOR GLOBALLY DISTRIBUTED *ALEXANDRIUM* (DINOPHYCEAE) SPECIFICS. II. SEQUENCE ANALYSIS OF A FRAGMENT THE LARGE SUBUNIT RIBOSOMAL RNA GENE

Christopher A. Scholin, Michel Herzog, Mitchell Sogin and Donald M. Anderson

A fragment of the large-subunit ribosomal RNA gene (LsrDNA) from the marine dinoflagellates *Alexandrium tamarense* (Lebour) Balech, *A. catenella* (Whedon et Kofoid) Balech, *A. fundyense* Balech, *A. affine* (Fukuyo et Inoue) Balech, *A. minutum* Halim, *A. lusitanicum* Balech and *A. andersoni* Balech have been cloned and sequenced in order to assess the organisms' inter- and intra-specific relationships. Cultures represent isolates from North America, Western Europe, Thailand, Japan, Australia and the ballast water of several cargo vessels, and include both toxic and non-toxic strains. Parsimony analyses revealed eight major classes of sequences, or "ribotypes," indicative of both species- and strain-specific genetic markers. Five ribotypes subdivide members of the "*A. tamarense/catenella/fundyense* species complex," but do not correlate with morphospecies designations, suggesting that morphological features are less specific indicators of these organisms' relationships than are their LsrDNA sequences. However, strains of *A. tamarense/catenella/fundyense* can be indicative of particular regional populations: representatives collected from the same geographic region appear the most similar, regardless of morphotype, whereas those from geographically separated populations are more divergent even when the same morphospecies are compared. Contrary to this general pattern, *A. tamarense* and *A. catenella* from Japan were found to be exceptionally heterogeneous, displaying sequences nearly identical to those of Australian, North American and Western European isolates. This diversity, at least in part, may stem from an introduction of *A. tamarense* to Japan from genetically distinct source populations. The three remaining ribotypes were associated with cultures that clearly differ morphologically from *A. tamarense, A. catenella* or *A. fundyense*; these distinct sequences are typified by: 1) *A. affine*; 2) *A. minutum* and *A. lusitanicum*; and 3) *A. andersoni.* LsrDnas from *A. minutum* and *A. lusitanicum* are indistinguishable, but differ from both *A. andersoni* and *A. affine.* An isolate's ability to produce toxin, or lack thereof, is consistent within LsrDNA phylogenetic terminal taxa. Relationships of selected *Alexandrium* isolates deduced from protein electrophoretic patterns agree with groupings defined by the same isolates' LsrDNA sequences. Some representatives of different *A. tamarense/catenella/fundyense* ribotypes appear capable of interbreeding. Results of the LsrDNA sequence analysis are in complete agreement with conclusions from a previous study using a restriction fragment length polymorphism (RFLP) assay of small-subunit rRNA genes (SsrDNAs), but LsrDNA sequences are finer-scale species and population indicators.

Submitted to: *Journal of Phycology.*

Supported by: NSF Grant OCE89-11226, URA 117, Ocean Ventures Fund.

WHOI Contribution No. 8259.

HYDRODYNAMIC ENHANCEMENT OF INVERTEBRATE LARVAL SETTLEMENT IN MICRODEPOSITIONAL ENVIRONMENTS: COLONIZATION TRAY EXPERIMENTS IN A MUDDY HABITAT

Paul V. R. Snelgrove

To test whether the distribution of settling larvae in muddy habitats is influenced by near-bed

hydrodynamics, colonization trays with different trapping characteristics were deployed flush with the ocean bottom at 20-m depth in Buzzards Bay, Massachusetts. The goal of these experiments was to determine whether different densities of settling larvae would be collected under different hydrodynamic conditions. Before deployment, trays were filled with pre-frozen, muddy sediment collected from the site, and some trays (Flush Trays) were filled so that the sediment surface would be flush with that of the ocean bottom when *in situ*. Other deeper trays (Depression Trays) were filled with a similar volume of sediment so that the sediment surface was approximately 8 cm below that of the surrounding ocean bottom when deployed. This latter treatment created a hydrodynamic regime that would trap passive particles, permitting a test of whether settling larvae at the site would be entrained like passive particles, and thus occur in higher densities in Depression Trays compared with Flush Trays. Experiments were deployed at five different times during the summer of 1990, and were recovered after 3- or 4-d periods depending on the sampling date. Total densities of organisms were higher in Depression Trays compared with Flush Trays on each sampling date, and of the five taxa that were consistently abundant, four were significantly more abundant in Depression Trays (bivalve larvae, gastropod larvae, juvenile *Mediomastus ambiseta* (Hartman) polychaetes, and nemerteans). Juvenile spionid polychaetes were abundant on only one date, and on that date they were significantly more abundant in Depression Trays. The only abundant taxon that was not significantly more abundant in Depression Trays was *Capitella* spp. polychaetes. To determine whether higher numbers in Depression Trays was an active response by settling larvae to elevated organic matter that is often associated with trapping environments such as depressions, some Flush Trays were enriched with *Thalassiosira* sp. on one of the sampling dates. Densities of organisms in *Thalassiosira* Trays were either comparable to or lower than those in Flush Trays, suggesting that higher carbon levels do not necessarily promote larval settlement of dominant colonizers at this site over the time scale of these experiments. Furthermore, some of the organisms that were more abundant in Depression Trays were species that normally occur at the site and might therefore be expected to find Flush Trays a suitable environment in which to settle. The most parsimonious explanation for these results is that larvae were passively entrained in Depression Trays, suggesting that near-bed hydrodynamics may, at least in part, determine where larvae settle. These field experiments complement earlier flume studies suggesting that the microdepositional environment of small depressions may result in passive entrainment of settling larvae, indicating that hydrodynamic, as well as behavioral, factors may determine where larvae in muddy habitats initially settle.

In Press: *Journal of Experimental Marine Biology and Ecology.*

Supported by: NSF Grant OCE88-12651, ONR Grant N00014-89-J-1637 and NSERC of Canada.

WHOI Contribution No. 8271.

POTENTIAL FLOW ARTIFACTS ASSOCIATED WITH BENTHIC EXPERIMENTAL GEAR: DEEP-SEA MUDBOX EXAMPLES

Paul V. R. Snelgrove, Cheryl Ann Butman and J. Frederick Grassle

In response to the growing recognition of the potential effects of near-bed hydrodynamics on various benthic processes, flume studies were conducted to document fine-scale flow patterns over several types of mudboxes that have been used to estimate colonization rates of deep-sea organisms. Mudboxes are typically filled with natural sediments or sediment treatments and placed in the field to observe how timing, larval supply and sediment composition may affect larval settlement rates. This study specifically addresses potential hydrodynamic biases of mudbox structures as obstructions to the near-bed flow. Detailed velocity profiles were made over two types of "free vehicle" mudboxes that could be deployed and recovered from a surface vessel. One of these ("Old Free Vehicle") was not designed with specific regard for potential hydrodynamic biases whereas the other ("New Free Vehicle") was designed specifically to minimize flow disturbances and maintain a realistic boundary-layer flow over the mudbox sediments. Flume velocity profiles also were made over two smaller mudboxes designed to be deployed by a submersible, one ("Flush Sediment Tray") which was specifically designed to be placed with the ocean bottom, thus minimizing flow disturbance, and another ("Single Tray Mudbox") which was not. Flume simulations indicated that the Old Free Vehicle and the Single Tray Mudbox cause considerable disturbance to the near-bed flow regime; flows over the mudbox sediment surface differed markedly from those predicted for the natural seabed and those observed over the flume bed in the absence of the mudboxes. Flow accelerations, growing secondary boundary layers and eddy formation were observed over these mudbox sediments, and vertical velocity profiles varied considerably in the along-channel direction. The alternative mudbox designs (New Free Vehicle and Flush Sediment Tray) were largely successful in reducing or eliminating these

flow artifacts. Boundary-layer flow over both the New Free Vehicle and the Flush Sediment Tray was much more uniform, and velocity profiles over the sediment surface were very similar to those in the empty flume channel and those predicted for a natural deep-sea habitat. In addition, there was no evidence of eddy formation and other major flow disturbances. These flume studies underscore the benefit of considering potential hydrodynamic effects in designing benthic experimental sampling gear. Careful designs that include hydrodynamic considerations can reduce potential flow disturbances that may bias data collections and confound data interpretation.

Submitted to: *Journal of Marine Research.*

Supported by: Natural Sciences and Engineering Research Council of Canada (NSERC) Postgraduate Scholarship, WHOI Ocean Ventures Award, NSF Grants OCE88-1651 and OCE92-16114, ONR Grant N00014-89-J-1637.

WHOI Contribution No. 8607.

MACROFAUNAL RESPONSE TO ARTIFICIAL ENRICHMENTS AND DEPRESSIONS IN A DEEP-SEA HABITAT

Paul V. R. Snelgrove, J. F. Grassle and R. F. Petrecca

To test whether small-scale patches of food and disturbance contribute to the unexpectedly high macrofaunal diversity of the deep sea, and evaluate the relative importance of active habitat selection for different patches of food and disturbance versus passive deposition of colonizing fauna, sediment tray and artificial depression colonization experiments were conducted on the deep-sea floor at 900-m depth, south of St. Croix, U.S. Virgin Islands. Trays and depressions were unenriched (Unenriched Controls) or enriched with either *Thalassiosira* sp. or *Sargassum* sp. Concurrent deployment of different types of enrichment and disturbance made it possible to evaluate whether macrofauna specialize on these patches. Depressions create a hydrodynamic regime that traps passive particles, allowing tests of the relative importance of active selection of different patch types versus passive deposition for abundant colonizers. By specializing on different patch types, organisms may avoid species interactions that might lead to competitive exclusion, thus contributing to deep-sea diversity. After 23 d, total densities and densities of the four abundant colonizers (*Capitella* spp., *Nereimyra* sp., *Cumella* sp. and *Nebalia* sp.) were extremely high in enriched trays, despite relatively low ambient densities. Densities in Unenriched Control Trays were very low, and did not attain ambient densities. After 24 d, total densities in all depression treatments were considerably lower than in enriched tray treatments, and only *Sargassum* Depression densities exceeded those in the ambient environment. Lower densities of organisms in depression treatments compared with trays, and the different densities observed in different depression treatments suggest that the dominant colonizers were highly active and selective and were not passively entrained in depressions. Analysis of samples indicted that faunas in trays and depressions were very different, and *Sargassum* Depression fauna was very different from other depression types. A strong difference was not observed between fauna in ambient sediments and *Thalassiosira* sp. or Unenriched Control Depressions, perhaps because *Thalassiosira* was dropped in depressions on the sediment surface and may have been more readily available to consumers and more rapidly consumed than in trays. Hurlbert rarefaction indicated that *Thalassiosira* Trays were colonized by a lower diversity fauna than *Sargassum* Trays, and Unenriched Control Trays were colonized by very low densities of a fauna that was comparable in diversity to ambient fauna and natural depressions, which were highly diverse. These experiments suggest that fauna may respond quickly and selectively to artificial food patches and disturbance, and this fauna is different from that observed in the ambient sediment. Thus, a patch mosaic may be part of the reason for the species richness of the deep sea. The different, highly diverse, fauna observed in natural depressions compared with flat ambient sediment suggests that natural analogs of these experiments may indeed contribute to high deep-sea diversity.

In Press: *Journal of Marine Research.*

Supported by: NOAA Grant NA88-AA-H-UR020, NSF Grant OCE88-12651, WHOI Ocean Ventures Fund Award, Natural Sciences and Engineering Research Council of Canada (NSERC).

WHOI Contribution No. 8327.

BIOCHEMISTRY AND MOLECULAR BIOLOGY OF MONOOXYGENASES: CURRENT DIRECTIONS IN FORMS, FUNCTIONS, AND REGULATION OF CYTOCHROME P450 IN AQUATIC SPECIES

J. J. Stegeman and M. E. Hahn

This chapter presents a review of the monooxygenase systems of aquatic animals, focusing on the cytochrome P450-dependent monooxygenases. Topics covered include the

diversity of P450 forms and their functions in aquatic species, their role in the toxicity and carcinogenesis of environmental contaminants, the regulation of P450 forms by endogenous and exogenous factors, isolated cell systems for studying P450 regulation and function, the use of P450 induction as a biomarker of environmental contamination, and evolution of P450 forms and their regulatory mechanisms.

In Press: *Aquatic Toxicology: Molecular, Biochemical and Cellular Perspectives.* G. Ostrander and D. Malin, eds. CRC Press, Boca Raton.

Supported by: EPA R81-7988, USPHS ES-04220, ES-06272, Stanley Watson Chair.

WHOI Contribution No. 8366.

AUTOMATED INSTRUMENTATION FOR TIME SERIES MEASUREMENT OF PRIMARY PRODUCTION AND NUTRIENT STATUS IN PRODUCTION PLATFORM-ACCESSIBLE ENVIRONMENTS

Craig D. Taylor, Brian L. Howes, and Kenneth W. Doherty

A major limitation to the assessment of the temporal and spatial variability of key ecological parameters is the ability to perform complex biological and chemical procedures autonomously *in situ*. We present new instrumentation for the automated *in situ* measurement of photosynthesis and other microbial processes, and for assessment of micro-nutrient pools in coastal and oceanic environments. High resolution time series studies of photosynthesis using a Submersible Incubation Device (SID) indicates that the standard sampling interval commonly employed in coastal and oceanic studies can lead to significant errors in the determination of the temporal patterns of photosynthesis, and quantification of integrated measures of production expressed on a seasonal or annual basis. Clearly, methodologies are needed which allow for the higher frequency measurements required to adequately quantify this key ecological parameter. In addition, SID technology was found to avoid both potential handling artifacts of standard techniques. Since photosynthesis rates must often be interpreted in context with the nutrient regime of the environment, an autonomous *in situ* Continuous Flow Chemical Analyzer (*in situ*-CFA) has been developed for parallel deployment with the SID. Both SID and *in situ*-CFA instruments, when incorporated into regional arrays of automated moorings that are supported by off-shore platform research programs, should greatly facilitate the gathering of data essential to our understanding of the meso-scale processes controlling biological systems in the coastal and oceanic environment.

Published in: *Marine Technology Society Journal,* 27(2):32-44, 1993.

Supported by: NOAA, Sea Grants NA86-AA-D-SG090, R/B-95-PD and R/P-34; NA90-AA-D-SG480, R/P-38, DOE Grant DE-FG02-92ER61426 and NSF Grants DPP-9118363, Amendment No. 01 and OCE-9000112.

WHOI Contribution No. 8353.

GRAZING RATES FOR THREE LIFE HISTORY STAGES OF THE DOLIOLID *DOLIOLETTA GEGENBAURI* ULJANIN (TUNICATA, THALIACEA)

Christopher M. Tebeau and Laurence P. Madin

Grazing rates for *Dolioletta gegenbauri* averaged 2.5 ml zooid^{-1} for trophozooids, 2.7 for phorozooids, and 5.8 for gonozooids. Average *in situ* rates were higher than laboratory rates by a factor of 2-3.

Submitted to: *Journal of Plankton Research.*

Supported by: NSF Grant OCE91-15453, Arthur Vining Dans SSF.

WHOI Contribution No. 8506.

UNUSUAL WHALE SOUND TRACKED BY NAVY SOSUS

William A. Watkins, Mary Ann Daher, Joseph George, Velma Ronquille, and Amy Stanley

Series of distinctive whale-like signals were analyzed and tracked for 59 days from 7 December 1992 through 3 February 1993 in the northeast Pacific with the help of the U.S. Navy underwater Sound Surveillance System (SOSUS) at NAVFAC Whidbey Island, WA. The signals had tonal components, with a primary mode averaging 51.75 Hz and a secondary mode at 69 Hz. Each signal (primary mode) exhibited a downward frequency sweep of about 2 Hz. These signals occurred in small groups of two to six per group, and groups of signals were produced at variable rates in long bouts of 1 to 19 hours or more per day. During this period, signal bouts varied without obvious pattern from day to day, but a slight increase in signal bouts was noted during the night. The signal source was tracked at 0.1 to 0.6 kts (0.05 to 0.30 m/sec) during periods of travel in an area about 210 miles long. These signals did not exactly match the acoustic features of finback whale sounds, but the resemblances in behavior

suggest either a variation of this species or a similar species as the source.

Submitted to: *Journal of Acoustical Society of America.*

Supported by: Woods Hole Oceanographic Institution.

WHOI Contribution No. 8517.

NITROGEN INCORPORATION INTO DECOMPOSING LITTER OF *SPARTINA ALTERNIFLORA*

David S. White and Brian L. Howes

Most of the above ground production of the dominant salt marsh grass *Spartina alterniflora* is not directly consumed by herbivores but enters a detrital food web. As *Spartina* litter decomposes, both the concentration and absolute amount of nitrogen increase due to incorporation from external sources. In this study we used the stable isotope ^{15}N to fractionate the total N pool of *Spartina alterniflora* into N originally incorporated during plant growth and that incorporated from external sources during decay. Comparison of decomposition of litter bag material incubated for 18 mo and a cohort of intact culms followed for 12 mo showed similar patterns of nitrogen and organic matter (as total organic carbon) loss typical of north temperature marshes. Both the original ^{15}N and total N pools declined through the fall but stabilized during the winter. With the onset of warmer temperatures in the spring, the original ^{15}N pool declined again but the total detrital nitrogen pool remained stable due to significant incorporation of nitrogen from external sources. It appears that 50-65% of the total detrital nitrogen pool at the mid-point in decomposition was incorporated from external sources and that at least part of this incorporation was biologically mediated. The apparent incorporation of external N based on ^{15}N techniques in this study is greater than previous estimates based on net N accumulation. We conclude that external nitrogen incorporation into decaying *Spartina alterniflora* is potentially a much more important mechanism of short term nitrogen retention in salt marsh ecosystems than previously thought.

In Press: *Limnology and Oceanography.*

Supported by: NSF Grants BSR85-07356, BSR87-17701 and Island Foundation.

WHOI Contribution No. 8272.

LONG-TERM ^{15}N-NITROGEN RETENTION IN THE VEGETATED SEDIMENTS OF A NEW ENGLAND SALT MARSH

David S. White and Brian L. Howes

^{15}N was used to directly quantify the amount, timing and mechanisms of annual N retention and loss in the short *Spartina alterniflora* (Loisel.) areas of a New England salt marsh. Transformations and loss of ^{15}N were monitored in the field for 7 years and in the laboratory for a single growing season. An initial rapid loss of about 25% of the ^{15}N was attributable to nitrification and denitrification at a daily rate of 25.2 mg N m^{-2} d^{-1}. Plant uptake and assimilation into biomass appeared to reduce further denitrification losses. There was a continual but declining loss of label from years 2-7 as the plant-associated ^{15}N became increasingly sequestered in the belowground dead organic N pool. About 40% of the injected label remained after 7 growing season.

The annual N budget for the short *Spartina* marsh shows a loss of 7.3-7.6 g N m^{-2} y^{-1} based on ^{15}N losses and estimates of the actively cycling total N pool. Removal through death and transport of particulate and dissolved organic N (2.1-3.3 g N m^{-2} y^{-1} and denitrification (4.0-5.5 g N m^{-2} y^{-1}) account for 28-45% and 53-75% of the total annual N loss respectively. Loss of N through uptake into live biomass and eventual burial in dead belowground organic matter was 3.7-4.1 g N m^{-2} y^{-1} similar estimates of 4.4 g N m^{-2} y^{-1} determined from direct accretion measurements. Recycling through remineralization following death and decay of belowground biomass (14.9-16.3 g N m^{-2} y^{-1}) was the major pathway in sediment N cycle equivalent to 62-73% of the annual plant demand. Annual N losses were balanced by inputs, primarily N_2 fixation in this marsh. It appears that long term N retention within *Spartina alterniflora* sediments is controlled primarily by the competition between the plants and bacterial nitrifiers-denitrifers, and secondarily by the relative incorporation into above versus belowground biomass.

Submitted to: *Limnology and Oceanography.*

Supported by: NSF Grants BSR85-18263, BSR85-07356 and the Island Foundation.

WHOI Contribution No. 8547.

TRANSLOCATION, REMINERALIZATION AND TURNOVER OF NITROGEN IN ROOTS AND RHIZOMES OF *SPARTINA ALTERNIFLORA*

David S. White and Brian L. Howes

We used ^{15}N-labelled *Spartina alterniflora* in field and laboratory studies to determine the rate of turnover and annual production of belowground biomass in Great Sippewissett Marsh, MA. Litter bag studies of root and rhizome decay indicated that 80% of the original plant (^{15}N-labelled) N was lost after 3 years with the remaining 20% being buried in the dead organic matter. In laboratory lysimeters 37% of the aboveground ^{15}N pool was translocated to belowground biomass from July through October. In the field study, ^{15}N was lost steadily from the live belowground biomass pool over a 7 year period, yielding a turnover time of 1.6 years. Since the ^{15}N in the live belowground biomass in the field at any point in time is an integration of decompositional losses and recycling through translocation and remineralization of label, when corrected for these two processes, the calculated turnover time of roots and rhizomes in the field was 1.0-1.1 years. When applied to peak belowground biomass estimates, these turnover times yielded estimates of belowground production ranging from 929-1022 g C m^{-2} yr^{-1} similar to estimates of belowground production from harvest and CO_2 budget techniques for the short *Spartina* areas of this marsh.

Submitted to: *American Journal of Botany.*

Supported by: BSR84-18268, BSR85-07356, BSR87-17701, and the Island Foundation

WHOI Contribution No. 8592.

CATALYTIC AND IMMUNOCHEMICAL CHARACTERIZATION OF HEPATIC MICROSOMAL CYTOCHROMES P450 IN BELUGA WHALE (*DELPHINAPTERUS LEUCAS*)

Renee D. White, Mark E. Hahn, W. Lyle Lockhart and John J. Stegeman

The content of native cytochrome P450 in hepatic microsomes of beluga whale (*Delphinapterus leucas*) from the Canadian arctic averaged 0.203 and 0.319 nmol/mg microsomal protein, cytochrome b5 content averaged 0.199 and 0.236 nmol/mg, and rates of NADPH- cytochrome c reductase were 79 and 76 nmol/min/mg, for females and males respectively. Ethoxyresorufin O-deethylase (EROD), pentoxyresorufin O-dependentylase (PROD), and benzo(a)pyrene (BP) hydroxylase (AHH) activities were significantly greater in males than in females, and were highly correlated with one another (r^2 between 0.853 and 0.912). HPLC analysis of *in vitro* BP metabolites revealed benzo-ring (7,8- and 9,10-) dihydrodiols, consistent with activation of this compound, as well as 4,5-dihydrodiol, 3-OH, 7-OH and 9-OH- BP and 1,6- and 3,6-quinones. Estradiol 2-hydroxylase activity did not differ between sexes, and rates did not correlate with those of the other activities. Antibodies against scup P450B (an apparent teleost CYP2B) and rat CYP2B1 did not recognize proteins in beluga liver microsomes, but there was a protein detected by antibodies to BP-inducible rabbit CYP2B4. Antibodies to ethanol and ketone-inducible rat CYP2E1 reacted with two proteins in beluga liver microsomes. Antibodies specific to hydrocarbon-inducible CYP1A1 and/or CYP1A2 forms showed a single protein band, apparently more closely related to CYP1A1. The content of CYP1A was five-fold greater in male than in female beluga. CYP1A content also correlated with EROD, PROD, and AHH activities, suggesting that this P450 form is a primary catalyst for these reactions in beluga. CYP1A content and activity were highly correlated with the concentrations in blubber of non-*ortho* and mono-*ortho* PCB congeners, compounds that induce CYP1A in other mammals. These results indicate that a CYP1A is a catalyst for the metabolism of aromatic hydrocarbon pollutants in the beluga whale, and strongly suggest that this protein is induced in these organisms by environmental contaminants, including PCBs. The function and evolutionary relationships of beluga proteins immunologically related to other P450 forms are uncertain.

In Press: *Toxicology and Applied Pharmacology.*

Supported by: NIH Grants ES-04220 and ES-05479; EPA Grant R817988; Stanley W. Watson Chair; WHOI Education Program.

WHOI Contribution No. 8461.

THE USE OF HIGH FREQUENCY ACOUSTICS IN THE STUDY OF ZOOPLANKTON SPATIAL AND TEMPORAL PATTERNS

Peter H. Wiebe and Charles H. Greene

Knowledge of the three-dimensional spatial structure of zooplankton populations and the change in this structure through time is fundamental to studies of plankton community dynamics. Although conceptual models portraying the time/space scales of plankton pattern and variability exist, data sets required to test their relationship to reality are lacking. High frequency

acoustical systems (100 kHz to 1MHz) are capable of simultaneously resolving individual zooplankton and mapping substantial ocean volumes. This approach provides investigators with new tools for investigating the processes controlling zooplankton distribution and abundance. The versatility of bioacoustical systems is exemplified by the variety of deployment modes already in existence, including use on submersibles, remotely operated vehicles, towed-bodies, net systems, moorings, and buoys. The processing and interpretation of bioacoustical data requires substantial development. Theoretical models of volume backscattering from zooplankton and visualization of three-dimensional data sets are needed. A fundamental limitation in existing system is the inability to discriminate and identify species which prevents the quantification of community composition.

In Press: *Proceedings NIPR Symposium on Polar Biology*, 7:134-158, 1994.

Supported by: NSF Grant OCE90-12150, NOAA Grant NA16RC0515, ONR Grant N00014-89-J-1729, ONR Subcontract 16460-5104.

WHOI Contribution No. 8334.

LONG RANGE NEEDS FOR DEEP-SEA PLATFORMS: THE DEEP-SEA OBSERVATORY CONCEPT

Peter H. Wiebe, David D. Moran, Robert Knox, Charles B. Miller and John A. McGowan

The international community of oceanographers and ocean engineers has faced an historical deficiency in long time-series data for all oceanographic and environmental variables in all sea states. Most measurements have been confined to short time-series data collection in the deep ocean during calm to moderate sea conditions by deployment of conventional oceanographic research ships. To a lesser extent, longer time-series have been obtained from moored or drifting autonomous instruments measuring selected (usually physical or optical) variables. A solution to this deficiency is to deploy a complete oceanographic Deep-Sea Observatory designed into a large mobile ocean platform with small water-plane area displacement. This Deep-Sea Observatory would be designed to maintain station at sea for periods in excess of five years with logistics and scientific resupply accomplished through the technologies developed during the last decade by the offshore ocean industry. The scientific suite consists of fixed core laboratory facilities and state-of-the-art scientific equipment. Additional specific purpose containerized laboratories would be transported from a companion shore-based laboratory complex. Personnel, scientific packages, and supplies are all transportable through conventional means while the Deep-Sea Observatory remains on a fixed point sea station. Platforms of this design will provide fundamental information about the structure and dynamics of open ocean ecosystems far from land and will enable greatly improved ground-truth information about the state of the ocean environment.

Published in: *Marine Technology Society Journal*, 27(2):24-31, 1993.

WHOI Contribution No. 8335.

P450 INDUCTION AND HISTOPATHOLOGY IN PRE-EMERGENT PINK SALMON FROM OILED STREAMS IN PRINCE WILLIAM SOUND, ALASKA

Michael Wiedmer, Mark J. Fink, John J. Stegeman, Roxanna Smolowitz, Gary D. Marty and David E. Hinton

After the March 1989 EXXON VALDEZ oil spill, cytochrome P450IA induction and histopathologic lesions were analyzed in pre-emergent pink salmon (*Oncorhynchus gorbuscha*) naturally exposed to oil contaminated stream sediments. Egg and alevin samples were collected from four oiled and five control sites in Prince William Sound, Alaska, between December 1989 and May 1991. Immunohistochemical staining for cytochrome P45IA was increased in alevins from 13 of 16 oiled sites, but was not increased in all seven samples from the control sites. Cytochrome P450IA induction was not detected in egg samples from either oiled or control sites. Persistent P450IA staining through the end of the study was evidence for persistent chronic exposure to hydrocarbon contamination. Histopathologic lesions were more frequent in alevins from oiled sites, but the differences were not statistically significant, and lesion occurrence seemed to be dependent on stage of development. These results provide evidence that pink salmon alevins in some heavily oiled streams were exposed to hydrocarbons more than two years after the initial spill, and that the hydrocarbons induced detectable physiological changes.

Submitted to: *Fisheries Bulletin.*

Supported by: State of Alaska.

WHOI Contribution No. 8600.

SUBJECT HEADING INDEX
Department of Biology
1993

ANIMAL BEHAVIOR

G. I. Mastumoto and G. R. Harbison B-11
Amélie H. Scheltema, Matthew Jebb B-15
Rudolf S. Scheltema and Michael Chin B-16
William A. Watkins, Mary Ann Daher, Joseph George, Velma Ronquille and Amy Stanley B-20

BENTHIC ECOLOGY

Tayasu Ichiro, Nanako Shigesada, Hiroshi Mukai and Hal Caswell B-7
Rudolf S. Scheltema and Michael Chin B-16
Paul V. R. Snelgrove, Cheryl Ann Butman and J. Frederick Grassle B-18
Paul V. R. Snelgrove, J. F. Grassle and R. F. Petrecca B-19

BENTHOS

Kathryn A. Burns, Manfred G. Ehrhardt, Brian L. Howes and Craig D. Taylor B-2
Brian L. Howes and Dale D. Goehringer B-6
Stacy L. Kim, Lauren S. Mullineaux and Karl R. Helfrich B-9
T. S. S. Rao B-14
Paul V. R. Snelgrove B-18
Paul V. R. Snelgrove, Cheryl Ann Butman and J. Frederick Grassle B-18
Paul V. R. Snelgrove, J. F. Grassle and R. F. Petrecca B-19

BIOACOUSTICS

Terrance Howald B-6
Pirjo Lindstrom-Seppa, Peter J. Korytko, Mark E. Hahn and John J. Stegeman B-10
William A. Watkins, Mary Ann Daher, Joseph George, Velma Ronquille and Amy Stanley B-20
Peter H. Wiebe and Charles H. Greene B-22

BIOCHEMISTRY

Kathryn A. Burns, Manfred G. Ehrhardt, Brian L. Howes and Craig D. Taylor B-2
Adria A. Elskus, John J. Stegeman, Jay W. Gooch, Dianne E. Black and Richard J. Pruell B-4
Mark E. Hahn and John J. Stegeman B-4
Mark E. Hahn, Alan Poland, Edward Glover and John J. Stegeman B-5
Holger W. Jannasch B-8
Kathleen M. Ledyard and John W. H. Dacey B-9
Newton P. Millham and Brian L. Howes B-12
J. J. Stegeman and M. E. Hahn B-20
Renee D. White, Mark E. Hahn, W. Lyle Lockhart and John J. Stegeman B-22
Michael Wiedmer, Mark J. Fink, John J. Stegeman, Roxanna Smolowitz, Gary D. Marty and David E. Hinton B-23

BIOGEOCHEMISTRY

Paul V. Dunlap and Sean M. Callahan B-3
Richard W. Hill, John W. H. Dacey and David A. Krupp B-6

Brian L. Howes and John M. Teal B-7
Newton P. Millham and Brian L. Howes B-13
J. J. Stegeman and M. E. Hahn B-20
David S. White and Brian L. Howes B-22
David S. White and Brian L. Howes B-22
David S. White and Brian L. Howes B-22

BIOGEOGRAPHY

M. Adachi, Y. Sako, Y. Ishida, D. M. Anderson, M. Kodama, T. Ogata and B. Reguera B-1
Kathryn A. Burns, Manfred G. Ehrhardt, Brian L. Howes and Craig D. Taylor B-2
Glenn R. Flierl and Cabell S. Davis B-4
T. S. S. Rao B-14
Rudolf S. Scheltema B-15
Christopher A. Scholin and Donald M. Anderson B-16
Christopher A. Scholin, Michel Herzog, Mitchell Sogin and Donald M. Anderson B-17
Peter H. Wiebe, David D. Moran, Robert Knox, Charles B. Miller and John A. McGowan B-23

BIOLOGICAL/CHEMICAL/PHYSICAL INTERACTIONS

Kathryn A. Burns, Manfred G. Ehrhardt, Brian L. Howes and Craig D. Taylor B-2
Glenn R. Flierl and Cabell S. Davis B-4
M. E. Hahn and J. J. Stegeman B-20
Mark E. Hahn, Alan Poland, Edward Glover and John J. Stegeman B-5
Richard W. Hill, John W. H. Dacey and David A. Krupp B-6
Brian L. Howes and Dale D. Goehringer B-6
Stacy L. Kim, Lauren S. Mullineaux and Karl R. Helfrich B-9
Pirjo Lindstrom-Seppa, Peter J. Korytko, Mark E. Hahn and John J. Stegeman B-10
T. S. S. Rao B-14
Paul V. R. Snelgrove, Cheryl Ann Butman and J. Frederick Grassle B-18
J. J. Stegeman and M. E. Hahn B-20
Craig D. Taylor, Brian L. Howes and Kenneth W. Doherty B-20
Peter H. Wiebe and Charles H. Greene B-22
Peter H. Wiebe, David D. Moran, Robert Knox, Charles B. Miller and John A. McGowan B-23

BIOTECHNOLOGY

M. Adachi, Y. Sako, Y. Ishida, D. M. Anderson, M. Kodama, T. Ogata and B. Reguera B-1
Donald M. Anderson B-1
Paul V. Dunlap and Sean M. Callahan B-3
Holger W. Jannasch, Carl O. Wirsen and Toshihiro Hoaki B-8
E. L. Lim, L. A. Amaral, D. A. Caron and E. F. DeLong B-10
Christopher A. Scholin and Donald M. Anderson B-16
Christopher A. Scholin, Michel Herzog, Mitchell Sogin and Donald M. Anderson B-17
Michael Wiedmer, Mark J. Fink, John J. Stegeman, Roxanna Smolowitz, Gary D. Marty and David E. Hinton B-23

COMMUNITY ECOLOGY

Tayasu Ichiro, Nanako Shigesada, Hiroshi Mukai and Hal Caswell B-7
Paul V. R. Snelgrove B-18
Paul V. R. Snelgrove, Cheryl Ann Butman and J. Frederick Grassle B-18

Paul V. R. Snelgrove, J. F. Grassle and R. F. Petrecca B-19
Peter H. Wiebe, David D. Moran, Robert Knox, Charles B. Miller and John A. McGowan B-23

DESCRIPTIVE/FUNCTIONAL/MORPHOLOGY

Lawrence C. Rome, Douglas Swank and David Corda B-14
Amélie H. Scheltema and Matthew Jebb B-15

ECOSYSTEM STUDIES

Glenn R. Flierl and Cabell S. Davis B-4
Brian L. Howes and Dale D. Goehringer B-6
Brian L. Howes and John M. Teal B-7
Dean M. Jacobson and Donald M. Anderson B-8
Newton P. Millham and Brian L. Howes B-12
Newton P. Millham and Brian L. Howes B-13
Newton P. Millham and Brian L. Howes B-13
Christopher A. Scholin and Donald M. Anderson B-16
David S. White and Brian L. Howes B-21
David S. White and Brian L. Howes B-22
David S. White and Brian L. Howes B-22
Peter H. Wiebe, David D. Moran, Robert Knox, Charles B. Miller and John A. McGowan B-23

EVOLUTION

Mark E. Hahn, Alan Poland, Edward Glover and John J. Stegeman B-5
J. J. Stegeman and M. E. Hahn B-20

FISHERIES

Adria A. Elskus, John J. Stegeman, Jay W. Gooch, Dianne E. Black and Richard J. Pruell B-4
Brian L. Howes and Dale D. Goehringer B-6

FISHES

Mark E. Hahn and John J. Stegeman B-4
Mark E. Hahn, Alan Poland, Edward Glover and John J. Stegeman B-5
Pirjo Lindstrom-Seppa, Peter J. Korytko, Mark E. Hahn and John J. Stegeman B-10
Michael J. Moore and Mark S. Myers B-13
Lawrence C. Rome, Douglas Swank and David Corda B-14
J. J. Stegeman and M. E. Hahn B-20
Michael Wiedmer, Mark J. Fink, John J. Stegeman, Roxanna Smolowitz, Gary D. Marty and David E. Hinton B-23

GENETICS

Paul V. Dunlap and Sean M. Callahan B-3
Christopher A. Scholin and Donald M. Anderson B-16

INSTRUMENTATION

Paul V. R. Snelgrove, Cheryl Ann Butman and J. Frederick Grassle B-18
Craig D. Taylor, Brian L. Howes and Kenneth W. Doherty B-20
Peter H. Wiebe and Charles H. Greene B-22

LARVAL ECOLOGY

Stacy L. Kim, Lauren S. Mullineaux and Karl R. Helfrich B-9
Rudolf S. Scheltema B-15
Rudolf S. Scheltema and Michael Chin B-16
Paul V. R. Snelgrove B-18
Paul V. R. Snelgrove, Cheryl Ann Butman and J. Frederick Grassle B-18
Paul V. R. Snelgrove, J. F. Grassle and R. F. Petrecca B-19

LIFE HISTORY

Rudolf S. Scheltema and Michael Chin B-16

MARINE MAMMALS

Mark E. Hahn, Alan Poland, Edward Glover and John J. Stegeman B-5
Terrance Howald B-6
J. J. Stegeman and M. E. Hahn B-20
William A. Watkins, Mary Ann Daher, Joseph George, Velma Ronquille and Amy Stanley B-20
Renee D. White, Mark E. Hahn, W. Lyle Lockhart and John J. Stegeman B-22

MARINE POLLUTION

Kathryn A. Burns, Manfred G. Ehrhardt, Brian L. Howes and Craig D. Taylor B-2
Adria A. Elskus, John J. Stegeman, Jay W. Gooch, Dianne E. Black and Richard J. Pruell B-4
Mark E. Hahn and John J. Stegeman B-4
Mark E. Hahn, Alan Poland, Edward Glover and John J. Stegeman B-5
Brian L. Howes and Dale D. Goehringer B-6
Pirjo Lindstrom-Seppa, Peter J. Korytko, Mark E. Hahn and John J. Stegeman B-10
Newton P. Millham and Brian L. Howes B-12
Newton P. Millham and Brian L. Howes B-13
Michael J. Moore and Mark S. Myers B-13
J. J. Stegeman and M. E. Hahn B-20
Michael Wiedmer, Mark J. Fink, John J. Stegeman, Roxanna Smolowitz, Gary D. Marty and David E. Hinton B-23
Renee D. White, Mark E. Hahn, W. Lyle Lockhart and John J. Stegeman B-22

MATHEMATICAL ECOLOGY

Glenn R. Flierl and Cabell S. Davis B-4
Tayasu Ichiro, Nanako Shigesada, Hiroshi Mukai and Hal Caswell B-7
Carlo C. Maley and Hal Caswell B-11
Mercedes Pascual B-14

MICROBIAL ECOLOGY

David A. Caron, Evelyn J. Lessard, Mary Voytek and Mark R. Dennett B-3
Paul V. Dunlap and Sean M. Callahan B-3
Toshihiro Hoaki, Carl O. Wirsen, Satoshi Hanzawa, Tadashi Maruyama and Holger W. Jannasch B-6
Holger W. Jannasch B-8
Kathleen M. Ledyard and John W. H. Dacey B-9
Kathleen M. Ledyard, Edward F. DeLong and John W. H. Dacey B-9
E. L. Lim, L. A. Amaral, D. A. Caron and E. F. DeLong B-10
Craig D. Taylor, Brian L. Howes and Kenneth W. Doherty B-20

David S. White and Brian L. Howes B-21
David S. White and Brian L. Howes B-22

MICROBIOLOGY

David A. Caron, Evelyn J. Lessard, Mary Voytek and Mark R. Dennett B-3
Paul V. Dunlap and Sean M. Callahan B-3
Toshihiro Hoaki, Carl O. Wirsen, Satoshi Hanzawa, Tadashi Maruyama and Holger W. Jannasch B-6
Holger W. Jannasch B-8
Holger W. Jannasch, Carl O. Wirsen and Toshihiro Hoaki B-8
Kathleen M. Ledyard and John W. H. Dacey B-9
Kathleen M. Ledyard, Edward F. DeLong and John W. H. Dacey B-9
E. L. Lim, L. A. Amaral, D. A. Caron and E. F. DeLong B-10

MODELLING

Glenn R. Flierl and Cabell S. Davis B-4
Stacy L. Kim, Lauren S. Mullineaux and Karl R. Helfrich B-9
Carlo C. Maley and Hal Caswell B-11

MOLECULAR BIOLOGY

Donald M. Anderson B-1
Paul V. Dunlap and Sean M. Callahan B-3
Mark E. Hahn and John J. Stegeman B-4
Mark E. Hahn, Alan Poland, Ed Glover and John J. Stegeman B-5
Kathleen M. Ledyard, Edward F. DeLong and John W. H. Dacey B-9
E. L. Lim, L. A. Amaral, D. A. Caron and E. F. DeLong B-10
Michael J. Moore and Mark S. Myers B-13
Christopher A. Scholin and Donald M. Anderson B-16
Christopher A. Scholin, Michel Herzog, Mitchell Sogin and Donald M. Anderson B-17
J. J. Stegeman and M. E. Hahn B-20

PATHOLOGY

Pirjo Lindstrom-Seppa, Peter J. Korytko, Mark E. Hahn and John J. Stegeman B-10
Michael J. Moore and Mark S. Myers B-13

PHYSIOLOGY

Paul V. Dunlap and Sean M. Callahan B-3
Brian L. Howes and J. M. Teal B-7
Lawrence C. Rome, Douglas Swank and David Corda B-14

PHYTOPLANKTON

M. Adachi, Y. Sako, Y. Ishida, D. M. Anderson, M. Kodama, T. Ogata and B. Reguera B-1
Donald M. Anderson B-1
Glenn R. Flierl and Cabell S. Davis B-4
Mercedes Pascual B-14
T. S. S. Rao B-14
Christopher A. Scholin and Donald M. Anderson B-16
Christopher A. Scholin, Michel Herzog, Mitchell Sogin and Donald M. Anderson B-17

PHYTOPLANKTON ECOLOGY

Donald M. Anderson B-1
Glenn R. Flierl and Cabell S. Davis B-4
Dean M. Jacobson and Donald M. Anderson B-8
Mercedes Pascual B-14
T. S. S Rao B-14
Christopher A. Scholin, Michel Herzog, Mitchell Sogin and Donald M. Anderson B-17
Craig D. Taylor, Brian L. Howes and Kenneth W. Doherty B-20

POPULATION ECOLOGY

Tayasu Ichiro, Nanako Shigesada, Hiroshi Mukai and Hal Caswell B-7
Carlo C. Maley and Hal Caswell B-11
Mercedes Pascual B-14
Christopher A. Scholin and Donald M. Anderson B-16
Paul V. R. Snelgrove B-18
Paul V. R. Snelgrove, Cheryl Ann Butman and J. Frederick Grassle B-18
Paul V. R. Snelgrove, J. F. Grassle and R. F. Petrecca B-19

RECRUITMENT

Stacy L. Kim, Lauren S. Mullineaux and Karl R. Helfrich B-9
Rudolf S. Scheltema and Michael Chin B-16
Paul V. R. Snelgrove B-18
Paul V. R. Snelgrove, Cheryl Ann Butman and J. Frederick Grassle B-19
Michael Wiedmer, Mark J. Fink, John J. Stegeman, Roxanna Smolowitz, Gary D. Marty and David E. Hinton B-23

REMOTE SENSING

Peter H. Wiebe and Charles H. Greene B-22

SYSTEMATICS

Amélie H. Scheltema and Michael Jebb B-15
Christopher A. Scholin and Donald M. Anderson B-16
Christopher A. Scholin, Michel Herzog, Mitchell Sogin and Donald M. Anderson B-17

TAXONOMY

M. Adachi, Y. Sako, Y. Ishida, D. M. Anderson, M. Kodama, T. Ogata and B. Reguera B-1
Amélie H. Scheltema and Michael Jebb B-15
Christopher A. Scholin and Donald M. Anderson B-16
Paul V. R. Snelgrove, J. F. Grassle and R. F. Petrecca B-19

TOXICOLOGY

Adria A. Elskus, John J. Stegeman, Jay W. Gooch, Dianne E. Black and Richard J. Pruell B-4
Mark E. Hahn and John J. Stegeman B-4
Mark E. Hahn, Alan Poland, Edward Glover and John J. Stegeman B-5
Pirjo Lindstrom-Seppa, Peter J. Korytko, Mark E. Hahn and John J. Stegeman B-10
Michael J. Moore and Mark S. Myers B-13
Christopher A. Scholin, Michel Herzog, Mitchell Sogin and Donald M. Anderson B-17
J. J. Stegeman and M. E. Hahn B-20

Michael Wiedmer, Mark J. Fink, John J. Stegeman, Roxanna Smolowitz, Gary D. Marty and David E. Hinton B-23

ZOOPLANKTON

Glenn R. Flierl and Cabell S. Davis B-4
L. P. Madin, P. Kremer and S. Hacker B-11
G. I. Mastumoto and G. R. Harbison B-11
T. S. S Rao B-14
Rudolf S. Scheltema B-15
Rudolf S. Scheltema and Michael Chin B-16
Christopher M. Tebeau and Laurence P. Madin B-20
Peter H. Wiebe and Charles H. Greene B-22

ZOOPLANKTON ECOLOGY

Glenn R. Flierl and Cabell S. Davis B-4
Michael W. Hart, Richard L. Miller and Laurence P. Madin B-5
Dean M. Jacobson and Donald M. Anderson B-8
Stacy L. Kim, Lauren S. Mullineaux and Karl R. Helfrich B-9
L. P. Madin, P. Kremer and S. Hacker B-11
G. I. Mastumoto and G. R. Harbison B-11
T. S. S Rao B-14
Peter H. Wiebe and Charles H. Greene B-22

DEPARTMENT OF GEOLOGY AND GEOPHYSICS

G. Michael Purdy, Chairman

ACCELERATOR MASS SPECTROMETRY

VARVE CALIBRATED RECORDS OF CARBONATE AND ORGANIC CARBON ACCUMULATION OVER THE LAST 2000 YEARS IN THE BLACK SEA

M. A. Arthur, W. E. Dean, E. D. Neff, B. J. Hay, J. King and G. A. Jones

Sedimentologic and geochemical studies of box and gravity cores recovered from the Black Sea during the first of a mullet-leg international Black Sea expedition in 1988 allow reconstruction of the basin wide Holocene environmental history of the Black Sea. In the deep parts of the basin, box cores typically recovered a flocculant surface "fluff" layer, laminated coccolith marls of Unit I (25 to 45 cm thick), and the upper 5 to 10 cm of finely laminated, dark-colored sapropels of Unit II. Fine-grained, homogeneous mud turbidites are interbedded with Units I and II over much of the basin, but the stratigraphic position of these turbidites differs from site to site. The deposition of individual turbidites up to 15 cm thick does not appear to have significantly disturbed underlying laminae.

Organic-carbon accumulation rates in Unit I are somewhat antithetic to those of carbonate, and, on the basis of this and additional constraints placed by pyrolysis and carbon isotopic analyses of organic material, it appears that terrestrial organic matter is an important component (perhaps >25%) of total organic carbon burial in the basin. Unit I in the western basin has a higher terrestrial organic component and higher accumulation rates of terrigenous clastic material than Unit I in the eastern basin, as expected because of the major rivers that empty into the western basin from eastern Europe and the former Soviet Union. Shallower slope sites, but still within anoxic bottom waters, have lower organic carbon accumulation rates and lower pyrolysis hydrogen indices than deep-water basinal sites, suggesting selective resuspension and oxidation of organic matter at basin margins and focusing of organic matter deposition towards the basin center. Comparison of productivity-normalized, organic-carbon accumulation rates from the anoxic Black Sea with open ocean oxic settings at similar water depths and bulk accumulation rates suggests that, although high, organic-carbon accumulation rates are not significantly higher under anoxic conditions than expected for the same bulk accumulation rates under oxic conditions.

In Press: *Global Biogeochemical Cycles.*

Supported by: NSF Grant OCE-8712181.

WHOI Contribution No. 8561.

AUTOMATED SAMPLE PROCESSING AT THE NATIONAL OCEAN SCIENCES AMS FACILITY

G. J. Cohen, D. L. Hutton, K. F. von Reden, E. A. Osborne, A. P. McNichol and G. A. Jones

The high throughput and high-precision requirements for the NOSAMS Facility have made it essential to automate many of the stages in sample processing. These automated procedures increase the sample capacity for the lab while reducing errors in sample preparation. Automation has also allowed sample histories to be recorded and saved in Sybase, a relational database.

In Press: *Nuclear Instruments and Methods.*

Supported by: NSF Grants OCE-9301015 and OCE-8702509.

WHOI Contribution No. 8564.

LAKE-LEVEL HISTORY OF LAKE MICHIGAN FOR THE PAST 12,000 YEARS: THE RECORD FROM DEEP LACUSTRINE SEDIMENTS

S. M. Colman, R. M. Forester, R. L. Reynolds, D. S. Sweetkind, J. W. King, P. Gangemi, G. A. Jones, L. D. Keigwin and D. S. Foster

Collection and analysis of an extensive set of seismic-reflection profiles and cores from southern Lake Michigan have provided new data that document the history of the lake basin for the past 12,000 years. Analyses of the seismic data, together with dating, magnetic, sedimentologic, isotopic, and paleontologic studies of core samples, have allowed us to reconstruct lake-level changes during this recent part of the lake's history.

The post-glacial history of lake-level changes in the Lake Michigan basin begins about 11.2 ka with the fall from the high Calumet level, caused by the retreat of the Two Rivers glacier, which had blocked the northern outlet of the lake. This lake-level fall was temporarily reversed by a major influx of water from glacial Lake Agassiz (about 10.6 ka), during which deposition of the distinctive gray Wilmette Bed of the Lake Michigan Formation interrupted deposition of red glaciolacustrine sediment. Lake level then continued to fall, culminating in the opening of the North Bay outlet at about 10.3 ka. During the resulting Chippewa low phase, lake level was about 80 m lower than it is today in the southern basin of Lake Michigan.

The rise of the early Holocene lake level, controlled primarily by isostatic rebound of the North Bay outlet, resulted in a prominent, planar, transgressive unconformity that eroded most of the shoreline features below present lake level. Superimposed on this overall rise in lake level, a second influx of water from Lake Agassiz temporarily raised lake levels an unknown amount about 9.1 ka. At about 7 ka, lake level may have fallen below the level of the outlet because of sharply drier climate. Sometime between 6 and 5 ka, the character of the lake changed dramatically, probably due mostly to climatic causes, becoming highly undersaturated with respect to calcium carbonate and returning primary control of lake level to the isostatically rising North Bay outlet. Post-Nipissing (about 5 ka) lake level has fallen about 6 m due to erosion of the Port Huron outlet, a trend around which occurred relatively small ($\pm$ $\sim$2 m), short-term fluctuations controlled mainly by climatic changes. These cyclic fluctuations are reflected in the sedimentological and sediment-magnetic properties of the sediments.

In Press: *Journal Great Lakes Research.*

Supported by: USGS/WHOI Cooperative Agreement and NSF Grant OCE-9301015.

WHOI Contribution No. 8536.

RADIOCARBON DATING OF LAKE BAIKAL SEDIMENTS – A PROGRESS REPORT

S. M. Colman, V. M. Kuptsov, G. A. Jones, and S. J. Carter

A suite of 34 new accelerator-mass spectrometer (AMS) radiocarbon ages on total organic carbon provides the first reliable chronology for late Quaternary sediments in Lake Baikal. The ages show more than an order of magnitude difference in sediment-accumulation rate among different sedimentary environments in Lake Baikal, from less than 0.03 mm/yr on isolated banks such as Academician Ridge, to nearly 0.3 mm/yr in the turbidite depositional areas beneath the deep basin floors, such as the Central Basin. Rates in the pro-delta area of the Selenga Delta are intermediate between these two extremes. Within each environment, Holocene sediment-accumulation rate appears to be nearly constant, and they are less than late Pleistocene rates. The new AMS ages clearly indicate that the dramatic increase in productivity in the lake, as evidenced by increases in biogenic silica and organic carbon, began before 12 ka, in contrast to previous estimates of the age of this transition (7 ka) based on conventional radiocarbon ages.

Several problems are inherent in the interpretation of these ages. In the Baikal cores, these manifest themselves as (1) the loss of the upper part of the sedimentary section in some cores, (2) apparent ages of the sediment surface that range from 0 to 1700 years, and (3) as stratigraphic reversals of ages in the deeper part of the cores. The first problem can be minimized by correlation to gravity and box cores. The second problem may be partly due to reworked or terrestrial organic carbon, but other factors, such as upward diffusion of bicarbonate, may also be involved; further work is underway to determine the cause of this effect. The last problem is probably due to slight contamination of the carbon in glacial clays, whose very low carbon content ($<$ 0.2 percent) and relatively great age ($>$ 20 ka) make then very susceptible to contamination.

In Press: *Geologie I Geofizica.*

Supported by: USGS/WHOI Cooperative Agreement and NSF Grants OCE-8702509, OCE-9301015.

WHOI Contribution No. 8555.

HOLOCENE CLIMATE AND DEEP OCEAN CIRCULATION CHANGES: EVIDENCE FROM AMS RADIOCARBON-DATED SEDIMENT DRIFTS OF THE ARGENTINE BASIN (SW ATLANTIC)

G. A. Jones

Accelerator Mass Spectrometer (AMS) radiocarbon analyses have been made on 51 samples of total organic carbon from four box and two piston cores collected from the "erosional" and "depositional" sides of two central Argentine Basin sediment waves. Throughout the Holocene, sediment from the geomorphically defined "depositional" side of each sediment wave accumulated at rates of 30 to 105 cm/1000 yrs. Sediments from the "erosional" side of each wave accumulated at rates of 2 to 10 cm/1000 yrs in the late and early Holocene, while the mid Holocene is characterized by sedimentation rates less than 1.0 cm/1000 yrs.

During the mid-Holocene, increased aridity reduced chemical weathering and the flow of the rivers draining to the continental shelf, causing a concomitant decrease in fine-grained terrigenous input to the basin as evidenced by decreased sedimentation rates, lower N/C ratios, and depleted $\delta^{13}C_{org}$ values. Bottom water flow speeds in the late Holocene averaged 14 cm/1000 yrs, and are in agreement with 10 cm/sec mean and 15-20 cm/sec maximum flow speeds measured by current meter. Flow speeds in the Argentine Basin were 10% higher than today from 8000 to 2000 yBP, and are consistent with a general invigoration of thermohaline circulation that began between 9000

and 8000 yBP. The introduction of warm, salty Indian Ocean water into the northern North Atlantic at 9000 yBP was the mechanism that provided the excess salt needed to stabilize the North Atlantic Deep Water (NADW) thermohaline circulation system in its present mode.

In Press: *Paleoceanography.*

Supported by: NSF Grants OCE-8511386 and OCE-9301015 and ONR Grant N00014-87-K-0007 and NOAA Grant NAl6RC0074-01.

WHOI Contribution No. 8552.

A NEW HYPOTHESIS FOR THE HOLOCENE APPEARANCE OF COCCOLITHOPHORES IN THE BLACK SEA

Glenn A. Jones

A recent accelerator mass spectrometer (AMS) radiocarbon study of Black Sea Holocene sediments (Jones and Gagnon, 1993, Deep-Sea Research in press) has resolved a long standing chronology controversy involving radioisotope (Ross and Degens, 1974, The Black Sea–Geology, Chemistry, and Biology, pp. 183-199; Crusius and Anderson, 1992, Paleoceanography, 7, 215-27) and varve counting (Degens et al., 1980, Neues Jahrbuch für Geologie und Paläontologie Monatshefte 5, 65-86; Neff et al., 1991, EOS, Transactions of the American Geophysical Union 72, 72) methodologies. The revised chronology combined with model results of the salinity evolution of the Black Sea since the last glacial maximum (Boudreau and Leblond, 1989, Paleoceanography, 4, 157-66) does not support the hypothesis of a salinity-controlled Holocene invasion of the Black Sea by coccolithophores, a planktonic golden-brown unicellular marine algae (Bukry, 1974, The Black Sea–Geology, Chemistry and Biology, pp. 353-63). Rather, evidence presented here suggests these organisms were inadvertently transported from the Mediterranean Sea by sailing vessels during the Greek exploration and colonization of the Black Sea in the 7th and 8th centuries B.C. As such this may be one of the earliest examples of anthropogenic transport of marine organisms between ocean basins, and a good example of the difficulties inherent in distinguishing natural from anthropogenic effects when studying Holocene biological systems (e.g., Haynes, 1991, Quaternary Research, 35, 438-450).

In Press: *The Holocene.*

Supported by: NSF Grant OCE-8712181.

WHOI Contribution No. 8470.

TIMING OF THE HOLOCENE REPOPULATION OF THE ATLANTIC OCEAN BY *G. MENARDII* AND *G. TUMIDA* AND IMPLICATIONS FOR SURFACE WATERMASS PALEOCEANOGRAPHY

G. A. Jones

The most recent repopulation of the Atlantic Ocean by the menardiform foraminiferal species *Globorotalia menardii* (d'Orbigny) and *Globorotalia tumida* (Brady) has been widely accepted as occurring at approximately 11,000 yBP (Ericson and Wollin, 1956, Micropaleontology, 2, 257-270) and used extensively to biostratigraphically define the boundary between Holocene and glacial sediments in the Atlantic Ocean. Accelerator mass spectrometer (AMS) radiocarbon dating of mixed planktonic foraminifera and monospecific samples of these two species have been made on a total of 188 samples from 3 Indian Ocean and 10 Atlantic Ocean cores. Both species were continuously present in the Indian Ocean during the last 30,000 years. The low abundances of *G. menardii* found throughout the late glacial section of southeastern South Atlantic core, RC17-43, suggests that the Agulhas Retroflection was still shedding warm-core rings containing Indian Ocean planktonic assemblages into the southeastern South Atlantic during that time. G. menardii was found to isochronously repopulate the rest of the Atlantic Ocean at 6350±100 yBP. In contrast, the pattern of Atlantic Ocean repopulation for *G. tumida* was found to be time-transgressive, averaging 9020±220 yBP in the equatorial and western North Atlantic Ocean and 7310 yBP in the eastern North Atlantic. *G. tumida* was not found to occur in the South Atlantic during the last glacial or the Holocene. The data presented here do not support the assumed isochroneity or long accepted age of the G. menardii-tumida Z/Y biostratigraphic datum. Not only does each species demonstrate a distinct and different mode of repopulating the Atlantic Ocean, but the timing of these events as a biostratigraphic tool must be interpreted in light of bioturbation modeling. *G. menardii-tumid* specimens are bioturbated downward into older sediments containing no specimens of these species, and it is the radiocarbon dating of the bulk sediments and not the individual specimens of *G. menardii-tumida*, that have resulted in the previous anomalously old age estimates. The maximum change in abundance should be used for defining a biostratigraphic datum, and not the first appearance, or 1% abundance levels as is common. It is further suggested that warm, salty Indian Ocean waters did not make it into the North Atlantic via the Agulhas-Benguela Current system until approximately 9000 yBP. This warm, salty

water is the catalyst by which the atmospheric and oceanic climate of the northern North Atlantic, and North Atlantic Deep Water stabilized in their present modes.

In Press: *Deep-Sea Research.*

Supported by: NSF Grant OCE-8608119.

WHOI Contribution No. 8532.

HIGH-PRECISION AMS RADIOCARBON MEASUREMENTS OF CENTRAL ARCTIC OCEAN SEAWATERS

G. A. Jones, A. R. Gagnon, R. J. Schneider, K. F. von Reden and A. P. McNichol

We report on the first high precision radiocarbon dataset measured on single targets using Accelerator Mass Spectrometry (AMS). Results from a thirteen sample water column profile collected in the Canada Basin (74°N, 150°W, 3850m water depth) of the central Arctic Ocean in September 1992 has been analyzed in duplicate and demonstrates that the average total precision achieved for each of the 26 targets was ±3.22 per mil. The reproducibility of the thirteen paired analyses averaged ±3.66 per mil. Comparison with a recently published AMS ^{14}C profile from the same basin suggests this data is accurate as well. Results suggests that the deep waters of the Canada Basin have a renewal rate of 430 years, in comparison with 250 years estimated for the deep waters of the Eurasian Basin. The major requirement of the World Ocean Circulation Experiment (WOCE) for a radiocarbon analysis precision of ±3 to 4 per mil for deep water samples has now been met with the AMS technology available at the National Ocean Sciences AMS Facility at the Woods Hole Oceanographic Institution.

In Press: *Nuclear Instruments and Methods.*

Supported by: NSF Grants OCE-9301015 and DPP-9024560, and NOAA Grant NAl6RC0074-01.

WHOI Contribution No. 8567.

WESTERN NORTH ATLANTIC EVIDENCE FOR MILLENNIAL-SCALE CHANGES IN OCEAN CIRCULATION AND CLIMATE

L. D. Keigwin and G. A. Jones

Two late Quaternary series of high resolution percent carbonate data from western North Atlantic sediment drifts (Bermuda Rise and Bahama Outer Ridge) show millennial-scale oscillations superimposed on the familiar, longer-period oscillations of orbital origin. The dominant high frequency oscillation in these records has a quasi period of about 4000 yrs. These % $CaCO_3$ changes most likely result from the influence of climate change on the flux of terrigenous material from eastern Canada, the resuspension of continental margin sediment by deep eddy kinetic energy, and carbonate dissolution. Sediment is transported to the Bermuda Rise by deep recirculating gyres and to the Bahama Outer Ridge by the deep western boundary current system. Stable isotope results on foraminifera across several of these oscillations from interstadial climate conditions and from a glacial inception display variability similar to that of % $CaCO_3$. Oxygen isotope ratios of planktonic foraminifera suggest large variations in near-surface temperature and/or salinity, and carbon isotope ratios of benthic foraminifera indicate that there were significant oscillations in the flux of North Atlantic Deep Water (NADW). These data support models which couple surface ocean conditions in the North Atlantic, production of NADW, North Atlantic heat flux, and evidence for temperature oscillations in ice cores.

In Press: *Journal of Geophysical Research.*

Supported by: NSF Grants OCE-8702509 and ATM-8706617 and NOAA Grant NA16RC0074-01.

WHOI Contribution No. 8530.

COMPARATIVE STUDY OF AMS TARGET PERFORMANCE USING THE NOSAMS RECOMBINATOR ION SOURCE

D. B. Klinedinst, A. P. McNichol, L. A. Currie, R. J. Schneider, G. A. Klouda, K. F. von Reden, R. M. Verkouteren and G. A. Jones

Using the National Ocean Science Accelerator Mass Spectrometer (NOSAMS) located at the Woods Hole Oceanographic Institute, a collaborative study was undertaken to compare the performance of two ^{14}C AMS target types: the Fe-C bead developed at the National Institute of Standards and Technology (NIST) and the more commonly used graphite powder. Targets were prepared according to a partial factorial design. A total of 29 targets that spanned a mass range of 7 to 1680 μg carbon and fraction of modern carbon range of 0 to 1.3 were analyzed. The study took place in order to compare the performance of the two target types, with a special view towards the limits of stability, sample size, and precision.

In Press: *Nuclear Instruments and Methods.*

Supported by: NSF Grants OCE-9301015 and OCE-8702509.

WHOI Contribution No. 8568.

RAPID ANALYSIS OF SEAWATER SAMPLES AT THE NATIONAL OCEAN SCIENCES ACCELERATOR MASS SPECTROMETRY FACILITY, WOODS HOLE, MA

A. P. McNichol, G. A. Jones, D. L. Hutton, A. R. Gagnon and R. M. Key

We have established a laboratory for extracting ΣCO_2 from seawater samples for AMS analysis of the radiocarbon content. The seawater samples are collected at sea, poisoned, and stored until analysis on land. Each sample is acidified, the inorganic carbon is stripped out as CO_2 with an inert carrier gas and then converted to graphite. In this paper we demonstrate our precision and accuracy in the analysis of seawater samples.

Submitted to: *Radiocarbon.*

Supported by: NSF Grants OCE-8702509, and OCE-9301015.

WHOI Contribution No. 8580.

TIC, TOC, DIC, DOC, PIC, POC - UNIQUE ASPECTS IN THE PREPARATION OF OCEANOGRAPHIC SAMPLES FOR ^{14}C-AMS

A. P. McNichol, E. A. Osborne, A. R. Gagnon, B. Fry and G. A. Jones

The radiocarbon content of discrete carbon pools (total (T), dissolved (D), and particulate (P) inorganic (I) and organic (O) carbon (C)) is a useful tracer of carbon cycling within the modern and past ocean. The isolation of different carbon pools in the ocean environment and conversion to CO_2 presents unique analytical problems for the radiocarbon chemist. In general, isolation and preparation of inorganic carbon presents few problems; dissolved carbon is easily extracted by acidifying the sample and stripping with an inert gas. Carbon is also readily isolated from particulate carbonate samples; in this case, CO_2 is prepared by hydrolysis of the substrate with phosphoric acid. The isolation and preparation of organic carbon presents a much greater problem. Dissolved organic carbon (DOC) must first be isolated from DIC and then oxidized in the presence of very high salt concentrations. We present results from a closed-tube combustion method in which the DIC-free seawater is evaporated to dryness, transferred to a clean combustion tube, and oxidized overnight at 550°C. Combustion of total organic carbon (TOC) in sediments with a high inorganic carbon content is also difficult. Removal of $CaCO_3$ with acid leaves severely deliquescent salts which, if not thoroughly dried, cause combustion tubes to explode. Removal of the salts by rinsing can also remove significant amounts of organic matter. Finally, we present results from a local coastal region.

In Press: *Nuclear Instruments and Methods.*

Supported by: NSF Grants OCE-9301015 and OCE-8702509.

WHOI Contribution No. 8550.

ELECTRIC DISSOCIATION OF NEGATIVE IONS-II

M-J. Nadeau, A. E. Litherland, M. A. Garwan and X-L. Zhao

As an alternative to naturally occurring negative ion discrimination, we have used electric dissociation to discriminate between isobars, thereby destroying the weaker negative ion of a pair. This technique also permits the determination of the properties of the quantum states and the binding energy of some weakly bound negative ions (Ca, Tm, Dy and Yb) some of which had not been studied previously (Tm, Dy, Yb). During the course of this study, it was also established that some very weakly bound negative ions (Dy and Yb) are destroyed by weak electric fields such as those in tandem accelerators. This fact was used to verify the theory of electric dissociation by the comparison of the dissociation probability under different field configurations and gradients. The results regarding the lanthanide elements indicate that in all three cases that the extra electron occupies a *p*-orbital which does not follow the "natural" filling of the periodic table. The study of Ca- concluded that the lowest states are the $4s^2 4p\ ^2p$ J=1/2,3/2 states with binding energy of 21.0 ± 2.5 meV and a spin-orbit splitting in the range 0.4-2.5 meV with a maximum probability at 0.75 meV. The ordering of the levels has not been established yet.

In Press: *Nuclear Instruments and Methods.*

Supported by: Natural Science and Engineering Research Council of Canada.

WHOI Contribution No. 8559.

INTERNAL AND EXTERNAL CHECKS IN THE NOSAMS FACILITY SAMPLE PREPARATION LABORATORY FOR TARGET QUALITY AND HOMOGENEITY

E. A. Osborne, A. P. McNichol, A. R. Gagnon, D. L. Hutton and G. A. Jones

When a sample reaches the NOSAMS facility, there are two sources that can contribute to a decrease in precision and accuracy of an analysis–the stability and cleanliness of the AMS and the cleanliness and reproducibility of the chemical procedures used to convert a sample to graphite. In the NOSAMS sample preparation laboratory (SPL) we have developed rigorous internal procedures aimed at ensuring that sample preparation introduces as little error into our analyses as possible and identifying problems rapidly. These procedures and standard laboratory practices are all documented and procedure numbers are stored for all samples processed in the SPL.

Our three major CO_2 preparation procedures are stripping inorganic carbon from seawater, hydrolyzing $CaCO_3$, and oxidizing organic matter. For seawater, approximately 10% of our analyses are standards or blanks which we use to demonstrate extraction of virtually all the inorganic carbon. Analysis of the stable carbon isotopic composition of the CO_2 extracted from our standards indicates a precision of better than 0.15‰. We also routinely process ^{14}C-free CO_2 in our stripping lines to demonstrate the absence of a significant process-dependent blank. For organic combustions and $CaCO_3CO$ hydrolyses, we use the carbon yield (%OC or $\%CaCO_2$ by weight) as a check on our sample procedures. For organic carbon analyses in sediments, we have found through experience that it is important to have a reliable estimate of the amount of organic present before proceeding with our combustions. We have analyzed the blank contribution of these procedures as a function of sample size. Our organic carbon blank is constant at approximately 0.4% modern for samples containing greater than 1 mg C and our carbonate blank is less than 0.2% modern for samples containing more than 0.5 mg C.

We use a standard Fe/H_2 catalytic reduction to prepare graphite from CO_2. We check the completeness of our reactions with the pressure data stored during the reaction as well as use a robot to determine a gravimetric yield. All graphite undergoes a visual inspection and is rejected if any heterogeneities are present. We have recombusted graphite made from CO_2 with $\delta^{13}C$ values ranging from -42 to 1‰and determined that the $\delta^{13}C$ of the recombusted carbon agrees with that from the pure gas to within 0.5‰, demonstrating little or no fractionation during the treatment of the sample. The $\delta^{13}C$ we measure on the CO_2 generated from more than 75% of our samples is compared to the δ^{13} measured on the AMS as a further check of our procedures.

We present ^{14}C results from CO_2 samples measured at WHOI and 2 other AMS laboratories as an external check on our accuracy. As further external checks, we analyzed the International Atomic Energy Association (IAEA) samples during the establishment of our laboratory and participated in the Third International Radiocarbon Intercalibration (TIRI) exercise.

In Press: *Nuclear Instruments and Methods.*

Supported by: NSF Grants OCE-9301015 and OCE-8702509.

WHOI Contribution No. 8582.

METHODS FOR DATA SCREENING, FLAGGING, AND ERROR ANALYSIS AT THE NATIONAL OCEAN SCIENCES AMS FACILITY

R. J. Schneider, G. A. Jones, A. P. McNichol, K. F. von Reden, K. L. Elder, K. Huang and E. D. Kessel

All data collection, from sample submittal, through processing into targets and AMS analysis is integrated within a large relational database (SYBASE). Over fifty tables are linked through key fields. Through structured queries, the information is analyzed and presented for a wide variety of applications. Benefits include enhanced quality control, more complete reports to users and more accurate transfer of data among the several laboratories on the network.

In Press: *Nuclear Instruments and Methods.*

Supported by: NSF Grant OCE-9301015.

WHOI Contribution No. 8558.

OPTIMIZED DATA ANALYSIS FOR AMS RADIOCARBON DATING

F. H. Séguin, R. J. Schneider, G. A. Jones and K. F. von Reden

Because the efficiencies of detection of ^{14}C and ^{12}C can and do vary with time during AMS data acquisition, it is desirable to have a data analysis technique which recognizes time variations and uses all available data to extract the maximum possible information content from a data set while providing meaningful statistical information about

measurement errors. Toward this end, a new method of data reduction and error analysis is being developed for the determination of ^{14}C to ^{12}C ratios for radiocarbon dating from data sets taken at the National Ocean Sciences AMS Facility.

In Press: *Nuclear Instruments and Methods.*

Supported by: NSF Grant OCE-9301015.

WHOI Contribution No. 8560.

PERFORMANCE CHARACTERISTICS OF THE 3 MV TANDETRON AMS SYSTEM AT THE NATIONAL OCEAN SCIENCES AMS FACILITY

K. F. von Reden, R. J. Schneider, G. J. Cohen and G. A. Jones

Operational and machine performance parameters are discussed for the National Ocean Sciences AMS System. The system now routinely measures between 50 and 100 carbon samples per week in largely unattended mode using one of the two functional high-current ion sources. System development and procedures are described that enable us to reach and maintain the high precision level required for the measurement of deep sea water dissolved inorganic carbon samples.

In Press: *Nuclear Instruments and Methods.*

Supported by: NSF Grants OCE-9301015 and OCE-8702509.

WHOI Contribution No. 8563.

RADIOCARBON AGES FROM TWO SUBMERGED STRANDLINE FEATURES IN THE WESTERN GULF OF MAINE AND A SEA-LEVEL CURVE FOR THE NORTHEASTERN MASSACHUSETTS COASTAL REGION

R. N. Oldale, S. M. Colman and G. A. Jones

New radiocarbon dates provide ages for two submerged strandline features on the Massachusetts inner shelf. These ages provide limited control on a relative sea-level (RSL) curve for the late Wisconsinan and Holocene. The curve indicates a late Wisconsinan high stand of RSL of +33 m about 14,000 yr ago and a very short-lived relative low stand of about -43 m at about 12,000 yr ago followed by a rise to present sea level. Rapid changes of RSL about 12,000 yr ago may be related to changes in global glacial meltwater discharge and eustatic sea-level change shown by dated corals of Barbados. Variations in the magnitude and timing of RSL change from south to north along the coast of the western Gulf of Maine are due to greater crustal depression and later deglaciation to the north.

Published in: *Quaternary Research*, 40:38-45, 1993.

Supported by: USGS/WHOI Cooperative Agreement and NSF Grant OCE-8702509.

A NEW HIGH-TEMPORAL RESOLUTION PALEOCEANOGRAPHIC TOOL FOR THE NORTHERN NORTH ATLANTIC: THE MOLLUSC *ARCTICA ISLANDICA*

C. R. Weidman and G. A. Jones

Annual and seasonal geochemical records of the surface subtropical oceans have been previously obtained from corals, but no comparable tools have been developed for the colder, higher latitude oceans – regions critical to the regulation of global climate and ocean circulation. The carbonate shell of the mollusc (Bivalvia) *Arctica islandica* offers tremendous potential as a long term monitor of ocean conditions on the continental shelves in the mid- to high-latitude North Atlantic due to this species' great longevity (>200 years), abundance, and wide latitudinal (35°N-70°N) and bathymetric distribution (10-200 m). The slow growth rate of this long-lived mollusc thwarted earlier attempts to exploit this potential, but now the application of micro-mass stable isotope mass spectrometry, automated micro-sampling technology, and accelerator mass spectrometry (AMS) have overcome this obstacle.

Our efforts have produced a $\delta^{18}O$ profile from a 38-year old *Arctica islandica* specimen collected from near the position of the former Nantucket Lightship (41°N, 69°W) for the annual band years 1956 to 1957 and 1961 to 1971. This record is in good agreement with the predicted $\delta^{18}O$ record derived from bottom temperature and salinity measurements taken at this lightship during this same period. In addition, we have obtained the first time-histories of bomb-^{14}C in the higher latitudes of the North Atlantic from Georges Bank (41°N, 67°W) and the North Sea (54°N, 6°E). Both of these results: 1) contribute new information on the life history of *A. islandica*, an important commercially harvested shellfish species in the U.S., confirming a consistent annual banding pattern for this species and showing a consistent shell growth shutdown temperature of ~8°C; and 2) demonstrate that *A. islandica's* shell can be used to help determine the annual maximum bottom temperature, shelf water origin, and the interannual variability of these parameters for the past two centuries.

In Press: *International Council for the Exploration of the Sea.*

Supported by: WHOI Ocean Ventures Fund, NOAA Grant NA36GPO0291 and NSF Grant OCE-9301015.

WHOI Contribution No. 8535.

DEVELOPMENT OF THE MOLLUSC ARCTICA ISLANDICA AS A PALEOCEANOGRAPHIC TOOL FOR RECONSTRUCTING ANNUAL AND SEASONAL RECORDS OF $\Delta^{14}C$ AND $\delta^{18}O$ IN THE MID-TO HIGH-LATITUDE NORTH ATLANTIC OCEAN

C. R. Weidman and G. A. Jones

Corals have been used, previously, to reconstruct high-resolution geochemical records of the surface subtropical oceans, but no comparable tools have been developed for the colder, higher latitude oceans. We report that the application of accelerator mass spectrometry and micro-sampling techniques now allows the carbonate shell of the long-lived (~200 yr) mollusc (Bivalvia) it Arctica islandica to be used to fulfill this role for the mid- and high-latitude North Atlantic Ocean. We describe the sampling methods used to produce the first time histories of bomb-^{14}C in the northern North Atlantic Ocean from Georges Bank (41°N, 67°W) and the North Sea (54°N, 6°E), and a record of seasonal bottom temperatures derived from the $\delta^{18}O$ profile of a shell collected on Nantucket Shoals (41°N, 69°W).

In Press: *Applications of isotope techniques in studying past and current environmental changes in the hydrosphere and atmosphere*, Rozanski, K., ed. International Atomic Energy Agency.

Supported by: WHOI Ocean Ventures Fund, NOAA Grant NA36GPO291 and NSF Grant OCE-9301015.

WHOI Contribution No. 8534.

THE LONG-LIVED MOLLUSC; *ARCTICA ISLANDICA*: A NEW PALEOCEANOGRAPHIC TOOL FOR THE RECONSTRUCTION OF MAXIMUM BOTTOM TEMPERATURES FOR THE CONTINENTAL SHELVES OF THE NORTHERN NORTH ATLANTIC OCEAN

C. R. Weidman and G. A. Jones

The carbonate shell of the bivalve *Arctica islandica* has been recognized, for more than a decade, as a potentially important marine geochemical bio-recorder owing to this species' great longevity (200+ years) and wide geographic distribution throughout the northern North Atlantic Ocean – a region vital to global climate and ocean circulation. However, until now, this potential has not been realized due to the difficulty of precisely sampling the shell of this slow growing species. Using newly available automated micro-sampling techniques combined with micro-mass stable isotope mass spectrometry, a stable oxygen isotope record (1956-1957 and 1961-1970) has been obtained from a live-captured 38-year old *A. islandica* specimen collected near the former position of the Nantucket Lightship (41°N, 69°W). The shell's $\delta^{18}O$ signal 1) is in phase with its growth banding, confirming the annual periodicity of this species' growth bands, 2) is in isotopic equilibrium with the ambient seawater and faithfully records the seasonal maximum bottom temperature, and 3) shows a consistent shell growth shutdown temperature of ~7-8°C, which translates into a 7-month, June-December, shell growth period at this location. These results add important information on the life history of this commercially important shellfish species and demonstrate that *A. islandica* shells can be used to reconstruct interannual records of the maximum bottom temperature.

In Press: *Journal of Geophysical Research.*

Supported by: WHOI Ocean Ventures Fund, NOAA Grant NA16RC0080-01 and NSF Grant OCE-931015.

WHOI Contribution No. 8520.

GEOCHEMISTRY

THE GEOCHEMISTRY OF MCMURDO GROUP VOLCANIC ROCKS

Stanley R. Hart and Philip R. Kyle

Young Cenozoic volcanic rocks from Marie Byrd Land (Futa and LeMasurier, 1983) and Scott Balleny Islands (Hart, 1988) are unusual in showing $^{87}Sr/^{86}Sr$ ratios lower than most oceanic island basalts, with some values approaching those typical of mid-ocean ridge basalt (MORB). To assess the geographic extent of this low 87/86 Sr province, and to decide whether a MORB-type mantle is involved, we have analyzed a reconnaissance sampling of basalts from the Hallett volcanic province, Northern Victoria Land, for Sr, Nd and Pb isotopic ratios. This data is shown in Figure 1, with data for basalts from Peter I Island, Jones Mountains, and Marie Byrd Land for comparison. A number of Hallett Province basalts show 87/86 Sr ratios less than 0.7030, comparable to the low values reported earlier for Marie Byrd Land and Scott/Balleny

islands. However, the Pb isotope data for all of these areas is quite radiogenic, with 206/204 Pb generally greater than 19.5. This is in marked contrast with MORB, which rarely show 206/204 Pb ratios higher than 19.0. The mantle end member reservoir designated HIMU by Zindler and Hart (1986) has 87/86 Sr ~0.70285 and 206/204 Pb ~21.8 and it is clear that many of the young Cenozoic volcanics from Antarctica are showing a strong involvement of this component.

In Press: *The Antarctic Journal of the United States.*

Supported by: NSF Grant DPP-9117853.

WHOI Contribution No. 8463.

ORPHAN STRONTIUM-87 IN ABYSSAL PERIDOTITES: DADDY WAS A GRANITE

Jonathan E. Snow, Stanley R. Hart and Henry J. B. Dick

The $^{87}Sr/^{86}Sr$ ratios in some bulk abyssal and alpine peridotites are too high to be binary mixtures of depleted mantle ($^{87}Sr/^{86}Sr \cong 0.7023$) and seawater ($^{87}Sr/^{86}Sr \cong 0.7092$) components. The apparent excess, or "orphan" ^{87}Sr appears to be separated from its radioactive parent. Such observations were widely held to be analytical artifacts. Study of several occurrences of orphan ^{87} shows that the orphan component in abyssal peridotite is located in the alteration products of olivine and enstatite in the peridotite. The orphan ^{87}Sr is most likely introduced by infiltration of low temperature (<200°C) seawater bearing suspended detrital particulates. These particulates include grains of detrital clay which are partly derived from continental (i.e., granitic) sources, and thus are highly radiogenic. Orphan ^{87}Sr and other radiogenic isotopes may provide a tracer for low temperature seawater penetration into the oceanic crust.

Published in: *Science*, 262(5141):1,861-1,863, 1993.

Supported by: NSF Grants EAR-9096194 and OCE-8918905.

WHOI Contribution No. 8531.

GEOLOGY

EFFECTS OF MULTIPLE INLET MORPHOLOGY ON TIDAL EXCHANGE: WAQUOIT BAY, MASSACHUSETTS

David G. Aubrey, Thomas M. McSherry and Pierre P. Eliet

Waquoit Bay, a nearly-enclosed embayment incised into outwash deposited during the last glaciation, has undergone dramatic geomorphic changes during the past century. Storms, and to an extent human influence, have varied the number of inlets in the Waquoit system through time, from a low of a single inlet to a high of three inlets. Water exchange rates between separate embayments within the system vary according to the number of inlets. The embayment is separated by a narrow tidal channel (Seapit River) into a western Bay (Eel River) and eastern Bay (Waquoit Bay). When only Waquoit Inlet was functioning, circulation and mixing processes in Eel River were sluggish, and residence times much longer. As the second inlet opened into Eel River, the circulation patterns changed dramatically. Residence times in Eel River were reduced, and residual currents were from Eel River into Waquoit Bay. Following Hurricane Bob in 1991, a third inlet opened, in the barrier protecting Eel River. This new inlet created increased exchange into Eel River, but its effect in general was smaller than the addition of the second inlet.

Published in: *Formation and Evolution of Multiple Tidal Inlets.* Coastal and Estuarine Studies, 44. American Geophysical Union, Washington, D.C., :213-235, 1993.

Supported by: Subcontract from Boston University and NSF LMER Contract OCE-8914729.

WHOI Contribution No. 8323.

PRODUCTION OF SMALL VOLCANOES IN THE SUPERSWELL REGION OF THE SOUTH PACIFIC

Karen G. Bemis and Deborah K. Smith

We use Sea Beam swath bathymetry and wide beam profiler data to investigate the production of small size (50-700 m high) volcanoes in the region of the Superswell in French Polynesia. Seamount population parameters are estimated for three study regions. We find that seamount abundances increase threefold going southward across the Marquesas fracture zone, the inferred northern boundary of the Superswell, indicating that more magma has been supplied to the surface to build small volcanoes in this region. In addition, we document that south of the Marquesas fracture zone, seamount abundances, on average, are equally as high on young crust (1-18 My) generated at the East Pacific Rise (9°-22°) as on the adjacent Superswell region (~20-60 My old crust). The high density of small-size seamount in both regions south of the Marquesas fracture zone suggests the following possibilities: (1) volcanic processes at the East Pacific Rise have produced more small-size seamounts south of the fracture zone than to the north for the last 60 My, (2)

off-axis volcanic processes (possibly related to the Superswell) have led to excess volcanism on both the Superswell region and the region adjacent to the East Pacific Rise, or (3) off-axis seamount production is anomalously high on the Superswell, and the production of seamounts has increased at the East Pacific Rise since 20 My.

Published in: *Earth Planetary Science Letters*, 118:251-262, 1993.

Supported by: ONR Grant N00014-89-J-1021.

WHOI Contribution No. 8373.

COMPARATIVE VOLCANOLOGY OF SMALL AXIAL ERUPTIVE CENTERS IN THE MARK AREA

Wilfred B. Bryan, Susan E. Humphris, Geoffrey Thompson and John F. Casey

We describe selected examples of small volcanic features identified during ODP site surveys in the MARK area for which additional observations and sample data have been obtained by manned submersible and/or drilling. Based on both morphologic relations and similarities in chemistry and petrography, Serocki Volcano, the site of bare rock drilling on ODP legs 106 and 109, appears to be a flat-topped megatumulus, a large rootless vent developed on a lava flow originating from an adjacent cone located above the true eruptive fissure. A linear set of five apparent volcanic centers on the east side of the median valley (the EastMARK cones) differ from one another in morphology and degree of tectonic degradation. They formed at different times and from different vents, but all were localized by damming of the flows against the steep walls of the linear valley containing them. The two northernmost features are probably megatumuli at the terminal ends of lava flows descending the valley walls. The other three vents are cones with breached craters and probably were more recently erupted in situ. The Snakepit hydrothermal area is located near the highest and widest part of a 35km-long ridge that appears to be a major, relatively young fissure eruption. The associated lavas are among the geochemically most primitive in the MARK area, but have their counterparts in several subsets of lavas associated with Serocki Volcano in spite of the morphologic contrasts and large geographic separation between the two features. We conclude that a volcano-like form, geographic proximity, and conformance to a linear geometry do not guarantee compositional or temporal coherence, nor is the alignment of apparent volcanic centers a reliable guide to underlying tectonic patterns.

The chemistry and petrography of the Serocki and EastMARK basalts resemble older adjacent lavas and also conform to subtle along-ridge variations. This, and the relatively old appearance of their flow surfaces, indicate that these lavas represent the waning stage of an older magmatic event. The more recent eruptions in the Snakepit area seem to reflect a renewed influx of the same relatively primitive (and presumably hotter) magma that initiated the Serocki eruptions. Residual pockets of this hotter magma in the shallow crust may provide the heat that drives the present hydrothermal system.

Published in: *Journal of Geophysical Research*, 99(B2):2,973-2,984, 1994.

Supported by: NSF Grants OCE-8510079 and OCE-8510847.

WHOI Contribution No. 8475.

CRUSTAL STRUCTURE OF NORTH ATLANTIC FRACTURE ZONES

R. S. Detrick, R. S. White and G. M. Purdy

Seismic studies have established that large-offset transforms along the slow spreading Mid-Atlantic Ridge exhibit anomalous crustal structures that fall well outside the range typically associated with oceanic crust. Seismically, fracture zone crust in the North Atlantic is extremely heterogeneous in both thickness and internal structure. It is frequently quite thin (<1-2 km thick) and is characterized by low compressional wave velocities and the absence of a normal seismic layer 3. A more gradual crustal thinning can extend up to several tens of kilometers from these fracture zones. Anomalously thin crust has also been inferred from both seismic and gravity studies at smaller ridge axis discontinuities along the Mid-Atlantic Ridge. The geological nature of the seismically anomalous crust found within Atlantic fracture zones, and how this crust forms, are still controversial. One interpretation consistent with available seismic observations is that the crust within North Atlantic fracture zones consists of a thin, intensely fractured and hydrothermally altered basaltic section overlying ultramafics that, in places, are extensively serpentinized. Variations in apparent seismic crustal thickness along fracture zones may reflect different degrees of serpentinization of the upper mantle section or changes in the thickness of the igneous crust. The existence of a thinner crustal section in fracture zones can be explained by a reduced magma supply within a broad region near ridge offsets due to the three-dimensional nature of upwelling beneath a segmented spreading center and by tectonic dismemberment of the crust by large-scale

detachment faults that preferentially form in the cold, brittle lithosphere near the ends of segments.

Published in: *Reviews of Geophysics*, 31:439-458, 1993.

Supported by: National Science Foundation, Office of Naval Research and Natural Environment Research Council.

WHOI Contribution No. 8451.

HYDRODYNAMICAL MODELING OF A MULTIPLE-INLET ESTUARY/BARRIER SYSTEM: INSIGHT INTO TIDAL INLET FORMATION AND STABILITY

Carl T. Friedrichs, David G. Aubrey, Graham S. Giese and Paul E. Speer

Two specific questions are addressed concerning the role of tidal hydrodynamics in determining the long-term morphologic evolution of the Nauset Beach-Monomoy Island barrier system and the Chatham Harbor-Pleasant Bay tidal estuary, Massachusetts: (1) why do the barrier and estuary exhibit a long-term (~150 yhr) cycle of new inlet formation, and (2) once a new inlet forms, why is the resulting multiple inlet system unstable? To address these questions, a branched 1-d numerical model is used to recreate the basic flow patterns in the tidal estuary at ten-year intervals during the last half century and also to recreate flow conditions shortly before and shortly after the formation of the new inlet. Results suggest that an inlet will form through Nauset Beach once southerly elongation of the barrier has led to a critical head across the barrier at high tide. If this critical head (enhanced by storm surge and wave set-up) exists at high tide during consecutive tidal cycles, flood currents can deepen the overwash channel sufficiently to enable the stronger ebb currents to complete the formation process. Once a new inlet has formed, the surface gradient and tidal discharge are drastically reduced along the pre-existing channel to the south of the inlet. This reduction eliminates the tidal action needed to keep the channel open. Rapid shoaling within the channel to the south of the new inlet completes the hydrodynamic decoupling of the northern and southern sections of the estuary.

Published in: *Formation and Evolution of Multiple Tidal Inlets.* Coastal and Estuarine Studies, 44. American Geophysical Union, Washington, D.C., :95-112, 1993.

Supported by: NOAA Sea Grant NA88-AA-D-SG90, Town of Chatham, U.S. Army Corps of Engineering (New England Division), and CRC/WHOI.

WHOI Contribution No. 8317.

EQUILIBRATION DURING MANTLE MELTING: A FRACTAL TREE MODEL

Stanley R. Hart

Many basalts from oceanic islands, ridges and arcs show strong trace element evidence for melting at great depths, where garnet is a stable phase in mantle peridotites. If partial melts ascend to the surface by porous (intergranular) flow processes, the high-pressure garnet signature will be obliterated by diffusive re-equilibration at shallower depths in the mantle. Spiegelman and Kenyon argued that partial melts must therefore be focused into a coarser transport network, for high-speed delivery to the surface.

Numerous natural network systems, such as rivers and the human vascular and bronchial systems, have fractal structures which are optimal for minimizing energy expenditure during material transport. I show here that a fractal magma "tree" with these optimal properties provides a network in which magma rapidly loses diffusive chemical "contact" with its host matrix. In this fractal network, magma conduits combine by twos, with the radius and flow velocities scaling as $(2^{n/3}$, where n is the generation number. For reasonable values of volume diffusivities, viscosities and aspect ratios, melts will experience only limited diffusive re-equilibration once they have traveled some hundreds of meters from their source. Melts thus represent rather local mantle domains, and there is little problem in delivering melts with deep (<100 km) geochemical signatures to the surface.

Published in: *Proceedings of the National Academy of Science*, 90:11,914-11,918, 1993.

Supported by: NSF Grant EAR-9096197 .

WHOI Contribution No. 8483.

MESOZOIC-CENOZOIC SEDIMENTATION IN THE KANE FRACTURE ZONE, WESTERN NORTH ATLANTIC, AND UPLIFT HISTORY OF THE BERMUDA RISE

Gary E. Jaroslow and Brian E. Tucholke

Seismic reflection profiles, basement structure-contour maps, and bathymetric data are used to analyze sedimentation patterns over a distance of ~2300 km along the Kane Fracture Zone and to interpret uplift history of the Bermuda Rise. Sediments within the fracture valley thin seaward on younger crust and with distance from continental sources. Superposed on this pattern are the effects of local and regional basement structure, variations in surface-water productivity,

influence of bottom currents, and local effects of sediment redistribution. Preservation of a thicker and more complete sedimentary record within the Kane fracture valley facilitates identification and eastward correlation of seismic reflections, and we have cross-correlated these reflections to synthesize an along-axis transect of the fracture zone. Stratigraphic correlations of key reflections to Deep Sea Drilling Project drill sites determine the composition and ages of the lithologic sequences. Observed pinch-outs of seismic horizons J_1, β, and A* on fracture-valley crust extend significantly seaward of previously mapped limits, and the younger pinch-out ages accord better with ages defined by deep-sea drilling.

Paleosedimentation patterns in successive stratigraphic intervals document the growth of the continental margin/basin sedimentary prism from Late Jurassic time and the uplift of the Bermuda Rise beginning in middle Eocene time. Middle Eocene cessation of turbidite deposition atop the Rise, as identified by Horizon A^1, marks initiation of regional uplift. A seismic discontinuity in turbidite ponds east of the Rise records a probable pulse of uplift during early Oligocene time. Structure of the overlying seismic reflection sequence suggests continued uplift, albeit at decreasing rates, through the late Oligocene and possibly through Miocene time. The anomalous elevation of the Rise subsequently has been maintained, but there is no clear stratigraphic evidence for further growth.

Turbidite ponds fill the Kane fracture valley east of the Bermuda Rise and terminate against a prominent structural dam at 55°20'W. These ponds began to fill with turbidites in middle Eocene to early Oligocene time, and the sediments were derived from local sources. Within the past 10 - 12 m.y., turbidity currents began to enter the ponds through connections with the encroaching Nares Abyssal Plain, and they probably now constitute the dominant sediment source for the fracture valley.

In Press: *Geological Society of America Bulletin*, 106:319-337, 1994.

Supported by: ONR Grant N00014-82-C-0019, N00014-85-C-0001, N00014-87-K-0007 and NSF Grant OCE-8716713.

WHOI Contribution No. 8289.

TIDAL RESIDUAL CURRENTS AND SEDIMENT TRANSPORT THROUGH MULTIPLE TIDAL INLETS

James T. Liu and David G. Aubrey

Tidal residual currents in a tidal channel connecting two water bodies having contrasting tides are most sensitive to the mean sea-level differences, less sensitive to the tidal amplitude differences, and least sensitive to the tidal phase differences between the two ends of the channel. On the other hand, tidal phase difference is the most important factor in generating M_4 overtide in the channel, the tidal amplitude difference has intermediate impact on M_4 generation, and the mean sea-level difference has little effect on M_4 generation. Residual currents and M_4 overtide are generated by different mechanisms. The former is related to the friction in the system, and the latter is related to the kinematic non-linearity in the system. The combined influence of the tidal phase, amplitude, and mean sea-level differences on the generation of tidal residual currents in a channel is complex and non-linear and can be predicted properly only by non-linear numerical models. The sediment transport patterns in a tidal channel that connects two bodies of water having different tidal characteristics can be attributed to residual currents that is primarily caused by the mean sea-level difference, and to a minor degree, by the tidal amplitude and phase differences between the two ends of the channel. Multiple inlets at Chatham, Massachusetts, are used as a case study.

Published in: *Formation and Evolution of Multiple Tidal Inlets.* Coastal and Estuarine Studies, 44. American Geophysical Union, Washington, D.C., :113-157, 1993.

Supported by: NOAA Sea Grant No. NA86-AA-D-SG-90; Town of Chatham, Commonwealth of Massachusetts, Department of Environmental Management; Coastal Engineering Research Center, U.S. Army Corps of Engineers; and the Coastal Research Center.

WHOI Contribution No. 8318.

MORPHODYNAMIC EVOLUTION OF A NEWLY FORMED TIDAL INLET

James T. Liu, Donald K. Stauble, Graham S. Giese and David G. Aubrey

A unique opportunity to document and understand the processes of tidal inlet evolution and morphodynamic interactions presented itself with the breach of Nauset Spit across from the town of Chatham, Massachusetts. In the first twenty-eight months since its formation, the morphological evolution of the new inlet can be characterized into four categories: 1) Inlet mouth widening, caused by the concurrent retreats of the north and south spits that flank the inlet mouth; 2) Cyclical spit elongation, breaching, and terminal detachment; 3) The southward migration of the thalweg of the main channel and its associated shoals; and 4) Shoal growth. Six major shoals both seaward and landward of the inlet

mouth developed between inlet formation and 1991. The growth of shoals and spit elongation indicate the trapping of littoral sediments within the inlet mouth area and the influx of ocean sediments entering the lagoon through the new inlet. The southward movement of the inlet channel is driven by its own channel configuration. As a result of the formation of this inlet, Chatham Harbor has evolved into two separate systems, each having its own hydrodynamic and morphological characteristics.

Published in: *Formation and Evolution of Multiple Tidal Inlets.* Coastal and Estuarine Studies, 44. American Geophysical Union, Washington, D.C., :62-94, 1993.

Supported by: NOAA Sea Grant No. NA86-AA-D-SG-90; Town of Chatham, Commonwealth of Massachusetts, Department of Environmental Management; Coastal Engineering Research Center, U.S. Army Corps of Engineers; and the Coastal Research Center.

WHOI Contribution No. 8316.

CHAOTIC DEPOSITION BY A GIANT WAVE, MOLOKAI, HAWAII

J. G. Moore, W. B. Bryan and K. R. Ludwig

A coral-basalt breccia-conglomerate is exposed more than 60 m above present sea level and nearly 2 km inland from the present shoreline on the southwest side of East Molokai Volcano. The conglomerate mantles interfluves between gullies, and forms a blanket-like deposit 0.5 to 3 m thick. No evidence of a wavecut terrace either within the blanket or at its upper or lower limits of exposure can be found. No coral was found in growth position. Basalt clasts and boulders vary from 2-3 to more than 30 volume percent. Measurements made at 20 localities indicate that the material is unsorted; basalt clasts vary from subrounded to angular and the tabular clasts are randomly oriented. The estimated size of the largest basalt and coral fragments, and the proportion of basalt to coral clasts, show almost no systematic variation with elevation, distance inland, or lateral position parallel to the shore.

Two distinct rock units are present in a few places: a lower carbonate-rich unit which we interpret as an "onwash facies" and an upper basalt-rich unit that we interpret as an "offwash facies". The carbonate-rich onwash facies is dominated by biogenic debris, especially fragments of coral and beach rock, and gastropod and pelecypod shells. The offwash facies contains 40 to more than 90 percent basalt cobbles and boulders in a matrix of finely broken biogenic fragments; the more carbonate-rich offwash also contains larger coral and gastropod fragments. Elsewhere, distinct facies are lacking, but the proportion of basalt clasts increases crudely from the lower to the upper part of the conglomerate at a single place and from lower to higher elevation outcrops. Other local variants include a lower mud-rich facies, sometimes partly mixed into the conglomerate, and several carbonate-bearing clastic dikes beneath the conglomerate that cut basalt cinders.

This deposit was apparently laid down by a giant wave that broke over an outer reef, similar to the present fringing reef, and advanced as a turbulent bore over the backreef flat, picking up a slurry of carbonate-rich debris and depositing it on the slopes inland as the wave advanced. The offwash picked up loose basalt debris on its return flow. U-series dating of coral fragments indicate that the age of this deposit is 240-200 ka, indicating the wave is distinct from that which produced a similar deposit on Lanai about 100 ka. This giant wave was most likely caused by one of the many large submarine landslides that have been identified on the lower slopes of the major Hawaiian Islands.

In Press: *Geological Society of America Bulletin.*

Supported by: Vetlesen Account 30005900.

WHOI Contribution No. 8551.

PRESSURE-TEMPERATURE-TIME PATHS FROM TWO-DIMENSIONAL THERMAL MODELS: PROGRADE, RETROGRADE, AND INVERTED METAMORPHISM

C. Ruppel and K. V. Hodges

Two-dimensional thermal models of time-transitive crustal thickening and subsequent unroofing in large-scale overthrust terrains generate pressure-temperature-time (PTt) paths that generally resemble those produced by earlier one-dimensional instantaneous models, but that differ in detail. These differences in PTt path morphology are most pronounced proximal to major fault zones, where postthrusting geotherms are characterized by large temperature inversions in one-dimensional models. Tests using the two-dimensional fault model developed here indicate that (1) burial rate (proportional to dP/dt), not thrust fault geometry (dip angle), controls the topology of synthrusting PT paths, but plays only a minor role in determining the maximum temperature that rocks attain during the later, unroofing stage in their thermal histories; (2) normal ranges of thrusting and erosion rates and fault parameters result in PT paths with the usual sense (clockwise on conventional PT diagrams; counterclockwise in our diagrams); (3)

the amount of heating and duration of heating following the end of thrusting are a function of the rate of unroofing (-dP/dt) during this period; (4) fast unroofing rates lead to the attainment of lower maximum temperatures after greater amounts of unroofing; (5) the initial thermal state of the lithosphere prior to thrusting has a profound effect on PT path morphologies and on the peak metamorphic conditions attained by samples; (6) for excess heat, distributed across the entire lithosphere (e.g., due to increased background thermal gradients), a plot of peak temperatures experienced by metamorphic rocks versus structural depth (TMAX plot) closely represents the initial geotherm; (7) excess heat in the crust only (e.g., increased radioactive heating in a layer) yields a different result, with the TMAX plot corresponding to the initial geotherm only near the top of the hanging wall (TMAX plots for both (6) and (7) show no temperature inversion which exceeds the nominal uncertainties (±50K) for geothermometric data); (8) shear heating can lead to significant temperature inversions at the fault zone if the frictional coefficient μ is 0.6 or greater; and (9) simultaneous thrusting and erosion produce PT loops significantly narrower than those resulting from sequential thrusting and erosion, suggesting that any formulation which fails to account for some degree of simultaneity between thrusting and erosion represents a far endmember model. Forward models like those presented here provide important guidelines for understanding the sensitivity of metamorphic PTt paths to various thermal, mechanical, and geometric factors related to tectonism, but they are generally inappropriate for reconstructing metamorphic thermal histories from actual petrologic and geochronologic data. Analytical inversion techniques that use a postthrusting thermal regime, consistent with two-dimensional forward models, and that integrate values of dP/dt, dT/dt, and radioactive heating rates extracted from suites of metamorphic rocks provide the best hope for furthering our understanding of the thermal evolution of metamorphic terrains.

Published in: *Tectonics*, 13(1):17-44, 1994.

Supported by: WHOI Postdoctoral Fellowship.

WHOI Contribution No. 8476.

BUILDING THE CRUST AT THE MID-ATLANTIC RIDGE

Deborah K. Smith and Johnson R. Cann

The morphology of the seafloor at mid-ocean ridge spreading centers provides a key to understanding how ocean crust is constructed. Images of the axial zone of the slow spreading Mid-Atlantic Ridge, obtained at a range of spatial scales, show that crustal construction is complex and highly variable, reflecting the three-dimensional variability in magmatic, tectonic, and hydrothermal processes.

In Press: *Nature*, 365, 1993.

Supported by: ONR Grant N00014-90-J-1615.

WHOI Contribution No. 8519.

SPRING SAPPING ORIGIN OF THE ENIGMATIC RELICT VALLEYS OF CAPE COD AND MARTHA'S VINEYARD AND NANTUCKET ISLANDS

Elazar Uchupi and Robert N. Oldale

Eroded on the outwash plains of Cape Cod, Martha's Vineyard and Nantucket islands are steep-sided, flat-floored linear valleys with amphitheater-like heads and lacking well developed tributaries. The valleys are restricted to the outwash plains and show no connection to possible water sources at the updip end of the plains. Their distribution and morphology lead us to propose that the valleys were eroded by groundwater seeps fed by proglacial lakes (their high hydrostatic heads led to the elevation of the water table) dammed by the outwash plains and associated moraines. The valleys on Cape Cod were initiated by seeps along the foreset surfaces of sandy deltas emplaced in lakes in Nantucket Sound and Cape Cod Bay after these lakes drained. The valleys on Martha's Vineyard and Nantucket islands were either eroded by seeps at the distal ends or toes of outwash plain wedges emplaced atop the subareal continental shelf south of the islands or along the foreset surfaces of sandy deltas emplaced on a lake behind a peripheral crustal bulge south of the glacial front. Valley erosion terminated after the lakes were drained and the water table dropped.

In Press: *Geomorphology.*

Supported by: None.

WHOI Contribution No. 8309.

CYCLIC SPIT MORPHOLOGY IN A DEVELOPING INLET SYSTEM

Christopher R. Weidman and James R. Ebert

A spit attached to the north end of South Beach, a barrier island in Chatham, Massachusetts, exhibits a cyclic pattern of accretion, breaching, and shoal generation. The flood-oriented spit is within a large (2 km wide)

developing tidal inlet system that was formed when Nauset Beach was breached in January 1987. Five cycles of spit growth and breaching have been observed in two years. Each cycle is characterized by: 1) elongation of spit for several months; 2) gradual narrowing and eventual breaching of the spit's mid-section, which creates a small tidal channel and terminates the growth cycle; and 3) evolution of the detached distal portion of the spit from a supratidal island to subtidal shoals. The growth and breaching of this spit are significant processes causing landward sediment transport within the inlet system. A conceptual model is offered which explains the cyclic behavior of this system as the result of interrelated morphological, tidal, and climatic controls.

Published in: *Formation and Evolution of Multiple Tidal Inlets.* Coastal and Estuarine Studies, 44. American Geophysical Union, Washington, D.C., :186-212, 1993.

Supported by: NOAA Sea Grant No. NA86-AA-D-SG-90; Town of Chatham, Commonwealth of Massachusetts, Department of Environmental Management; Coastal Engineering Research Center, U.S. Army Corps of Engineers; and the Coastal Research Center.

WHOI Contribution No. 8322.

GEOPHYSICS

THE MAGMA BODY AT KILAUEA IKI LAVA LAKE: POTENTIAL INSIGHTS INTO MID-OCEAN RIDGE MAGMA CHAMBERS

G. A. Barth, M. C. Kleinrock and R. T. Helz

Kilauea Iki is an extensively studied passive lava lake formed during the 1959 eruption of Kilauea Volcano. The lava lake magma body has been the site of a time-series of boreholes, with core recovery near 100% for each of the 23 deep holes drilled since 1967. Geophysical studies including active and passive seismics and electromagnetic profiling have yielded remotely-gathered images of the lake contents. This contribution first presents an overview of the geological and geophysical observations from the lava lake, including some new data, and a reinterpretation of the results. Despite the fact that the analogy is imperfect, observations at Kilauea Iki lead to insights into processes at mid-ocean ridge magma chambers. The data suggest fine structure at the top of the mid-ocean ridge magma body in the form of horizontal segregation veins (e.g., sills) and indicate that sustained convection at a mid-ocean ridge magma chamber is highly unlikely. The lava lake also exhibits a dry-out zone above the magma body and below the deepest penetration of hydrothermal circulation; a similar zone may exist under mid-ocean ridge conditions. Physical and petrologic constraints at the lava lake and at mid-ocean ridges strongly suggest very rapid and frequent replenishment of mid-ocean ridge magma chambers at high magma supply ridges where quasi-steady-state melt zones are present.

In Press: *Journal of Geophysical Research.*

Supported by: ONR Contract N00014-89-J-1021.

WHOI Contribution No. 8290.

MANTLE-PLUME-HEAD INSTABILITIES AND VENUS CORONAE

David Bercovici and Jian Lin

Coronae on Venus are possibly the surface expression of mantle plumes or melt induced diapirs. Venus coronae commonly display circular ridges and moats which have been explained in terms of viscous relaxation of diapirically uplifted plateau, or in the case of large coronae, flexural response to subduction. However, discrepancies between these models and observations, as well as the likely rheological weakness of Venus' lithosphere, warrant investigation of alternative mechanisms. Plume-head instabilities may provide the necessary dynamics for the formation of corona structures. Here we specifically examine the plume-head wave (PHW) instability which has been suggested to occur in laterally spreading sublithospheric plume heads. A simple theoretical analysis implies that terrestrial plume heads are susceptible to this instability, which is expressed as growing perturbations in plume-head thickness and temperature. The dominant instability can appear as a plateau bounded by a moat and with a slight central depression; this is strongly reminiscent of the essential corona structure. Transient wave-like perturbations lead to features suggestive of secondary corona structures. Basic plume-head dynamics is thus capable of generating corona-like morphology and therefore provides a simple alternative mechanism for the formation and evolution of Venus coronae.

Submitted to: *Nature.*

Supported by: Subcontract to University of Hawaii No. 8936001 (Prime NASA Grant NAGW-3531).

WHOI Contribution No. 8459.

DEEP STRUCTURE OF THE EARTH: CONSTRAINTS PROVIDED BY SPATIAL VARIABILITY OF THE GRAVITY POTENTIAL FIELD AND ITS VERTICAL DERIVATIVES

Carl Bowin

From spherical harmonic coefficients for the Earth's gravity potential field, plots of Cumulative Contribution Curves (CCC) at the center locations of the Earth's major geoid anomalies demonstrate that the Earth's regional degree 10 field (which has virtually no relation with surface topography and plate tectonic pattern) is comprised of two distinct packets of mass anomalies. The greatest mass anomalies are represented in the spherical harmonic degrees 2-3 packet and account for the strong 'red' power spectrum of our planet. The second largest mass anomalies are reflected in the degree 4-10 packet which has linear belts of positive mass anomalies in a pattern consistent with present day subduction zone sites. The masses of the residual geoid anomalies (i.e. represented in spherical harmonic degrees 11 to infinity) are very small compared to the masses producing the magnitude of the degree 2-3 contribution. Fortunately, two small cracks in the opaque gravity window have been identified and utilized to provide definitive constraints on the depths to both of the great mass anomalies within the Earth's deep interior. Crack number 1 recognizes that the "cone of solutions" diagram (which shows the equivalence of surface anomaly patterns from broad shallow mass distributions with deep compact mass anomalies, and therefore the inability to distinguish deep from shallow sources) is only completely valid for an infinite flat Earth. A consequence of this recognition, and new methodology for estimating point mass depths from harmonic degree contributions at geoid anomaly center locations, demonstrate that the degrees 2-3 field of the Sri Lanka/Indian low and the New Guinea high must arise from mass anomalies in the lower mantle or deeper. To achieve the great magnitude of the requisite mass anomalies, vertical perturbations of the core/mantle boundary are the most reasonable source because of the 4.4 gm/cc density contrast across that boundary, and the lack of strong seismic tomography velocity anomalies at the lowermost mantle. Crack number 2 recognizes that analyses of multiple vertical derivatives of the potential field are useful in identifying whether at a particular location mass anomalies at multiple depths contribute to an anomaly observed at the surface. It is demonstrated that the geoid high at the South America Andes is caused by a mass anomaly at about 1200 km depth and that it is part of the 4-10 degree packet. A phase change of the subducted lithosphere to high density material in the lower mantle is inferred to account for the degree 4-10 linear belt of positive mass anomalies. These mass anomalies thus also confirm that whole mantle convection occurs in the Earth and contributes to plate tectonics. The hotspot plume sources for Iceland and Crozet, which have prominent geoid contributions from degrees 3 through 6, therefore lies in the lowermost lower mantle.

Submitted to: *Tectonophysics.*

Supported by: ONR Grant N00014-90-C-0098 and the World Gravity Project.

WHOI Contribution No. 8595.

ON ELECTRIC AND MAGNETIC GALVANIC DISTORTION TENSOR DECOMPOSITIONS

Alan D. Chave and J. Torquil Smith

The physics governing galvanic distortion of natural source electromagnetic induction measurements is re-examined beginning from first principles. The conditions under which a tensor decomposition of measured magnetotelluric response tensors and magnetic transfer functions is applicable are described, and the form of the decomposition describing distortion of the electric and magnetic fields is derived directly from the integral equation describing the scattering of electric and magnetic fields by surface heterogeneities. The inclusion of magnetic field galvanic distortion is shown to lead to indeterminacy in the regional magnetotelluric response in the form of scaling by frequency-dependent, complex factors controlled by two unknown real constants. This is a generalization of the well-known static shift effect from electric field galvanic distortion, and can be resolved if the magnitude and phase of the regional response are known at some frequency. Distortion of the magnetic transfer function is shown to be even more indeterminate, containing a term proportional to one of the regional magnetotelluric responses which is inseparably additive to the regional transfer function, as well as the complex scaling seen for magnetotellurics. A set of simultaneous nonlinear equations describing the full electric and magnetic field galvanic distortion decomposition of the magnetotelluric response tensor and magnetic transfer function is derived, and methods for their solution, including implementation of jackknife error estimates, is described. The full magnetotelluric decomposition is applied to severely distorted data from the Canadian shield and seafloor data from the

EMSLAB experiment. In both cases, magnetic field galvanic distortion is important at periods under a few thousand seconds. This suggests that greater attention to galvanic distortion of the magnetic field is needed during magnetotelluric surveys.

In Press: *Journal of Geophysical Research.*

Supported by: NSF Grant OCE-9196236.

WHOI Contribution No. 8489.

SEISMIC CONSTRAINTS ON SHALLOW EMPLACEMENT PROCESSES AT THE FAST-SPREADING EAST PACIFIC RISE

G. L. Christeson, G. M. Purdy and G. J. Fryer

We present the results of nine on-bottom seismic refraction experiments carried out over young East Pacific Rise crust. The experiments are unusual in that both the source and receiver are located within a few meters of the seafloor, allowing high-resolution determinations of shallow crustal structure. Three experiments were located within the axial summit caldera (ASC), over 'zero-age' crust. The seismic structure at these three locations is fundamentally the same, with a thin (<60 m) surficial low-velocity (<2.5 km/s) layer, an ~100-150 m thick transition zone with velocities increasing by ~2.5 km/s, and a layer with velocities of ~5 km/s at a depth beneath the seafloor of ~130-0190 m. The surficial low-velocity layer and transition zone are defined as seismic layer 2A, and the ~5 km/s layer as the top of layer 2B. Both the surficial low-velocity layer and the transition zone double in thickness within ~1 km of the rise axis, with the depth to the 2A/2B boundary increasing from ~150 m to ~300-250 m over this range. The seafloor velocities increase from ~2.1-2.35 km/s for zero-age crust to ~2.4-2.85 km/s for 10,000 to 120,000 year old crust, consistent with a decrease in porosity from ~27% to ~20%. Amplitude modeling of the on-bottom seismic refraction data determines that the Poisson's ratio at the seafloor must be at least 0.43, suggesting that the shallow crustal porosity is largely due to high-aspect ratio cracks. Our preferred seismic model includes high attenuation within layer 2A (Qp~25), and lower attenuation (Qp~500) in layer 2B. We model layer 2A as the extrusive sequence and transition zone, and the 2A/2B boundary as the top of the sheeted dikes. The thickening of the extrusive layer is interpreted to be due to lava that either overflows the ASC walls, is emplaced through eruptions outside of the ASC, or travels laterally from the ASC through conduits. According to this model, the shallow crustal architecture is in place within 1 km of the rise axis. A comparison with the structure observed from drilling at DSDP Hole 504B suggests that the subsidence of the sheeted dikes is more than double at intermediate-spreading centers (~800 m) than for the fast-spreading EPR (~300-350 m). Additionally, this implies that the volume of magma emplaced as extrusives at intermediate spreading centers is at least as great as that emplaced at fast-spreading centers.

Submitted to: *Journal of Geophysical Research.*

Supported by: ONR Grant N00014-89-J-1015 and NSF Grant OCE-8917750.

WHOI Contribution No. 8597.

THE SHALLOW ATTENUATION STRUCTURE OF THE FAST-SPREADING EAST PACIFIC RISE NEAR 9°30'N

G. L. Christeson, W. S. D. Wilcock and G. M. Purdy

Seven on-bottom seismic refraction experiments are analyzed in an effort to resolve the shallow compressional wave attenuation structure of young crust at the fast-spreading East Pacific Rise. All models depict a low-Q layer 2A (apparent Q=11-22), and several models resolve a layer 2B with a much higher Q (apparent $Q > 70$). This structure is consistent with a layer 2A composed of extrusives overlying a layer 2B composed of sheeted dikes.

In Press: *Geophysical Research Letters.*

Supported by: ONR Grant N00014-89-J-1015.

WHOI Contribution No. 8602.

FLOW STRUCTURE AND DISPERSION WITHIN ALGAL MATS

J. Escartin Guiral and David G. Aubrey

Shallow-water estuaries such as Waquoit Bay (Cape Cod, Massachusetts) are characterized by the presence of large algal mats with thicknesses that can represent more than 25% of the total water depth. Flume experiments show these algal mats strongly affect the hydrodynamic circulation by reducing the effective water depth and increasing the friction between the flow and the top of the algal mat. Approximately 90% of the total water flux occurs over the algal mat whereas less than 10% flows through the mat itself. The flow over the algae corresponds to a shear flow, but within the mat it has the characteristics of a pressure-driven flow, with shear restricted to the upper and lower boundaries of the algal mat. Estimated vertical dispersion coefficients within

the algal mat vary between 0.03 and 1.6 cm^2/s, and are comparable or one order of magnitude larger than those calculated for the shear flow over the algal mat. Experiments also revealed that the observed flow characteristics and dispersion coefficients are insensitive to the density of the algal mat, mean flow velocity and/or water depth for the range of parameters used throughout the experiments, indicating that heterogeneities within the mat are important. The introduction of buoyancy forcing due to internally-produced heat (as a product of metabolism and/or decomposition of organic matter) or solar heating of the algal mat considerably augments the turbulent kinetic energy; a 1.5°C increase of the water temperature at the base of the algal mat augments the vertical dispersion coefficients by a factor of three.

In Press: *Coastal, Estuarine and Shelf Sciences.*

Supported by: Subcontract from Boston University, NSF LMER Contract OCE-8914729 and Caixa de Pensiones"La Caixa" Fellowship.

WHOI Contribution No. 8374.

TERRESTRIAL HEAT FLOW IN LAKE SUPERIOR

S. R. Hart, J. S. Steinhart and T. J. Smith

Using oceanographic heat flow techniques, 162 measurements of heat flow were made in Lake Superior during the summers of 1966 and 1967. This data is of high quality, with precisions with respect to intercomparisons typically in the 3-5% range. The data define two very clear features. One is a trough of low heat flow values which runs continuously for 650 km along the northern edge of the lake, with values ranging between 0.46-0.98 HFU. This feature correlates with surface exposure of Keweenawan mafic volcanics, and is believed to delineate a major crustal separation associated with the Mid-Continent Rift, and filled to crustal thicknesses with mafic intrusives and extrusives. This feature has not been imaged with the seismic reflection profiling of GLIMPCE. The other heat flow feature is an arcuate ridge of high (1.0-1.45 HFU) heat flow values, parallel to and south of the heat flow trough. The highest areas of this ridge correspond to areas of thick rift-filling Keweenawan sediments. The high heat flow is modulated to lower values in areas where the thick sediments overlie highly-thinned crust now containing large thicknesses of mafic volcanic rock. The heat flow features show very good correlation with the magnetic anomaly map of Lake Superior, but only spotty correlation with the Bouguer gravity anomaly features.

In Press: *Canadian Journal of Earth Sciences.*

WHOI Contribution No. 8311.

SUPPRESSION OF PREVIOUS SHOT NOISE ON MARINE WIDE-ANGLE SEISMIC DATA

W. Steven Holbrook and Edmund C. Reiter

Wide-angle, ocean-bottom seismic data recorded during shooting of marine multichannel seismic data often contain previous shot noise (PSN) – high-amplitude, low-apparent-velocity water-borne noise – that interferes with deep crustal reflections and refractions. In data shot at a constant distance interval, PSN is incoherent and thus resistant to elimination by standard processing techniques. We present a simple and effective technique for suppressing PSN by applying static shifts to align the PSN, followed by FK filtering and unshifting. The efficacy of this technique implies that PSN should not be a major consideration in designing joint multichannel/wide-angle seismic surveys. In particular, there is no need to sacrifice dense shot spacing or to shoot MCS and wide-angle data separately, simply to avoid recording PSN.

In Press: *Geophysics.*

Supported by: NSF Grant OCE-8917599.

WHOI Contribution No. 8276.

DEEP STRUCTURE OF THE U.S. ATLANTIC CONTINENTAL MARGIN, OFFSHORE SOUTH CAROLINA, FROM COINCIDENT OCEAN-BOTTOM AND MULTICHANNEL SEISMIC DATA

W. S. Holbrook, E. C. Reiter, G. M. Purdy, D. Sawyer, P. L. Stoffa, J. A. Austin, Jr. , J. Oh and J. Makris

We present the results of a combined multichannel seismic reflection (MCS) and wide-angle, ocean-bottom seismic profile collected in 1988 across the Carolina Trough on the U.S. East Coast continental margin. Inversion of vertical-incidence and wide-angle traveltime data has produced a velocity model of the entire crust across the continent-ocean transition. The margin consists of three structural elements: (1) rifted continental crust, comprising 1-4 km of post-rift sedimentary rocks overlying a 30-34 km thick subsedimentary crust; (2) transitional crust, a 60- to 70-km-wide zone comprising up to 12 km of post-rift sedimentary rocks overlying a 10- to 22-km-thick subsedimentary crust; and (3) "marginal" oceanic crust, comprising 8 km of sedimentary rocks overlying an 8-km-thick crystalline crust. The transitional crust, which includes seaward-dipping reflections observed on the MCS section in the mid-crust, has high seismic

velocities in the mid-crust (6.5-6.9 km/s) and lower crust (7.1-7.5 km/s). Modeling of potential field data shows that the transitional crust also produces the prominent, margin-parallel gravity and magnetic anomalies (e.g., the East Coast magnetic anomaly). These observations support the interpretation that the transitional crust was formed by volcanism during continental separation. The prodigious thickness (up to 22 km) of igneous material rivals that interpreted on continental margins of the North Atlantic (e.g., Hatton Bank and Vøring Plateau), which formed in the vicinity of the Iceland hotspot. This result is not easily explained by existing models of rift-margin volcanism, in view of the lack of an obvious nearby hotspot track or of basement structure associated with secondary convection models. This suggests either that the Cape Verdes hotspot was much closer to the Carolina Trough margin during continental separation than previously thought, or that the voluminous volcanism was unrelated to a hotspot.

In Press: *Journal of Geophysical Research.*

Supported by: NSF Grant OCE-8917599.

WHOI Contribution No. 8277.

MANTLE TEMPERATURES ALONG THE PRESENT AND PALEO-AXES OF THE GALAPAGOS SPREADING CENTER AS INFERRED FROM RESIDUAL GRAVITY ANALYSES

Garrett T. Ito and Jian Lin

To better understand the effects of hot spots on mid-ocean ridge thermal structure, we investigate the subsurface density structure of the Galapagos spreading center and nearby lithosphere of ages zero to ~7.7 m.y. Using shipboard gravity and bathymetry data, we obtain maps of mantle-Bouguer anomalies by removing from the free-air gravity the attractions of seafloor topography and a 6-km-thick model crust; we also obtain maps of residual mantle-Bouguer anomalies (RMBA) by further removing the 3D gravity effects of a cooling lithosphere. Comparison of observed and theoretical mantle-Bouguer gravity profiles along isochrons for ages 0.0-7.7 m.y. suggest that seafloor topography is isostatically compensated by mass anomalies primarily in the upper 100 km of the mantle. This result is consistent with the notion that seafloor topography along the Galapagos spreading center is supported by lateral changes of crustal thickness and mantle density, both of which are controlled by temperatures in the upper mantle where decompression melting occurs. Along the ridge axis, the RMBA decreases from the east and west toward the Galapagos hot spot by ~110 mgal, reaching a minimum nearest the hot spot at 91°W. Seafloor topography mirrors the RMBA along axis, increasing by ~1.2 km toward the hot spot. These variations in RMBA and bathymetry can be explained by crustal thickening and mantle density variations resulting from a gradual axial temperature increase of 65±30°C towards the hot spot. We predict a crustal thickening of 2-4 km nearest the hot spot, accounting for 70-80% of the along-axis RMBA and 60-80% of the along-axis bathymetric anomaly; mantle density variations account for the rest of the anomalies. The mantle temperature gradient along-axis, however, is only a small fraction (~5-10%) of the temperature gradient from the Galapagos hot spot to the ridge axis. Studies of off-axis mantle Bouguer anomalies further suggest that approximately 7.7 m.y. ago, when the hot spot was near or at the ridge axis, the temperature anomaly beneath the spreading center was ~180°C; such a value is much higher than the present-day ridge axis temperature anomaly (~65°C) but very close to the estimated temperature anomaly (~200°C) beneath the Galapagos Archipelago. This result suggests that the mantle temperature anomaly of the Galapagos hot spot has remained approximately constant in the past ~7.7 m.y.; but as the hot spot migrated away from the ridge axis, its effect on the along-axis temperature anomaly decreased in proportion to the increasing distance separating the hot spot and the ridge axis.

Submitted to: *Journal of Geophysical Research.*

Supported by: NSF Grant OCE-9020408 and ONR Grant N00014-91-J-1433.

WHOI Contribution No. 8601.

THE UNIFORM ACCRETION OF OCEANIC CRUST SOUTH OF THE GARRETT TRANSFORM AT 14°15'S ON THE EAST PACIFIC RISE

Graham M. Kent, Alistair J. Harding, John A. Orcutt, Robert S. Detrick, John C. Mutter and Peter Buhl

Using migrated common depth point reflection profiles, we find the structural differences along the ultrafast spreading (> 150 mmy/yr) East Pacific Rise south of the Garrett fracture zone are second-order suggesting a remarkably uniform process of crustal accretion. The rise axis south of the Garrett transform is underlain by a narrow (< 1.0-km) melt lens which shows great along-strike continuity. The depth of the axial melt sill is approximately 1200 m beneath the seafloor which is about 400 m shallower than along the slower spreading East Pacific Rise at 9°30'N. This

observation strengthens the argument that the depth to the top of the crustal velocity inversion is spreading rate dependent. Melt sill width, however, shows little variation along the East Pacific Rise, suggesting no dependence of magma chamber size on spreading rate. The melt reservoir decreases in width toward/across the 14°27'S ridge axis discontinuity by a modest 250-300 m and appears to be continuous across this feature. Given the small aspect ratio (~1.0 km by ~50 m by ten's kilometers) of the axial melt lens, the previously recorded jump in MgO content across the 14°27'S offset is likely the result of a mixing boundary which is sustained through an along-strike impedance in convection. Wide-angle reflections originating at the base of seismic layer 2A, assumed to coincide with the extrusive layer, reveal a twofold to threefold increase (200-250 to 500-600 m) in thickness within 1-2 km of the rise axis. The pattern of extrusive thickening imaged south of the Garrett transform is similar to that observed along the slower spreading (110-120 mm/yr) East Pacific Rise at 9°N. Outside of the neovolcanic zone mean extrusive thickness is relatively invariant along a profile and from profile to profile. This implies a degree of temporal stability of along-strike magma supply when integrated over the 10 ka that corresponds to the width of the neovolcanic zone. The inferred uniformity of off-axis mean extrusive thickness is inconsistent with the conjecture that decreases in axial volume toward the 14°27'S discontinuity are caused by long-term reductions in magma supply. Second-order differences in the style of extrusive thickening may be related to structural differences within the low-velocity zone underlying the rise axis, and/or changes within the stress field in the overlying carapace which results in the diffuse emplacement of lavas near the rise axis. Images of Moho on cross-axis profiles may be traced to within ~1.0 km of the melt sill edge; this observation is in agreement with recent rise crest models which generate the lower crustal section through the advection of material down and outward from the axial melt lens rather than through cumulate deposition at the base of a large magma chamber.

In Press: *Journal of Geophysical Research.*

Supported by: NSF Grant OCE-9012596.

WHOI Contribution No. 8378.

STATIC STRESS CHANGES AND THE TRIGGERING OF EARTHQUAKES

Geoffrey C. P. King, Ross S. Stein and Jian Lin

To understand whether the 1992 M=7.4 Landers earthquake changed the proximity to failure on the San Andreas fault system, we examine the general problem of how one earthquake might trigger another. We use the Coulomb criterion, in which changes in both the shear and normal stress influence a fault's tendency to failure. As a result of an earthquake, the Coulomb stress change on a particular fault depends on its geometry, sense of slip, and the coefficient of friction. We use this method to calculate stress changes on the San Andreas and San Jacinto faults caused by the Landers event. We further consider a Coulomb criterion appropriate for the production of aftershocks, where faults most likely to slip are those optimally oriented for failure as a result of the regional stress and the stress change caused by the main shock. We find that the distribution of aftershocks for the Landers earthquake, as well as several other moderate events in its vicinity, can be explained by the Coulomb criterion: aftershocks are abundant where the Coulomb stress on optimally oriented faults rose by more than one-half bar, and aftershocks are sparse where the Coulomb stress dropped by a similar amount. We find that several moderate shocks raised the stress at the future Landers epicenter and along much of the Landers rupture zone by about a bar, advancing the Landers shock by perhaps a century. The Landers rupture, in turn, raised the stress at site of the future M-6.5 Big Bear aftershock site by 3 bars, and together the Landers and Big Bear earthquakes raised the stress along the San Bernardino segment of the southern San Andreas fault by 5 bars, hastening the next great earthquake there by about a decade.

In Press: *Bulletin of the Seismological Society of America.*

Supported by: Subcontract to University of Southern California No. 608805 (Primary Grant NSF EAR-8920136).

WHOI Contribution No. 8479.

THE SOUTHEASTERN BOUNDARY OF THE JUAN FERNANDEZ MICROPLATE: BRAKING MICROPLATE ROTATION AND DEFORMING THE ANTARCTIC PLATE

Martin C. Kleinrock and Robert T. Bird

Data from a 1991 multibeam, sidescan sonar, and geophysical survey of the Juan Fernandez microplate at the Pacific-Nazca-Antarctic triple junction strongly support a model of edge-driven microplate rotation. They reveal the nature of the microplate's southeastern boundary with the Antarctic plate and show that plate boundary interactions are capable of significantly altering plate motions. Microplate rotation slowed

progressively from >30°/m.y. to <10°/m.y. between Anomaly 2 time (~1.9 Ma) and the early Brunhes (~0.6 Ma). Magnetics, bathymetry, and morphology suggest that this deceleration resulted from coupling across a rapidly evolving Juan Fernandez-Antarctic (JF-A) plate boundary. Over the past ~2 m.y., the JF-A plate boundary has lengthened, changed orientation, and migrated to the southeast, into the Antarctic plate. This deformed and transferred to the Juan Fernandez plate about 3000 km^2 of the Antarctic plate. Curved lineaments within this deformed zone are thought to represent N-S abyssal hills originally generated at the Pacific-Antarctic Ridge that were later sheared by dextral slip bookshelf faulting within the migrating sinistral shear zone of the JF-A boundary. This is supported by kinematic and morphologic observation. Deformation within this system documents that shear zone migration, not rift propagation, is the key process associated with development of carved lineaments and transferred lithosphere. The JF-A plate boundary shear-zone may have been quite narrow (~10-20 km) despite its migration through the Antarctic plate. Narrow migrating plate boundaries are also observed at other systems, such as the Galapagos 95.5°W migrating offset which too has a width of ~20 km. Such narrow deformation zones may be common along migrating plate boundaries in a variety of tectonic environments. Triple junction systems in this area appear to represent a suite of plates and triple junctions crossing a range of scales. The observations here support models for triple junctions having complex evolutionary histories involving rapid changes in plate boundary configuration and stress field.

In Press: *Journal of Geophysical Research.*

Supported by: NSF Grant OCE-8917941.

WHOI Contribution No. 8292.

CONSTRUCTION AND DESTRUCTION OF VOLCANIC KNOBS AT THE COCOS-NAZCA SPREADING SYSTEM NEAR 95°W

Martin C. Kleinrock and Benjamin A. Brooks

Characterization of volcanic knobs observed in Sea Beam bathymetry near the 95°W Galapagos propagator system on the Cocos-Nazca spreading axis provides insight into volcanic and tectonic processes at propagators and mid-ocean ridges. Despite evidence suggesting a higher magma supply rate at the propagator axis, crust accreted there contains fewer knobs than crust created at the failing or doomed spreading axes. Figure-fed flows rather than seamount construction are more important along the propagator. The process of transferring lithosphere via bookshelf faulting from one plate to another as this ridge offset migrates through a region destroys about half of the knobs on preexisting crust. Sparse data tentatively suggest that at slow and intermediate spreading rates on-axis volcanic cones increase in size and contribution to crustal construction but decrease in abundance with decreasing spreading rate.

In Press: *Geophysical Research Letters.*

Supported by: ONR Grants N00014-91-J-1434, N00014-89-J-1021 and NSF Grant OCE-8822199.

WHOI Contribution No. 8291.

LARGE-SCALE ELECTRIC FIELD MEASUREMENTS ON THE EARTH'S SURFACE: A REVIEW

L. J. Lanzerotti, A. D. Chave, C. H. Sayres, L. V. Medford and C. G. Maclennan

There exist only a few reported measurements of quasi-stationary (near DC) electric potentials over very large spatial scales (hundreds of kilometers or more) on the Earth's surface. Such measurements have typically been made using unpowered submarine telecommunications cables. The measurements pose unique experimental challenges and require careful procedures to avoid data contamination by electrode contact potentials and local ground currents. In addition, there are possible interpretation problems from pervasive, poorly understood, low frequency electric fields induced by ocean water motion through the Earth's stationary magnetic field. Nevertheless, estimates of the magnitude of the electric field computed from large-scale potential difference measurements, made principally to date in the Pacific Ocean, can be used to place a limit on the size of the toroidal magnetic field at the core-mantle boundary under certain conditions on the Earth's electrical conductivity profile. Thus, large-scale electric potential measurements can serve as an adjunct probe of the Earth's dynamo process in addition to measurements of the poloidal magnetic field and its secular changes made at and above the surface of the Earth. A review of all of these data suggests that the toroidal and poloidal magnetic fields at the top of the core are comparable in magnitude.

Published in: *Journal of Geophysical Research,* 98:23,525-23,534, 1993.

Supported by: NSF Grant EAR-9121278.

WHOI Contribution No. 8249.

SURFACE AND SUBSURFACE TECTONIC LOADING ON THE OCEANIC LITHOSPHERE AT THE MID-ATLANTIC RIDGE

Jian Lin and Y. John Chen

The oceanic plates deform in response to both subsurface loading from crustal and mantle density anomalies and surface loading from seafloor topography. By finite-element modeling of gravity and topography data collected over the Mid-Atlantic Ridge between 27°and 31°N, we estimate the relative importance of subsurface and surface loads on the young oceanic plates. We show that subsurface loading may cause ~300-800 m of seafloor deepening near non-transform offsets and ~1100 m of deepening near the Atlantis FZ. After subsurface loads are removed, the residual topography reveals a rift structure with strong asymmetry. The degree of asymmetry is, however, smaller near non-transform offsets than near the Atlantis transform fault. Further theoretical modeling reveals that the enhanced asymmetry near the Atlantis transform is partially caused by regional isostatic compensation of the deep transform valley. Such three-dimensional effects are smaller at non-transform offsets because of the lack of a deep transform valley there.

Submitted to: *Geophysical Research Letters.*

Supported by: NSF Grant OCE-9012576 and ONR Grant N00014-91-J-1433.

WHOI Contribution No. 8619.

WAVELET ANALYSIS OF A BATHYMETRIC PROFILE REVEALS ANOMALOUS CRUST

Sarah A. Little, Patricia Carter and Deborah Smith

A 200 km anomalous topographic zone was discovered using wavelet scale analysis in a 1600 km linear Sea Beam profile taken northeast of Hawaii. A spectral analysis of the zone shows that the power in wavelengths shorter than 25 km averages 5-10 times lower than the surrounding topography. Conversely, wavelengths longer than 25 km have 2-3 times greater power than nearby topography. Further research reveals that this low-frequency zone correlates with the eastern flank of a regional bathymetric high which has been described by J. Mammerickx (1981). Details of the features suggest that this zone is a small, abandoned, slow-spreading rift overprinted by a regional thermal swell. The magnitude of the feature is smaller than other, known, abandoned spreading centers, making it easy to overlook without the application of the wavelet transform.

Published in: *Geophysical Research Letters,* 20(18):1,915-1,918, 1993.

Supported by: ONR Grant N00014-93-1-0179.

WHOI Contribution No. 8419.

CRUSTAL STRUCTURE ACROSS THE BRUNSWICK MAGNETIC ANOMALY, OFFSHORE GEORGIA, FROM COINCIDENT OCEAN-BOTTOM AND MULTICHANNEL SEISMIC DATA

Daniel Lizarralde and W. Steven Holbrook

We present results from a coincident wide-angle and deep-penetrating, multichannel reflection seismic experiment conducted on the continental shelf of the Southeast Georgia Embayment. Over 5000 airgun shots were recorded by a 6-km-long, towed streamer and six ocean-bottom seismic instruments along a ~250-km north-south profile crossing the Brunswick magnetic anomaly (BMA). These data indicate a transition in seismic properties across the BMA, including higher seismic velocities south of the BMA, particularly in the upper crust (7-15 km depth), and a transition from reflective to transparent crust from north to south. We interpret this transition to be the result of massive mafic intrusion south of the BMA. This interpretation and magnetic modeling based on our seismic results support previous suggestions that the BMA is sourced by mafic material emplaced outboard of the BMA. We suggest that the distribution of this material is controlled by Mesozoic extensional features and not an Alleghanian suture, for which there is no clear indication in the data. The southern portion of the seismic profile trends subparallel to and just inboard (0-30 km) of the northwestern Blake Plateau Basin hinge zone, crossing the hinge towards the south. Seaward-dipping reflectors observed beyond the hinge zone on this and other seismic profiles nearby suggest rift-related igneous activity along this portion of the hinge similar to that interpreted for the Carolina Trough. Our seismic data include no direct evidence for a thick, high velocity (<7.0 km/s), mid- to lower-crustal underplate such as observed in the Carolina trough. This suggests that the emplacement of the high velocity underplate is confined to a region outboard of the hinge zone.

In Press: *Journal of Geophysical Research.*

Supported by: NSF Grant OCE-8917599.

WHOI Contribution No. 8372.

ESTIMATION OF THE SPATIAL VARIABILITY OF TRANSMISSION LOSSES AT LOW FREQUENCY IN SHALLOW WATER USING MULTICHANNEL SEISMIC REFLECTION DATA

G. M. Purdy, D. L. DuBois and J. I. Ewing

Spectral studies of commercial marine multichannel reflection profiling data demonstrate their utility for providing estimates of the degree of spatial variability in low-frequency (<100-Hz) transmission characteristics that is present in contrasting shallow water environments. The excellent spatial sampling provided by these readily available datasets allow them to resolve ~10-dB changes in returned energy levels occurring over distances of as little as a few hundred meters. At frequencies below the cutoff frequency, when the wave field is no longer dominated by water-borne energy, these small scale variabilities in transmission losses cannot be straightforwardly predicted from routinely collected mapping data (e.g., reflection profiles and reflection profiling datasets constitute an important resource for the mapping of changes in propagation characteristics in shallow water.

Published in: *Journal of the Acoustical Society of America*, 92(3):1,631-1,640, 1992.

Supported by: ONR Grant N00087-14-K-0007.

WHOI Contribution No. 7843.

IMPLICATIONS OF NEW GRAVITY DATA FOR BAIKAL RIFT ZONE STRUCTURE

C. Ruppel, M. G. Kogan and M. K. Mcnutt

Newly available, 2D Bouguer gravity anomaly data from the Baikal Rift zone, Siberia, indicate that this discrete, intracontinental rift system is regionally compensated by an elastic plate ~50 km thick. However, spectral and spatial domain analyses and isostatic anomaly calculations show that simple elastic plate theory does not offer an adequate explanation for compensation in the rift zone, probably because of significant lateral variations in plate strength and the presence of subsurface loads. Our results and other geophysical observations support the interpretation that the Baikal Rift zone is colder than either the East African or Rio Grande rift.

Published in: *Geophysical Research Letters*, 20(15):1,635-1,638, 1993.

Supported by: NASA Grant NAGS-1084 and a WHOI Postdoctoral Fellowship.

WHOI Contribution No. 8409.

AN ESTIMATE OF LATE PLEISTOCENE GEOMAGNETIC INTENSITY VARIATION FROM SULU SEA SEDIMENTS

David A. Schneider

Sediments from Site 769 of the Ocean Drilling Program's Leg 124 provide a record of geomagnetic intensity variation over the past 110 thousand years. Using exclusively continuous shipboard measurements, I estimate the variation in the geomagnetic field strength by employing low-field magnetic susceptibility as a normalization parameter for the measured remanence intensity. By calibrating the resultant relative paleointensity record against previously available Holocene age estimates of absolute paleointensity, I derive an estimate of virtual dipole moment since 110 ka. The record obtained from these Sulu Sea sediments is strikingly like that previously obtained from sediments of a similar age in the Mediterranean Basin with distinct intervals of low intensity near 15, 20, 40 and 65-70 ka. The Sulu sediments also indicate a low intensity feature near 108 ka. Important differences in paleointensity estimates obtained from these different regions for the interval between 30 and 20 ka suggest that a relatively large non-dipolar component of the geomagnetic field might have been present at that time.

In Press: *Earth and Planetary Science Letters.*

Supported by: W.H.O.I. Postdoctoral Fellowship.

WHOI Contribution No. 8383.

PALEOMAGNETISM OF SOME LEG 138 SEDIMENTS: DETAILING MIOCENE MAGNETOSTRATIGRAPHY

David A. Schneider

The aims of this study are twofold. First, the study tries to provide the most reliable chronology possible for two critical sections by correlating the magnetic polarity stratigraphy measured in these sediments with a newly revised geomagnetic polarity time scale. Second, this study attempts to examine in detail the nature of seven short events not included in the shipboard standard time scale, but for which abundant magnetostratigraphic evidence was obtained during the Leg.

Data presented here force some modifications to the shipboard interpretations of the magnetostratigraphy of Sites 845 and 844 on the basis of new data generated using discrete samples

and from a greater appreciation of the magnetostratigraphic signature of Miocene-age short evens. Those short events can be classified into two groups: those that probably reflect short, full-polarity intervals, and those that more likely represent an interval of diminished geomagnetic intensity. Three of the seven events documented here correspond well with three subtle features, as seen in marine magnetic profiles, that have been newly included in the geomagnetic polarity time scale as short, full-polarity chrons. One of the seven events corresponds to a poorly defined feature of the marine magnetic record that has also been newly included in the geomagnetic polarity time scale, but which was considered of enigmatic origin. The three remaining events investigated here, although they have not been identified with features in the seafloor magnetic record, are suggested to be events of a similar nature, most likely times of anomalously low geomagnetic intensity.

In addition to the Miocene magnetostratigraphic results given, several sets of averaged paleomagnetic inclinations are presented. Although these results clearly show the effects of a residual coring overprint, they demonstrate that paleomagnetic estimates of paleolatitudes can be made which are in good general agreement with ancient site positions calculated using hot spot-based plate reconstructions.

In Press: *Proceedings of the Ocean Drilling Program, Scientific Results Leg 138.*

Supported by: W.H.O.I. Postdoctoral Fellowship and JOI-USSAC Grant 26060100.

WHOI Contribution No. 8380.

EDGE-DRIVEN MICROPLATE KINEMATICS

Hans Schouten, Kim D. Klitgord and David G. Gallo

It is known from plate-tectonic reconstructions that oceanic microplates undergo rapid rotation about a vertical axis and that the instantaneous rotation axes describing the microplate's motion relative to the bounding major plates are frequently located close to its margins with those plates — close to the tips of propagating rifts. We propose a class of edge-driven block models to illustrate how slip across the microplate margins, block rotation, and the propagation of rifting may be related to the relative motion of the plates on either side. An important feature of these edge-driven models is that the instantaneous rotation axes are always located on the margins between block and two bounding plates. According to those models the pseudofaults or traces of disrupted seafloor resulting from the propagation of rifting between microplate and major plates, may e used independently to approximately trace the continuous kinematic evolution of the microplate back in time. Pseudofault geometries and matching rotations of the Easter microplate show that for most of its 5 Ma history, block rotation could be driven by the drag of the Nazca and Pacific plates on the microplate's edges rather than by a shear flow of mantle underneath.

Published in: *Journal of Geophysical Research,* 98(B4):6,689-6,701, 1993.

Supported by: ONR Grant N00014-89-J-1020.

WHOI Contribution No. 8270.

CONDUCTIVITY DISCONTINUITIES IN THE UPPER MANTLE BENEATH A STABLE CRATON

A. Schultz, R. D. Kurtz, A. D. Chave and A. G. Jones

We present evidence for approximate collocation of seismic and electrical transitions in the upper mantle. More than two years of very long period magnetotelluric (MT) data were recorded at a lakebottom observatory in the central Canadian Shield. After processing to contend with non-stationary source effects, and removal of galvanic distortion, the underlying structure is 1D for periods of one hour to four days. The response was extended to periods of 100 days by appending Geomagnetic Depth Sounding data to the MT curves. Minimum structure linearized inversion, nonlinear extremal inversion, and a new genetic algorithm for nonlinear hypothesis testing, reveal discrete jumps in conductivity at depths near the major upper mantle seismic discontinuities. The jumps occur over limited depth ranges.

Published in: *Geophysical Research Letters,* 20:2,941-2,944, 1993.

Supported by: NSF Grant EAR-9121278.

WHOI Contribution No. 8442.

SEGMENTATION AND MORPHOTECTONIC VARIATIONS ALONG A SLOW-SPREADING CENTER: THE MID-ATLANTIC RIDGE (24°00'N - 30°40'N

Jean-Christophe Sempere, Jian Lin, Holly S. Brown, Hans Schouten and G. M. Purdy

Analysis of Sea Beam bathymetry along the Mid-Atlantic Ridge between 24°00'N and 30°40'N reveals the nature and scale of the segmentation of

this slow-spreading center. Except for the Atlantis Transform, there are no transform offsets along this 800-km-long portion of the plate boundary. Instead, the Mid-Atlantic Ridge is offset at intervals of 10-100 km by non-transform discontinuities, usually located at local depth maxima along the rift valley. At these discontinuities, the horizontal shear between offset ridge segments is not accommodated by a narrow, sustained transform zone. Non-transform discontinuities along the MAR can be classified according to their morphology, which is partly controlled by the distance between the offset neovolcanic zones, and their spatial and temporal stability. Some of the non-transform discontinuities are associated with off-axis basins which integrate spatially to form discordant zones on the flanks of the spreading center. These basins may be the fossil equivalents of the terminal lows which flank the neovolcanic zone at the ends of each segment. These traces, which do not lie along small circles about the pole of opening of the two plates, reflect the migration of the discontinuities along the spreading center. Based on the orientation of the off-axis discordant zones, we calculate an average, northward migration rate on the order of 2 km Ma^{-1} over the last 2 Ma.

The spectrum of rift valley morphologies ranges from a narrow, deep-hourglass-shaped valley to a wide valley bounded by low-relief rift mountains. A simple classification of segment morphology involves two types of segments. Long and narrow segments are found preferentially on top of the long-wavelength, along-axis bathymetric high between the Kane and Atlantis Transforms. These segments are associated with circular mantle Bouguer anomalies which are consistent with focused mantle upwelling beneath the segment mid-points. Wide, U-shaped segments are preferentially found in the deep part of the long-wavelength, along-axis depth profile. These segments do not appear to be associated with circular mantle Bouguer anomalies, indicating perhaps a more complex pattern of mantle upwelling and/or crustal structure. Thus, the long-recognized bimodal distribution of segment morphology may be associated with different patterns of mantle upwelling and/or crustal structure. We propose that the range of observed, first-order variations in segment morphology reflects differences in the flow pattern, volume and temporal continuity of magmatic upwelling at the segment scale. However, despite large first-order differences, all segments display similar intra-segment, morphotectonic variations. We postulate that the intra-segment variability represents differences in the relative importance of volcanism and tectonism along strike away from a zone of enhanced magma upwelling within each segment. The contribution of volcanism to the morphology will be more important near the shallowest portion of the rift valley within each segment, beneath which we postulate that upwelling of magma is enhanced, than beneath the ends of the segment. Conversely, the contribution of tectonic extension to the morphology will become more important toward the spreading center discontinuities. Variations in magmatic budget along the strike of a segment will result in along-axis variations in crustal structure. Segment mid-points may coincide with regions of highest melt production and thick crust, and non-transform discontinuities with regions of lowest melt production and thin crust. This hypothesis is consistent with available seismic and gravity data. The rift valley is, as a rule, an asymmetric feature. Near segment mid-points, the rift valley is in general symmetric but, away from the segment mid-points, one side of the rift valley often consists of a steep, faulted slope while the other side forms a more gradual ramp. These observations suggest that half-grabens rather than full-grabens are the fundamental building blocks of the rift valley. They also indicate that the pattern of faulting varies along strike at the segment scale, and may be a consequence of the three-dimensional thermo-mechanical structure of segments associated with enhanced mantle upwelling beneath their mid-points.

Published in: *Marine Geophysical Researches*, 15:153-200, 1993.

Supported by: NSF Grants OCE-8722980, OCE-9012536 and OCE-9000285 and ONR Grant N00014-91-J-1433.

WHOI Contribution No. 8288.

AGE VARIATIONS OF OCEANIC CRUST POISSON'S RATIO: INVERSION AND A CRUSTAL EVOLUTION MODEL

Peter R. Shaw

Porosity in the oceanic crust is one of the most important factors influencing measured seismic velocities. Porosity is particularly important in the uppermost young crust, where rapid variations in velocities with depth and crustal age are observed. Knowledge of the concentration and aspect ratios of inferred crack populations can be improved considerably if estimates of Poisson's ratio are available from observations of compressional and shear seismic velocities v_p and v_s. In this paper I present a joint seismic waveform inversion for v_p and v_s; velocities are found while maximizing or minimizing Poisson's ratio using a hypothesis-testing mechanism. I apply this method to OBH data in 140 Ma Atlantic crust; the resulting solution corridor agrees with laboratory

measurements without the low Poisson's ratio anomalies at depths of 0.8-1.5 km found by Spudich and Orcutt (1980) and Au and Clowes (1984) on younger (<15 Ma) Pacific crust. Compiling other published v_p and v_s solutions, an age-dependent pattern emerges: none of the solutions for crust older than 60 Ma display the Poisson's ratio anomaly. I propose a simple crustal and evolution model, using thin and thick cracks, to explain these observations: thin cracks preferentially close at shallow depths in the crust, producing the localized Poisson's ratio anomaly. Sealing of all cracks by hydrothermal deposits as the crust ages restores the seismic velocities to be consistent with the laboratory measurements. This model is consistent with similar models of crack populations and their evolution from shallow measurements.

Published in: *Journal of Geophysical Research*, 99(B2):3,057-3,066, 1994.

Supported by: ONR Grant N00014-89-J-1018.

WHOI Contribution No. 8452.

CAUSES AND CONSEQUENCES OF VARIATIONS IN FAULTING STYLE AT THE MID-ATLANTIC RIDGE

Peter R. Shaw and Jian Lin

Both volcanism and faulting contribute to the rugged topography that is created at the Mid-Atlantic Ridge and preserved off-axis in Atlantic abyssal hill terrain. Distinguishing volcanic from fault-generated topography is essential to understanding the variations in these processes and how these variations are affected by the three-dimensional pattern of mantle upwelling, ridge segmentation and offsets. Here we describe a new quantitative method for identifying fault-generated topography in swath bathymetry data by measuring topographic curvature. The curvature method can distinguish large normal faults from volcanic features whereas slope methods cannot because both faults and volcanic constructs can produce steep slopes. The combination of curvature and slope information allows inward- and outward-facing fault faces to be mapped. We apply the method to Sea Beam data collected along the Mid-Atlantic Ridge between 28°-29°30'N. The fault styles mapped in this way are strongly correlated with their location within the ridge segmentation framework: long, linear, small-throw faults occur toward segment centers while shorter, larger-throw, curved faults occur toward ends; these variations reflect those of active faults within the axial valley. We investigate two different physical mechanisms that could affect fault interactions and thus underlie variations in abyssal hill topography at the MAR. In the first model only one fault is active at a time on each side of the rift valley. Each fault grows while migrating away from the volcanic center due to dike injection; extension across the fault causes a flexural rotation of nearby inactive faults. The amount of stress necessary to displace the fault increases as the fault grows. When reaching a critical size the fault stops growing as fault activity jumps inward as a new fault starts its growth near the rift valley. This model yields a realistic terrace-like morphology from the rift valley floor into the rift mountains, the relief is caused by the net rotation accumulated in the lithosphere from the active faults (e.g., 10°reached 20 km from the active fault). Fault spacing is controlled by lithospheric thickness, fault angle, and the ratio of amagmatic to magmatic extension. We hypothesize that this mechanism may e dominant toward ridge segment offsets. An alternative model considers multiple active faults; each fault relieves stresses as it grows and inhibits the growth of nearby faults, causing a characteristic fault spacing. Such fault interactions would occur in a region of necking instability involving deformation over an extended area. This mode of extension would drive a feedback mechanism that would act to regulate the size of nearby faults. We hypothesize that this mechanism may be active in the relatively weak regions of strong mantle upwelling near segment mid-points, causing the homogeneous abyssal hill fabric in these regions.

Published in: *Journal of Geophysical Research*, 98(B12):21,839-21,851, 1993.

Supported by: NSF Grant OCE-9012576 and ONR Grants N00014-89-J-1021, N00014-90-J-1615 and N00014-91-J-1433.

WHOI Contribution No. 8379.

THE SEAFLOOR BOREHOLE ARRAY SEISMIC SYSTEM (SEABASS) AND VLF AMBIENT NOISE

R. A. Stephen, D. E. Koelsch, H. Berteaux, A. Bocconcelli, S. Bolmer, J. Cretin, N. Etourmy, A. Fabre, R. Goldsborough, M. Gould, S. Kery, J. Laurent, G. Omnes, K. Peal, S. Swift, R. Turpening and C. Zani

The Seafloor Borehole Array Seismic System (SEABASS) has been developed to measure the pressure and three dimensional particle velocity of the VLF sound field (2-50 HZ) below the seafloor in the deep ocean. The system consists of four three-component borehole seismometers (with an optional hydrophone), a borehole digitizing unit, and a seafloor control and recording package. The system can be deployed using a wireline re-entry

capability from a conventional research vessel in Deep Sea Drilling Project (DSDP) and Ocean Drilling Project (ODP) boreholes. Data from below the seafloor are acquired either on-board the research vessel via coaxial tether or remotely on the seafloor in a self-contained package. If necessary the data module from the seafloor package can be released independently and recovered on the surface. This paper describes the engineering specifications of SEABASS, the tests that were carried out, and preliminary results from an actual deep sea deployment. VLF ambient noise levels beneath the seafloor acquired on the Low Frequency Acoustic-Seismic Experiment (LFASE) are within 20 dB of levels from previous seafloor borehole seismic experiments and from land borehole measurements. The ambient noise observed on LFASE decreases by up to 12 dB in the upper 100m of the seafloor in a sedimentary environment.

In Press: *Marine Geophysical Researches.*

Supported by: APL Johns Hopkins University Contract No. 602809-0, and ONR Grants N00014-89-J-1018, N00014-89-J-1012, N00014-90-C-0098.

WHOI Contribution No. 8340.

FINITE DIFFERENCE MODELING OF GEOACOUSTIC INTERACTION AT ANELASTIC SEAFLOORS

Ralph A. Stephen and Stephen A. Swift

A major problem in understanding seismic wave propagation in the seafloor is to distinguish between the loss of energy due to intrinsic attenuation and the loss of energy due to scattering from fine scale heterogeneities and bottom roughness. Energy lost to intrinsic attenuation (heat) disappears entirely from the system. Energy lost to scattering is conserved in the system and can appear in observations as incoherent noise (reverberation, time spread, angle spread) and/or mode converted waves. It has been shown by a number of investigators that the seafloor scattering problem can be addressed by finite difference solutions to the elastic wave equation in the time domain. However, previous studies have not considered the role of intrinsic attenuation in the scattering process. In this paper we present a formulation which includes the effects of intrinsic attenuation in a two dimensional finite difference formulation of the elastodynamic equations. The code is stable and yields valid attenuation results.

Published in: *Journal of the Acoustical Society of America*, 95(1):60-70, 1994.

Supported by: ONR Grant N00014-89-J-1012.

WHOI Contribution No. 8480.

FINE-SCALE MAGNETIC ANOMALY FIELD OVER THE SOUTHERN JUAN DE FUCA RIDGE: THE AXIAL MAGNETIZATION LOW AND IMPLICATIONS FOR CRUSTAL STRUCTURE

Maurice A. Tivey

Sea surface, deeptow and submersible magnetic surveys show that the spreading axis of the Cleft Segment of the Southern Juan de Fuca Ridge (SJDF) is overlain by a distinctive magnetic anomaly low in contrast to the more typical magnetic anomaly high found over the adjacent Vance Segment and most midocean ridge spreading centers. Forward iterative thickness modelling, based on the near-bottom magnetic data, shows that this axial magnetic low anomaly can be produced by a thin magnetic source layer beneath the Cleft axial valley. Thick crust is required to produce the magnetic anomaly high over the Vance axial valley. This magnetic modelling demonstrates that variations in the base of the magnetic source layer, which is assumed to be equivalent to the base of the extrusive lavas, can produce a significant proportion of the observed short-wavelength magnetic anomaly signal. These magnetic layer thickness models also correlate quite well with nearby seismic results which show seismic layer 2A thin beneath the axial valley of the Cleft and thicker beneath the Vance axial valley. Recent seismic results over other fast- and medium-spreading rifts also show rapid changes in the thickness of the uppermost crust near the axis of spreading, which could produce significant magnetic contrasts. The results of this study and the correlation with independent seismic measurements suggest that while magnetization may vary due to geomagnetic behavior or because of petrology or alteration, first-order changes in upper crustal thickness is one of the most important variables to consider in the production of fine-scale magnetic anomalies in young ocean crust.

Published in: *Journal of Geophysical Research*, 99(B3):4,833-4,855, 1994.

Supported by: ONR Grant N00014-89-J-1022 and a WHOI subcontract to University of Washington.

WHOI Contribution No. 8303.

HIGH-RESOLUTION MAGNETIC SURVEYS OVER THE MIDDLE VALLEY MOUNDS, NORTHERN JUAN DE FUCA RIDGE

Maurice A. Tivey

High-resolution, near-bottom magnetic surveys were carried out over two hydrothermal mound sites in Middle Valley; a thickly sedimented (0.2 to 1.5 km thick) abandoned spreading center, 20 km east of the current spreading axis of the northern Juan de Fuca Ridge. ODP Leg 139 drilled both the relict Bent Hill mound area (Site 856, 48°26'N 128°41'W) and the hydrothermally active Dead Dog mound area (Site 858, 48°27'N 128°43'W). No magnetic anomalies were found over the active Dead Dog hydrothermal mound area, but a large-amplitude (6000 nT), short-wavelength (<200 m) positive magnetic anomaly was measured over the massive sulfide mound, south of the Bent Hill mound. No anomalies were found over the Bent Hill mount itself. A magnetic anomaly was also found over the active 264°C vent site 300m south of Bent Hill. Drilling at the sulfide mound revealed sulfide and magnetic mineralization to at least 95 m depth with at least 60 m horizontal extent. The shape and limited extent of the magnetic anomaly is consistent with a positively magnetized, three-dimensional body at depth. The magnetic anomaly can be modeled by a buried sphere centered at 60 m below seafloor with a radius of 60 m or a long rod buried at 30 m below seafloor. A more realistic pipelike body of radius 60 m and magnetization 14 A/m predicts that the mineralized zone extends to 180 m in depth. In all cases, the magnetic field predicts continued magnetic mineralization at depth. Although basaltic sills were intersected in a number of the drillholes, no magnetic anomalies were found associated with them. The lack of anomalies in the Dead Dog area suggests that no buried bodies of magnetic material exist at depth equivalent to those found in the Bent Hill area.

In Press: *Proceedings of the Ocean Drilling Program Leg 139 Scientific Results.*

Supported by: JOI/USSAC 4505-3765 and OCE-8409478.

WHOI Contribution No. 8297.

VARIATIONS IN OCEANIC CRUSTAL STRUCTURE AND IMPLICATIONS FOR THE FINE-SCALE MAGNETIC ANOMALY SIGNAL

Maurice A. Tivey and H. Paul Johnson

Marine magnetic anomalies are traditionally modeled using a constant thickness source layer, usually defined as the extrusive lavas associated with seismic layer 2A. Recent seismic studies reveal that the thickness of layer 2A can vary by more than a factor of two, an observation which has important implications for the magnetic anomaly source layer. We model deep-tow magnetometer data from the Endeavour Segment of the Northern Juan de Fuca Ridge, in combination with nearby seismic data and find a positive correlation between the thickness of the seismically-defined layer 2A and the magnetic anomaly source layer. This suggests that short-wavelength magnetic anomalies observed within individual magnetic polarity units can arise from variations in the thickness of the extrusives, rather than geomagnetic field variations or secondary magnetization.

Published in: *Geophysical Research Letters,* 20(17):1,879-1,882, 1993.

Supported by: ONR Grant N00014-89-J-1022 and WHOI Subcontract to University of Washington.

WHOI Contribution No. 8302.

REDUCED CRUSTAL MAGNETIZATION BENEATH THE ACTIVE SULFIDE MOUND, TAG HYDROTHERMAL FIELD, MID-ATLANTIC RIDGE 26°N

Maurice A. Tivey, Peter A. Rona and Hans Schouten

A detailed near-bottom magnetic field survey was carried out by the submersible ALVIN over the actively venting mound located within the TAG (Trans-Atlantic Geotraverse) hydrothermal field on the Mid-Atlantic Ridge at 26°08'N 44°49'W. Three-dimensional analysis of these data clearly shows a distinct zone of reduced magnetization directly beneath the active mound. This magnetization low is consistent with the highly altered upflow zone of a hydrothermal vent system that feeds the actively venting mound structure. In contrast, the sea surface magnetic anomaly is associated with a broad 2 by 8 km magnetization low elongated along the axis, that includes both the active and inactive mounds. The short-wavelength (250 meter), near-bottom magnetic anomaly over the active mound is far too small to produce the long-wavelength (8 km) sea surface magnetic anomaly at TAG however, and even a collection of mounds with similar magnetic structure cannot produce the magnetic moment needed to generate the sea surface anomaly. Other hypotheses, including reversely magnetized crust and structurally thinned crust could account for the sea surface anomaly, but are considered unlikely. The existence of vigorous hydrothermal

activity at TAG and the lack of microseismic activity in the TAG area suggests that thermal demagnetization is the prime contributor to the sea surface anomaly. The thermal halo associated with a largely solid but still hot intrusion would provide sufficient demagnetization on a kilometer scale to produce the long-wavelength sea surface anomaly. Pervasive alteration at depth would also be an important factor in the destruction of crustal magnetization and is the only way that such a long-wavelength magnetic signal could be preserved in the crust. The overall model of crustal magnetization at a hydrothermal field with discrete zones of demagnetization in the upper crust and a broader zone of demagnetization at depth is consistent with studies of hydrothermal systems in ophiolite suites. These studies show narrow alteration pipes in the upper crust feeding the exhalative seafloor deposits and pervasive alteration at depth which commonly have associated late-stage intrusive bodies. While detailed magnetic surveys may provide some clues to the location of oceanic hydrothermal upflow zones, only drilling will ultimately test these hypotheses.

Published in: *Earth and Planetary Science Letters*, 115:101-115, 1993.

Supported by: NSF Grant OCE-9200905.

WHOI Contribution No. 8298.

A NOTE ON THE SEAFLOOR COUPLING CHARACTERISTICS OF THE NEW ONR OBS

Anne Trehu and George H. Sutton

A series of transient tests were conducted to determine the seafloor coupling characteristics of a new ocean-bottom seismometer (OBS) developed for the United States Office of Naval Research (ONR). The OBS comprises a large recording package and a separate sensor package that is deployed from the recording package. In addition to the coupling characteristics of both the sensor and the recording packages, the seismic energy radiated from the main recording package as a result of motion of the recording package was measured. The observed vertical coupling resonances of both the recording package and the sensor package are in good agreement with those predicted by a simple model of soil-structure interaction. The most important result of this study is that significant energy is radiated from the recording package in response to horizontal motions of the recording package. When the sensor package is 1 m from the recording package, the amplitude of the recorded signal is similar to that recorded in the recording package. In the field, this effect will result in distortion of seismic signals and increased background noise recorded by the sensor package if the recording package is disturbed by seafloor currents or biological activity. The amplitude of this signal attenuates by approximately a factor of two as sensor/recorder separation is increased from 1 to 6 m, suggesting that an improved response can be achieved by increasing the separation between the recording package and the sensors. This effect is much less severe for vertical disturbances of the recording package.

Published in: *Marine Geophysical Research*, 16(2):91-103, 1994.

Supported by: Rondout Associates and Oregon State University ONR Grant N00014-89-J-1635.

WHOI Contribution No. 8313.

A GEOLOGICAL MODEL FOR THE STRUCTURE OF RIDGE SEGMENTS IN SLOW-SPREADING OCEAN CRUST

Brian E. Tucholke and Jian Lin

First-order (transform) and second-order ridge-axis discontinuities cause a fundamental tectonic segmentation of mid-ocean ridges, and in slow-spreading crust they are commonly associated with exposure of subvolcanic crust and upper mantle. We have analyzed available morphological, gravity, and rock-sample data from the Atlantic Ocean to determine whether consistent structural patterns occur at these discontinuities and to constrain the processes that control the patterns. We find that both the first- and second-order discontinuities are characterized by thinned crust and/or mantle exposures along their older, "inside-corner" sides, as well as by irregular fault patterns and a paucity of volcanic morphologic features. On the young, "outside-corner" sides of discontinuities the crust has more normal thickness, regular fault patterns, and common volcanic forms. These results are consistent with tectonic thinning of inside-corner crust by a low-angle detachment fault as previously suggested for transform offsets by Dick et al. (1981) and Karson (1990). The volcanic upper crust forms the hanging wall at the outside corner and is stripped from the inside-corner footwall. Gravity and morphological data suggest that detachment faulting is relatively continuous, long-lived process in crust spreading at <25-30 mm/yr, that it may be intermittent at intermediate rates of 30-40 mm/yr, and that it is unlikely to occur at faster rates. The detachment surfaces are cut by later, high-angle faults formed during crustal uplift into the rift mountains; these faults may cut through the entire crust and are probably the types of

faults imaged by seismic reflection profiling over Cretaceous North Atlantic crust. Slow-spreading crust experiences cyclic magmatic/amagmatic extension; from observations of off-axis gravity anomaly variations, a typical cycle appears to last on the order of 2 m.y. During magmatic phases the footwall of the detachment fault probably exposes lower-crustal gabbros, and these rocks locally may have an unconformable volcanic carapace. We suggest that during amagmatic extension the detachment dives into the lithosphere and can exhume upper-mantle ultramafics very rapidly, probably in as little as 0.5 m.y. Together, detachment faulting and cyclic magmatic/amagmatic extension create heterogeneous lithosphere both along and across isochrons in slow-spreading crust.

In Press: *Journal of Geophysical Research.*

Supported by: ONR Grants N00014-90-J-1621 and N00014-91-J-1433 and NSF Grants OCE-8716713 and OCE-9020408.

WHOI Contribution No. 8369.

EVIDENCE FROM EARTHQUAKES FOR BOOKSHELF FAULTING AT LARGE NON-TRANSFORM RIDGE OFFSETS

Laura Reiser Wetzel, Douglas A. Wiens and Martin C. Kleinrock

Migrating non-transform offsets, which occur along mid-ocean ridges when a propagating segment gradually elongates and takes over spreading from a doomed rift segment, represent a significant modification of the plate tectonic paradigm. However, the mechanism of deformation within the migrating offset zone between the two spreading segments has been controversial. Study of source parameters and locations of earthquakes at such offsets allows discrimination between previously proposed instantaneous transform, distributed transform, and bookshelf faulting models for deformation between the two rifts. Earthquakes at large non-transform offsets at medium and fast spreading rates show strike-slip mechanisms rotated relative to the expected transform fault orientation. One set of nodal planes is parallel to curved seafloor lineaments which shows increased rotation as a function position in the deforming zone. A bookshelf faulting model in which initially ridge-parallel faults are rotated by simple shear is consistent with observed lineament orientation, focal mechanisms, and earthquake distributions.

Published in: *Nature*, 362:235-237, 1993.

Supported by: ONR Grant N00014-89-J-1021.

WHOI Contribution No. 8293.

MORPHOLOGY AND CRUSTAL STRUCTURE OF THE ATLANTIS TRANSFORM, MID-ATLANTIC RIDGE

Christopher E. Zervas, Jean-Christophe Sempere and Jian Lin

The Atlantis Fracture Zone (30°N) is one of the smallest transform faults along the Mid-Atlantic Ridge. It corresponds to a spatial offset of 70 km and to an age offset of ~6 Ma. The morphology of the Atlantis Fracture Zone is typical of that of slow-slipping transforms. The transform valley is 15-20-km wide and 2-4-km deep. The locus of strike-slip deformation is confined to a narrow band of a few kilometers wide. Terrain created at the ridge-nontransform corners of the fracture zone is characterized by ridges which curve toward the ridge-transform intersections and depressions which resemble nodal basins. Hooked ridges are not observed on the transform side of the ridge-transform intersections. The orientation of the inactive and active parts of the transform differ slightly. This difference may indicate that the Atlantis Transform has recently responded to changes in the direction of relative plate motion, but our limited coverage of the fracture zone does not allow us to study these plate motion changes in detail. We have performed a three-dimensional inversion of the surface magnetic field over our survey area. Accretionary processes appear to be sufficiently organized within 3-4 km of the transform fault to produce lineated magnetic anomalies. The magnetization solution documents a 15-km, westward relocation of the axis of accretion immediately south of the transform about 0.25 Ma ago. The Atlantis Transform is associated with a band of high mantle Bouguer anomalies. This pattern suggests the presence of high densities in the crust and/or mantle along the transform, or thin crust beneath the transform. Assuming that all the mantle Bouguer anomalies are due to crustal thickness variations, we calculate that the crust may be 2-3 km thinner than a reference 6-km thickness beneath the transform valley, and 2-4 km thicker beneath the spreading segments which bound the transform. Our results indicate that crustal thinning is not uniform along the strike of the fracture zone. We have studied the state of compensation of the Atlantis Transform and conclude that the depth anomaly associated with the fracture zone valley is not compensated everywhere by thin crust. The relationship between bathymetry and gravity is best explained by regional compensation with an elastic plate with an effective thickness of ~4 km or greater.

Submitted to: *Marine Geophysical Research.*

Supported by: NSF Grant OCE-9012576 and ONR Grant N00014-91-J-1433.

WHOI Contribution No. 8618.

HYDRODYNAMICS

UNIFORM BOTTOM SHEAR STRESS AND EQUILIBRIUM HYPSOMETRY OF INTERTIDAL FLATS

Carl T. Friedrichs and David G. Aubrey

Hypsometry is the distribution of horizontal surface area with respect to elevation. Recent observations of tidal flat morphology have correlated convex hypsometry with large tide ranges, long-term accretion and/or low wave activity. Concave hypsometry, in turn, has been correlated with small tide ranges, long-term erosion and/or high wave activity. The present study demonstrates that this empirical variation in tidal flat hypsometry is consistent with a simple morphodynamic model which assumes tidal flats to be at equilibrium if maximum bottom shear stress (τ) is spatially uniform. Two general cases are considered: (i) dominance of τ by tidal currents, where τ is equal to maximum tidally-generated shear stress (τ_{itT}), and (ii) dominance by wind waves, where τ is equal to maximum wave-generated shear stress (τ_{itW}). Analytic solutions indicate that a tidal flat which slopes linearly away from a straight shoreline does not produce a uniform distribution of τ_{itT} or τ_{itW}. If the profile is adjusted until either τ_{itT} or τ_{itW} is uniform, then domination by tidal currents favors a convex hypsometry, and domination by wind waves favors a concave hypsometry. Equilibrium profiles are also derived for curved shorelines. Results indicate that an embayed shoreline significantly enhances convexity and a lobate shoreline significantly enhances concavity – so much so that the potential effect of shoreline curvature on equilibrium hypsometry is of the same order as the effect of domination by τ_{itT} or τ_{itW}.

In Press: *Mixing Processes in Estuaries and Coastal Seas.* C. Pattiaratchi, ed. Estuarine Studies Series, American Geophysical Union, Washington, D.C.

Supported by: NSF Grant OCE-9102429.

WHOI Contribution No. 8294.

TIDAL PROPAGATION IN STRONGLY CONVERGENT CHANNELS

Carl T. Friedrichs and David G. Aubrey

Simple first- and second-order analytic solutions are derived for tidal propagation in strongly convergent channels which diverge markedly from classical views of co-oscillating tides. Theoretical predictions compare well with observations from typical examples of shallow, "funnel-shaped" tidal estuaries. A scaling of the governing equations appropriate to these channels indicates that at first order, gradients in cross-sectional area dominate velocity gradients in the continuity equation and the friction term dominates acceleration in the momentum equation. Finite amplitude effects, velocity gradients due to wave propagation, and local acceleration enter the equations at second-order. Applying this scaling, the first-order governing equation becomes a first-order wave equation, which is inconsistent with the presence of a reflected wave. The solution is of constant amplitude and has a phase speed near the frictionless wave speed, like a classical progressive wave, yet velocity leads elevation by 90°, like a classical standing wave. The second-order solution at the dominant frequency is also a unidirectional wave, however its amplitude is exponentially modulated. If inertia is finite and convergence is strong, amplitude increases along channel, whereas if inertia is weak and convergence is limited, amplitude decays. Compact solutions for second-order tidal harmonics quantify the partially canceling effects of (i) time variations in channel depth, which slow the propagation of low water, and (ii) time variations in channel width, which slow the propagation of high water. Finally, it is suggested that phase speed, along-channel amplitude growth, and tidal harmonics in strongly convergent channels are all linked by morphodynamic feedback.

Published in: *Journal of Geophysical Research,* 99(C2):3,321-3,336, 1994.

Supported by: NSF Grant OCE-9102429.

WHOI Contribution No. 8422.

ISOTOPE GEOCHEMISTRY

VARIATIONS OF THE $^{187}OS/^{186}OS$ RATIO OF SEAWATER OVER THE PAST 28 MILLION YEARS AS INFERRED FROM METALLIFEROUS CARBONATES

Greg Ravizza

The Os concentration and isotopic composition of metalliferous carbonates deposited near the East Pacific Rise over the past 28 Ma are reported with complementary Sr isotope data. Variations in the Os isotopic composition of these samples are interpreted as a record of past changes in the Os isotopic composition of seawater. These results are consistent with isotopic analyses of leachable Os in

pelagic clays which have also been interpreted as a temporal record of the $^{187}Os/^{186}Os$ ratio of seawater through time (Pegram et al. 1992). The metalliferous carbonate record clearly shows that seawater Os and Sr isotope systems are decoupled from one another over the past 28 Ma. Accelerated weathering of ancient organic-rich sediments is suggested as a possible mechanism to account for this decoupling and the rapid increase in the $^{187}/^{186}Os$ ratio of seawater over the past 15 Ma. This rapid increase suggests that the seawater Os record can be utilized as a stratigraphic tool in some Neogene marine deposits.

Published in: *Earth and Planetary Science Letters*, 118:335-348, 1993.

Supported by: NSF Grants OCE-9115253 and EAR-9204409.

WHOI Contribution No. 8349.

THE GEOCHEMICAL CYCLE OF RHENIUM: A RECONNAISSANCE

Debra Colodner, Julian Sachs, Gregory Ravizza, Karl Turekian, John Edmond and Edward Boyle

Rhenium (Re) is one of a suite of elements (including uranium and molybdenum) that display conservative behavior in seawater and are enriched in anoxic sediments. The decay of ^{187}Re to ^{187}Os provides a geochronometer in ancient sedimentary rocks and gives rise to Os-isotopic variations in nature. In order to better characterize its sources to seawater, Re was measured in three major rivers (Amazon, Orinoco, Ganges-Brahmaputra) and some of their tributaries. Re concentrations span four orders of magnitude (from <0.02 to 400 pmol/kg), with the highest concentrations found in rivers draining black shales in the Venezuelan Andes. Mainstream Re levels in the three rivers are between 1 and 10 pmol/kg, with a flux weighted average of 2.3 pmol/kg. The residence time for Re in the oceans is estimated to be 750,000 yr with respect to river inputs.

Re profiles from the Atlantic and Pacific Oceans confirm that Re behaves conservatively in seawater, with no significant uptake onto particles and/or recycling within the water column. This is also true in the anoxic water column of the Black Sea. Re removal into anoxic sediments occurs at or below the sediment water interface, as demonstrated in sediment pore waters from Chesapeake Bay. In oxic sediments, Re is not cycled with manganese oxides, and it is not enriched in very slowly accumulating pelagic sediments with a large hydrogenous iron and manganese component, or in manganese nodules. Burial of Re in anoxic sediments, which accumulate on 0.3% of the ocean floor, removes approximately 50% of the riverine Re flux to the oceans. Hence, oceanic Re concentrations may be very sensitive to changes in the area of anoxic sedimentation.

Published in: *Earth and Planetary Science Letters*, 117:205-221, 1993.

Supported by: NSF Grants OCE-9115253 and WHOI Postdoctoral Fellowship.

A POSSIBLE LINK BETWEEN THE SEA WATER OSMIUM ISOTOPE RECORD AND WEATHERING OF ANCIENT SEDIMENTARY ORGANIC MATTER

Greg Ravizza and B. K. Esser

The Os isotopic composition of leachable Os from a North Pacific pelagic clay sequence (Pegram et al. 1992) and bulk sediment samples of metalliferous carbonates deposited near the East Pacific Rise (Ravizza 1993) display similar patterns of temporal variation (Fig. 1). This similarity indicates that the composite record of $^{187}Os/^{186}$ ratio variations reflect changes in the Os isotopic composition of sea water. Temporal changes in the Sr isotopic composition of sea water record changes in the relative rates of continental weathering and oceanic crustal alteration. The Os isotopic composition of sea water should be influenced by similar processes. In both the Rb-Sr and Re-Os signatures to continental material. However, the sea water Sr and Os records are decoupled from one another over the past 27 Ma. From 27 to 15 Ma $^{87}Sr/^{86}Sr$ increased rapidly while the $^{187}/^{186}$ ratio of sea water remained nearly constant. At 15 Ma the $^{187}Os/^{186}$ ratio of sea water began to increase rapidly but the rate of increase in the $^{87}Sr/^{86}Sr$ ratio diminished. Accelerated weathering of ancient sedimentary organic matter may account for this decoupling and the rapid increase in the $^{187}Os/^{186}$ ratio of sea water over the past 15 Ma (Pegram et al. 1992, Ravizza 1993). Calculations described here suggest this is a viable hypothesis which has implications for our understanding of changes in the size of the buried organic carbon reservoir during the Neogene.

In Press: *Chemical Geology.*

Supported by: NSF Grant EAR-9204409.

WHOI Contribution No. 8351.

OSMIUM ISOTOPIC VARIATIONS IN METALLIFEROUS SEDIMENTS FROM THE EAST PACIFIC RISE AND THE BAUER BASIN

Greg Ravizza and Gary M. McMurtry

The osmium concentration and isotopic composition of metalliferous sediments from the

East Pacific Rise (EPR) and Bauer Basin have been determined. $^{87}Sr/^{86}Sr$ ratios range from 7.9 to 8.6, with EPR samples between 8.4 and 8.6 and Bauer Basin samples between 7.9 and 8.2. The Os isotopic composition of EPR samples is indistinguishable from the inferred Os isotopic composition of sea water requiring that nearly all the Os in these sediments is hydrogenous in origin. This result is used to place broad constraints on the behavior of Os in ridge crest hydrothermal systems. While Bauer Basin samples also contain predominantly hydrogenous Os an additional source of Os with low $^{187}Os/^{186}$ is required to account for the lower measured ratios. Calculation of total Os burial fluxes in the Bauer Basin show that the background flux of cosmic Os is adequate to produce the observed depression in Bauer Basin $^{187}Os/^{186}$ ratios. Burial flux calculations also suggest that metalliferous sediment deposition is a significant sink in the marine Os cycle.

Published in: *Geochimica et Cosmochimica Acta*, 57:4,301-4,310, 1993.

Supported by: NSF Grant OCE-9115253.

WHOI Contribution No. 8348.

OCEANOGRAPHY

THE WESTERN BLACK SEA RIM CURRENT

T. Oguz, S. Besiktepe, D. G. Aubrey, V. Diaconu, L. Ivanov and U. Unluata

The Black Sea possesses a remarkably strong Rim current, with pronounced current meanders and eddies along its entire length. The narrow Rim Current frontal zone, of width ~50-75 km, has a uniform upper layer (up to 100 m) speed exceeding 50 cm/s, with maximum measured currents of ~100 cm/s. Following a strong sear zone across the permanent pycnocline, uniform currents of ~20 cm/s extend to a depth of ~300 dbar (the approximate limit of the ADCP measurements). The lower layer currents, measured up to ~40 cm/s at 300 dbar, are much stronger than previously reported. The cross-stream Rim Current structure has a narrow (~10 km) core confined over the upper topographic slope, flanked by narrow, intense shear zones. Except in localized regions of the onshelf meanders of the Rimcurrent, the northwestern shelf circulation is decoupled from the influence of the basin-wide circulation, and characterized by much weaker currents of ~10 cm/s.

Submitted to: *Deep Sea Research, Part II.*

Supported by: TUBITAK, NATO Science for Stability Program in Turkey, Intergovernmental Oceanographic Commission, NSF Grant INT-9310226, Regional Environmental Center for Central and Eastern Europe, A.W. Mellon Foundation awarded to Coastal Research Center.

WHOI Contribution No. 8507.

PALEOCEANOGRAPHY

A MODEL FOR VARIATION IN THE CHEMISTRY OF PLANKTONIC FORAMINIFERA DUE TO SECONDARY CALCIFICATION AND SELECTIVE DISSOLUTION

G. P. Lohmann

A quantitative model for describing the within-population variation in planktonic foraminifer shell chemistry that results from secondary calcification and selective dissolution is presented. The objective is to construct a basis for inferring the chemistries of different shell components and estimating the extent of shell dissolution. Variation is modeled as mixtures of two kinds of shell calcite, a primary calcite that forms the chambers and a secondary calcite that forms crust. Bulk shell chemistries are intermediate between the chemistries of these calcites and lie on mixing lines between them. For two component systems, mass balance relationships can be reformulated as a linear regression and solved for the chemistries of the primary and secondary calcites and for the uncertainties associated with the estimates.

To apply this model, one needs measurements of bulk shell chemistries and estimates of the relative proportions of secondary and primary calcites. For most planktonic foraminifer species, the proportion of secondary calcite can be estimated from differences in the relationship between shell size and mass before and after crusting.

Preliminary results are consistent with previous work showing that secondary calcites are added at depth. However, even deep-dwelling species appear to grow most of their primary shell in surface waters and some surface-dwelling species add secondary calcite in the deep ocean.

In contrast to the model's simple description of secondary calcification, the variation in chemistry from selective dissolution is more complicated because undissolved shells are themselves mixtures of primary and secondary calcites and present a wide range of initial shell compositions. Nevertheless, the model allows both the compositions of different components to be

inferred and the amount of dissolution to be estimated. Preliminary results indicate that dissolution of planktonic foraminifera is apparent nearly 2 km above the foraminifer lysocline and even apparently well-preserved shells may be over 50% dissolved.

In Press: *Paleoceanography.*

Supported by: NSF Grants OCE-9101553 and OCE-9301722.

WHOI Contribution No. 8571.

VERTICAL δ ^{13}C GRADIENT IN THE SOUTH ATLANTIC OCEAN DURING THE LAST GLACIAL MAXIMUM

G. P. Lohmann and K. C. Lohmann

North Atlantic waters are cooled at the surface in sub-polar marginal seas and then sink to ventilate the deep Atlantic and eventually the Indo-Pacific basins. During the last glacial maximum, when these subpolar regions were covered with ice, vertical $\delta^{13}C$ gradients suggest that deep water formation diminished and the North Atlantic was ventilated primarily by intermediate waters [Curry et al., 1988; Boyle and Keigwin, 1987; Oppo and Fairbanks, 1987; Slowey and Curry, 1992; Oppo and Lehman, 1993]. At the same time, it has been suggested that expansion of Antarctic sea ice shifted the circumpolar wind field northward, causing the North Atlantic intermediate waters to bypass the Southern Ocean and flow directly into the Indo-Pacific [Imbrie et al., 1992]. The Rio Grande Rise stands in the path of these waters as they flow through the South Atlantic. It intersects the entire water column, from the main thermocline through intermediate, deep and bottom waters, and any circulation changes should be evident in the sediments deposited on its slopes. Unfortunately, low sedimentation rates and severe biological mixing have confused the sediment record on the Rio Grande Rise, precluding accurate reconstructions of the past ocean. Here we attempt to unmix these records by using the $\delta^{18}C$ chemistry of individual particles to distinguish those formed today from those formed during the last glacial maximum. We then use their associated $\delta^{13}C$ chemistry to reconstruct vertical gradients for today's ocean and for the last glacial. These reconstructions indicate that the glacial South Atlantic, like the North Atlantic, was ventilated by intermediate waters, but the source of these waters is unclear. Their $\delta^{13}C$ decreases from north to south, consistent with aging as they flow from the North Atlantic, however, this difference does not rule out the possibility that South Atlantic intermediate waters originated as $\delta^{13}C$-depleted surface waters in the Southern Ocean. Furthermore, a large decrease in the $\delta^{13}C$ of surface waters over the Rio Grande Rise during the last glacial suggests that Southern Ocean surface waters were pushed farther northward then they are today. This result supports the conclusion of Imbrie et al. (1992) that circumpolar winds shifted and pushed surface waters farther northward during the last glacial maximum. The Southern Ocean, rather than the North Atlantic, may have been the source of the intermediate waters that ventilated the glacial Pacific.

Submitted to: *Nature.*

Supported by: NSF Grants OCE-9101553 and OCE-9102438.

WHOI Contribution No. 8583.

REASSESSMENT OF THE INFLUENCE OF TEMPERATURE ON THE DISTRIBUTION OF ^{13}C IN THE UPPER OCEAN

G. P. Lohmann, D. W. Oppo and W. B. Curry

Before the influence of temperature on the distribution of ^{13}C in the ocean can be assessed, adjustments must be made for the redistribution of carbon isotopes by biological processes. Broecker and Maier-Reimer [1992] used dissolved PO_4 concentrations to estimate the amount of organic matter decomposition and adjust for its contribution to observed $\delta^{13}C$. After this adjustment, they found that a significant component remained in the $\delta^{13}C$ of southern ocean surface waters, which they attributed to thermodynamic processes. Here we consider an alternative means of estimating the biological component of $\delta^{13}C$, based on the O_2 consumed by decomposition rather than on the PO_4 released. In principle, both estimates should yield the same results. However, estimates of biological $\delta^{13}C$ based on PO_4 typically assume that all surface waters are initially PO_4-free. Not only is there significant PO_4 in cold, high latitude surface waters, but the mixing of these waters with warm, PO_4-depleted tropical surface waters produces a strong correlation between temperature and performed PO_4 within the upper ocean. This correlation imposes an apparent temperature-dependency on biological $\delta^{13}C$ when regional preformed PO_4 differences are ignored, leading to an overestimate of the influence of temperature. In contrast, when oxygen utilization is used to adjust for biological activity, there is no evidence that local temperature differences produce regional $\delta^{13}C$ gradients in the upper ocean. Boyle (1992) has shown that discordancies between $\delta^{13}C$ and [Cd] (the proxy for $[PO_4]$) arise

when their past distribution is explained only in terms of biological processes. Broecker (1993) has suggested that these reflect past changes in the efficiency of air-sea exchange of carbon isotopes. Based on our reassessment, we raise the alternative possibility that the discordancies reflect changes in the relative proportions of nutrient-free versus nutrient-rich surface waters subducted into the deep ocean. The apparent lowering of preformed nutrients entering the deep ocean during the last glaciation supports the hypothesis that increased utilization of nutrients in surface waters contributed to the lowering of atmospheric CO_2 (Knox and McElroy, 1984).

In Press: *Paleoceanography.*

Supported by: NSF Grants OCE-9102458, OCE-9101553 and OCE-9012279.

WHOI Contribution No. 8385.

DEPTH PROFILES OF $\delta^{13}C$ IN BOTTOM WATER AND CORE-TOP *C. WUELLERSTORFI* ON THE ONTONG-JAVA PLATEAU AND EMPEROR SEAMOUNTS

Daniel C. McCorkle and Lloyd D. Keigwin

We have measured the carbon isotopic composition of dissolved inorganic carbon in bottom waters of the Ontong-Java Plateau (Western Equatorial Pacific) and on the northern Emperor Seamounts (Northwest Pacific). Each of these locations is several hundred miles from the nearest GEOSECS stations, and the observed $\delta^{13}C$ values at each site differ substantially from regionally averaged GEOSECS $\delta^{13}C$ profiles. We discuss the possible causes of these differences, including real horizontal variability, near-bottom effects, and problems with the Pacific GEOSECS $\delta^{13}C$ data.

We also measured the isotopic composition (C and O) of core-top *C. wuellerstorfi* from a depth transect of cores at each location. The $\delta^{13}O$ data are used to verify that our samples are Recent. Comparison of foraminiferal and bottom water $\delta^{13}C$ values shows that this species faithfully records bottom water $\delta^{13}C$ at both sites, and demonstrates that there is no depth-related artifact in the DIC - *C. wuellerstorfi* $\delta^{13}C$ relationship.

In Press: *Paleoceanography.*

Supported by: NSF Grants OCE-9101154, OCE-8710783 and OCE-9000437.

WHOI Contribution No. 8339.

GLACIAL-HOLOCENE PALEOPRODUCTIVITY OFF WESTERN AUSTRALIA: A COMPARISON OF PROXY RECORDS

D. C. McCorkle, H. H. Veeh and D. T. Heggie

We compare paleoproductivity proxy records from a set of gravity cores from the Exmouth Plateau ($\approx$ 19°S, 113°E, 950 to 2250 m) and the Perth Basin ($\approx$ 27°S, 111°E, 2750 m) in the southeastern Indian Ocean. In general, these proxies indicate higher surface-ocean productivity in this region at the last glacial maximum (LGM, isotope stage 2). LGM sediment accumulation rates and the accumulation rates of biogenic sediment components ($CaCo_3$ and organic carbon) are a factor of 1.5 to 2 higher than Holocene values. Benthic foraminiferal abundances and accumulation rates are both higher in glacial sediments, as are the concentrations and accumulation rates of authigenic uranium in the sediments. These benthic foraminiferal abundance and authigenic uranium data suggest higher surface ocean productivity during the glacial, but we cannot yet relate them to carbon flux quantitatively. In contrast to these three approaches, a productivity proxy based on paired-special benthic foraminiferal $\delta^{13}C$ differences shows little Glacial-Holocene change. Possible explanations for this disagreement are discussed.

Together, the data suggest that the Glacial productivity off Western Australia was elevated relative to Holocene values, and support the hypothesis that a north-flowing west Australian current led to enhanced coastal upwelling and primary productivity off western Australia at the last Glacial maximum (LGM). However, Glacial productivity was high only relative to the low productivity characteristic of this region in the modern ocean. We see no evidence of strong upwelling similar to that observed in the modern ocean off the southwestern coasts of Africa and South America.

In Press: *Carbon Cycling in the Glacial Ocean: Constraints on the Oceans' Role in Global Change,* NATO Advanced Research Workshop Volume.

Supported by: NSF Grant OCE-8817620.

WHOI Contribution No. 8251.

CD/CA CHANGES IN A DEEP CAPE BASIN CORE OVER THE PAST 388,000 YEARS: RESPONSE OF CIRCUMPOLAR DEEP WATER VARIABILITY TO NORTHERN HEMISPHERE ICE SHEET MELTING?

Delia W. Oppo

A comparison of cadmium/calcium (cd/Ca) records of benthic foraminifera from a deep Cape Basin and a deep eastern equatorial Pacific core suggests that over the past 388,000 years, the nutrient concentration of Circumpolar Deep Water (CDW) has always been lower than that of the deep Pacific. The data further suggest that at the 100,000 and 23,000 year orbital periods, the contribution of North Atlantic Deep Water (NADW) to CDW is at a maximum during periods of ice growth and at a minimum during periods of ice decay. These results are not in agreement with results based on carbon isotope records of benthic foraminifera, which suggest intervals of CDW nutrient-enrichment relative to the deep Pacific, and an approximately in-phase relationship between CDW nutrient concentration and ice volume. Resolution of the apparent conflict between $\delta^{13}C$ and Cd/Ca data may provide important constraints on past deep ocean circulation and nutrient variability.

In Press: *Paleoceanography.*

Supported by: NSF Grant OCE-9012279.

WHOI Contribution No. 8310.

PALEOCLIMATOLOGY

DEEP CIRCULATION CHANGE LINKED TO HEINRICH EVENT 1 AND YOUNGER DRYAS IN A MIDDEPTH NORTH ATLANTIC CORE

Lloyd D. Keigwin and Scott J. Lehman

A core from the Mid-Atlantic Ridge at 43.5°N and ~3 km water depth shows distinct evidence of the deglacial events known as Heinrich event 1 (probably the marine equivalent of Oldest Dryas cooling in Europe) and the Younger Dryas. The Heinrich event, dated at three levels to between 14.3 and 15.0 ka, is marked by a minimum in foraminifera per gram, by maxima in rates of sedimentation, ice rafted debris per gram, and relative abundance of *N. pachyderma* (s.), and by a $\delta^{18}O$ minimum in planktonic foraminifera. The Younger Dryas event is marked by peak abundance of *N. pachyderma* (s.) and a planktonic $\delta^{18}O$ maximum. Benthic foraminiferal $\delta^{18}C$ reaches minimum values during both the Heinrich event and the Younger Dryas. Our data indicate pronounced changes in surface water properties were coupled with reduced production of North Atlantic Deep Water at each of these times.

In Press: Paleoceanography.

Supported by: NOAA Grant NA16-RC-0074-01 and NSF Grants OCE-9019660 and OCE-9116259.

VARIABILITY OF ATLANTIC CIRCULATION ON SUB-MILLENNIAL TIMESCALES

Scott J. Lehman

New sediment records from the southeastern Norwegian Sea documents a series of abrupt changes in poleward flow of warm surface waters during the last deglaciation (15,000 - 8,000 yr BP), some of which produced shifts in sea surface temperature of more than 5°C in fewer than 40 years. These findings confirm the timing, magnitude and rates of circum-Atlantic climate change implied by ice-core data and predicted by numerical models, and support the theory that the intensity of thermohaline overturning controlled air temperatures around and downstream of the North Atlantic.

Unlike the deglacial interval, the last ~8,000 years have been marked by relatively stable climate conditions in the North Atlantic region. But, as pointed out earlier by Broecker (1987), the conditions that conferred stability over this interval are not yet understood, and thus is can not be assumed that such conditions will persist in the face of the gradual changes already forecast as a response to anthropogenic perturbation of the climate system.

In Press: Workshop on Decade to Century Time Scales of Natural Climate Variability, National Research Council, National Academy Press, Washington, D.C.

Supported by: NSF Grant OCE-9019660.

TRANSPORT OF FRESHWATER INTO THE DEEP OCEAN BY THE CONVEYOR

Scott J. Lehman, Daniel G. Wright and Thomas F. Stocker

The upper limb of the ocean's conveyor-belt circulation transports about one petaWatt of heat across the equator in the Atlantic, of which approximately two-thirds is released to the atmosphere in the northern part of the basin as a

result of deepwater formation. If all of this heat were taken up in melting ice, it would yield approximately 60,000 km^3 of meltwater per year. Thus it is conceivable that peak melting rates of 5,000-15,000 km^3/yr at the end of the last glaciation (Fairbanks 1989) were achieved in response to sudden start-up or strengthening of the conveyor. Of course, a portion of the heat borne and released by the conveyor radiates to space, and much of the glacial ice at high elevation and high latitude must have been warmed prior to melting, consuming additional energy. But the point here is that even without sunlight at high latitudes, the transient heat gain associated with strengthening of the conveyor may have been sufficient or near-sufficient to account for the melting of the former ice sheets of the Northern Hemisphere. The potential role of the conveyor in melting the ice sheets is further underscored by Figure 1 showing that melting rates during the last deglaciation varied in accordance with the relative strength of the conveyor's upper limb (Lehman and Keigwin 1992). However, in most numerical ocean models the convection which drives the conveyor circulation is extremely sensitive to small changes in the freshwater balance at the surface (Maier-Reimer and Mikolajewicz 1989; Stocker et al. 1992). If such model sensitivities are close to being correct, it is difficult to understand how the conveyor remained "on" long enough to promote the large pulses of ice sheet melting seen in Figure 1.

A second observation of relevance to this problem is that high-resolution oxygen isotopic records in benthic foraminifera often show a two-step depletion in ^{18}O during the deglaciation (cf. Duplessy et al. 1981). A few records with exceptional resolution show that, at some locations, these steps correspond to two depletion "spikes" separated by an enrichment at approximately the time of the Younger Dryas (Figure 2). The low-$\delta^{18}O$ spikes may be explained in several ways: 1) by transient freshening of the deep ocean before and after the YD, 2) by transient warming of the deep ocean before and after the YD, or 3) by a change in the relationship between $\delta^{18}O$ and salinity in deep water source areas before and after the YD, due either to a change in the amount and/or isotopic composition of glacial meltwater or in the extent of brine-rejection by sea ice. As the timing of maximum ice sheet melting and benthic ^{18}O-depletion are similar the simplest explanation is that $\delta^{18}O$ dropped temporarily when and where the rate of addition of ^{18}O-depleted meltwater exceeded the mixing capacity of the deep ocean. If the conveyor remained "on" during much or all of the periods of greatest melting, discrete pulses of meltwater may then have been advected into the deep ocean and recorded in the oxygen isotopic composition of benthic foraminifera. But, once again, if deepwater formation and conveyer-belt circulation in the real ocean had a sensitivity to freshening close to that of most models, how could such discrete pulses of freshwater have been advected to depth?

Wright and Stocker (this volume hereafter WS-93) have recently made progress in addressing the sensitivity problem by investigating the dependence of the transient behavior of the thermohaline circulation on the strength of the hydrological cycle. Using a two-dimensional, coupled ocean - sea ice - atmosphere model forced by realistic deglacial meltwater fluxes, they identified a circulation response similar to the one inferred from Figure 1; thermohaline overturning collapsed following the first meltwater pulse, recovered spontaneously after about a millennium, and survived the second meltwater pulse. As this simulation produces a credible history of circulation change during the deglaciation, we use the same model in this study to explore the mechanisms by which ^{18}O-depleted freshwater is incorporated into the deep ocean. We find that some of the most significant changes in $\delta^{18}O$ of deepwater (and in carbonates precipitated in equilibrium with seawater) occur immediately upon re-establishment of the overturning circulation at the end of the YD. This occurs because, in these simulations, ^{18}O-depleted freshwater is sequestered at the ocean surface while the circulation is in the collapsed state. The accumulated freshwater is then advected rapidly through the deep Atlantic as the circulation abruptly recovers. Because the model has been spun-up under initial conditions approximating those of the present-day (or Allerød), this occurs only once in the simulations. In the real ocean the same phenomena may have occurred twice, first when the conveyor circulation increased following the last glaciation (at the transition from the Oldest Dryas to the Bølling), and then again at the termination of the YD. Thus, the "store and advect" mechanism may be useful in explaining the isotopic record in sediments, which commonly display two negative excursions, one before and the other after the YD.

In Press: NATO ASI Series, Vol. I 12, *Ice in the Climate system*, W.Richard Peltier, ed. Springer-Verlag, :187-209, 1993.

Supported by: NSF Grant OCE-9019660.

WHOI Contribution No. 8387.

PALEONTOLOGY

EVOLUTION OF DEPTH ECOLOGY IN THE PLANKTIC FORAMINIFERA LINEAGE *GLOBOROTALIA (FOHSELLA)*

R. D. Norris, R. M. Corfield and J. E. Cartlidge

After over 15 million years of evolution in near surface waters of the Western Pacific and Caribbean, planktic foraminifera in the lineage *Globorotalia (Fohsella)* abruptly invaded thermocline habitats 13 Ma ago. Stable isotope data demonstrate that this habitat shift took about 50,000 years to complete, a duration similar to that of the fastest measured rates of speciation in marine protistans. The ecological change occurred near the end of a long series of gradual morphological transitions and demonstrates that at least some of the chronospecies in this lineage had distinctive ecologies and were probably biological species. Other than this one shift in depth distribution, skeletal evolution is largely disconnected from depth changes in *Globorotalia (Fohsella)*. Morphological trends of globorotaliid foraminifera may not record changes in water depth ecology contrary to existing models for foraminiferal diversification.

Published in: *Geology*, 21:975-978, 1993.

Supported by: NSF Grant EAR-9106108.

WHOI Contribution No. 8460.

PETROLOGY

THE INFLUENCE OF WATER ON THE PETROGENESIS OF SUBDUCTION-RELATED IGNEOUS ROCKS

Glenn A. Gaetani, Timothy L. Grove and Wilfred B. Bryan

Experimental evidence shows that the olivine and high-Ca clinopyroxene assemblages found in subduction-related volcanic rocks and ultramafic cumulates crystallized in the shallow crust (-6 km depth) from liquids that contained elevated amounts of dissolved magmatic H_2O (- 2-4 wt%). The compositional variations that occur in high-Ca clinopyroxene in response to changes in pressure and H_2O content of the crystallizing magma allow discrimination between a high-pressure origin (upper mantle depths of ~24-45 km) under anhydrous conditions, and a low pressure origin (crustal depths of ~6 km) involving H_2O-rich magmas. Subduction-related olivine and clinopyroxene bearing lavas contain phenocrysts that are nearly identical to clinopyroxenes from wehrlite xenoliths in arc lavas, and wehrlite cumulates from ophiolites. The occurrence of cumulate wehrlites in ophiolites indicates the presence of H_2O-rich melts, and supports other geochemical evidence that many ophiolites spent some portion of their history in a subduction-related setting (i.e., back-arc or inter-arc basins).

Published in: *Nature*, 365(6444):322-334, 1993.

Supported by: JOI USSAC P.O. #20561.

WHOI Contribution No. 8393.

EVIDENCE FOR HOTSPOT-RELATED CARBONATITE METASOMATISM IN THE OCEANIC UPPER MANTLE

Erik H. Hauri, Nobu Shimizu, Julie J. Dieu and Stanley R. Hart

Four peridotite xenoliths from the islands of Savai'i (Western Samoa) and Tubuai (Austral Islands) contain primary olivine of lithospheric origin, and secondary assemblages of clinopyroxene+spinel±apatite. Trace element results show these secondary assemblages to be the first known occurrences in oceanic xenoliths which can be demonstrated to be in equilibrium with carbonatitic melts. Isotopic results indicate that the carbonatitic melts were derived from recycled crustal endmembers in the convecting mantle, and place constraints on the origins of these endmember compositions.

Published in: *Nature*, 365(6443):221-227, 1993.

Supported by: NSF Grant EAR-9219958.

WHOI Contribution No. 8493.

SEDIMENTOLOGY

AUTOMATED ICE-OCEAN ENVIRONMENTAL BUOYS (IOEBS) FOR THE TELEMETRY OF AIR, ICE AND OCEAN DATA FROM THE POLAR OCEANS

R. Krishfield, S. Honjo, W. B. Tucker III, T. Nakanishi and T. Takizawae

The Ice-Ocean Environmental Buoy (IOEB) was developed to acquire and telemeter in near real-time inter-relatable time-series data on atmospheric, oceanographic and ice physics in

ice-covered oceans during all seasons. Mechanically, the IOEB consists of an extremely durable surface flotation package and an underwater mooring line of instruments and sensors. The apex contains data loggers for meteorological, ice physics and engineering measurements, microcontroller modules for accumulating the data, and ARGOS platform transmit terminals (PTTs) for broadcasting the data. The ocean sensors include conductivity/temperature recorders, an Acoustic Doppler Current Profiler (ADCP), a dissolved oxygen sensor, a transmissometer and two fluorometers. Furthermore, a suspended particle collector and sediment trap collect biogeochemical samples at the bottom of the 110 m suspended mooring. In April 1992, two IOEBs were successfully deployed at two separate ice camps in the Arctic Ocean with battery power adequate to sustain the systems for over two years.

Published in: *Oceans II*, :47-52, 1993.

Supported by: ONR Grant N00014-89-J-1288, JAMSTEC.

WHOI Contribution No. 8484.

PRODUCTION AND ACCUMULATION OF CALCIUM CARBONATE IN THE OCEAN: BUDGET OF A NON-STEADY STATE

John D. Milliman

Present-day production of $CaCO_3$ in the world ocean is calculated to be about 5 billion tons (bt) per year, of which about 3 bt accumulate in sediments; the other 40 percent is dissolved. Nearly half of the carbonate sediment accumulates on reefs, banks and tropical shelves, and consists largely of metastable aragonite and magnesian calcite. Deep-sea carbonates, predominantly composed of calcitic coccoliths and planktonic foraminifera, have orders of magnitude lower productivity and accumulation rates than shallow-water carbonates, but they cover orders of magnitude larger basin area. Twice as much calcium is removed from the oceans by present-day carbonate accumulation as is estimated to be brought in by rivers and hydrothermal activity (1.6 bt), suggesting that outputs have been overestimated or inputs underestimated, that one or more other inputs have not been identified, and/or that the oceans are not presently in steady state. One "missing" calcium source might be groundwater, although its present-day input is probably much smaller than that of rivers. If, as seems likely, $CaCO_3$ accumulation presently exceeds terrestrial and hydrothermal input, this imbalance presumably is offset by decreased accumulation and increased input during lowered sea level: shallow-water accumulation decreases by an order of magnitude with a 100m drop in sea level, while groundwater influx increases because of heightened piezometric head and the diagenesis of metastable aragonite and magnesian calcite from subaerially exposed shallow-water carbonates.

In Press: *Global Biogeochemical Cycles*, 4(4):927-957, 1993.

Supported by: NSF Grant DPP-9000214.

WHOI Contribution No. 8518.

DEPARTMENT OF MARINE CHEMISTRY AND GEOCHEMISTRY

Geoffrey Thompson, Chairman

TRACING THE DOWNWARD FLUX OF NITROGEN AND CARBON INTO THE DEEP OCEAN DURING THE JGOFS N. ATLANTIC BLOOM EXPERIMENT

Mark A. Altabet

Large increases in the $\delta^{15}N$ (12‰) and $\delta^{13}C$ (5‰) of suspended and sinking POM were observed with time during the JGOFS N. Atlantic Bloom experiment. Isotopic fractionation during the uptake of NO_3^- by phytoplankton resulted in ^{15}N enrichment as this substrate was depleted. Decreasing $[CO_2(aq)]$ caused an apparent decrease in the isotopic fractionation factor for photosynthetic carbon fixation. Nevertheless, a 2-week lead in the time-series signal of $\delta^{13}C$ relative to $\delta^{15}N$ was observed due in part to a relatively high $\sum CO_2$ to NO_3^- depletion ratio at the beginning of the bloom and underscoring their fundamental independence as tracers. In contrast to oligotrophic sites previously studies, $\delta^{15}N$ and C/N values for sinking particles collected at 80 m were indistinguishable from values for near-surface suspended particles during the bloom. Small, suspended particles were apparently efficiently converted into large, fast sinking particles in the euphotic zone without significant biological reworking at this time. While sharing several features, the deep (>1000 m) isotopic time-series of sinking particles were substantially modified with respect to near-surface signals. These differences can be explained by a simple time-varying model in which the deep particle flux is separated into two components: one that sinks directly from surface waters and one which undergoes exchange with deep suspended particles through disaggregation and reaggregation. The first component is strongly coupled to surface productivity and undergoes relatively large seasonal variations in flux, whereas the latter's contribution is much more constant. Even during the period of peak particle flux during the bloom, about 20% of total flux appeared to be derived from this second 'background' component. The two-component model also explains well apparent discrepancies between particle sinking speeds previously estimated from Th isotopic data and from time lage with depth in flux maxima. These results indicate that the processes contributing to particle flux in the deep ocean are more complex and temporally variable than previously thought requiring some re-evaluation of existing chemical and isotopic tracer depth.

Supported by: NSF Grants OCE-8817830 and OCE-9115641.

WHOI Contribution No. 8472.

SPECTROSCOPIC CHARACTERIZATION AND REMOTE SENSING OF NON-LIVING ORGANIC MATTER

Neil V. Blough and S. A. Green

Optical absorption and luminescence spectroscopies have played a key role in characterizing the "colored" components of dissolved organic matter (CDOM), which constitute a significant fraction of the total non-living organic matter (NLOM) in the environment. These techniques have also been essential for establishing the ways that CDOM might be viewed by remote sensors. However, our current understanding of the spatial and temporal variability in the optical properties and their relation to CDOM structure remains rudimentary. This article emphasizes the need to examine the relationship between the optical and molecular properties of CDOM in a more systematic fashion, and the importance of this information for both field and remote sensing studies. The optical properties of CDOM are first reviewed, followed by a brief examination of available correlations between the optical and molecular properties of this material. Possible experimental approaches to better define these relationships are then presented. Finally, the use of remote sensing to track the distribution and dynamics of CDOM in natural waters is discussed.

In Press: Dahlem Konferenzen Proceedings on *The Role of Non-Living Organic Matter in the Earth's Carbon Cycle.*

Supported by: ONR Grant N00014-89-J-1260, NASA Grant NAGW-2431, and NSF Grant OCE-9115608.

WHOI Contribution No. 8401.

REACTIONS OF OXYGEN SPECIES IN NATURAL WATERS

Neil V. Blough and Richard G. Zepp

The methods of detection, sources and sinks and environmental significance of photochemically-generated reactive oxygen species are reviewed.

In Press: *Reactive Oxygen Species in Chemistry.*

Supported by: ONR Grant N00014-89-J-1260 and NSF Grant OCE-9115608.

WHOI Contribution No. 8260.

SEASONAL VARIATIONS IN THE NITROGEN ISOTOPIC COMPOSITION OF SEDIMENT TRAP MATERIALS COLLECTED IN LAKE MALAWI

R. Francois, C. H. Pilskaln, and Mark A. Altabet

We have measured the nitrogen isotopic composition of sediment trap materials collected in northern Lake Malawi between June 1987 and January 1991. Short-lived but prominent flux maxima, which occurred irregularly during the dry season, were accompanied by significant decreases in the $\delta^{15}N$ of the settling material. We interpret this observation as reflecting preferential uptake of $^{14}NO_3^-$ during diatom blooms triggered by spurious upwelling events which brought nitrate-rich water to the surface of the lake. We suggest that isotopic fractionation during nitrate uptake by phytoplankton might provide a means of identifying permanent or recurring upwelling centers from lacustrine sedimentary records, from which it might be possible to infer secular changes in regional wind patterns.

Supported by: Project Probe and NSF Grant ATM-8811615, and Research Grant from Mobil and Texaco.

WHOI Contribution No. 8420.

VARIATIONS OF MARINE PLANKTON $\delta^{13}C$ WITH LATITUDE TEMPERATURE AND DISSOLVED CO_2 IN THE WORLD OCEAN

Ralf Goericke and Brian Fry

Variations of the ^{13}C content of marine particulate organic carbon ($\delta^{13}C_{POC}$) in the modern ocean were studied using literature data to test the assumptions underlying the calculation of atmospheric pCO_2 through geological time from the $\delta^{13}C$ of sedimentary organic matter. These assumptions are (1) that concentrations of CO_2 in the atmosphere and the surface ocean are at equilibrium at all times and latitudes, and (2) that carbon isotopic fractionation of phytoplankton (ϵ_p) covaries primarily with the concentrations of dissolved molecular CO_2 ($[CO_2]_{aq}$). Previous studies and compilations have shown that the first assumption does not strictly hold, although $[CO_2]_{aq}$ may be predicted with a reasonable degree of accuracy from sea surface temperature (SST) for specific regions of the world ocean. The second assumption is shown to be questionable due to the weak covariation of ϵ_p and $[CO_2]_{aq}$ in the modern ocean. The large residual variance for regressions of ϵ_p against $[CO_2]_{aq}$ suggests that other factors but $[CO_2]_{aq}$ affect carbon isotopic fractionation in phytoplankton. It is concluded that the relationship between ϵ_p and $[CO_2]_{aq}$ cannot be calibrated using $\delta^{13}C_{POC}$ data from the modern ocean.

Supported by: NSF Grant OCE-9101384.

WHOI Contribution No. 8603.

CHLOROPHYLLS *A* AND *B* AND DIVINYL CHLOROPHYLLS *A* AND *B* IN THE OPEN SUBTROPICAL NORTH ATLANTIC OCEAN

Ralf Goericke and Daniel J. Repeta

Divinyl chlorophyll *a* (chl a_2) and divinyl chlorophyll *b* (chl b_2) are chemotaxonomic tracers for the marine photooxytrophic procaryote *Prochlorococcus marinus*. Here we report the complete separation of chlorophyll *a* (chl a_1) and chl a_2 on a reverse-phase high-pressure liquid chromatography system that also achieves good separation of most other chemotaxonomically important pigments. Chlorophyll *b* (chl b_1) and chl b_2 are partially resolved, and their relative abundances are estimated with an on-line spectrophotometric method. Using these methods, we determined that chl a_2 and chl b_2 contributed up to 40% to total chl *a* (the sum of chl a_1 and a_2) and up to 95% to total chl *b*, respectively, in samples from the subtropical North Atlantic. The results suggest that *Prochlorococcus* represented a significant fraction of the total phytoplanktonic biomass. A comparison of chl *b*/*a* ratios observed in the field of chl *b*/*a* ratios measured in cultures of *P. marinus* suggests the presence of two strains of this organism in the subtropical North Atlantic. The spectroscopic differences between chl a_1 and chl a_2 would have led to small underestimates of total chl *a* in these samples had these been analyzed by spectrophotometric methods. However, the standard fluorometric method would have underestimated total chl *a* on the average by 8% with maximum values of 20%.

Supported by: NSF Grant OCE-9101384 and NASA Grant NAGW-2431.

WHOI Contribution No. 8501.

A HIGH RESOLUTION HISTORICAL RECORD OF HOLOCENE ANOXYGENIC PRIMARY PRODUCTION IN THE BLACK SEA

Daniel J. Repeta

I reconstruct the historical record of anoxygenic primary production in the Black Sea

over the last 8200 years by an analysis of *Chlorobium* carotenoids in sediments. Anoxygenic photosynthesis in the Black Sea occurs only when hydrogen sulfide-containing deep water penetrates the euphotic zone. The data show that the Black Sea has experienced large fluctuations in the extent of anoxygenic primary production and therefore the depth of the H_2S chemocline throughout much of the Holocene. Changes in the depth of the H_2S chemocline also shift the dominant phytoplankton populations in the water column to noncarbonate bearing species and result in the formation of intense dark bands in sediments.

Published in: *Geochimica et Cosmochimica Acta*, 57:4337–4342, 1993.

Supported by: NSF Grants OCE-8614398 and OCE-9017626.

WHOI Contribution No. 8423.

REASSESSMENT OF THE OCEANIC RESIDENCE TIME OF PHOSPHORUS

K. C. Ruttenberg

Phosphorus (P) is an essential nutrient for the growth of all organisms and is believed to limit marine productivity, especially on geologic time scales. As a result of the link between marine photosynthetic productivity and atmospheric CO_2, phosphorus along with other nutrients present in short supply in the euphotic zone have been cited as potential players in the ocean's role in climate change. This link has been referred to as the "nutrient-CO_2" connection.

Model simulations which aim to quantify the role of oceanic nutrient inventories in promoting or enhancing climate change rely on the most currently formulated element budgets for the ocean. In this paper significant modifications to the currently accepted marine phosphorus budget are proposed. The modified P budget presented here requires a reassessment of phosphorus residence time in the ocean, and a concomitant review of the role of P as a potential player in climate change over glacial-interflacial time scales.

Published in: *Chemical Geology*, 107:405–409, 1993.

Supported by: NSF Grant OCE-9101495.

WHOI Contribution No. 8357.

THE ROLE OF BOTTOM SEDIMENTS IN THE AQUATIC PHOSPHORUS CYCLE

K. C. Ruttenberg

Bottom sediments are the locus of early diagenetic reactions which result in build-up of dissolved P in sediment pore waters. Sediment pore waters can be a source of dissolved P delivered to bottom waters via diffusion. If periodic resuspension of bottom sediments occurs, release of P from bottom sediments re-exposed to overlying water can occur. Diagenetic changes in solid-phase P-distribution which occurred between the time of deposition and resuspension can enhance P-release from resuspended bottom sediments. In order to quantitatively evaluate the bioavailability of sedimentary P, it is imperative to understand the processes controlling release of P from sediments, whether resuspended or on the bottom, and the time and space scales over which this release occurs. Measurement of total-P in bulk particulate samples will not reveal the mechanisms which control release of bioavailable P from sediments. Such understanding must be based on quantitative determination of solid-phase P-speciation. Several analytical approaches are evaluated for revealing the chemical nature of sedimentary P. Selective sequential extraction methods are the most promising, especially when coupled with pore water chemical data. Interpretation of early diagenetic chemical reactions inferred from coupled sequential extraction and pore water data can be significantly bolstered by diagenetic modeling of the data. Future work to improve selective leaching schemes is suggested. Algal and microbial culture work using well-characterized sedimentary-P materials as the sole source of nutrient-P could provide useful information on the nature of bioavailable-P in sediments.

Published in: *Proceedings of the National Workshop on Phosphorus in Australian Freshwaters*, Occasional Paper No. 03/93, 1993.

Supported by: NSF Grant OCE-9101495.

WHOI Contribution No. 8439.

TRANSPORT OF SLUDGE-DERIVED ORGANIC POLLUTANTS TO DEEP-SEA SEDIMENTS AT DEEP WATER DUMP SITE 106

Hideshige Takada, John W. Farrington, Michael H. Bothner, Carl G. Johnson, and Bruce W. Tripp

Linear alkylbenzenes (LABs), used in synthetic detergents; coprostanol and epicoprostanol, fecal indicators, were detected in sediment trap and bottom sediment samples at the Deep Water Dump Site 106 located 185 km off the coast of New Jersey, U.S.A. in water depths from 2400 to 2900 m. These findings clearly indicate that organic pollutants derived from dumped sludge are transported through the water column

and have accumulated on the deep sea floor. No significant difference in isomeric composition of LABs was observed among sludge, sediment trap, and sediment samples, indicating little biodegradation of these compounds in the water column and sediments. LABs and coprostanol have penetrated down to a depth of 6 cm in a sediment core, indicating mixing of these compounds into the sediment by biological and physical processes. Also, in artifically resuspended surface sediments, high concentrations of LABs and coprostanols were detected, implying that sewage-derived organic pollutants initially deposited on the deep sea floor can be further dispersed by resuspension and transport.

Small but significant amounts of coprostanol were detected in the sediment from a control site at which no LABs were detected. The coprostanol is probably derived from feces of marine mammals and sea birds, and/or from microbial or geochemical transformations of cholesterol. The polycyclic aromatic hydrocarbons (PAHs) in sediment trap samples from the dump site were largely from the sewage sludge and had a mixed petroleum and pyrogenic composition. In contrast, PAHs in sediments in the dump site were mainly pyrogenic; contributed either from sewage sludge or from atmospheric transport to the overlying waters and subsequent deposition.

In Press: *Environmental Science and Technology.*

Supported by: NOAA's National Undersea Research Program.

WHOI Contribution No. 8471.

AN EXPERIMENTAL MODEL OF THE CHROMOPHORIC DISSOLVED ORGANIC MATTER SOLAR-STIMULATED FLUORESCENCE SPECTRUM

Anthony Vodacek, Sarah A. Green, and Neil V. Blough

We present an experimental model of CDOM solar-stimulated fluorescence. 3D fluorescence spectra of natural waters were employed to determine the solar-stimulated emission from an optically thin sample for a given solar irradiance. Inclusion of the spectrally-dependent fluorescence quantum yield provides emission values in units of photons s^{-1} cm^{-2} 5 nm^{-1}. Attenuation of light in the water column is also modeled, allowing the determination of total upwelled emission. The upwelled fluorescence is compared to irradiance reflectance calculated from a semianalytical model. The fluorescence contribution to reflectance in the blue-green to green can be as high as 70% for blackwater, but is rapidly reduced by the introduction of scattering particles. Excepting blackwaters, CDOM fluorescence does not significantly affect irradiance reflectance ratios commonly employed in remote sensing applications. In water with moderate amounts of CDOM (absorption coefficient at 355 nm ~0.5 m^{-1}), the fluorescence will dominate water Raman scattering as a secondary influence on the light field in the green spectral region.

In Press: *Limnology and Oceanography.*

Supported by: NASA Grant NAGW-2431 and ONR Grant N00014-89-J-1260.

WHOI Contribution No. 8300.

ORGANIC GEOCHEMISTRY

EPR STUDY OF KEROGENS FROM THREE ALASKAN NORTH SLOPE WELLS

Trudy A. Dickneider, Jean K. Whelan, and Neil V. Blough

Whole rock and isolated kerogens from the Seabee, Inigok, and Ikpikpuk wells of the alaskan North Slope have been analyzed by electron paramagnetic resonance (EPR) spectroscopy. The sample suit includes representatives of the Torok, Kingak, Lisburne, Sadlerochit and Endicott formations. Power saturation studies show a definite correlation with the expected downhole maturation, the extent of aromaticity of the sample as defined by ^{13}C NMR, and with the beginning of the oil window for the Kingak formation. Strong correlations within formations across the depositional basin are seen. Abrupt changes in EPR parameters indicate a change in the nature of the organic matter present and may reflect a facies change. Peak widths and spin densities correlate with the usual organic geochemical parameters including vitrinite reflectance and solid state ^{13}C NMR spectra.

In Press: *Organic Geochemistry.*

Supported by: DOE Grant DE-FG02-86ER13466.

WHOI Contribution No. 8437.

CARBON ISOTOPIC EVIDENCE FOR THE ORIGIN OF MACROMOLECULAR ALIPHATIC STRUCTURES IN KEROGEN

Timothy I. Eglinton

This study describes compound-specific stable carbon isotopic analyses of aliphatic hydrocarbon

products from flash pyrolysis (800°C, 20 s) of kerogens representing a range of depositional environments (marine, estuarine, lacustrine) and ages (Recent to Ordovician). The carbon isotopic measurements were obtained, using isotope-ratio-monitoring gas chromatography-mass spectrometry (irmGC-MS), for the major aliphatic pyrolysis products (*n*-hydrocarbons, acyclic isoprenoids and hopanoids). While isotopic compositions of *n*-hydrocarbons varied substantially between samples (average values ranged from -35 to -14‰), δ-values of *n*-alkenes and *n*-alkanes generated from a given sample generally ranged over less than ±3‰. This isotopic uniformity implies a common origin for *n*-hydrocarbons (probably from thermal dissociation of biopolymers), supporting the concept of selective preservation of highly resistant aliphatic structures in kerogens. There are notable exceptions to this general relationship, in which either mixed biopolymeric sources (e.g., Guttenberg Fm) or minor contributions from aliphatic biopolymers (e.g., Monterey) must be inferred. In several cases, average *n*-hydrocarbon values also closely match the corresponding total organic carbon (TOC) δ-value, indicating that the *n*-hydrocarbons in these samples are derived from structurally important, or at least isotopically representative, constituents of the kerogen. In other samples, significant discrepancies were observed between the δ-values for these products and $\delta^{13}C_{TOC}$. In these cases the presence of additional components not yielding hydrocarbons on pyrolysis is indicated. Isotopic compositions of isoprenoid hydrocarbons varied non-systematically relative to those of *n*-hydrocarbons, whereas hopanoid hydrocarbons were consistently depleted in ^{13}C relative to both TOC and *n*-hydrocarbons, with δ-values as low as -50‰.

In Press: *Organic Geochemistry.*

Supported by: NSF Grant OCE-9019166.

WHOI Contribution No. 8522.

RELATION OF SHALE COMPACTION TO DEEP OVERPRESSURES AND HYDROCARBON EXPULSION IN THE GULF COAST

John M. Hunt, Jean K. Whelan, Lorraine Buxton Eglinton, and Lawrence M. Cathles III

The porosities of Tertiary and Cretaceous shales in many wells of the Texas and Louisiana Gulf Coast appear to follow the traditional concept of an exponential decrease of porosity mainly at shallow depths (152 to 305 m, 500 to 1000 ft) during which porosities decrease from about 90% to 30–35%. At greater depths in the normally compacted areas, shale porosities tend to decrease linearly until they reach a porosity of around 9 to 12% at a temperature of 82° to 110°C (180 to 230°F). Beyond this, there is no significant decrease in shale porosity (no compaction) through thousands of feet of burial in many normally compacted Gulf Coast shales.

The tops of deep (>3 km or 10,000 ft) overpressured fluid compartments occur most commonly within the interval of no porosity decrease indicating that compaction does not play a significant role in creating overpressures in these deep high pressure compartments. In addition, the generation and expulsion of hydrocarbons from the source rocks in the Gulf Coast generally occurs at temperatures exceeding 100°C (212°F), which is deeper than the interval of significant shale compaction. Consequently, compaction does not appear to be a factor in expelling hydrocarbons from the source rocks studied herein. Model studies suggest that gas generation is the dominant force causing the deep (>3 km) overpressures and the expulsion of hydrocarbons.

Supported by: Grant from the Gas Research Institute.

WHOI Contribution No. 8573.

THERMAL EVOLUTION OF SEDIMENTS FROM LEG 139, MIDDLE VALLEY, JUAN DE FUCA RIDGE: AN ORGANIC PETROLOGICAL STUDY

Shaozhi Mao, Lorraine Buxton Eglinton, Jean Whelan, and Li Liu

This study is a petrographic examination of the thermal evolution of organic material in sediments from the Ocean Drilling Program leg 139, Middle Valley, Juan de Fuca Ridge. Thermal Alteration Indices (TAI), vitrinite reflectance (%VR_o) and spore fluorescence color (SFC) are used to provide thermal maturation data from four distinct hydrologic environments in this sedimented rift system. Extremely sharp increases in thermal maturity at Sites 856 and 858 characterize past and present hydrothermally active systems, respectively. Site 857 also shows accelerated maturation but may differ from Site 856 and 858 in that lateral fluid flow may be involved. Site 855A is presently immature and gives a good indication of the regional background thermal maturity. A paleotemperature correlation between TAI and other maturity and thermal indicators has has been attempted in conjunction with laboratory experiments.

In Press: *Proceedings of the Ocean Drilling Program,* Scientific Results, Vol. 139.

Supported by: DOE Grant DE-FG02-86ER13466 and a grant from the Ocean Drilling Program.

WHOI Contribution No. 8261.

METASTABLE EQUILIBRIUM AS A CONTROL ON THE ABUNDANCE OF LOW MOLECULAR WEIGHT HYDROCARBONS

Jeffrey S. Seewald

Thermal maturation of sedimentary organic matter reflects reaction progress towards a state of thermodynamic equilibrium. Although it is clear that kinetic barriers allow thermodynamically unstable species to persist in a metastable state for geologically significant periods of time, local equilibrium between more reactive species may substantially influence their abundance. Reported here for the first time are the results of redox buffered hydrothermal experiments that indicate reversible metastable thermodynamic equilibrium is attained between dissolved ethane, ethene, water, and inorganic redox sensitive minerals. Because water participates directly in this equilibrium, it represents a reactive and abundant source of hydrogen for hydrocarbon generation in sedimentary basins. The data presented here provide a basis for the development of new models for the description of chemical processes involving organic species in nature.

Supported by: NSF Grant OCE-9116537 and DOE Grant DE-FG02-86ER13466.

WHOI Contribution No. 8572.

ORGANIC GEOCHEMICAL INDICATORS OF DYNAMIC FLUID FLOW PROCESSES IN PETROLEUM BASINS

Jean K. Whelan, Mahlon C. Kennicutt, James M. Brooks, Dietmar Schumacher, and Lorraine B. Eglinton

A variety of geophysical, geochemical, geological, and well production data have led to the remarkable hypothesis that fluid injection into Eugene Island Block 330 (EI-330) in the US Louisiana Gulf Coast is occurring at the present time. These data include (i) coherence of temperature and pressure contours for reservoirs (pressure decays more rapidly with time than temperature, (ii) abnormally low oil and gas depletion over the time the field has been in production, and (iii) bright seismic amplitude trails coming up from depth along faults. This "dynamic fluid injection hypothesis" is consistent with initial gas and oil compositional data presented here, including

1. Whole oil chromatograms show sharp well-resolved peaks superimposed over a "humpane" type baseline typical of biodegraded oils in the shallowest reservoirs. GCMS shows these sharp peaks to be predominantly highly biodegradable light n-alkanes. The presence of the light n-alkane together with the biodegraded oils shows injection into the shallower reservoirs on very short time scales, possibly as little as years.
2. Ratios of n-heptane/methylcyclohexane (F) plotted against those of toluene/n-heptane (B) for EI-330 oils lie in a region of either very high maturity or within the "condensate" field of an evaporative fractionation event. High maturity is ruled out by ethane vs. propane $\delta^{13}C$ values. Thus, the generally high F values for EI-330 oils are proposed to represent the "condensate" end of an evaporative fractionation event consistent with recent injection of gasoline range hydrocarbons into these reservoirs. For comparison, nearby South marsh Island Block 128 (SMI-128) oils, located on the opposite side of a salt ridge, show higher gas maturities along with a tight clustering of F versus B values consistent with little or no evaporative fractionation or biodegradation.
3. A comparison of whole oil and C7 hydrocarbon data for EI-330 reservoirs taken in 1985 and 1988 shows temporal changes in both light and heavy hydrocarbon compositions. New samples are currently being collected and analyzed from the same platforms to further follow these changes and to rule our sampling or analytical artifacts as the cause of these changes.
4. Vitrinite reflectances for sediment kerogens are higher nearer a fault system thought to feed these reservoirs than in samples away from the fault.

An extensive drilling and sampling program is just beginning at EI-330 with the goal of gaining additional evidence regarding the viability of the "dynamic fluid injection" hypothesis as well as evaluating its usefulness in exploration strategy. A process of episodic pressure build-up followed by rapid breakout of gas and oil through geopressure and injection into overlying reservoirs is proposed.

In Press: European Association of Organic Geochemists.

Supported by: DOE Grant DE-FG02-86ER13466.

WHOI Contribution No. 8499.

TIME-TEMPERATURE HISTORIES OF KEROGEN AND MINERAL AMMONIA FROM ODP LEG 139 (MIDDLE VALLEY) SEDIMENTS

Jean K. Whelan, Jeffrey Seewald, Lorraine Eglinton, and Fran Miknis

Sediments from four sites in the Middle Valley Hydrothermal area were analyzed for thermal maturity by solid state ^{13}C nuclear magnetic resonance (^{13}C NMR) and thermal gravimetric Fourier transform infrared spectroscopy (TG-FTIR). General trends matched those found from vitrinite reflectance profiles indicating increases in thermal maturity from 200 to 400 meters in Hole 857C and from 0 to 300 m in Hole 858A. Holes 858B, 858D, and 858C all showed high maturities in samples shallower than 50 m via both ^{13}C NMR and TG-FTIR. Some samples showed relatively high maturities via these two techniques but relatively low vitrinite reflectance values suggesting that thermal alteration is reflected more rapidly via ^{13}C NMR and TG-FTIR than by Ro in these hydrothermal systems. The TG-FRIR analyses showed strong nitrogen depletion and alteration of the nitrogen containing material in samples exposed to higher temperatures.

For Hole 857C, maximum temperature exposures estimated from the vitrinite reflectance data using Ro/maximum temperature calibrations of Barker (1983) and Barker and Pawlewicz (1986) are less than 30°C at depths shallower than 47 m, 200 to 225°C at 378 m and 256 to >270°C at 433 m. These values closely match present day temperatures of <30°C, 210 to 225°C, and 260°C, respectively, for the same intervals as measured by downhole temperature and ^{18}O. Maximum temperature exposures for other Leg 139 samples for which downhole measurements were not available were estimated to be in the range of <20 to 40°C for 855C-1R-2,141-144 at 2.91 m; <20 to 70°C for 856A-2H-4, 86-101 at 8.06 m; and 260 to >280°C for samples 856A-13X-2, 143-149 at 108.23 m.

At the bottom of geothennally cold Hole 855C, preferential biodegradation of aliphatic portions of kerogen by aerobic microorganisms, activated by a flow of oxygenated cold seawater from basement, is postulated to be responsible for the absence of aliphatic and the predominance of aromatic carbon atoms detected by ^{13}C NMR. Vitrinite reflectance measurements show this section to be immature.

In Press: *Proceedings of the Ocean Drilling Program Scientific Results.*

Supported by: DOE Grants DE-FG05-89ER75506 and DE-FGO2-86ER13466, NSF Grant OCE-9116537, and Grant from Ocean Drilling Program at Texas A& M University.

WHOI Contribution No. 8295.

GEOCHEMISTRY—INORGANIC, ISOTOPIC

A VIEW OF THE LOWER CRUSTAL COMPONENT OF HYDROTHERMAL SYSTEMS AT THE MID-ATLANTIC RIDGE

Kathryn M. Gillis, Geoffrey Thompson, and Deborah S. Kelley

An extensive suite of hydrothermally gabbros was recovered by *Alvin* and dredging from the Mid-Atlantic Ridge, in the vicinity of the eastern ridge-transform intersection (RTI) of the Kane Fracture Zone (MARK), where tectonic extension has provided a window into the lower crustal component of hydrothermal cells. Four alteration types are distinguished on the basis of metamorphic assemblage, mineral composition, and deformation textures. A conceptual model is presented that places temperature-fluid/rock ratio relationships, in conjunction with styles of deformation, into a spatial and temporal framework. Exsolution of late-stage magmatic fluids in the vicinity of the magma-hydrothermal interface at temperatures >700°C marks the on-set of fluid-rock interaction in the MARK gabbros [*Kelley et al.*, this issue], with subsequent alteration involving seawater-derived fluids being strongly influenced by deformation mechanisms. In zones of ductile shear, hydration was initiated at temperatures between 550° to 700°C and moderate fluid/rock ratios. Elsewhere in the lower crust, the on-set of seawater penetration occurred at temperatures of 400° to 550°C and was facilitated by brittle fracturing. Early vein networks indicate that initial fluid/rock ratios were very low, and are interpreted as being related to the solidification of plutons. Later fractures indicate higher water/rock ratios, and may be related to the downward propagation of shallow fault systems. Throughout the crust, fluid-rock interaction ceased at temperatures 180°–300°C. Subsequent cataclastic deformation associated with the unroofing and emplacement of crustal blocks in the RTI massif produced moderate fluid/rock ratios within localized zones. Hydrothermal alteration in the crustal section exposed at MARK was initiated at lower temperatures, and water/rock interaction proceeded to lower temperatures than in many other plutonic suites. These differences must reflect the temporal and spatial evolution of magmatic and tectonic extension that is particular to each section of sampled crust.

Published in: *Journal of Geophysical Research*, 98(B11):19597–19619, 1993.

Supported by: NSF Grant OCE-8917352.

WHOI Contribution No. 8343.

FLUID EVOLUTION IN SUBMARINE MAGMA-HYDROTHERMAL SYSTEMS AT THE MID-ATLANTIC RIDGE

Deborah S. Kelley, Kathryn M. Gillis, and Geoff Thompson

Fluid inclusions in a suite of gabbro, quartz-breccia, and metabasalt samples recovered from the MARK area on the Mid-Atlantic Ridge are the product of a complex hydrothermal history involving late stage magmatic fluids at temperatures >700°C and penetration by modified seawater at 300–400°C. The evolution of volatiles during the early stages of solidification and cooling of magma bodies near the ridge-transform intersection is marked by exsolution of CO_2 fluid, entrapped within primary inclusions in fluorapatites. Attendant with progressive melt fractionation, residual evolved melts reached water saturation, and locally, supercritical CO_2+H_2O+NaCl+Fe brines (>50 wt% NaCl) and cogenetic H_2O+CO_2-rich vapors (1–2 wt% NaCl) were exsolved as immiscible phases. Concomitant or subsequent fracturing, perhaps in response to volatile exsolution from the melts, allowed migration of these fluids along macrofracture networks at >700°C. Trondhjemitic-hosted inclusions, which homogenize by halite dissolution, indicate that the last fluids exsolved from the melts may have been 35–40 wt% brines. The transition from magmatic to seawater-dominated hydrothermal conditions in the gabbros is marked by initial penetration of lower salinity fluids (1–7 wt% NaCl) at temperatures in excess of 400°C, with the general cessation of fluid flow occurring at minimum temperatures of ≈250°C. The relative enrichment and depletion of NaCl with respect to seawater in these fluids may record supercritical phases separation of seawater or boiling of hydrothermal fluids enriched in NcCl. Migration along microfracture networks of CH_4-rich, 350°C fluids, may reflect deeper seated hydrothermal processes involving hydration of underlying mantle material in response to fluid flow along deeply penetrating fault systems. In shallow crustal rocks, circulation of seawater-derived fluids occurred at temperatures up to 400°C, with subsequent collapse of the active hydrothemal system at minimum temperatures of 200–250°C. In fault-related upflow zones, multiple hydrothermal pulses involving 180–340°C and 3.5–10 wt% NaCl fluids, pervasively altered bounding wall rocks, forming chlorite-rich pyrite- and chalcopyrite-bearing breccias. At shallow crustal depths, fluids reached temperatures of 150–300°C and contained salinities of 3.8–6.9 wt% NaCl. Following collapse of the axial-related hydrothemial system, the plutonic and shallow crustal rocks were uplifted and emplaced as allocthonous blocks attending formation of the ridge-transform intersection massif.

Published in: *Journal of Geophysical Research*, 98(B11):19579–19596, 1993.

Supported by: NSF Grant OCE-8917352.

WHOI Contribution No. 8342.

ACTIVE AND RELICT SEA-FLOOR HYDROTHERMAL MINERALIZATION AT THE TAG HYDROTHERMAL FIELD, MID-ATLANTIC RIDGE

Peter A. Rona, Mark D. Hannington, C. V. Raman, Geoffrey Thompson, Margaret K. Tivey, Susan E. Humphris, Claude Lalou, and Sven Petersen

The TAG hydrothermal field is a site of major active and inactive volcanic-hosted hydrothermal mineralization in the rift valley of the slow-spreading Ntd-Atlantic ridge at 26°N. The TAG field occupies an asymmetric area at least 5 km × 5 km of the floor and wall of the rift valley between water depths of 2300 and 4000 m situated between 2 and 8 km east of an axial high along the center of the spreading segment. The axial high is the principal locus of present magmatic intrusions.

The TAG field contains three main areas of present and past hydrothermal activity: (1) an actively venting high-temperature sulfide mound 200 m in diameter by 35 m high at a water depth of 3670 m on the floor of the rift valley near the base of the east wall; (2) two former high-temperature vent areas known as the MIR zone and the ALVIN zone containing multiple sulfide bodies that are undergoing deformation and mass wasting during uplift on fault blocks on the adjacent section of the lower east wall between water depths of 3400 m and 3600 m; (3) a zone of low-temperature venting and precipitation of Fe- and Mn-oxide deposits farther from the axial high and higher on the east wall between water depths of 2300 m and 3100 m.

The active sulfide mound and the MIR and ALVIN zones are situated near the margins of discrete volcanic centers. The volcanic centers occur at the intersections between ridge axis-parallel normal faults and projected axis-transverse transfer faults. The intersections of these active fault systems may act as conduits both for magmatic intrusions from sources beneath

the axial high that build the volcanic centers and for hydrothermal upwelling that taps the heat sources. Convective heat transfer from a central black smoker vent complex (365°C; calculated convective heat flux 225 ± 25 × 10^6 W), white smoker vents (≤300°C), and widespread diffuse flow predominate on the active sulfide mound. Values of conductive heat flow measured at the margins of the active mound and the MIR zone appear to vary inversely with distance from adjacent volcanic centers, supporting the inference that episodic intrusions at the centers have driven hydrothermal circulation at the hydrothermal zones. A low in magnetic intensity coincides with the entire TAG field. The low is modeled as the combined effect of alteration pipes beneath the high-temperature hydrothermal zones and thermal degmagnetization of a still hot but largely solid intrusion beneath the axial high.

Radiometric dating of sulfide samples and manganese crusts in the hydrothermal zones and dating of sediments intercalated with pillow lava flows in the volcanic center adjacent to the active sulfide mound indicate multiple episodes of hydrothermal activity throughout the field driven by heat supplied by episodic intrusions over a period of at least 140 × 10^3 yr. The sulfide deposits are built by juxtaposition and superposition during relatively long residence times near episodic axial heat sources counterbalanced by mass wasting in the tectonically active rift valley of the slow-spreading oceanic ridge. Hydrothermal reworking of a relict hydrothermal zone by high-temperature hydrothermal episodes has recrystallized sulfides and concentrated the first visible primary gold reported in a deposit at an oceanic ridge. Supergene reactions of older sulfides with seawater produces secondary gold enrichment. Preservation of the recrystallized sulfides is favored by silicification or an armoring of oxides.

In Press: *Economic Geology*, 88:1989–2017, 1993.

Supported by: NSF Grant OCE-9013150.

WHOI Contribution No. 8590.

RARE EARTH ELEMENT COMPOSITION OF PRECIPITATION, PRECIPITATION PARTICLES AND AEROSOLS

Edward R. Sholkovitz, Thomas M. Church, and Richard Arimoto

The rare earth elements (REEs), because of their unique solution and chemical properties, can provide new insights into atmospheric chemical reactions of trace elements and the geochemical processes which distribute REEs between the continents, atmosphere and oceans. Here we report the REE composition of aerosols and precipitation (dissolved and particle phases) from Bermuda, Lewes (Delaware, USA) and Woods Hole (Massachusetts, USA). There is large-scale fractionation of REE between the continents, atmosphere and the oceans. The REE compositions of atmospheric samples are highly fractionated relative to (1) each other (e.g., aerosol/precipitation pairs), (2) the upper crust of the earth and (3) seawater. Precipitation samples exhibit markedly convex-up shale-normalized patterns, large negative Eu-anomalies and large and systematic depletions in the heavy REE (Lu>Yb>Er>Gd). We argue that the in-situ selective dissolution of mineral aerosol particles is responsible for the unusual REE composition of precipitation. This has major implications for the interpretation of the biogeochemical cycles of trace elements in the oceans, particularly the partitioning between solution and particle phases, controls on the Nd isotopic composition of seawater, and the chemical weathering of minerals in the aquatic geosphere.

Published in: *Journal of Geophysical Research (Atmospheres)*, 98:20,587–20,599, 1993.

Supported by: NSF Grant OCE-9101466.

WHOI Contribution No. 8296.

HEINRICH EVENTS IN THE NORTH ATLANTIC: RADIOCHEMICAL EVIDENCE

Roger Francois and Michael P. Bacon

Heinrich events are a series of apparently synchronous sediment horizons in the North Atlantic with unusually high ratios of lithic fragments to foraminifera in the coarse fraction. They occur more prominently during cold climatic periods and could have been produced either by dramatic decreases in surface water productivity, by brief increases in carbonate dissolution on the seafloor, or by rapid accumulation of ice-rafted debris. The excess ^{230}Th activity profile in core CHN82 31 11PC (42°23'N; 31°48'W) provides evidence in support of the last of these explanations for the two most recent events (H1 and H2). Sediment flux reconstruction based on the constant ^{230}Th flux model indicates that sediment rain rates increased from an average of *ca* 1.6 g cm^{-2}ka^{-1} to at least 18 g cm^{-2}ka^{-1} during Heinrich event H1 and 11 g cm^{-2}ka^{-1} during Heinrich event H2. These estimates are lower limits, as bioturbation likely smoothed the ^{230}Th profile. Our data also suggest a maximum of 600 y for the duration of H1 and 800 y for H2.

Two independent approaches provide similar estimates of sediment mass accumulation (g cm^{-2})

at the site during the two events; *ca* 10 g cm^{-2} and *ca* 9 g cm^{-2} were deposited from the overlying water column during event H1 and H2. An additional *ca* 4 g cm^{-2} were brought to the site by sediment focussing during event H1. These methods provide a means of mapping and quantifying IRD mass accumulation over the North Atlantic for studying the processes which controlled the distribution of the Heinrich deposits.

In Press: *Deep-Sea Research.*

Supported by: NSF Grant OCE-8922707.

WHOI Contribution No. 8262.

SIZE-FRACTIONATED ^{234}TH IN CONTINENTAL SHELF WATERS OFF NEW ENGLAND: IMPLICATIONS FOR THE ROLE OF COLLOIDS IN OCEANIC TRACE METAL SCAVENGING

S. Bradley Moran and Ken O. Buesseler

Measurements of ^{234}Th ($t_{1/2}$ = 24.1 days) in dissolved, colloidal, and particulate forms have been made to investigate the role of colloids in reactive metal scavenging in the surface waters of Buzzards Bay, over an annual cycle, and in the shelf and slope waters off New England. At-sea sampling involved prefiltering seawater through 0.2 μm filters followed by cross-flow filtration using a 10,000 nominal molecular weight filter to collect colloidal (10,000 NMW-0.2 μm) and dissolved (<10,000 NMW) phases. Total ^{234}Th activities increase with distance from shore, indicative of enhanced scavenging in the particle-rich nearshore waters. Clearly seen in Buzzards Bay are seasonal changes in total ^{234}Th, with activities ranging from ~0.7 dpm l^{-1} in the winter, preceeding a phytoplankton bloom, to ~0.2 dpm l^{-1} in the summer. Throughout the annual cycle, 2–15% of total ^{234}Th is colloidal, 23–43% is dissolved, and 44–75% is particulate. In the offshore waters, ~1% of total ^{234}Th is colloidal, 2–5% is particulate, and 93–98% is dissolved. The ^{234}Th size-distribution exhibits a systematic increase in the association of ^{234}Th with particulate and, to a lesser extent, colloidal matter with increasing suspended particle concentration (C_p). Moreover, a first-order prediction of the fractionation of ^{234}Th between the various size classes is demonstrated using measured solid-solution partition coefficients. Box model calculations indicate a mean residence time of colloidal ^{234}Th with respect to aggregation into particles of 0.4 days in Buzzards Bay, which compares with 2 days for dissolved and 4 days for particulate ^{234}Th. In the offshore surface waters, colloidal and particulate ^{234}Th residence times are ~0.5 days and 1–2 days, respectively, compared with 32–100 days for the dissolved phase. The short residence time of colloidal ^{234}Th is consistent with the hypothesis that colloids play a role as intermediates in the transfer of reactive metals from solution onto particulate matter. Using the size-fractionated ^{234}Th data, we demonstrate that K_d values for thorium are invariant with C_p and that scavenging rate constants exhibit a first-order dependence on C_p. Thus, "particle-concentration effects" are negligible for oceanic waters (C_p ~0.01–1 mg l^{-1}).

In Press: *Journal of Marine Research.*

Supported by: DOE Grant DE-FG02-92ERG1429, NSF Grant OCE-9201186, and NOAA Sea Grant NA90-AA-D-SG480.

WHOI Contribution No. 8458.

VARIATIONS IN THE CHEMICAL AND STABLE ISOTOPE COMPOSITION OF CARBON AND SULFUR SPECIES DURING ORGANIC-RICH SEDIMENT ALTERATION: AN EXPERIMENTAL AND THEORETICAL STUDY OF HYDROTHERMAL ACTIVITY AT GUAYMAS BASIN, GULF OF CALIFORNIA

Jeffrey S. Seewald, William E. Seyfried, Jr., and Wayne C. Shanks III

Organic-rich diatomaceous ooze was reacted with seawater and a Na-Ca-K-Cl fluid of seawater chlorinity at 325 to 400°C, 400 to 500 bars, and fluid/sediment mass ratios of 1.6 to 2 to constrain factors regulating the abundance and stable isotope composition of carbon and sulfur species during hydrothermal alteration of sediment from Guaymas Basin, Gulf of California. Alteration of inorganic and organic sedimentary components resulted in extensive exchange reactions, the release of abundant H_2S, CO_2, CH_4, and $C_{organic}$ to solution, and recrystallization of the sediment to an assemblage containing albitic plagioclase, quartz, pyrrhotite and calcite.

The stable isotope composition of dissolved H_2S varied from -10.9 to +4.3‰ during seawater sediment interaction at 325 and 400°C and from -16.5 to -9.0‰ during Na-Ca-K-Cl fluid-sediment interaction at 325 and 375°C. In the absence of seawater SO_4, H_2S is derived from the recrystallization and transformation of pyrite to pyrrhotite, and from sulfur release during the degradation of organic matter. In the presence of seawater SO_4, reduction of SO_4 contributes directly to H_2S production. Sedimentary organic matter acts as the reducing agent during pyrite and SO_4 reduction. Requisite acidity for the reduction of SO_4 is provided by Mg-fixation during

early-stage sediment alteration and by albite and calcite formation in Mg-free solutions.

Thermal maturation of sedimentary organic matter under hydrothermal conditions resulted in the release of abundant CO_2, CH_4, and $C_{organic}$ to solution. Organically derived CH_4 was characterized by $\delta^{13}C$ values ranging from -20.8 to -23.1‰ whereas $\delta^{13}C$ values for dissolved $C_{organic}$ varied from -14.8 to -17.7‰. Mass balance calculations indicate $\delta^{13}C$ values for organically derived CO_2 were $\geq$-14.8‰. Residual solid sedimentary organic matter showed small but significant depletions in ^{13}C relative to the starting sediment.

The experimental results are consistent with the isotopic and chemical composition of natural hydrothermal fluids and minerals at Guaymas Basin, Gulf of California and permit us to better constrain sources and sinks for carbon and sulfur species in sub-seafloor hydrothermal systems at sediment-covered spreading centers. The sulfur isotope composition of hydrothermal sulfide minerals from Guaymas Basin indicate derivation of sulfur from diagenetic sulfide and seawater sulfate. Mobilization of basaltic sulfur may also be contributing to sulfide deposits but is not required. Estimates of seawater/sediment mass ratios based on sulfur isotopic composition of sulfide minerals and the abundance of dissolved NH_3 in vent fluids range from 3 to 29 during hydrothermal circulation. Sources of carbon in Guaymas Basin hydrothermal fluids include thermal degradation of organic matter, bacteriogenic methane production, and dissolution of diagenetic carbonate.

In Press: *Geochimica et Cosmochimica Acta.*

Supported by: NSF Grants OCE-9116537 and OCE-8400677.

WHOI Contribution No. 8438.

THE USE OF NITROGEN ISOTOPIC RATIO FOR RECONSTRUCTION OF PAST CHANGES IN SURFACE OCEAN NUTRIENT UTILIZATION

Mark A. Altabet and Roger Francois

Sedimentary $^{15}N/^{14}N$ can be used as a unique measure of past changes in surface ocean nutrient utilization which in turn is a function of past changes in productivity and nutrient input from deeper waters. Due to isotopic fractionation during nitrate uptake by phytoplankton, partial nutrient utilization produces substantial ^{15}N enrichment in particulate matter reaching the seafloor. Examples are given from the N. Atlantic, Equatorial Pacific, and Southern Ocean. In the latter two regions where there are large variations in nutrient utilization with latitude, corresponding gradients in both near-surface ocean and core top $^{15}N/^{14}N$ are observed. Thus isotopic signals generated in surface waters are transferred and preserved in sediments. First down core results from the Southern Ocean indicate that only modest increases in nutrient utilization and perhaps productivity occurred in Subantarctic waters during the last glacial maximum.

In Press: *Carbon Cycling in the Glacial Ocean,* R. Zahn, M. A. Kaminski, L. Labeyrie, and T. F. Pederson, eds. NATO ASI Series.

Supported by: NSF Grant OCE-9115641 and DPP-9118031.

WHOI Contribution No. 8473.

INTRODUCTION TO ATLANTIC HYDROTHERMAL ACTIVITY

Peter A. Rona and Geoffrey Thompson

Seafloor hydrothermal research has advanced rapidly from the discovery in mid-1960's of hot metalliferous brines and sediments ponded in deeps along the slow-spreading (half-rate 1 cm yr^{-1}) axis of the Red sea [Charnock, 1964; Miller, 1964; Swallow and Crease, 1965; Miller et al., 1966; Hunt et al., 1967; Bischoff, 1969]; recognition of a hydrothermal metalliferous component in sediments of the East Pacific Rise [Skornyakova, 1964; Arrhenius and Bonatti, 1965; Bostrom and Peterson, 1966]; discovery in 1972 and 1973 of warm springs and low-temperature hydrothermal precipitates at the TAG hydrothermal field at the slow-spreading (half-rate 1.2 cm yr^{-1}) Mid-Atlantic Ridge near 26°N [Rona, 1973; Rona and R.B. Scott, 1974; M.R. Scott et al., 1974; R.B. Scott et al., 1974; Rona et al., 1975]; discovery in 1977 of warm springs and chemosynthetic vent biota at the intermediate spreading (half-rate 3 cm yr^{-1}) Galapagos spreading center [Williams et al., 1974; Lonsdale, 1977; Corliss et al., 1979]; prediction based on extrapolation to pure and member of the mixed Galapagos hydrothermal solutions (Edmond et al., 1979], discovery in 1978 of massive sulfide deposits (CYAMEX Scientific Team, 1979], and in 1979 of high-temperature black smoker-type venting at the East Pacific Rise near 21°N spreading at an intermediate rate (half-rate 3 cm yr^{-1} [CYAMEX Scientific Team, 1979; RISE Project Group 1980]; discovery in 1985 of high-temperature black smoker-type venting, massive sulfides, and vent biota in the Atlantic at the TAG hydrothermal field (Rona, 1985; Rona et al., 1986], and at the Snakepit hydrothermal field (Scientific Party, Leg 106, 1986] at 26°N and 23°N, respectively, at the Mid-Atlantic Ridge. Additional hydrothermal sites are being found at spreading centers in the northeast Pacific, the southeast

Pacific, the Indian Ocean, and in back-arc basins of the western Pacific leading to recognition of seafloor hydrothermal activity as a global phenomenon [Rona, 1988).

The basic hydrothermal process is similar at different locations consisting of subseafloor circulation of seawater driven convectively by magmatic heat sources at or near spreading centers involving reaction of the heated seawater with permeable rocks of the crust and sometimes the upper mantle. However, significant differences in solution chemistry, heat transfer, mineralization and biology are also being found. The ten papers presented in this special section, *Atlantic Hydrothermal Activity*, are part of the initial series of papers which define chemical, physical and biological characteristics of the hydrothermal systems at the TAG and Snakepit hydrothermal sites based on the detailed investigations at these sites. These investigations include the initial intensive dive series at Snakepit (11 dives) by Deep Submergence Vehicle (DSV) *NAUTILE* in 1988 [Mevel et al., 1989]; at TAG (16 dives) and Snakepit (3 dives) by DSV *ALVIN* in 1990 [Mid-Atlantic Ridge Hydrothermal Research Team, 1990]; and by the two MIR submersibles in the TAG area in 1988 (18 dives) [Zonenshain et al., 1989; Lisitsyn et al., 1989], and in 1991 (6 dives) [Rona et al., this issue]. Earlier versions of most of the papers were presented orally in two sessions at the Fall 1990 American Geophysical Union meeting [Rona and Thompson, 1990; Thompson and Rona, 1990].

Published in: *Journal of Geophysical Research*, 98:9621–9623, 1993.

Supported by: NSF Grant OCE-9013150.

WHOI Contribution No. 8347.

RELICT HYDROTHERMAL ZONES IN THE TAG HYDROTHERMAL FIELD, MID-ATLANTIC RIDGE 26°N, 45°W

P. A. Rona, Y. A. Bogdanov, E. G. Gurvich, N. A. Rimski-Korsakov, A. M. Sagalevitch, M. D. Hannington, and G. Thompson

Two relict hydrothermal zones were delineated between water depths of 3400 m and 3500 m at the lower part of the east wall of the rift valley of the Mid-Atlantic Ridge in the TAG hydrothermal field using a deep-towed side-scan sonar tow and a camera-temperature tow along the northern 3 km of the wall, and a submersible transect. Named the North and MIR relict zones, they are located about 4 km and 2 km northeast, respectively, of the known active high-temperature sulfide mound between water depths of 3625 and 3670 m on the rift valley floor near the base of the east wall. The North zone extends about 2 km along the northern end of the lower east wall. The zone includes two mound-like features up to 30 m high by 200 m in diameter imaged by side-scan sonar within a 2 km-long line of discontinuous hydrothermal deposits comprising inactive toppled and standing chimneys, layered material, and patchy dark stains on sediment photographed by the camera-temperature tow. Several other mound-like features were imaged with the side-scan sonar outside of the photographic coverage. The MIR relict hydrothermal zone 2 km south of the North zone, named after the MIR submersible used to investigate it, consists of three subzones: (1) a 200 m-wide area of diverse types of hydrothermal materials exposed by normal faulting at its western margin; (2) a 400 m-wide by 700 m-long central area of discrete groups of toppled and standing inactive sulfide chimneys up to 25 m high on a substrate of red metalliferous sediment and carbonate lutite; spires sampled on the highest chimneys are composed of coarse-grained, recrystallized sulfides dominated by pyrite and chalcopyrite which contain the first primary, free gold grains (2–3 microns diameter) found at a hydrothermal site on a mid-ocean ridge; (3) a 150 m-wide hummocky area of layered hydrothermal material with the appearance of low temperature precipitates and carbonate lutite with patchy dark stains at its eastern margin. The active sulfide mound, the North zone, and the MIR zone are each located on the fractured western margins of gentle, dome-shaped areas of pillow flows typically 500 m in diameter interpreted as summits of volcanic centers that may have supplied heat to drive adjacent hydrothermal activity. The distribution and size of the active and inactive hydrothermal zones of the TAG field, the chronology and the characteristics of relict samples recovered indicate a long history of high-temperature hydrothermal episodes with multiple overprinting stages of mineralization accompanied by alteration.

Published in: *Journal of Geophysical Research*, 98:9715–9730, 1993.

Supported by: NSF Grant OCE-9013150.

WHOI Contribution No. 8345.

PH OF THE NORTH ATLANTIC OCEAN: IMPROVEMENT TO THE GLOBAL MODEL FOR SOUND ABSORPTION IN SEA WATER

Peter G. Brewer, David M. Glover, Catherine Goyet, and Deborah K. Shafer

At frequencies below 1 kHz sound absorption coefficients in the ocean are a function of pH, and at higher frequencies are dependent upon $MgSO_4$. The pH dependent terms are attributable to relaxation of $B(OH)_3$ and $MgCO_3$ species, and the ensemble effect has been given (*Mellen et al.* [1987]) as:

$$\alpha = \alpha_1(MgSO_4) + \alpha_2(B(OH)_3) + \alpha_3(MgCO_3)$$

where α is the absorption coefficient (db/km) and

$$\alpha_n = \frac{S}{35} A_n \frac{f^2 f_n}{(f^2 + f_n^2)}$$

Overall accuracy of $\pm 15\%$ in α requires that pH be known to 0.05 units.

The presently used oceanic pH field for sound absorption models is derived from a combination of GEOSECS data, and Soviet data from the Gorshkov atlas (*Gorshkov* [1974]) for the North Atlantic where GEOSECS data are absent. We compare the North Atlantic fields with the well constrained TTO North Atlantic CO_2 data set and find large differences. We further show that sufficiently strong correlations exist between CO_2 system variables and other hydrographic properties that improved renditions of the pH field in other regions of the ocean area possible once equivalent local correlations are established.

Supported by: Office of Naval Technology Grant N00014-90-C-0098.

WHOI Contribution No. 8548.

STABILITY OF THE OXIC/ANOXIC INTERFACE IN THE BLACK SEA

K. O. Buesseler, H. D. Livingston, L. Ivanov, and A. Romanov

We have examined the position of the oxic, suboxic, and anoxic interfaces in the Black Sea between 1965–1992. It appears as if the suboxic zone (i.e., depths where DO and $H_2S < 5\ \mu M$) has been a common feature throughout the Black Sea, and only recandy been observed due to advances in sampling and analytical procedures. The upper boundary of the suboxic zone is identified based upon a minimum in the PO_4 profile at a density of 15.95 σ_t. The lower boundary at 16.20 σ_t is identified by the onset of H_2S. These densities show seasonal and interannual variations on the order of 0.05–0.10 σ_t, but no directional trend over the past 2–3 decades. The position of the suboxic zone is consistent with T/S data. Large variations in T/S characteristics are seen between years and seasons above the suboxic layer, as ventilation is quite rapid. Below the DO $< 5\ \mu M$ horizon, entrainment processes bring surface water to depth, thus forming a suboxic layer as DO and H_2S are consumed. T/S characteristics vary slightly below 16.2 σ_t, and are constant below 17.0 σ_t, indicating that these waters are ventilated less frequently.

In Press: *Deep-Sea Research.*

Supported by: NSF Grant OCE-8917465 and EPA Grant R817047-01-3.

WHOI Contribution No. 8400.

LONG-TERM VARIABILITY OF PARTICLE FLUX IN THE DEEP SARGASSO SEA

W. G. Deuser

The particulate flux to the deep Sargasso Sea has now been measured continuously for over 15 years. More than 85% of the time elapsed since April of 1978 is represented in the sample suite from 3200 m. This suite was the first in which an annual cycle in deep-ocean flux, tied to the cycle of primary production in the surface water, was observed. This feature has since been observed in a variety of oceanographic settings. However, while a distinct annual cycle persists throughout the record, a significant amount of spectral energy is also in periods both longer and shorter than the annual. A reliable assessment of these periods offers the greatest promise for identifying forcing functions through the study of spectral coherence with oceanographic and meteorologic variables. The reason lies in the fact that an annual cycle is common to all of them and, therefore, is of little diagnostic value. The definition of the high-frequency variability is, of course, limited by the sampling frequency. A compromise always has to be struck between the desirability of high temporal resolution (short sampling intervals) and the requirements of minimum sample size for the purposes of chemical and other analyses. Our bimonthly sampling scheme of the first 11 years was not well-suited to studying variability on less than about semiannual periods. We quadrupled the sampling frequency to biweekly in mid-1989 and can now begin to assess monthly variability. The periodogram for those four years (94%

temporal coverage) shows secondary peaks at periods of 6, 4.4, 3.2 and 2 months. The periodogram for fifteen years of bimonthly sampling has secondary peaks at periods of 4.5 and 2.7 years (beyond the annual and shorter periods). For the detection of any periods longer than that, e.g., of sunspot-cycle length, the series is still far too short.

Is it likely that the series will be continued that long? It certainly is desirable. We do need long series of observations and measurements in order to identify forcing functions of carbon input to the deep ocean and to detect secular changes. While time series definitely have gained more respect in recent years, their establishment and maintenance are still entirely dependent on the rules and priorities of short-term funding schemes. This is clearly not a good situation because not even a large number of series of just one or a few years' duration can replace a single series of a few decades' length. Similarly, once a series is stopped, a restart is unlikely and of questionable value (see, for example, the demise of the Ocean Weather Ships: while widely lamented, it is now irreversible!). Also, it is increasingly appreciated that rare, episodic events, the occurrence of which, by definition, is unpredictable, can have major impact on ecosystems, far beyond their duration. Their effect on the sedimentary record can also be highly significant. Such events are very unlikely to be recorded by short measurement series or even by long but discontinuous series. Only continuously recording, long-term sampling schemes offer any prospect of assessing them.

Supported by: NSF Grants OCE-9017114 and OCE-9215350.

WHOI Contribution No. 8498.

OPTICAL ABSORPTION AND FLUORESCENCE PROPERTIES OF CHROMOPHORIC DISSOLVED ORGANIC MATTER IN NATURAL WATERS

Sarah A. Green and Neil V. Blough

Complete optical absorption and fluorescence spectra were collected for a diverse suite of 0.2-μm filtered marine, riverine and estuarine waters, as well as for colored dissolved organic matter (CDOM) isolated from several of these waters by C-18 extraction. Absorption and fluorescence parameters for these samples are reported. For surface waters, variations in the fluorescence quantum yields obtained with 355 and 337 nm excitation fell within a narrow window (<2.5-fold variation about the mean values), demonstrating that fluorescence measurements can be employed to determine absorption coefficients of CDOM in the ultraviolet with reasonably good accuracy. Methods for predicting absorption coefficients and lineshapes from the fluorescence data are introduced and tested. The absorption and fluorescence spectra of CDOM extracted from some seawaters were found to differ significantly from those of the original waters, clearly illustrating that great care must be taken when these extracts are used to infer the optical properties of natural waters.

Supported by: ONR Grant N00014-91-J-1260, NASA Grant NAGW-2431, and NSF Grant OCE-9115608.

WHOI Contribution No. 8589.

OCEAN PARTICLE CHEMISTRY: THE FRACTIONATION OF RARE EARTH ELEMENTS BETWEEN SUSPENDED PARTICLES AND SEAWATER

Edward R. Sholkovitz, William M. Landing, and Brent L. Lewis

Sargasso Sea suspended particles were sequentially digested with three chemical treatments (acetic acid, mild HCl-HNO_3 and HF/HNO_3/HCl in a bomb). The latter two treatments dissolve detrital minerals while the acetic acid removes surface coatings (organic matter and Mn oxides). The rare earth element (REE) composition of the surface coatings, in marked contrast to the crust-like REE composition of the two detrital phases, is extensively fractionated with respect to both filtered seawater and the crust. Surface coatings are responsible for the removal and fractionation of REEs from seawater and, as such, play a key role in the marine geochemcial cycles of trace elements.

Relative to seawater, the surface coatings are systematically enriched 10-fold across the trivalent REEs from Lu to La and develop large positive Ce-anomalies. The Ce-anomalies of the coatings switch from being negative (seawater-like) in the upper 100 m to being strongly positive at greater depths. The in-growth of and Ce and light REEs on particle surfaces reflects the *in situ* oxidation of dissolved Ce (III) to particulate Ce (IV), and the preferential removal of light REE (III) over heavy REE (III). REEs (III) fractionation of this type is consistent with particle/solution models. Both processes appear to be related to the *in situ* formation of Mn oxide particles from the oxidation of dissolved Mn (II) in the upper 200 m of the water column. Preferential removal of light REEs in the upper waters is countered by their preferential release at depth due to remineralization of surface coatings on particles.

Our results support a recent argument by Bertram and Elderfield (1993) that the vertical variation in the Nd isotopic composition of seawater is being driven by the reversible exchange of Nd between particles and seawater, a concept consistent with REE adsorption onto surface coatings.

A new method is explored for estimating the residence time of suspended particles by combining Ce concentration data of dissolved and surface-bound phases with the Ce (III) oxidation rate measurements of Moffett (1990). A Ce-based residence time of 13 days is similar in magnitude to the value calculated from U-Th^{234} disequilibria in the Sargasso Sea (Moran and Buesseler, 1992).

In Press: *Geochimica et Cosmochimica Acta.*

Supported by: NSF Grants OCE-8711032 and OCE-9101466.

WHOI Contribution No. 8464.

INSTRUMENTS AND METHODS

MOORING LINE MOTIONS AND SEDIMENT TRAP HYDROMECHANICS: IN-SITU INTERCOMPARISON OF THREE COMMON DEPLOYMENT DESIGNS

G. Gust, A. F. Michaels, R. Johnson, W. G. Deuser, and W. Bowles

Trap array characteristics were monitored concurrent with particle collections for tethered and bottom-moored cones and cylinders (MultiPITs) at the North Atlantic OFP/JGOFS site in the Sargasso Sea. At depths ranging from 145 m to 3200 m, velocities of approaching fluid and those inside the traps were recorded at 5 Hz in bursts of 3–10 min every half hour during particle collections. A thermistor, a high resolution pressure gauge, and two inclinometers concurrently monitored trap movements. Burst-averaged slip velocities experienced by both shallow and deep tethered traps reached 37 cm/s, while a bottom-moored trap recorded 10-d averaged speeds of 4 cm/s. For both cones and cylinders, flow cells inside the traps led to an intense flushing of fluid and particles. While none of the traps ever tilted more than 8 degrees from vertical, even under strong flow accelerations, tether-line motions induced by the surface waves introduced high flow acceleration peaks into trap arrays at all depths, even for bungie-cord decoupled tethers of MultiPIT arrays. The flow cells inside traps were thus agitated with intense turbulence found close to the collection cup in the apex of cones. Trap fluxes by tethered cones were up to a factor of 8 smaller than by MultiPITs at the same depth, cones (and perhaps cylinders) collected more material when experiencing higher approaching fluid flows, and for the same conical geometry tethered traps collected less material than bottom-moored traps. In MultiPITs, the internal flow cell and collection characteristics changed in response to a density interface established between the dense preservation fluid and sea water. The in-situ deployments revealed substantial differences in collection behavior among different trap arrays, all of which deviated from steady-state flume simulations. Indications are that the diameter of the retention cup at the trap apex, rather than the diameter of the trap mouth, may be the design parameter controlling particle collection rates of conical traps. To advance efforts to link trap and in-situ fluxes, line motions and hydrodynamics of individual trap arrays must be monitored. Trap simulation studies utilizing steady-state flume flows may be accurate only under very specialized conditions.

In Press: *Deep-Sea Research.*

Supported by: NSF Grants OCE-8716589 and OCE-9017114.

WHOI Contribution No. 8263.

ANALYSES OF DISSOLVED ORGANIC CARBON IN SEAWATER: THE JGOFS EQPAC METHODS COMPARISON

Jonathan H. Sharp, Ronald Benner, Lenore Bennett, Craig A. Carlson, Steve E. Fitzwater, Edward T. Peltzer, and Luis M. Tupas

Results of a dissolved organic carbon (DOC) methods comparison are presented here in which five high temperature combustion (HTC) instruments and a wet chemical oxidation (WCO) method were used on a series of oceanic samples. The samples were collected during U.S. JGOFS Equatorial Pacific Ocean cruises (EqPac) and most of the authors were involved with DOC analyses for the EqPac Program. Samples were collected with a "clean" protocol and were immediately quick frozen in replicate sample bottles. They were distributed by the first author to the other authors for "blind" analyses later on land on the stored samples.

Comparable results (±7.5%) were found by three HTC instruments and the WCO method. There were difficulties with the other two HTC methods for which explanations and improvements are offered. The single most critical element for good DOC values appears to be assessment and subtraction of the total instrument blank (or reagent and handling blank for WCO methods). A

"zero" carbon (very low C) water sample assisted in having all analysts achieve a uniform assessment of individual instrument or methods blanks. Conditioning of the catalyst bed in the combustion tube is critical to achieve consistent low instrument blanks. Failure to thoroughly condition the catalyst bed may be a significant error that can give erroneously high DOC values for oceanic samples. Reference standards available to all analysts also allowed comparison of instrument and methods performance. Contamination problems were demonstrated and it was shown that careful preparation and handling can reduce the potential for errors from contaminated samples.

Results indicate Equatorial Pacific oceanic DOC values in near surface waters that are on the order of 60–70 μM C and deep water values on the order of 35–40 μM C. Since the "zero" carbon water contained a small, but measurable, amount of DOC, the sample values reported here may be slightly low. Because the lowest instrument blanks were equivalent to about 10 μM C, it is suggested that even if there were no instrument blank at all and all this "blank" were in the "zero" carbon water, the oceanic sample concentrations could not be underestimated by more than 10 μM C.

Supported by: NSF Grant OCE-9115201.

WHOI Contribution No. 8581.

PHYSICAL OCEANOGRAPHY

DEPARTMENT OF PHYSICAL OCEANOGRAPHY

James Luyten, Chairman

OCEAN CIRCULATION & LOW FREQUENCY VARIABILITY

A CLOSER LOOK AT PARTICLE EXCHANGE IN THE GULF STREAM

Amy S. Bower and M. Susan Lozier

Isopycnal floats deployed in the Gulf Stream in the last decade have shown that a substantial amount of particle exchange takes place between the Gulf Stream and the surrounding fluid at the level of the main thermocline: 75% of the floats released in the center of the jet northeast of Cape Hatteras escaped from the current in less than 30 days. Re-entrainment of floats was also frequently observed. This exchange is suggestive of significant cross-stream eddy mixing. However, to accurately interpret the float exchange in terms of property exchange, it is necessary to determine where the floats were deployed relative to the strong property front which is aligned with the Gulf Stream's cyclonic flank. Toward this end, the cross-stream structure of potential vorticity in the Gulf Stream has been examined in four layers of the main thermocline (7–17° C) and the behavior of the floats has been analyzed in light of the potential vorticity structure in each layer.

In the lower half of the main thermocline (7–12° C) it was found that potential vorticity is nearly uniform across the stream. Eighty percent of the floats deployed in this layer escaped from the Gulf Stream in less than 30 days, but due to the homogeneity of the potential vorticity field at this level, this *particle* exchange is not representative of a significant *property* exchange. In the upper layer of the main thermocline, 14.5–17.0° C, a strong potential vorticity front is consistently present and aligned with the Gulf Stream's cyclonic flank in the upper ocean. Furthermore, it was determined that the floats released in this layer were launched *offshore* of the potential vorticity front in water of subtropical origin. In contrast to the lower main thermocline, where the vast majority of floats escaped in less than one month, in the upper main thermocline, most of the floats (60%) stayed in the stream for at least that long. The remaining 40% (eight floats) were lost equally to both sides of the current. Since the floats in this layer were deployed on the offshore, or south, side of the potential vorticity front, it is only the trajectories of the four floats that escaped from the Gulf Stream to the north at this level that can be identified as indicative of a cross-stream property/flux. This is only 4% of all floats deployed in the main thermocline. It is therefore concluded that almost all of the observed particle exchange between the Gulf Stream and its surroundings is *not* associated with a cross-stream property flux, but instead represents fluid particles circulating within the same water mass. These results are viewed in light of a study of particle behavior in a quasi-geostrophic EGCM and are found to be generally compatible with the model results.

Submitted to: *Journal of Physical Oceanography.*

Supported by: ONR Contract N00014-91-J-1425.

WHOI Contribution No. 8407.

EXCHANGE THROUGH THE STRAIT OF GILBRALTAR

Harry L. Bryden, Julio Candela and Thomas H. Kinder

To measure the exchange between the Atlantic and Mediterranean through the Strait of Gibraltar, an array of current meter moorings was deployed for a year in the Strait during 1985–86. A novel aspect of these measurements is the inclusion of conductivity as well as temperature and pressure sensors on each current meter so that the salinity of the flows could be monitored continuously. These salinity measurements determine the water mass characteristics of the flows crossing the sill; they allow definition of the 37‰-isohaline as the interface between inflowing fresher Atlantic water and outflowing saltier Mediterranean water, and they enable time series to be developed for the depth of this interface, for the upper layer inflow, and for the lower layer outflow.

From these measurements, the time-averaged outflow of Mediterranean water is estimated to be -0.68 Sv and the outflow salinity transport, defined to be the outflow times the salinity excess above a basic Atlantic water salinity of 36.1‰, is estimated to be -1.50 Sv‰, equivalent to a net evaporation over the Mediterranean basin of 52 cm yr^{-1}. Extrapolated measurements of the inflow from current meters generally deployed below 100 m depth yield an estimate for the time-averaged inflow of 0.93 Sv, which is believed to be unrealistically high in view of the better measured outflow and net evaporation. Thus, a more realistic estimate of the inflow is 0.72 Sv, equal to the sum of the outflow and net evaporation as required by the mass budget for the Mediterranean Sea. Such estimates of the exchange are smaller by almost a factor of 2 than previous values for the exchange by Lacombe and Richez (1982).

The exchange across the Gibraltar sill is found to be due in nearly equal parts to the mean currents and to tidal fluctuations. The mean currents are smaller than had been expected reaching a peak value of only about -60 cm s^{-1} in the deep outflow over the sill. The tidal exchange is due to a strong correlation over the tidal period between the depth of the interface and the

strength of the inflowing currents. For the M_2-tide at the sill, the amplitude of the interface depth is 51 m and the amplitude of the tidal currents is 1.2 m s^{-1}; furthermore, the inflow and interface depth have similar phases. As a consequence, the upper layer is deep on the inflowing tide so that a large slug of Atlantic water crosses the sill into the Mediterranean; on the outflowing tide, the interface is shallow so that a large slug of Mediterranean water crosses the sill into the Atlantic. Similar processes occur for the S_2, O_1 and K_1 tides, though the amplitudes are smaller. In this manner, tidal oscillations lead to a time-averaged exchange of water masses across the Gibraltar sill.

The inflow and outflow, defined to be the instantaneous transports above and below the 37‰-isohaline interface, exhibit M_2-tidal amplitudes of 2.3 Sv and 1.3 Sv respectively. Thus, the tides are large enough to reverse the mean upper layer inflow and lower layer outflow. Daily averaged inflow and outflow transports exhibit low-frequency fluctuations with standard deviations of 0.37 Sv and 0.22 Sv respectively. Such low frequency fluctuations have been shown previously to be associated with barotropic flows through the Strait of Gibraltar compensating for sea level variations over the Mediterranean due to atmospheric pressure fluctuations (Candela, Winant and Bryden, 1989). Finally, from these measurements there appears to be little fortnightly or annual period fluctuations in the exchange through the Strait of Gibraltar.

Submitted to: *Progress in Oceanography.*

Supported by: ONR Contract N00014-87-K-0007.

WHOI Contribution No. 8525.

SALT FLUX AS A MECHANISM OF LARGE-SCALE CIRCULATION IN THE BLACK SEA

S. N. Bulgakov, G. K. Korotaev and J. A. Whitehead

The hypothesis is discussed that formation of the large-scale cyclonic system of currents in the Black Sea is due to river run-off and inflow of salty Marmara Sea waters through the Bosphorus strait. A theoretical investigation of dynamics induced by lateral boundary salt flux was carried out using analytical and numerical modelling in an open channel for the linear, quasi- and nonlinear cases. On the basis of these results, the formation of the general cyclonic current system (and other large-scale dynamic elements that are known from the observation of the Black Sea) are interpreted as being driven by river run-off and inflow of salty Marmara Sea water. To test the theoretical results about the formation of buoyancy flux induced circulation and stratification in the Black Sea, a series of laboratory experiments was carried out. A cylindrical rotating tank was used with intrusion of fresh water at the surface and salt water at intermediate depth. Other experiments were conducted with thermal forcing composed of a warm temperature in the upper part of the cylinder wall and cold temperature below. The stable regime of the quasi-steady circulation in the laboratory tests has good agreement with the theoretical predictions. Surface buoyancy induced circulation is cyclonic. The circulation has a jetstream character and a three-layer vertical structure with a counter-current at intermediate depth. It does not depend on the symmetrical or asymmetrical way that fresh or salt water fluxes are distributed along the side wall. The importance of orography influence on the gyre formation, so-called "Knipovich glasses" in the Black Sea, has also been observed in the salt-driven experiments.

Submitted to: *Journal of Marine Research.*

Supported by: ONR Contract N00014-89-J-1037.

WHOI Contribution No. 8598.

BAROTROPIC RESPONSE OF THE WESTERN MEDITERRANEAN TO OBSERVED ATMOSPHERIC PRESSURE FORCING

Julio Candela and Carlos J. Lozano

The barotropic response of the Western Mediterranean Sea to observed atmospheric pressure derived from twice daily ECMRWF analyses is studied using a space spectral representation of the shallow water equations for the entire Mediterranean Sea that includes exchanges across the Strait of Gibraltar. The atmospheric pressure induced transport is the predominant barotropic signal at the Straits of Gibraltar and Sicily. Cross-spectra of the model transports through the Straits of Gibraltar and Sicily indicate high coherence at low frequencies (periods $\geq$ 10 days) and in bands centered around 2.5 and 1.4 day periods. There is a broad band between 3 to 10 days where the barotropic flows in the two straits are incoherent, even though both straits, specially Sicily, show energetic flows at these periods. The latter behavior is due to excitation of some of the rotational basin modes. The response of the Sea to atmospheric pressure has a marked seasonal variability with circulation patterns 2 to a times more intense during the winter months. The frictional dissipation of energy at Gibraltar is two orders of magnitude larger than the dissipation related to either the irrotational or rotational motions induced by the atmospheric

pressure in the interior. The conspicuous rotational circulation in the basin are generated via topographic and planetary β effects and dissipation mechanisms. The atmospheric pressure induced sea surface signal is dominant over tidal or wind related surface changes and its variability is described via Empirical Orthogonal Functions (EOF).

Submitted to: *The Seasonal and Interannual Variability of the Western Mediterranean Sea.* Paul La Violette, ed. American Geophysical Union.

Supported by: ONR Contract N00014-93-1-0415.

WHOI Contribution No. 8255.

CHANGES IN ANTARCTIC BOTTOM WATER PROPERTIES IN THE WESTERN SOUTH ATLANTIC IN THE LATE 1980'S

Victoria J. Coles, Michael S. McCartney, Donald B. Olson and William M. Smethie, Jr.

Antarctic Bottom Water properties within the Argentine Basin are shown to have evolved during the 1980's to a fresher, less dense watermass. Comparisons of hydrographic property data from several time periods are shown in 4 locations following the western boundary current. These figures indicate that the Antarctic Bottom Water potential temperature to salinity relationship freshened, and the coldest temperatures warmed between 1984 and 1988. Data collected in 1988–89, as part of the South Atlantic Ventilation Experiment, have been combined with the historical database to produce a map of potential temperature at 4000m. Used as an indication of geostrophic shear, the map defines a south and western intensified crescent shaped abyssal recirculation. The volume of water in each temperature class has been computed to quantify the change in dominant mode from colder to warmer water below the 0.2° C isotherm. This change corresponds to a net heat flux into the basin over the time period of 1.22×10^5 J/m^3. Comparison of 1983 and 1988 sections in the Brazil Basin shows northward penetration of the fresh watermass in the deep western boundary current to between 18° S and 10° S. It is suggested that open ocean convective events within the Weddell Sea contributed to the change in Antarctic Bottom Water documented here.

Submitted to: *Journal of Geophysical Research.*

Supported by: NSF Grants OCE86-14486 and OCE92-01314.

WHOI Contribution No. 8587.

BIO-OPTICAL AND PHYSICAL VARIABILITY IN THE SUB-ARCTIC NORTH ATLANTIC OCEAN DURING THE SPRING OF 1989

T. Dickey, J. Marra, M. Stramska, C. Langdon, T. Granata, R. Weller, A. Plueddemann and J. Yoder

A unique set of physical, bio-optical, and meteorological observations were made from a mooring located in the open ocean south of Iceland (59° 29.5' N 20° 49.8' W) from April 13 to June 12, 1989. The present measurements are apparently the first to resolve the rapid transition to springtime physical and biological conditions at such a high latitude site. Our data, which were collected with bio- optical and physical moored systems every few minutes, captured the abrupt onset of springtime stratification with the mixed layer shoaling from ≈550 m to ≈50 m in about 5 days along with a major phytoplankton bloom indicated by a tenfold increase in near surface chlorophyll concentration in less than three weeks. Our statistical analysis indicates that the velocity shear in the upper layer is driven primarily by local wind stress. Mesoscale variability is also apparent from these and concurrent Airborne Oceanographic Lidar observations. Our complementary modeling results suggest that the near surface layer may be reasonably well described by a one-dimensional model and that the spring bloom was initiated during incipient near surface restratification.

Submitted to: *Journal of Geophysical Research.*

Supported by: ONR Contracts N00014-89-J-1498, N00014-89-J-1150, N00014-89-J-1683; NASA Contracts NAGW-1500-1854 and NAGW-1500-1891.

WHOI Contribution No. 8576.

THE INFLUENCE OF DISTRIBUTED SOURCES AND UPWELLING ON THE BAROCLINIC STRUCTURE OF THE ABYSSAL CIRCULATION

Christopher A. Edwards and Joseph Pedlosky

We report the study of a simple, continuously stratified model of the abyssal ocean driven by source fluid entering the basin through lateral boundaries and by upwelling out of the abyss into the main thermocline.

Our approach divides the deep ocean into inviscid interior and frictional boundary layer regions. The interior circulation is fully determined by the horizontal upwelling distribution and by the *net, vertical* distribution of sources entering the basin. Forcing by the local upwelling drives a

barotropic velocity field, and remote forcing by both the upwelling and sources generate an underlying baroclinic flow, which can be considerably stronger and of opposite sign at some depths. The boundary current functions to redistribute around the perimeter fluid entering the boundary regions either through the basin walls or from the interior. In contrast to the interior flow, it depends also on the *geographical* location of sources. The boundary current is divided into three sublayers, one barotropic layer that is required to satisfy an overall mass balance, and two baroclinic layers which close the baroclinic circulation. The outer baroclinic layer has a width that depends on the vertical scale of the flow and can extend far into the interior. Stratification induces the sub-division of both the interior and boundary layers into an upper region, dominantly driven by the upwelling, and a lower one, predominantly influenced by the sources.

Submitted to: *Journal of Physical Oceanography.*

Supported by: NSF Grant OCE89-05890.

WHOI Contribution No. 8593.

DEEP CIRCULATION IN THE TROPICAL NORTH ATLANTIC

Marjorie A. M. Friedrichs and Melinda M. Hall

A transatlantic CTD/ADCP (Conductivity, Temperature, Depth/Acoustic Doppler Current Profiler) section along 11N, taken in March 1989, has been used to compute geostrophic velocities; geostrophic transport is required to balance *in situ* values of the Ekman and shallow boundary current transports. The horizontal flow structure is described for eight layers, with particular emphasis on deep and bottom waters (four layers below $\theta = 4.7°$ C). In the shallow layers, total North Brazil Current (NBC) transport agrees with other observations previously made in the month of March, while net northward flow of these layers across the western basin is also consistent with recent observations to the north. For each of the four deep layers, circulation patterns are illustrated by means of schematic cartoons. Each of these layers flows southward in the Deep Western Boundary Current, which has a magnitude of 26.5 Sv. Roughly half of this flow returns northward to the west of the Mid-Atlantic Ridge, confirming the existence of a hypothesized cyclonic recirculation gyre in the western basin of the tropical Atlantic. To varying degrees the deep and bottom waters also circulate cyclonically in the eastern basin, with net northward flow across this basin.

Partly as a result of the unusual appearance of the North Equatorial Countercurrent in March 1989, the *in situ* values of the meridional overturning cell (5.2 Sv), heat flux (3.0 $\times 10^{14}$ W), and freshwater flux (-0.65 Sv) computed from the 11N section depart significantly from estimates of these quantities in the literature. By forcing the 11N geostrophic velocities to balance annual average Ekman and NBC transports, annual average values of these fluxes (12 Sv; 11 $\times 10^{14}$ W; -0.6 Sv) are obtained, and are shown to agree well with historical estimates.

Published in: *Journal of Marine Research,* 51(4):697–736, 1993.

Supported by: NSF Grants OCE87-16314 and OCE91-01636; and a Graduate Fellowship from ONR through the American Society for Engineering Education.

WHOI Contribution No. 8346.

HEMISPHERIC ASYMMETRY OF DEEP WATER TRANSPORT MODES IN THE ATLANTIC

Marjorie A. M. Friedrichs, Michael S. McCartney and Melinda M. Hall

Subtropical studies of the Atlantic meridional cold water flow show a hemispheric contrast in the dominant southward transport mode below 2000 meters: in the North Atlantic lower deep water (LDW: 1.8° C$\leq \theta \leq$ 2.4° C) dominates with small transport of middle deep water (MDW: 2.4° C$\leq \theta \leq$ 3.2° C), while in the South Atlantic the opposite is observed. We use numerous observations in the western basins of the tropics to show that the transition occurs rapidly near the equator in the western Atlantic, rather than smoothly due to gradual warming and upwelling following the flow. A meridional section in the central Brazil Basin reveals zonal flows that are responsible for the transition. LDW transport from the Guiana Basin (north of the equator) flows eastward at about 4° S in the Brazil Basin, and is inferred to continue on through the Romanche Fracture Zone into the eastern Atlantic. An opposing flow of MDW from the eastern tropical Atlantic flows towards the western boundary, where it bifurcates to supply MDW to the DWBC of the Brazil Basin, as well as to feed the northward flow of MDW in the Guiana Basin offshore of the DWBC. The intensity of the opposing flows is about 7 Sv, and in the eastern basin the zonal flows appear to be connected predominantly by upwelling from LDW to MDW within the tropics.

The overall deep water transport system below 2000 meters in mid- and low latitude Atlantic is thus found to comprise three distinct components: 1) A strong DWBC transport of LDW with

associated recirculation dominates the Guiana Basin north of the equator; 2) A zonal overturning cell south of the equator absorbs the exported LDW and carries it eastward, and imports MDW into the western basin where it bifurcates; 3) The southward branch of this flow causes the MDW dominance in the Brazil Basin, where the MDW dominated DWBC and associated recirculations are the third component of the deep water transport system.

Submitted to: *Journal of Geophysical Research.*

Supported by: NSF Grants OCE92-01314 and OCE91-01636; NOAA Grant NA16RC0527-01.

WHOI Contribution No. 8523.

MEAN SEA SURFACE HEIGHT OF THE ANTARCTIC CIRCUMPOLAR CURRENT FROM GEOSAT DATA: METHOD AND APPLICATION

Sarah T. Gille

The mean sea surface height across the Antarctic Circumpolar Current has been reconstructed from height variability measured by the Geosat altimeter, without assuming prior knowledge of the geoid. For this study, an automated technique has been developed to estimate mean sea surface height for each satellite ground track using a meandering Gaussian jet model, and errors have been estimated using Monte Carlo simulation. The results are objectively mapped to produce a picture of the mean Subantarctic and Polar Fronts (SAF and PF) which together comprise the major components of the Antarctic Circumpolar Current. The meandering jet model explains between 40% and 70% of the height variance along the jet axes. The results show that the fronts are substantially steered by topography, though they do not precisely follow contours of f/H, and that the jets have an average Gaussian width of about 44 km in the meridional direction and meander about 75 km to either side of their mean locations. The average height difference across the SAF is 0.7 m and across the PF 0.6 m. The mean widths of the fronts are correlated with the size of the baroclinic Rossby radius.

Submitted to: *Journal of Geophysical Research - Oceans.*

Supported by: ONR Graduate Student Fellowship NASA Contract NAGW-1666.

WHOI Contribution No. 8524.

MEAN CIRCULATION OF THE UPPER LAYERS OF THE WESTERN EQUATORIAL PACIFIC OCEAN

Yves Gouriou and John Toole

Hydrographic (0–1000 db) and direct current measurements (0–600 db) along 165° E (20° S–10° N) between January 1984 and July 1991 are used to investigate the mean circulation and its relationships with the distributions of salinity and potential vorticity on isopycnal surfaces. Less well documented mean sections along 142° E and 137° E are used to complement the 165° E analysis.

The Equatorial Undercurrent is centered on the equator at 165° E and at 0.5° N at 142° E. No variation in its transport (15. 10^6 m^3s^{-1}) is found between those longitudes. We find indication of the Equatorial Undercurrent at 137° E–0.75° N in the geostrophic field. The northern and southern Subsurface Countercurrents are clearly identified by extrema of eastward velocity at 165° E around 3° N and (250 dbars). No evidence of a southern Subsurface Countercurrent is found at 142° E. At 137° E the northern Subsurface Countercurrent is not characterized by a local extrema of eastward velocity: the North Equatorial Countercurrent seems to extend from the surface to 400 dbars with a southward shift of its core. Analysis of the seasonal variability at 165° E indicates that the Equatorial Undercurrent transport increases by a factor two between January (10.7 10^6 m^3s^{-1}) and July (21.5 10^6 m^3s^1) and the Equatorial Intermediate Current transport is halved (6.3 10^6 m^3s^{-1} in January, 3.5 10^6 m^3s^{-1} in July). In contrast the transport of the Subsurface Countercurrents does not vary substantially between those two months.

The meridional distributions of salinity and potential vorticity show that the axes of the main eastward currents are associated with strong meridional property gradients, not with property extrema. The eastward currents thus represent a barrier to the northward extension of the high salinity Tropical Water. Relatively weak meridional gradients of salinity and potential vorticity are observed in the westward directed South Equatorial Current and Equatorial Intermediate Current.

Submitted to: *Journal of Geophysical Research.*

Supported by: NSF Grant OCE91-15347; ORSTOM.

WHOI Contribution No. 8404.

SYNTHESIZING THE GULF STREAM THERMAL STRUCTURE FROM XBT DATA

Melinda M. Hall

Thirty-six XBT temperature profiles have been used in a parametric model introduced by Hendry (1988) to model the Gulf Stream's thermal structure at 65° W between 200 and 1200 dbars, with an rms residual error of 0.64° C. Velocity has been computed geostrophically relative to 1200 dbar, and has been included in calculating potential vorticity analytically from the model. The resulting potential vorticity section for 65° W has been compared with the analogous result from Hendry's parametric model at 59° W, as well as the observed potential vorticity at 68° W from Hall and Fofonoff (1993). Potential vorticity is found to exhibit relative maxima and minima along thermocline isopycals crossing the current, and there is a change in structure from the western locations (68°, 65° W) to the eastern location (59° W).

Submitted to: *Journal of Physical Oceanography.*

Supported by: ONR Contracts N00014-87-K-0001, NR 083-004, N00014-88-K-0612 and N00014-89-J-1056.

WHOI Contribution No. 8394.

OBSERVATIONS OF GULF STREAM MEANDER INDUCED DISTURBANCES

Nelson G. Hogg

Using moored array data collected across the Gulf Stream at 55°W we have investigated the dynamical signatures of the velocity fluctuations at the thermocline (550 m) and near bottom (4000 m) levels. The cross-stream amplitude and phase structures for motions with period from 64 to 12 days, in a coordinate frame aligned with the instantaneous Stream, have a striking resemblance to those computed from small amplitude instability theory. In addition, the mean downstream velocity at the two levels is consistent with a model for the mean flow in which the lower layer has uniform potential vorticity. Some puzzles remain. It is the sinuous or asymmetric mode that appears to dominate the observed fluctuations whereas the varicose mode is predicted to have a substantially larger growth rate. The model for the mean flow when fit to the data predicts a value for the rate of change of the Coriolis parameter appropriate to this latitude but one would expect it to be augmented by a factor of two or so by the significant slope of the bottom in this region.

Submitted to: *Journal of Physical Oceanography.*

Supported by: ONR Contract N00014-85-C-0001; NSF Grant OCE86-08258.

WHOI Contribution No. 8429.

THE LONG-TERM HYDROGRAPHIC RECORD AT BERMUDA

Terrence M. Joyce

A long time-series (by oceanographic standards) of hydrographic observations at Bermuda was begun in 1954 and continues to the present. Analysis of this data set has shown the temperature and salinity variations on interannual time-scales to be largely independent in the surface layer (0-500 m depth) and highly correlated in the thermocline and below. Salinity changes in the deepest layer observed at Bermuda station "S" (1500-2500 m) are masked by measurement errors in the early years of the time-series. The reason for correlated temperature and salinity changes is because the interannual variability between 500-1500 m is due to vertical oscillations of the thermocline with amplitudes of $\pm$ 50 m. Inclusion of earlier data of opportunity near Bermuda has permitted the time-series of temperature change to be extended backward 22 years to 1932. Over the entire 58 year period, temperature change is characterized by decadal time-scale changes at all depths, but notably the deepest layer (1500-2500 m) also shows a trend of increasing temperature. The rate of increase appears to be constant and equal to about 0.5° C/century. This rate of temperature rise amounts to a sequestration of 0.7 watts m^{-2} of 'excess' heat flux in the deep water and, because of thermal expansion of seawater, should produce a rise in steric sea level of approximately 7 cm/century.

Submitted to: *Nature.*

Supported by: NSF Grant OCE90-06184.

WHOI Contribution No. 8398.

SPATIAL VARIABILITY OF SUBDUCTING WATER IN THE NORTH ATLANTIC: A PILOT STUDY

Terrence M. Joyce and William J. Jenkins

Hydrographic and tritium-^{3}He data obtained on a small scale survey conducted in 1986 south of the Azores show strong horizontal and isopycnic gradients across the Azores Front. Examination of small-scale spatial variability reveals a dominant scale for salinity, oxygen and tritium-^{3}He age of order 160 km, comparable to estimates of sea

surface height correlation scales from Geosat data. This spatial variability correlates strongly with large-scale horizontal gradients. Two mesoscale resolving surveys separated by 300 km reveal spatial scales and amplitudes of thickness variability that decrease rapidly with age, becoming incoherent on scales greater than 18 km within 1 year, and approaching internal wave background values. There appears to be a substantial reduction in mode thickness between the two surveys, which may be the result of non-conservation of potential vorticity, or the result of interannual changes in formation. Subduction rates computed from tritium-^{3}He age gradients are comparable to or larger than Ekman pumping estimates based on climatological data.

Published in: *Journal of Geophysical Research,* 98(C6):10,111–10,124, 1993.

Supported by: NSF Grants OCE85-15642 and OCE89-09908; ONR Contract N00014-89-J-1312.

WHOI Contribution No. 8365.

MONITORING GULF STREAM TRANSPORT BY RADAR ALTIMETER AND INVERTED ECHO SOUNDERS

Kathryn A. Kelly and D. Randolph Watts

The Gulf Stream has both path and transport fluctuations on seasonal and interannual time scales. Fluctuations in the Gulf Stream surface transport of about 10% with spatial scales of more than 1000 km and temporal scales of several months were observed using the radar altimeter on board the U.S. Navy's Geodetic Satellite (Geosat). Anomalously large surface transports were found to be correlated with more northerly paths. The structure of the transport fluctuations suggests large-scale changes in the Gulf Stream recirculation gyres. Fluctuations were also monitored using moored inverted echo sounders (IES) as part of the Synoptic Ocean Prediction (SYNOP) program. Here we show a high degree of correlation between upper layer transport fluctuations estimated from the IES and the altimetric surface transport fluctuations and excellent correspondence between path fluctuations. These comparisons demonstrate that large-scale fluctuations in both transport and path of the Gulf Stream can be monitored directly using the satellite-mounted radar altimeter.

In Press: *Journal of Physical Oceanography.*

Supported by: NASA Contract NAGW-31666; NSF Grant OCE87-17144; ONR Contract N00014-90-J-1568.

WHOI Contribution No. 8287.

ANOMALOUS ANOMALIES IN AVERAGED HYDROGRAPHIC DATA

M. Susan Lozier, Michael S. McCartney and W. Brechner Owens

A comparison of a recently assembled hydrographic database for the North Atlantic (Lozier *et al.* 1993) with data from the Levitus atlas (1982) shows striking differences in the vicinity of the Gulf Stream and the North Atlantic Current. On isopycnal surfaces in the main thermocline, isolated pools of warm, saline water are found in the Levitus database but are absent in the new database. Using synoptic data as a proxy for temporally-averaged climatological data, it is shown that the anomalous features can be accounted for by the difference in the averaging process. To produce a gridded database from irregularly-spaced station data Levitus averaged the data on pressure surfaces while Lozier *et al.* (1993) averaged on potential density surfaces. It is shown that averaging on a pressure surface in an area of sharply sloping isopycnals produces a water mass with a θ-S signature uncharacteristic of the surrounding synoptic water mass(es). The anomalous potential temperatures and salinities that result are compared to the background water mass anomalies of the North Atlantic and are shown to be of comparable strength. As a caution to users of averaged data the consequences of having sizable averaging artifacts are discussed.

In Press: *Journal of Physical Oceanography.*

Supported by: NSF Grant OCE91-03364; NOAA Grants NA36GP-0137 and NA16RC-1527-01.

WHOI Contribution No. 8487.

GULF STREAM-GENERATED TOPOGRAPHIC ROSSBY WAVES

Robert S. Pickart

An inverse ray tracing model is applied to observations of 40 day topographic Rossby waves off of Cape Hatteras to determine their origin. The model shows that as the rays extend into the region of the Gulf Stream the bottom slope remains strong enough that topographic β dominates planetary β. This enables coupling to occur between eastward propagating Gulf Stream meanders and topographic waves with eastward phase speed and matching zonal wavelength. The most frequency occurring Gulf Stream meanders have a period of 40 days, and the model reveals that as these meanders pass a topographic bend near 71–72°W they are able to couple to the observed topographic waves traced back from Cape Hatteras. The 40 day Gulf Stream meanders occur

in bursts, apparently due to enhanced baroclinic instability, which leads to associated bursts of the topographic waves.

Submitted to: *Journal of Physical Oceanography.*

Supported by: ONR Contract N00014-92-J-1910.

WHOI Contribution No. 8513.

INTERACTION OF GULF STREAM AND DEEP WESTERN BOUNDARY CURRENT WHERE THEY CROSS

Robert S. Pickart

The long time scale variability of the deep western boundary current (DWBC) where it crosses under the Gulf Stream is analyzed using a three-year array of bottom current meters and inverted echo sounders. The relationship of this variability to fluctuations in the upper layer Gulf Stream is specifically addressed. At periods shorter than a year the DWBC variability shows no relationship to the local Gulf Stream: 100 day fluctuations show a pulsing of the DWBC transport, whereas longer period fluctuations are indicative of a meandering-type variability. By contrast, on time scales greater than a year variations in the orientation and transport of the DWBC are directly related to such fluctuations in the local Gulf Stream. The coupling reveals that the DWBC is forced by changes in the Gulf Stream rather than causing such variations, which contradicts earlier modeling results.

Submitted to: *Journal of Geophysical Research.*

Supported by: ONR Contract N00014-92-J-1910.

WHOI Contribution No. 8512.

DETERMINING THE MEAN GULF STREAM AND ITS RECIRCULATIONS THROUGH COMBINING HYDROGRAPHIC AND ALTIMETRIC DATA

Bo Qiu

The altimetric data from the first 2.5-year Geosat Exact Repeat Mission were used to estimate the mean sea surface height (SSH) field in the region of the Gulf Stream and its recirculation gyres. Assuming the instantaneous surface velocity field is composed of an eastward flowing jet and two westward recirculating flows, we used the time-varying surface data from the altimeter to determine the shape of the along-track mean SSH profiles and the historical hydrographic data to constrain the net SSH difference across the Gulf Stream system. The two-dimensional mean SSH field was determined by objectively mapping the mean height profiles along the ascending and descending tracks. The SSH jump across the mean Gulf Stream has a maximum of 1.15 m around 65° W and drops to an almost constant 0.9 m downstream of the New England Seamount Chain (NESC). While the SSH jump associated with the mean northern recirculating flow is mostly uniform, we found that the Gulf Stream's southern recirculation has two local gyres that are separated by the NESC. An attempt was then made to estimate the mean deep circulation in this region by comparing the mean SSH field derived from the altimetry data and the surface dynamic height field based on the historical hydrographic data. Despite the large uncertainties, we found that the mean deep flow pattern thus estimated agreed well with the overall circulation pattern suggested by the long-term current meter observations. Like the well defined northern recirculation gyre, a continuous southward flow along 57.5° W also follows closely along the deep layer potential vorticity contours. To the south of the Gulf Stream, the deep circulation consists of two separated recirculation gyres; divided by the NESC, the gyre to the west appears to circulate around the Corner Rise.

Published in: *Journal of Geophysical Research,* 99(C1):951–962, 1994.

Supported by: NOAA Grant NA16RC-0468-01; ONR Contract N00014-92-J-1656.

WHOI Contribution No. 8341.

UPPER OCEAN HEAT BALANCE IN THE KUROSHIO EXTENSION REGION

Bo Qiu and Kathryn A. Kelly

A horizontally two-dimensional mixed-layer model is used to study the upper-ocean heat balance in the Kuroshio Extension region (30°–40° N, 141°–175° E). Horizontal dependency is emphasized because, in addition to vertical entrainment and surface thermal forcing, horizontal advection and eddy diffusion make substantial contributions to changes in the upper-ocean thermal structure in this region. By forcing the model using the wind and heat flux data from ECMWF and the absolute sea surface height data deduced from the Geosat ERM, the mixed-layer depth (h_m) and temperature (T_m) changes in the Kuroshio Extension are hindcast for a 2.5-year period (November 1986–April 1989). Both phase and amplitude of the modeled T_m and h_m variations agreed well with the climatology. The horizontal thermal patterns were also agreed favorably with the available *in-situ* SST observations, but this agreement depended crucially on the inclusion of horizontal advections.

Although the annually averaged net heat flux from the atmosphere to the ocean (Q_{net}) is negative over the Kuroshio Extension region, the effect of the surface thermal forcing, when integrated annually, is to increase T_m because the large, negative Q_{net} in winter is redistributed in a much deeper mixed layer than it is in summer when $Q_{net} > 0$. This warming effect is counterbalanced by the vertical turbulent entrainment through the base of the mixed layer (35% when annually integrated), the Ekman divergence (16%), the geostrophic divergence (12%), and the horizontal eddy diffusion (35%). Though small when averaged in space and time, the temperature advection by the surface flows makes a substantial contribution to the local heat balances. While it warms the upstream region of the Kuroshio Extension (west of 150° E), the current advection tends to cool the upper ocean over the vast downstream region due to the presence of the recirculation gyre.

Published in: *Journal of Physical Oceanography,* 23(9):2027–2041, 1993.

Supported by: ONR Contract N00014-92-J-1656; NOAA Grant NA16RC-0468-01.

WHOI Contribution No. 8253.

NORTH BRAZIL CURRENT RETROFLECTION EDDIES

P. L. Richardson, G. Hufford, R. Limeburner and W. S. Brown

During 1989–1992 five different anticyclonic eddies were observed to translate up the coast of South America between 7N and 12N. These eddies which are similar to those recently observed with CZCS images, current meters, and altimetry, are inferred to have formed from pieces of the North Brazil Current that retroflects or veers offshore near 7N to flow eastward. The overall near surface diameter of the eddies when newly formed is estimated to be 400 km. The retroflection eddies were identified in trajectories of four surface drifters and two SOFAR floats at 900 m that looped as they translated northwestward with a mean velocity of 10 cm/sec. The two longest trajectories were (1) by a 900 m float beginning near 7N in August 1989 that looped 14 times over 151 days with a maximum diameter of 140 km and (2) by a surface drifter beginning near 7N in October 1990 that looped 9 times over 116 days with a maximum diameter of 250 km and maximum swirl speed of 80 cm/sec at that diameter. The mean rotation period of the two eddies was 8 days and 13 days (respectively), with the rotation period of small loops at 900 m around 7 days. Three the eddies were observed during the period August 1989 to April 1990. Retroflection eddies are considered to provide significant northward volume transport ~ 3 Sv along the western boundary even during the months when the North Brazil Current has been observed to retroflect into the countercurrent.

In Press: *Journal of Geophysical Research.*

Supported by: NSF Grants OCE85-21082, OCE88-12917, OCE91-15712 and OCE91-14656.

WHOI Contribution No. 8434.

OBSERVATIONS OF SUPER-INERTIAL AND NEAR INERTIAL WIND-DRIVEN FLOW

Daniel L. Rudnick and Robert A. Weller

The super-inertial and near-inertial wind-driven flow in the western North Atlantic is examined using data from two recent experiments. The Frontal Air-Sea Interaction Experiment (FASINEX) took place at 27° N, 70° W during 1986. The Long-Term Upper-Ocean Study (LOTUS) took place at 34° N, 70° W during 1982. Each experiment included moored measurements of meteorological variables that allowed estimation of the wind stress and oceanic currents. The directly wind-driven flow is isolated from other sources of variability, such as internal waves and mooring motion, using a transfer function between geocentric acceleration and wind stress. The transfer function is examined in rotary spectral bands bounded by periods of 36 and 12 hours, and 12 and 2 hours. For surface-moored observations, wind-driven mooring motion is found to cause a response that extends at least to 1000 m (much deeper than the frictional layer of direct wind forcing). Once this artifact is removed the directly wind-driven flow is identified. This response is found to rotate to the left (right) for clockwise (counterclockwise) rotating super-inertial wind stress, in agreement with the solution of the time-dependent Ekman spiral. When vertically integrated the Ekman transport relation is satisfied, indicating that all of the wind-driven flow has been isolated.

Submitted to: *Journal of Physical Oceanography.*

Supported by: ONR Contracts N00014-90-J-1496 and N00014-84-C-0134.

WHOI Contribution No. 8274.

WAVE-INDUCED ABYSSAL RECIRCULATIONS

Michael A. Spall

The forcing of abyssal recirculation gyres by cross isopyncal mixing and wave fluxes near the

deep western boundary is investigated. A three-layer isopycnal primitive equation model is applied in a series of experiments to an idealized basin with bottom topography. In the absence of deep western boundary current instabilities, cross isopycnal mixing forces a cyclonic recirculation gyre, modified by topography, which is consistent with the traditional Stommel-Arons model. Instabilities of the boundary current fundamentally alter the mean basin-scale deep flow from a cyclonic recirculation to an anticyclonic recirculation. The forcing mechanism is the downslope propagation of energy carried by topographic waves from the boundary current into the interior. The offshore variation in the deep stratification results in a horizontal divergence of the momentum flux carried by the waves which drives a poleward mean flow over the western sloping bottom and forces the anticyclonic recirculation. This is essentially an adiabatic process. The addition of cross isopycnal mixing forces the large scale interior recirculation towards the pole, partially into boundary currents, through linear vorticity dynamics. Vorticity budgets reveal three dynamical regimes for the eddy-driven flows, the western boundary current, the recirculation region, and the interior. Similarities and differences between the mean flow and recent observations in the Brazil Basin are discussed.

Submitted to: *Journal of Marine Research.*

Supported by: Bundesminister für Forschung and Technologie Grant 03F0050D and NSF Grant OCE93-01323.

WHOI Contribution No. 8556.

ADVECTION AND EDDY MIXING IN THE MEDITERRANEAN SALT TONGUE

Michael A. Spall, Phillip L. Richardson and James Price

Lagrangian trajectories from the SOFAR float Mediterranean outflow experiment are used to estimate the low frequency variability and mixing in the vicinity of the Mediterranean salt tongue. Two dominant patterns of Lagrangian variability are observed, (1) nearly zonal low frequency motions and (2) wave-like oscillations with northwest to southeast orientation. The zonal motions are found near the core of the salt tongue in the Canary Basin while the oscillations are generally found to the south and east. It is suggested that the zonal motions are the result of baroclinic instability of the large-scale flow. They have zonally enhanced low frequency variability (periods greater than 200 days) and nearly isotropic mesoscale variability (periods 50 to 200 days). The wave motions are believed to be the signature of radiating baroclinic Rossby waves generated to the south at the Cape Verde Frontal Zone. They are strongly peaked at the mesoscale band and have an essentially isotropic low frequency component. Integral time scales for the zonal motions are relatively long (23 and 13 days for the zonal and meridional directions) while for the wave motions they are short (7.7 and 5.0 days). The resulting eddy diffusivities are found to be non-isotropic and non-homogeneous with $(K_{xx}, K_{yy}) = (21 \text{ and } 8.4 \times 10^6 \text{ cm}^2 \text{ s}^{-1})$ in the core of the salt tongue (mainly zonal motions) and $(K_{xx}, K_{yy}) = (4.3 \text{ and } 3.5 \times 10^6 \text{cm}^2 \text{ s}^{-1})$ to the south of the core (mainly wave-like motions). A simple scale analysis indicates that these time dependent motions play the dominant role in the spread of the Mediterranean salt tongue in both the zonal and meridional directions.

Published in: *Journal of Marine Research,* 51:797–818, 1993.

Supported by: NSF Grant OCE90-09463.

WHOI Contribution No. 8329.

A HYDROGRAPHIC SECTION ACROSS THE SUBTROPICAL SOUTH INDIAN OCEAN

John M. Toole and Bruce A. Warren

Features of the water-property and circulation fields at the southern limit of the continentally bounded Indian Ocean are described on the basis of a transoceanic hydrographic section occupied along roughly Lat. 32° S by the R.R.S. *Charles Darwin* in November–December 1987. Primary observations consisted of 106 full-depth CTD/O_2 stations with discrete measurements of the concentrations of dissolved silica, phosphate and nitrate. The section lies in the southern part of the South Indian subtropical gyre; water-property features in the upper kilometer indicate that the northward interior flow is predominantly in the eastern half of the ocean there, consistent with the forcing pattern of wind-stress curl. The southward return flow is the Agulhas Current, whose transport at Lats 31–32° S is estimated as $85 \times 10^6 \text{ m}^3 \text{ s}^{-1}$. Circumpolar Deep Water flows northward to fill the greater deep Indian Ocean by means of western-boundary currents in the Crozet Basin, Central Indian Basin and Perth Basin. North Atlantic Deep Water entering directly from the mid-latitude South Atlantic is almost entirely confined to the southwestern Indian Ocean (Mozambique Basin, Natal Valley) by the topography of the Madagascar Ridge and Mozambique Channel.

Geostrophic transport figures are presented based on a zero-velocity surface constructed along

the section from the tracer-property evidence of where deep water was moving northward and where southward. Ekman transport, deduced from shipboard acoustic-Doppler profiler measurements, as well as synoptic and historical wind stress data, is found to be small (about 1×10^6 m^3 s^{-1} northward). Net transport (geostrophic and Ekman) across the section is estimated to be 7×10^6 m^3 s^{-1} southward, which implies a similarly sized Indonesia throughflow. Ambiguity in the geostrophic referencing scheme, and the magnitude of baroclinic eddy noise on the section, suggest this figure is uncertain by at least $\pm 10 \times 10^6$ m^3 s^{-1}. The calculations obtain a figure for net transport of water below 2000 dbars of 27×10^6 m^3 s^{-1} northward, which specifies an average upwelling speed at the 2-km level north of 30°S of 6.9×10^{-5} cm s^{-1}. This estimate, perhaps uncertain by 20– 30%, nonetheless contributes to growing evidence for an anomalously vigorous meridional circulation in the Indian Ocean. The associated calculations of heat and fresh water flux divergences demonstrate that the Indian Ocean thermohaline circulation essentially expresses a conversion of bottom and deep water to mid-depth thermocline, and near-surface water.

Published in: *Deep-Sea Research,* 40(10):1973–2019, 1993.

Supported by: NSF Grant OCE86-14497; and a subcontract with Oregon State University.

WHOI Contribution No. 8264.

A WESTERN ATLANTIC SECTION FROM SOUTH GEORGIA ISLAND (54° S) NORTHWARD ACROSS THE EQUATOR

Mizuki Tsuchiya, Lynne D. Talley and Michael S. McCartney

A long CTD/hydrographic section with closely spaced stations was made in the Atlantic Ocean between Iceland (63° N) and South Georgia (54° S). The northern half of the section (Iceland to 3° S) was occupied in July–August 1988 and has been reported in a previous paper (Tsuchiya *et al.*, 1992). The present paper deals with the southern half (O° 40'N to South Georgia) occupied by R/V Melville (Hydros 3 and 4) in February–April 1989 along a nominal longitude of 25° W. Vertical sections of potential temperature, salinity, and potential density from CTD measurements and of oxygen, silica, phosphate, and nitrate based on discrete water-sample measurements are presented and discussed in terms of the large-scale circulation of the South Atlantic Ocean.

The most significant result is a detailed description of the complex structure of the North Atlantic Deep Water (NADW), made possible by the high quality and high resolution, both horizontal and vertical, of the present data. The NADW north of 25° S contains two vertical maxima of oxygen separated by intervening low-oxygen water of circumpolar characteristics. Each maximum is associated with a maximum of salinity and minima of silica, phosphate, and nitrate. The deeper salinity maximum is only weakly defined and is limited to north of 18° S, appearing more as vertically uniform salinity. The deeper minima of nutrients are also limited to north of 18° S. South of 25° S the NADW shows only a single maximum of salinity, a single maximum of oxygen, and a single minimum of each nutrient, all lying close together. The salinity maximum south of 25° S and the deeper oxygen/salinity maximum north of 11° S are derived from the same source waters. The less dense NADW containing the shallower extrema of characteristics turns to the east at lower latitudes and does not reach the region south of 25° S. As the NADW spreads southward in the South Atlantic, it exhibits a number of cores interrupted by domains of intensified 2 circumpolar characteristics. This structure is closely related to the basin-scale zonal circulation pattern.

Other features of interest include: 1) the Subtropical, Subantarctic, and Polar Fronts clearly defined in the thermal and salinity fields, and additional fronts at 36° S and 20–22° S, the former being the Brazil Current Extension which is a boundary between the denser and lighter types of the Subantarctic Mode Water (SAMW) and the latter marking the boundary between the anticyclonic subtropical and cyclonic subequatorial gyres, 2) two pycnostads with temperatures 20–24° C with one in the subtropical and the other in the subequatorial gyre between 10° and 25° S, 3) confirmation of the thermostad at temperatures 8–9° C that was observed near the equator in the previous year, 4) a weak thermostad centered at 4° C in the Antarctic Intermediate Water (AAIW) between the Subtropical Front and the Subantarctic Front and its similarity to the densest variety of the SAMW, 5) a complicated pattern of eastward and westward flows of the AAIW near the equator suggested by the property distributions and reflected deeper in the NADW, 6) the termination of the high-oxygen tongue of the AAIW at the anticyclonic/cyclonic gyre boundary at 22° S despite the northward penetration of the AAIW salinity minimum across the equator, 7) identification of the nutrient maxima north of 22° S with the AAIW rather than with the Upper Circumpolar Water, 8) separate temperature minima at ~1600 m between 41° S and 33° S and at ~1000 m north of 21° S, 9) a steep northward descent of isopycnals at all depths along the

southern flank of the Falkland Ridge, accompanied by a reversal of the isopycnal slope just above the Ridge, 10) a weak vertical maximum of silica 400–800 m above the bottom of the Georgia Basin, which appears to have its origin in the Weddell Sea, and 11) the vertical and lateral homogeneity of the Lower Circumpolar Water that occupies the abyssal layer of the Brazil Basin.

Submitted to: *Journal of Marine Research.*

Supported by: NSF Grants OCE86-14486 and OCE92-01314.

WHOI Contribution No. 8330.

A HOMOGENEOUS MODEL OF THE WIND-DRIVEN OVERTURNING CELL IN THE SOUTHERN OCEAN

Liping Wang and Rui Xin Huang

An idealized two-layer homogeneous model with an infinitesimal surface Ekman layer on top of a homogeneous layer for the wind-driven overturning cell in the Southern Ocean, *i.e.*, the Deacon Cell, is discussed. It is shown that a supercritical high ridge is of critical importance to break down the geostrophic constraint in the latitudes of the circumpolar zone. In the model it is found that the Deacon Cell is a fundamentally three-dimensional system. Dynamically, the surface, sinking and rising branches of the cell are rather uniform and governed by the Ekman layer dynamics; while the lower branch is rather inhomogeneous and governed by both the boundary layer and Sverdrupian dynamics. It is demonstrated that associated with the surface Ekman drift is a strong inter-basin water mass exchange among the different oceanic basins in the Southern Ocean.

Submitted to: *Journal of Physical Oceanography.*

Supported by: NSF Grant OCE90-17158.

WHOI Contribution No. 8575.

A SIMPLE MODEL OF ABYSSAL CIRCULATION IN A CIRCUMPOLAR OCEAN

Liping Wang and Rui Xin Huang

Over the world oceans, there are several distinct source regions of deep water formation, such as that in the North Atlantic Ocean. Warren (1981) gave an excellent review of the deep water formation in the world oceans. In compensation for the deep water formation in small source regions, there is a general slow upward movement of deep water over the rest of the world oceans. This upward advection of cold water balances the downward diffusion of heat, thus maintaining the vertical structure of the temperature field (Stommel, 1958, Munk, 1966). Based upon this idea and with the assumption of planetary geostrophy for flow away from the western boundaries, Stommel and Arons developed a theoretical conceptual model for the abyssal circulation in both closed basins and global ocean basins (Stommel *et al.*, 1958; Stommel, 1958; Stommel and Arons, 1960a and b). The model predicted intense western boundary currents in each closed basin. And this prediction was indeed, to some extent, confirmed by Swallow and Worthington, 1957, in the North Atlantic and by obvservations in other closed basins.

In Press: *Journal of Physical Oceanography.*

Supported by: NSF Grant OCE90-17158.

WHOI Contribution No. 8503.

TOPOGRAPHIC CONTROL OF THE ANTARCTIC CIRCUMPOLAR CURRENT. PART I: A LINEAR HOMOGENEOUS CHANNEL MODEL

Liping Wang and Rui Xin Huang

An analytical solution is sought for a wind-driven circulation in the inviscid limit in a linear barotropic channel model of the Antarctic Circumpolar Ocean in the presence of a bottom ridge. There is a critical height of the ridge, above which all geostrophic contours in the channel are blocked. In the subcritical case, the Sverdrup balance does not apply and there is no solution in the inviscid limit. In the supercritical case, however, the Sverdrup balance applies and an explicit form for the zonal transport in the channel is obtained.

In the case with a uniform wind stress, the transport in the $\beta-$ plane channel is independent of the width of the ridge, linearly proportional to the wind stress and the length of the channel, while inversely linearly proportional to the ridge height. In the $f-$ plane with $\beta = 0$, the transport is even independent of the width of the channel. In the case with a nonuniform wind stress $\tau_x = \tau_0(1 - \cos \pi y/D)$, the Sverdrup flow driven by the vorticity input always induces a form drag against the mean wind stress. Now, the transport depends on the width of the ridge but not on the length of the channel.

The model clearly demonstrates how the topographic form-drag is generated in a linear barotropic model, which is fundamentally different from the nonlinear Rossby wave drag generation. Here in this linear model, the presence of a supercritical high ridge is essential in the inviscid

limit. The form-drag is generated regardless of the flow direction. Besides, the model demonstrates that most of the potential vorticity dissipation occurs at the northern boundary where the ridge is located.

Submitted to: *Journal of Physical Oceanography.*

Supported by: NSF Grant OCE90-17158.

WHOI Contribution No. 8606.

DRIVING THE MERIDIONAL OVERTURNING IN THE INDIAN OCEAN

Bruce A. Warren

Accumulating evidence suggests that the overall deep upwelling velocity in the Indian Ocean is several times bigger than that in the Pacific, and that the mean surface heat flux per unit area is much greater into the Indian than into the Pacific Ocean. A simple physical model is developed, through which it is hypothesized that the Indian heat-flux distribution is the principal agent driving the apparent relatively vigorous meridional overturning there.

Submitted to: *Deep-Sea Research.*

Supported by: NSF Grant OCE91-16284.

WHOI Contribution No. 8511.

SLIGHT NORTHWESTWARD INFLOW TO THE DEEP SOUTH FIJI BASIN

Bruce A. Warren, Thomas Whitworth, III., Mike I. Moore and Worth D. Nowlin, Jr.

Inflow to the South Fiji Basin from the deep boundary current east of New Zealand and the Kermadec Ridge occurs only in the potential-temperature interval 2.0-2.2° C, at a rate of about 0.2×10^6 m^3 s^{-1}.

In Press: *Deep-Sea Research.*

Supported by: NSF Grants OCE89-17338 and OCE90-02708.

WHOI Contribution No. 8299.

DIRECT OBSERVATIONS OF THE EKMAN BALANCE AT 10° N IN THE PACIFIC

Susan Wijffels, Eric Firing and Harry Bryden

The wind-driven Ekman transport and velocity structure are estimated from direct current measurements and geostrophic shears along a transpacific section at 10° N. The velocity field is dominated by the North Equatorial Current and its eddies, but near-inertial oscillations and an Ekman spiral are robust features of the shear. The ageostrophic component of shear averaged across the section can be approximated as a slab layer with a velocity of 5 cms^{-1} in the top 30–40 m, overlying a shear layer in which the velocity goes to zero below 80 m. The zonally-integrated mass transport of this Ekman layer is $62\ (\pm 0) \times 10^9$ kgs^{-1} to the north, similar to the estimate of $52\ (\pm 10) \times 10^9$ kgs^{-1} based on winds measured from the ship. Climatological winds also yield similar transports. The zonally-averaged velocity relative to the velocity at the top of the thermocline forms a clockwise spiral, decaying with depth. As has been found at higher latitudes, this mean Ekman spiral results from diurnal cycling of the mixed layer.

Submitted to: *Journal of Physical Oceanography.*

Supported by: NASA Graduate Student Fellowship in Global Change; NSF Grants OCE87-16910 and OCE91-04211.

WHOI Contribution No. 8307.

THEORETICAL AND LABORATORY MODELS

THERMALS WITH BACKGROUND ROTATION AND STRATIFICATION

Karl R. Helfrich

Scaling analysis and experiments are used to study the evolution of thermals in the presence of background rotation. When the ambient environment is homogenous the thermal rises and expands until it reaches a critical height where the Rossby number becomes ~1. The thermal then stops expanding and rises in a column. Both the critical height and column radius scale with $(F_0 f^{-2})^{\frac{1}{4}}$. F_0 is the initial thermal buoyancy and f is the Coriolis frequency. The thermal vertical is independent of f. When the background is stratified with buoyancy frequency N, the thermal rises to a neutral buoyancy level which scales with $(F_0 N^{-2})^{\frac{1}{4}}$. For $\frac{N}{f} < 0.6$ column formation occurs before the thermal reaches the neutral level. For $\frac{N}{f} > 0.6$ the thermal reaches the neutral level before rotation is important. In both regimes, geostrophic adjustment eventually causes the formation of a baroclinic vortex consisting of an anticyclonic lens of thermal fluid at the neutral level and cyclonic circulation below. The lens has $\frac{Nh}{fl} \sim 1$. The lens thickness $2h$ and the radius l obey relations of the form $(F_0 N^{-2})^{\frac{1}{4}} (\frac{N}{f})^m$.

However, the exponents m are different in the two regimes. The relevance of these results to deep convection and hydrothermal venting is discussed.

In Press: *Journal of Fluid Mechanics.*

Supported by: NSF Grant OCE92-16628.

WHOI Contribution No. 8252.

TIME-DEPENDENT TWO-LAYER HYDRAULIC EXCHANGE FLOWS

Karl R. Helfrich

A theory is presented for time-dependent two-layer hydraulic flows through straits. The theory is used to study exchange flows forced by a periodic barotropic (tidal) flow. For a given strait geometry the resulting flow is a function of two non-dimensional parameters, $\gamma = (g'H)^{1/2}T/L$ and $q_{b0} = u_{b0}/(g'H)^{1/2}$. Here g', H, L, T and u_{b0} are, respectively, the reduced gravity, strait depth and length scales, the forcing period and the barotropic velocity amplitude. γ is a measure of the dynamic length of the strait and q_{b0} a measure of the forcing strength. Numerical solutions for both a pure contraction and an offset sill-narrows combination show that the exchange flow, averaged over a tidal cycle, increases with q_{b0} for a fixed γ. For fixed q_{b0} the exchange increases with increasing γ. The maximum exchange is obtained in the quasi-steady limit $\gamma \to \infty$. The minimum exchange is found for $\gamma \to 0$ and is equal to the unforced steady exchange. The usual concept of hydraulic control occurs only in these two limits of γ. In the time-dependent regime complete information on the strait geometry, not just at a finite number of control points, is required to determine the exchange. The model results are compared to laboratory experiments for the pure contraction case. Good agreement for both interface evolution and average exchange is found if account is made for the role of mixing which acts to reduce the average salt (density) transport.

The relevance of these results to ocean straits is discussed. It is shown that many typical straits lie in the region of parameter space where time-dependence is important. Application to the Strait of Gibraltar helps explain the success of the unforced steady hydraulic theory.

Submitted to: *Journal of Physical Oceanography.*

Supported by: NSF Grant OCE90-22088; ONR Contract N00014-93-1-0263.

WHOI Contribution No. 8528.

THERMOHALINE CIRCULATION: INTERMEDIATE WATER FORMATION AND ENERGETICS OF HALOCLINE CATASTROPHE

Rui Xin Huang

A series of numerical experiments have been carried out to explore the structure of thermohaline circulation, especially intermediate water formation and the energetics of halocline catastrophe. It is found that when the amplitude of freshwater flux is smaller than a critical value, the thermohaline circulation is in a thermal mode, with deep water formed in the north. When the freshwater flux amplitude is supercritical, the thermohaline circulation can not reach a single steady state. Instead, the model ocean is in a continuous transition between a slow, quasi-steady saline mode and an energetic, unsteady thermal mode. For cases with no wind stress, the saline mode is characterized by sinking along the equator. For cases with wind stress, the saline mode is characterized by intermediate water formation at mid-latitude.

During the saline mode phase, the deep water gradually becomes warm and salty. Thus, at the end of the saline mode phase, within the northern basin there is cold and relatively fresh water laying on top of warm and salty water. Such a vertical structure is potentially very unstable because small perturbations can grow, supported by release of the Diabatic Available Potential Energy. Thus, a final equilibrium in the saline mode cannot be reached; instead, the model ocean flips to a very energetic thermal mode in which violent overturning fed by the Diabatic Available Potential Energy destroys the vertical stratification. After the energy is released, the saline cell supported by precipitation in the subpolar basin advances southward and the model ocean returns to the saline mode and the whole cycle will be repeated.

Submitted to: *Journal of Geophysical Research.*

Supported by: NSF Grant OCE90-17158.

WHOI Contribution No. 8275.

THREE-DIMENSIONAL STRUCTURE OF THE WIND-DRIVEN CIRCULATION IN THE SUBTROPICAL NORTH PACIFIC

Rui Xin Huang and Bo Qiu

The subduction rate is calculated for the North Pacific based on Levitus climatology data and Hellerman & Rosenstein wind stress data. Because the period of effective subduction is rather

short, subduction rates calculated in Eulerian and Lagrangian coordinates are very close. The subduction rate defined in the Lagrangian sense consists of two parts. The first part is due to the vertical pumping along the one-year trajectory, and the second part is due to the difference in the winter mixed layer depth over the one-year trajectory. Since the mixed layer is relatively shallow, the vertical pumping term is very close to the Ekman pumping, while the sloping mixed layer base enhances subduction, especially near the Kuroshio. For most of the subtropical North Pacific, the subduction rate is no more than 75 m/year, which is slightly larger than the Ekman pumping. The water mass volume and total amount of ventilation integrated for each interval of 0.2 σ_θ unit is computed. The corresponding renewed time for each water mass is obtained. The inferred renewed time is of 5–6 years for the shallow water masses (σ_θ = 23–25), and about 15 years for the subtropical mode water σ_θ = 25.2–25.4).

The maximum barotropic mass flux of the subtropical gyre is about 46 Sv (east of 135°E). This mass flux is partitioned as follows. The total horizontal mass flux in the ventilated thermocline, the seasonal thermocline and the Ekman layer is about 30 Sv, and the remain 16 Sv is in the unventilated thermocline. Thus, about 1/3 of the mass flux in the wind-driven gyre is sheltered from direct the air-sea interaction.

Submitted to: *Journal of Physical Oceanography.*

Supported by: NOAA Grant NA36GP-0270.

WHOI Contribution No. 8443.

ROTATING HYDRAULIC MODELS OF CONTINENTAL SHELF AND CIRCULAR EDDY FONTS

Ryuji Kimura and J. A. Whitehead

We explore a mechanism for inertia to produce steady cross frontal flux across a geostrophic front that separates two fluids of differing density in a rotating fluid. We ask *"when the front is forced to be narrower than the Rossby Radius R so the full Rossby adjustment cannot be reached, will fluid continue to flow in a cross-frontal direction and if so at what rate?"* A simplified model is considered with flow in a submerged horizontal slot between two very deep basins containing motionless water. The inviscid rotating nonlinear equations for exchange flow are solved for two configurations: In one the slot is infinitely wide but of length l and height h. In the other case both the slot and basins are cylindrical. Volume flux Q_l per unit slot width is determined. For the Cartesian case Q_l decreases with R and goes to zero when slot length equals R. For the cylindrical case Q_l decreases to zero when the difference beween radii equals R times $2\frac{3}{2}\gamma/(1+\gamma)(1+\gamma^2)^{\frac{1}{2}}$ where γ is the outer radius divided by the inner radius. This may be important for eddies or cyclones in the ocean or atmosphere. A lock-exchange experiment driven by electrical heating produced temperature difference measurements for given heat flux and rotation. A cylindrical heated chamber of radius 15 cm was separated from an outer cold water basin of 20 cm radius by a horizontal slot. The temperature difference between the two chambers was measured for various rotation rates. There is good agreement with theory for small rotation but poor agreement above a critical rotation rate where a transition to a flow with eddies (probably from baroclinic instability) shows evidence of increased heat flux.

Submitted to: *Geophysical Astrophysical Fluid Dynamics.*

Supported by: ONR Contract N00014-89-J-1037.

WHOI Contribution No. 8609.

THERMOCLINE FORCED BY ANNUAL AND DECADAL SURFACE TEMPERATURE VARIATION

Z. Liu and J. Pedlosky

A two-layer thermocline model is modified by adding an essentially passive mixed layer above it. The surface temperature variation is simulated by a moving outcrop line. The outcrop line is specified during the whole cycle while the mixed layer depth can only be specified during part of the cycle. It is found that, in contrast to a surface wind stress (Liu, 1991 a, b), a surface temperature variation causes strong variability in the ventilated zone through subducted water while it affects the shadow zone very little.

Two types of buoyancy-forced solution are found. When the outcrop line moves slowly, the solutions are non-entrainment solutions. For these solutions, the surface heat flux is mainly balanced by the horizontal advection in the permanent thermocline. The mixed layer never entrains. The time-mean thermocline is close to the steady thermocline with the time-mean outcrop line. When the outcrop line moves southward rapidly during the cooling season, the solutions become entrainment solutions. Now, deep vertical convection must occur, because the horizontal advection in the permanent thermocline is no longer strong enough to balance the surface cooling. The mixed layer penetrates rapidly such that water mass is entrained into the mixed layer through the bottom. The time-mean then thermocline resembles the steady thermocline with the early spring mixed layer, as suggested by

Stommel (1979). The local variability in the permanent thermocline is most efficiently produced by decadal forcings.

According to water mass formation, there are three stages during each cycle: the seasonally subducting stage, the entraining stage and the subducting stage. Waters subducted during the seasonally subducting stage will be re-entrained in the following entraining stage to form the seasonal thermocline. The waters subducted during the subducting stage establish the permanent thermocline.

In Press: *Journal of Physical Oceanography.*

Supported by: NSF Grant ATM89-03890.

WHOI Contribution No. 8469.

STRATIFIED ABYSSAL FLOW IN THE PRESENCE OF FRACTURED RIDGES

Joseph Pedlosky

A linear, two-layer model for abyssal flow driven by a specified upwelling into the thermocline is studied when the ocean basin is *partially* blocked by a meridional barrier in the lower layer. The barrier is meant to represent a midoceanic ridge, and the space between the termination points of the ridge and the northern and southern basin boundaries represents the gaps that pierce most ridge systems.

It is found that the deep flow is only partially blocked by the barrier. A substantial flow threads through the gaps in the form of zonal jets. The portion of the flow that is blocked by the ridge produces a recirculating, cyclonic gyre east of the ridge, and its latitudinal extent is typically smaller than the unbroken interval of the ridge. The overall structure of the recirculation and the degree of blocking are related to robust integral conditions constraining the circulation around the ridge.

Although weaker, a similar recirculation is often found in the *unblocked* layer above the ridge as an upward extension of the deep circulation.

Published in: *Journal of Physical Oceanography,* 24(2):403–417, 1994.

Supported by: NSF Grant ATM89-03890.

WHOI Contribution No. 8390.

PREDICTING EDDY DETACHMENT FOR AN EQUIVALENT BAROTOPIC THIN JET

Elise A. Ralph and Larry Pratt

The time-dependent meandering of thin ocean jets in reduced gravity models has recently been shown to obey a natural coordinate version of the standard modified Korteweg deVries (mKdV) equation. The detachment of eddies from such a jet begins when different segments of the jet path come into contact, causing the initially simply connected jet to "pinch" together. It is shown that this pinching process if effected primarily by breather solutions to the mKdV equation. For a given initial condition the solution will evolve into a dispersive wave train plus a finite number of breathers, the connectivity of which is determined by a steepness parameter λ. Using the scattering transform for the mKdV equation the value(s) of λ can be calculated in a straight forward manner, and the detachment (or lack thereof) of meanders can be forecast to a high degree of confidence by calculating λ. Examples with simple meander disturbances show a remarkable degree of stability and resistance to detachment.

In Press: *Journal of Nonlinear Science.*

Supported by: NSF Grant OCE89-16446; ONR Contract N00014-89-31182.

WHOI Contribution No. 8527.

DOES STOMMEL'S MIXED-LAYER 'DEMON' WORK?

Richard G. Williams, Michael A. Spall and John C. Marshall

The subduction process is examined using diagnostics from a time-dependent coupled mixed-layer/primitive equation model of the North Atlantic (CME). The influence of the mixed layer on the properties of the main thermocline is investigated using two methods. In the first, the rate and timing of subduction into the main thermocline is diagnosed using kinematic methods from the CME fields. In the second, idealized tracer 'age' and 'date' fields are examined to understand the seasonal coupling of the mixed layer and thermocline. The tracer 'age' highlights the ventilated regime and the 'date' identifies the time period of effective subduction. Over the subtropical gyre, both methods generally support Stommel's hypothesis that fluid is only transferred from the mixed layer into the main thermocline over a short period, $\sim$ 1 month, in late winter/early spring.

Submitted to: *Journal of Physical Oceanography.*

Supported by: NOAA Grant NA90AA-D-AC498.

WHOI Contribution No. 8405.

COASTAL CIRCULATION & DYNAMICS

THE SEMI-DIURNAL TIDES ON THE AMAZON SHELF

Robert C. Beardsley, Julio Candela, Richard Limeburner, W. Rockwell Geyer, Steven J. Lentz, Belmiro Castro, David Cacchione and Nelson Carneiro

As part of A Multi-disciplinary Amazon Shelf Sediment Study (AMASSEDS), shipboard acoustic Doppler current profiler and moored and shipboard current measurements made over the Amazon shelf during 1990–1991 have been analyzed to determine the principle semi-diurnal (M_2, S_2, and N_2) tidal current constituents. These results have been combined with coastal sea level data from within the Amazon and Para Rivers, the adjacent shelf, and with satellite-derived tidal elevation data from off the shelf to provide a more complete description of the semi-diurnal tides in this complex river/shelf system.

Due to the near-resonant forcing of the semi-diurnal tides in the equatorial Atlantic, the semi-diurnal tides exhibit a broad area of large amplitude and relatively constant phase offshore of the Amazon shelf. There the three principal semi-diurnal constituents have relative amplitudes of 1.00 (M_2), 0.31 (S_2), and 0.21 (N_2). This leads to large spring/neap and monthly variations in tidal forcing. The response of the Amazon river/shelf region is then largely determined by the geometry of the system and dissipation. Our description here focuses on the M_2 since it is the dominant and most accurately observed constituent, and the physical processes governing the M_2 should also govern the S_2 and the N_2 to lowest order.

Since the Amazon shelf spans the equator where the Coriolis acceleration is dynamically unimportant, the observed M_2 tidal currents are nearly rectilinear and oriented primarily across the local isobaths. Near the Amazon River mouth, the M_2 tide propagates across the shelf and through the mouth as a damped progressive wave, with its amplitude decreasing and phase increasing upriver. Over the adjacent shelf north of Cabo Norte, the M_2 tide approaches a damped standing wave, with large amplitudes (greater than 1.5 m) near the coast due to near-resonance within the coastal embayment formed by the Cabo Norte shoal to the south and Cabo Cassipore to the north. Comparisons between tidal observations in both the North Channel and the Cabo Norte-Cabo Cassipore embayment and a simple variable-width channel tidal model indicate that (a) most of the M_2 tidal energy dissipation occurs over the mid- and inner shelf (in water depths less than 20 m) and (b) fluid muds found there cause a significant reduction in the effective bottom friction felt by the M_2 tide. The approximate resonant period of the Cabo Norte-Cabo Cassipore embayment is 11.9 hrs, and at resonance the average energy dissipation per forcing period is roughly 2.2 times the average mechanical energy in the embayment. This damping rate is large enough that the tidal amplification is rather insensitive to forcing frequency so that the response of the embayment to forcing over the semi-diurnal band should be essentially the same.

The vertical structure of the M_2 tidal current is examined at one outer-shelf site located in 65-m water depth. The observed semi-major axis increases logarithmically with height above bottom within the lowest 1–2 m and reaches a maximum in excess of 0.5 m/s at approximately 11 m above bottom. The mean ellipticity is small ($\leq .1$) and positive, indicating clockwise rotation of a nearly rectilinear current, and the semi-major axis is oriented with 10° of the local cross-isobath direction. The M_2 phase increases within height above bottom, with flood at the bottom leading flood at the surface by about one hour. A simple local homogeneous tidal model with time- and space-dependent eddy viscosity simulates the observed near-bottom velocity reasonably well, however, the model suggests that stratification above the lowest few meters may significantly affect the tidal boundary layer structure at this site.

Estimates of the net M_2 energy flux onto the Amazon shelf and into the Amazon and Para Rivers have been made combining the variable-width channel model results with observed current and surface elevation data. The net M_2 energy flux into the Amazon and Para Rivers at their mouths is 0.47×10^7 kW and 0.19×10^7 kW, respectively. A net M_2 energy flux of about 3.3×10^7 kW occurs onto the shelf between the North Channel of the Amazon River and Cabo Cassipore. This shelf region accounts for about 1.3% of the global dissipation of the M_2 tide.

Submitted to: *Journal of Geophysical Research.*

Supported by: NSF Grants OCE88-12917, OCE88-13399 and OCE91-15712; and the Brazilian Conselho Nacional de Desenvolvimento Cientifico e Technologico Grant FAFESP 89/3508-4.

WHOI Contribution No. 8554.

THE EFFECT OF SHORT-SCALE WIND VARIATIONS ON SHELF CURRENTS

K. H. Brink, J. H. LaCasce and J. D. Irish

Most existing models of shelf currents (such as

coastal-trapped wave models) usually disagree with observations in that the cross-shelf currents are weaker than observed, and that the predicted coherence length scales of cross-shelf currents are much longer. We seek to test the hypothesis that these inconsistencies can be resolved by including, in the forcing, realistic wind variations with alongshore length scales down to about 10 km. We use the Coastal Ocean Dynamics Experiment (CODE) Northern California, 1982, wind observations to drive a linear, stratified stochastic ocean model which includes bottom friction. The model results are expressed as statistics of the flow field which can be checked against observations. CODE aircraft winds from 1982 low-level alongshore flight tracks were converted to stresses and then subjected to wavenumber spectral analysis. Results show about 1 order of magnitude more energy at wavelengths shorter than 50–100 km than would be expected from the extrapolation of larger-scale spectral estimates based on buoy wind time series. Thus, for the CODE region, the forcing is energetic at relatively short length scales. The model results for cross-shelf velocity support our hypothesis, in that the modeled alongshore coherence length scales are indeed much shorter than those from a large-scale-only model. For example, at a 7-day period, the present calculations predict a coherence squared of 0.3 at a 35-km separation, while the large-scale-only model predicts 0.3 at 250 km. The observations show a 35–50 km scale for 0.3 coherence squared. However, while cross-shelf current variances are increased, they are still about a factor of 5 or more smaller than the CODE shelf observations over the shelf.

Published in: *Journal of Geophysical Research,* 99(C2):3305–3315, 1994.

Supported by: NSF Grant OCE89-22648; ONR Contract N00014-92-J-1643.

WHOI Contribution No. 8375.

AN UPDATE ON THE FORMATION AND MAINTENANCE OF SHELFBREAK FRONTS

David C. Chapman and Glen Gawarkiewicz

The model for the formation and maintenance of a shelfbreak front presented by Gawarkiewicz and Chapman (*Journal of Physical Oceanography,* 22:753–772, 1992) is extended to cases of stronger stratification and spatially and temporally varying vertical mixing coefficients which are functions of the local Richardson number. Stronger stratification leads to larger cross-shelf density gradients near the shelf break and an associated surface-intensified geostrophic alongshelf jet, but does not change the basic frontal formation mechanism. However, with Richardson-number-dependent mixing coefficients, the mixing is greatly reduced outside the bottom boundary layer, and the shelf does not become vertically homogeneous despite the continued offshore flow in the bottom boundary layer. Strong horizontal density gradients still form near the shelf break where the bottom boundary layer separates from the bottom, but the shelfbreak front no longer extends to the surface. Thus, the mechanism proposed by Gawarkiewicz and Chapman is probably, not capable of forming a surface-to-bottom shelfbreak front, but the circulation patterns suggest that the underlying dynamics may be important in maintaining a shelfbreak front and isolating the shelf water from the slope water.

Submitted to: *Journal of Physical Oceanography.*

Supported by: NSF Grant DPP91-13940.

WHOI Contribution No. 8411.

VARIABILITY OF WATER PROPERTIES AND CURRENTS IN LATE SPRING IN THE NORTHERN GREAT SOUTH CHANNEL. PART I. WATER PROPERTIES

Changsheng Chen, Robert C. Beardsley and Richard Limeburner

As part of the South Channel Ocean Productivity Experiment (SCOPEX), three regional CTD/ADCP surveys were made in the northern Great South Channel (GSC) during April 26–29, 1988, May 18–21, and June 6–11, 1989 to study water property distributions and the subtidal circulation. The surface salinity patterns observed in late April, 1988 and June, 1989 differ significantly in the extent of the freshwater plume which occurs east of Cape Cod in spring. In April, 1988, the surface plume was just beginning to form along the outer coast of Cape Cod while six weeks later in 1989, the minimum salinity was about $1.5°/_{oo}$ less, and a large pool of water fresher than $31.6°/_{oo}$ had pushed eastward over much of the northern GSC region. The difference in the amount of freshening observed between the two surveys is due primarily to the six-week difference in the seasonal cycle and increased river discharge in 1989. The offshore spreading of the low-salinity plume was driven by the deeper circulation and upwelling-favorable winds.

The distribution of Maine Intermediate Water (MIW) also significantly differed between April, 1988 and June, 1989. In April, 1988, the seasonal thermocline was just beginning to form, and the spatial structure of MIW was relatively uniform.

In June, 1989, a narrow core of temperature minimum water (with T_{min} in a range of 3.2° to 4.4° C) was found along the western flank of the northern GSC between 40 m and 120 m. This colder and fresher water spread to mix with the interior MIW as the core flowed southward into the central GSC.

Hydrographic data plus satellite sea surface temperature images showed a relatively permanent continuous thermal front (with a 10 km cross-isobath variation) along the eastern flank of Nantucket Shoals, across the northern shallow region of the GSC and along the northern western flank of Georges Bank, which separated the well-mixed water over the shallow region of GSC from stratified water in the center of northern GSC. Comparison of the location of this front with theoretical predictions by Loder and Greenberg (1986) suggests that enhanced tidal mixing due to the spring-neap cycle is important in determining the relative balance between buoyancy import and tidal mixing in the GSC region.

Submitted to: *Continental Shelf Research.*

Supported by: NSF Grants OCE87-13988 and OCE91-101034.

WHOI Contribution No. 8395.

VARIABILITY OF WATER PROPERTIES AND CURRENTS IN LATE SPRING IN THE NORTHERN GREAT SOUTH CHANNEL. PART II. CURRENTS

Changsheng Chen, Robert C. Beardsley and Richard Limeburner

As part of the South Channel Ocean productivity Experiment (SCOPEX), continuous Acoustic Doppler Current Profiler (ADCP) data were collected aboard the *R/V Endeavor* using a 150-kHz RDI ADCP during three regional hydrographic surveys (April 26–29, 1988, May 18–21, and June 6–11, 1989) and several small-scale biological surveys during May–June, 1989. The ADCP data were detided using an empirical least-squares method. The resulting residual flow field clearly shows different circulation patterns in the near-surface and deeper regions in the Great South Channel (GSC) area in late spring. In the upper 50 m, the residual flow in the northern GSC consists of three principal currents: (1) a southward coastal current located along the western flank of the GSC; (2) a broad cyclonic circulation crudely following the local topography in the interior region of the northern GSC; and (3) a northeastward current along the western flank of Georges Bank. Below 50 m, the residual flow tended to be cyclonic along the local 100-m isobath in the northern GSC.

The residual ADCP current patterns are consistent with the vertical distributions of water properties described in Part I by Chen *et al.* (1992) and the trajectories of satellite-tracked drifters drogued at 5 and 50 m which were released in the northern GSC as part of SCOPEX. Comparisons with geostrophic current shears and numerical model results suggest that the residual flow in spring is driven primarily by tidal rectification over the shallower sides of the northern GSC and by buoyancy forcing over the deeper flanks of the GSC. The southward transports of low-salinity plume surface water and MIW were about 0.07 ± 0.03 Sv and 0.31 ± 0.38 Sv in April, 1988 and about 0.12 ± 0.06 Sv and 0.66 ± 0.14 Sv in June, 1989. The larger transport of low-salinity plume water and MIW found in June, 1989 is believed due to the increased freshwater river discharge in 1989 and occurrence of a subsurface coastal jet current along the western flank of the GSC.

The dense aggregations of the zooplankton *Calanus finmarchicus* that occur in the northern GSC during late spring appear to be related to the regional circulation. In particular, a large-scale near-surface convergence appears to be a necessary condition for high zooplankton concentration while the horizontal shift of the region of maximum zooplankton concentration from 1988 to 1989 may be a direct result of the movement of the low-salinity surface plume.

Submitted to: *Continental Shelf Research.*

Supported by: NSF Grants OCE87-13988 and OCE91-101034.

WHOI Contribution No. 8396.

QUANTIFYING THE EFFECT OF DISCRETE CONTAMINANT DISCHARGE ON THE MARINE ENVIRONMENT

James H. Churchill

This paper is directed at the effects of material released from a spatially confined source during its initial transport through a marine region (*i.e.*, before becoming incorporated in bottom sediment or the food chain). Developed are risk assessment parameters which incorporate information on fluid motions, mixing and rates of contaminant uptake and depuration. These parameters include the mean concentration of recently discharged material, the frequency of discharged plume visitation, the probability of at least one plume encounter over a specified time period and indices for judging the impact of a particular contaminant on a target marine species. Examples considering the effects of sewage sludge released east of New Jersey at the 106-Mile Disposal Site are presented.

In Press: *Journal of Marine Environmental Engineering.*

Supported by: NOAA Grant NA90-AA-D-SG-480.

WHOI Contribution No. 8486.

TRANSPORT OF SOUTH ATLANTIC BIGHT SHELF WATER TO THE SHELF EDGE OF THE MIDDLE ATLANTIC BIGHT

James H. Churchill, Jonathan A. Hare, Robert K. Cowen, Paul Dragos, Scott M. Glenn and Peter C. Cornillon

Two distinct oceanographic regimes are found off the U.S. east coast: the South Atlantic Bight (SAB) which extends from the Florida Straits to Cape Hatteras, and the Middle Atlantic Bight (MAB) which stretches from Cape Hatteras to the Great South Channel. Previous studies of fish larvae suggest that water from the SAB shelf is routinely transported to the shelf edge of the MAB, even though the mean currents of the MAB tend to the southwest. Here we present physical oceanographic measurements in support of an hypothesized mode of transport from the SAB shelf to the MAB shelf edge. It is one in which water is drawn from the SAB shelf into the Gulf Stream current, carried eastward along the northern edge of the Gulf Stream and then extracted from the Gulf Stream and transported to the MAB shelf edge by the circulation of a Gulf Stream warm-core ring. For the case in which water is transported from the Carolina Shelf to the shelf edge near Hudson Canyon, estimated transit times along this route fall in the range of 7–16 days.

Submitted to: *Journal of Marine Research.*

Supported by: Dept. of Energy 11041800; NSF Grant OCE81-277800.

WHOI Contribution No. 8314.

HEAT AND SALT BALANCES OVER THE NORTHERN CALIFORNIA SHELF IN WINTER AND SPRING

E. P. Dever and S. J. Lentz

Heat and salt balances over the northern California shelf from early December 1988 through late February 1989 and from early March through early May 1989 are estimated from moored meteorological and oceanographic time series 93 m of water 6.3 km from the coast. Though the northern California shelf is a site of strong persistent coastal upwelling during late spring and summer, persistent upwelling does not occur in winter or early spring and the heat budget differs markedly from the summer upwelling heat budget in this and other coastal upwelling regions.

Between early December 1988 and late February 1989 (winter), there is a mean offshore heat flux of 7.8×10^5 W/m. This is about a factor of five smaller than estimates of the mean offshore heat flux on the northern California shelf in the summer upwelling season. It occurs predominantly in the upper 30 m. The offshore heat flux is balanced by an eddy along-shelf temperature gradient flux and a long term cooling trend making the mean winter heat balance fundamentally three dimensional. The cross-shelf eddy heat flux and sea surface heat flux, while often important in upwelling mean heat budgets, are small components of the winter mean heat budget. A winter heat budget for 1981–1982 from more limited data yields similar results.

Between early March and early May 1989 (spring), the mean heat budget is primarily two dimensional, like mean upwelling budgets. There is a mean offshore heat flux of 5.3×10^5 W/m during spring which occurs predominantly in the upper 10 m. In contrast to winter, the mean sea surface heat flux is an important component of the mean spring heat budget, contributing 7.1×10^5 W/m. Heat is also added by an eddy along-shelf temperature gradient flux, as in winter, and the heat content increases in spring.

On time scales of days, the dominant terms in the fluctuating heat budget are the cross-shelf heat flux and local changes in heat content. This is true in both winter and spring. These two components are well correlated with each other and with the local along-shelf wind stress. The along-shelf temperature gradient flux is apparently unrelated to the local along-shelf wind. It is usually weak on time scales of days. Occurrences when it is strong are interpreted as effects of mesoscale features. Mean and fluctuating cross-shelf salt fluxes provide essentially the same information as cross-shelf heat fluxes. This is not surprising in light of the strong $T - S$ relationship and similar processes of advection and mixing for temperature and salinity on the northern California shelf.

Submitted to: *Journal of Geophysical Research.*

Supported by: NSF Grant OCE91-15713.

WHOI Contribution No. 8477.

A NUMERICAL STUDY OF DENSE WATER FORMATION AND TRANSPORT ON A SHALLOW, SLOPING CONTINENTAL SHELF

Glen Gawarkiewicz and David C. Chapman

The circulation and transport of dense water formed over a limited area on a gently sloping

continental shelf is studied using a three-dimensional primitive equation model. Starting with a homogeneous, quiescent ocean, a constant negative buoyancy flux is imposed at the surface over a half- elliptical region adjacent to a coastal boundary to study the circulation generated by an idealized coastal polynya. The flow response can be divided into three phases; geostrophic adjustment, instability, and eddy- eddy interactions. During geostrophic adjustment, the flow at the edge of the forcing region accelerates as the fluid within the forcing region becomes denser and density gradients strengthen. Eventually, the flow at the leading edge of the forcing region (relative to Kelvin wave propagation) becomes unstable and a train of counter-rotating eddies is formed. These eddies then interact and transport dense water offshore, across isobaths. Eddy scales and velocities are consistent with observations in the Arctic. The results are qualitatively insensitive to weakening of the negative buoyancy forcing, to changing of the bottom slope, and various vertical mixing parameterizations. The results suggest that instability processes and eddy fluxes are important in transporting dense water off continental shelves and into marginal seas, while stream-tube flows of dense water on continental shelves appear unlikely to occur in the absence of along- shelf variations in bottom topography.

Submitted to: *Journal of Geophysical Research - Oceans.*

Supported by: NSF Grant DPP91-13940.

WHOI Contribution No. 8588.

SUMMERTIME SYNOPTIC VARIABILITY OF FRONTAL SYSTEMS IN THE NORTHERN BERING SEA

Glen Gawarkiewicz, J. Christopher Haney and Michael Caruso

Hydrographic observations in the Bering Sea during August and September, 1987, indicate the presence of a warm, fresh coastal current along the north-western coast of St. Lawrence Island near the Anadyr Strait. The surface salinities were as low as 29.5 PSU with a maximum temperature of 10° C. The geostrophic velocities relative to the bottom had a maximum value at the surface of between 0.07 and 0.14 m s^{-1} eastward in different transects. The width of the coastal current increased by 80 km in ten days. The buoyancy-driven geostrophic transports varied from 41,000 to 72,000 m^3 s^{-1}. The wind-driven Ekman transports ranged from very small values to values four times larger than the buoyancy-driven flow, which implies that the coastal current may reverse in strong wind conditions. It is likely, based on prior observations further east, that this coastal current extends the length of the northern coastline of St. Lawrence Island during the summer.

Submitted to: *Journal of Geophysical Research - Oceans.*

Supported by: NSF Division of Polar Programs Arctic Systems Science Initiative Grant DPP-9113940.

WHOI Contribution No. 8256.

CURRENT DYNAMICS OVER THE NORTHERN CALIFORNIA INNER-SHELF

Steven J. Lentz

Current observations from a northern California inner-shelf site in 30 m of water reveal a simple cross-shelf circulation pattern. The near-surface inflow was typically offshore in response to equatorward winds, with a return flow in the lower water column. The depth-averaged cross-shelf velocity was consistently zero to the accuracy of the observations, suggesting a two-dimensional circulation. Results from a simple two-dimensional eddy-viscosity model reproduced the basic features of the observations. The four eddy-viscosity profiles used do not depend on the stratification which was generally weak at this inner-shelf site during the deployment period (summer of 1981). The model results were generally not very sensitive to the form of the eddy-viscosity profile. The agreement between the observations and model results supports the assumption that the observed flow is two-dimensional and is driven locally by an alongshelf wind stress and alongshelf pressure gradient. A notable difference between the model results and observations was that model alongshelf currents were about twice as large as observed alongshelf currents. Analyses suggest that the drag on the inner-shelf currents may have been larger than suggested by bottom tripod measurements at the site due to the presence of large rock outcrops. The observations reveal a factor of four decrease in the alongshelf current standard deviations from mid-shelf to inner-shelf. Analyses suggest this was due to a decrease in the wind stress toward the coast, shallower water resulting in a weaker body force due to the alongshelf pressure gradient, and an increased drag on the flow over the inner-shelf.

Submitted to: *Journal of Physical Oceanography.*

Supported by: NSF Grant OCE91-15713; ONR Contract N00014-89-J-1074.

WHOI Contribution No. 8308.

SEASONAL VARIATIONS IN THE AMAZON PLUME STRUCTURE INFERRED FROM HISTORICAL HYDROGRAPHIC DATA

Steven J. Lentz

Near-surface salinity observations from the NODC hydrographic data archive for the region 4° S–10° N, 60–40° W show that the Amazon River discharge forms a plume of low-salinity water that extends northwestward into the western equatorial North Atlantic. The average near-surface salinity within the plume increases away from the Amazon River mouth due to entrainment of oceanic water. The average entrainment is estimated to be about 4×10^5 m^3/s (twice the Amazon River discharge) every 1° of latitude. In the vicinity of the Amazon River mouth (0–2° N) the plume extends about 400 km eastward on average. However, from March to May the plume was occasionally wider in the vicinity of the river mouth, possibly due to the combination of near maximum river discharge and southeastward winds which may temporarily impede or block the northwestward transport of freshwater. From 2–5° N the average Amazon Plume is a band of low-salinity water (20–30 psu) about 200 km wide, with no resolvable seasonal variation in width. North of 5° N the Amazon Plume fans out over a broad region of the western equatorial North Atlantic. During January through June low-salinity Amazon Plume water is primarily found west of 52° W, spreading northwestward toward the Caribbean. Beginning in May, however, some of the Amazon Plume water begins to be deflected eastward in the North Brazil Current (NBC) retroflection. From July through October a majority of the Amazon Plume water is carried eastward in the NBC retroflection. The observations indicate however that some of the Amazon Plume water continues to flow northwestward toward the Caribbean even when the NBC retroflection is present.

Submitted to: *Journal of Geophysical Research.*

Supported by: NSF Grant OCE91-15712.

WHOI Contribution No. 8377.

SENSITIVITY OF THE INNER-SHELF CIRCULATION TO THE FORM OF THE EDDY VISCOSITY PROFILE

Steven J. Lentz

The sensitivity of the inner-shelf circulation to the form of the eddy viscosity profile is examined using a steady, linear, two-dimensional model. For both wind stress and alongshelf pressure gradient forcing the inner-shelf alongshelf circulation is insensitive to the form of the eddy-viscosity profile, however, the cross-shelf circulation is sensitive to the form of the eddy-viscosity profile. In particular, the location and width of the cross-shelf divergence in the Ekman transport over the inner-shelf, and hence the corresponding upwelling or downwelling, depend on the form of the eddy-viscosity profile.

Submitted to: *Journal of Physical Oceanography.*

Supported by: NSF Grant OCE91-15713; ONR Contract N00014-89-J-1074.

WHOI Contribution No. 8331.

THE AMAZON RIVER PLUME DURING AMASSEDS: SUBTIDAL CURRENT VARIABILITY AND THE IMPORTANCE OF WIND FORCING

Steven J. Lentz

Current variability over the North Brazilian shelf, particularly within the Amazon Plume, is characterized using observations from a moored array deployed about 300 km north of the Amazon River mouth from February to June 1990 as part of AMASSEDS (A Multidisciplinary Amazon Shelf SEDiment Study). The moored array consisted of a transect perpendicular to the coast with inner-shelf (18 m depth) and mid-shelf (65 m) moorings and a third mooring near the shelf break, in 100 m of water. The current variability is dominated by two components: semi-diurnal cross-shelf currents with peak velocities of 50–200 cm/s and vertically-sheared subtidal (time scales days to weeks) along-shelf currents. This study focuses on the subtidal flow within the Amazon Plume which is strong and variable with along-shelf currents ranging from -50 cm/s to over 150 cm/s. This along-shelf current variability within the plume is shown to be wind-driven. The relatively weak (<0.5 dynes/cm^2) along-shelf wind stresses in this region drive strong along-shelf currents because the Amazon Plume is thin and the drag is weak. In the absence of an along-shelf wind stress the plume flow is northwestward at 40 to 80 cm/s indicating that direct wind forcing does not account for the mean northwestward flow of the Amazon Plume. In the cross-plume direction there is a tendency for the wind stress due to the persistent onshore trade winds to balance the typically offshore buoyancy force and the Coriolis force associated with the wind-driven along-shelf flow. Thus the wind stress is a key factor influencing variability in both the flow and cross-shelf structure of the Amazon Plume in the vicinity of the moored array.

Submitted to: *Journal of Geophysical Research.*

Supported by: NSF Grants OCE88-12917 and OCE91-15712.

WHOI Contribution No. 8399.

THE AMAZON RIVER PLUME DURING AMASSEDS: SPATIAL CHARACTERISTICS AND SALINITY VARIABILITY

Steven J. Lentz and Richard Limeburner

The Amazon River discharge forms a plume of low salinity water that extends offshore and northwestward over the North Brazilian shelf. Shipboard CTD (Conductivity, Temperature, Depth) and moored temperature-conductivity observations, acquired as part of AMASSEDS (A Multidisciplinary Amazon Shelf SEDiment Study), are used to characterize the structure and variability of the Amazon Plume and salinity variability within the plume.

Four shipboard CTD surveys spanned the shelf from 1°S to 5°N during rising (March 1990), maximum (May 1990), falling (August 1989) and minimum (November 1991) discharge. Based on the CTD profiles the Amazon Plume, defined as the region with salinities less than 35.5 psu, is typically 3 to 10 m thick and 80 to over 200 km wide. A bottom front separating the low-salinity plume water from oceanic water is consistently located between the 10 and 20-m isobaths. Northwest of the river mouth the plume is often characterized by a wedge of low-salinity water adjacent to the coast and a separate tongue of low salinity water extending offshore over the mid to outer shelf.

A moored array deployed about 300 km northwest of the river mouth from February to June 1990, included inner and mid-shelf moorings in 18 and 65 m of water on which temperature-conductivity measurements were made. The salinity time series from instruments within the Amazon Plume (3 m below the surface on both moorings) reveal salinity variations of over 10 psu on time scales of days to weeks. Estimates of the salinity balance within the plume indicate that both cross-plume and along-plume advection contribute to these fluctuations. Volume budgets indicate the Amazon Plume entrains roughly twice the river discharge between the river mouth at the equator and 3°N. Estimates of gradient Richardson numbers from the moorings suggest entrainment occurs where the plume intersects the bottom due to the strong semidiurnal tidal currents and over the outer portion of the plume where the plume salinity approaches oceanic values.

The AMASSEDS observations indicate there are intermittent events in which plume water pools up in the vicinity of the river mouth and the plume width can exceed 200 km. These accumulation events are apparently due to wind events with a southeastward component which impede or block the normally northwestward freshwater transport. The resulting bulges in the plume are then released and propagate northwestward when the wind reverses.

In Press: *Journal of Geophysical Research.*

Supported by: NSF Grants OCE88-12917 and OCE91-15712.

WHOI Contribution No. 8494.

LANGRANGIAN FLOW OBSERVATIONS OF THE AMAZON RIVER DISCHARGE IN THE NORTH ATLANTIC

Richard Limeburner, Robert C. Beardsley, Ivan D. Soares and Steven J. Lentz

Nine satellite-tracked drifters with drogues centered near-surface were launched in the mouth of the Amazon River on the North Brazil shelf during 1989–1991 at four different stages of river discharge (rising in March, 1990, high in May, 1990, falling in August, 1989, and low discharge in November, 1991). The drifters initially flowed along-shelf toward the northwest over the North Brazil shelf with mean speeds varying from 42 to 128 cm/s and a maximum along-shelf velocity of 197 cm/s. Many drifters showed strong accelerations near 2° N between the 5 and 20 m isobaths; this may be caused by the sharp reduction in cross-shelf cross-sectional area due to the shore-perpendicular Cabo Norte Shoal. Residence times for the drifters over the North Brazil shelf varied from 6 to 28 days and were not simply related to river discharge. The drifter trajectories showed strong cross-shelf tidal variability in the flow field near the Amazon River mouth, and the strongest low-frequency, along-shelf variability was located over the open shelf just north of Cabo Norte. Three drifters flowed northwestward parallel to the northeast coast of South America, crossed the shelf break near 8° N, and moved into deeper North Atlantic water where they began looping in anticyclonic eddies (often called retroflection eddies or loopers) with periods of approximately 11 days as they moved northwestward to the Caribbean Sea. Four drifters initially flowed along-shelf toward the northwest and then offshore into deep North Atlantic water between 3° N and 7° N where they retroflected in the North Brazil Current. Only one drifter entered the zonal current system that characterizes the equatorial Atlantic circulation. When the drifter velocities were low, there was a weak correlation between the along-shelf drifter velocity and wind stress components.

Submitted to: *Journal of Geophysical Research.*

Supported by: NSF Grants OCE88-12917 and OCE91-81572; and the European Center for Medium-Range Weather Forecasting.

WHOI Contribution No. 8526.

INSTRUMENTATION & EXPERIMENTAL NUMERICAL METHODOLOGY

DETERMINATION OF LONGWAVE HEAT FLUX AT THE AIR-SEA INTERFACE USING MEASUREMENTS FROM BUOY PLATFORMS

T. D. Dickey, D. V. Manov, D. A. Siegel and R. A. Weller

A theory of operation for a downwelling longwave radiation sensor or pyrgeometer shows that only the instrument's sensitivity is needed as a free parameter for its laboratory calibration. In addition, the incident shortwave radiation fluxes are important for daytime determinations of downwelling longwave radiation. Errors in downwelling longwave measurements are primarily due to differences in temperatures of the pyrgeometer body and dome compared to the temperature of the atmosphere. Using the present theory and laboratory and field observations, it is possible for downwelling longwave heat fluxes to be measured with errors less than 6 W m^{-2}. Examples of determinations of longwave heat flux from surface buoy observations in four different oceanic regions are also presented. These observations suggest the following: 1) incoming longwave measurements from buoys are possible and repeatable; two calibrated sensors on the same platform return time series that are in good agreement, 2) uncertainties in the calibration of the Eppley radiometers are significant and appear systematic in that all radiometers calibrated on a given day have similar shifts in calibration, and 3) radiometers deployed in the field are sensitive to incoming shortwave radiation when deployed in conditions where solar heating of the sensors and buoy might be anticipated; differences between longwave sensors on the same platform are correlated to the magnitude of the incoming shortwave radiation. Further, it is not possible to conclude how closely present radiometers come to being absolutely correct and the size of the uncertainty associated with the calibration is similar in magnitude to the difference signal observed in the field. Thus, improvement in calibration procedures is needed as well as a radiometer which could be used as a transfer standard to determine if in situ measurements are accurate as well as repeatable. Finally, a hybrid measurement system for the determination of net longwave heat flux at the air-sea interface is described. Uncertainties in sea surface skin temperature and emissivity are major contributors to the error in the net longwave heat flux. A targeted error limit of $\pm$ 10 W m^{-2} for the net longwave heat flux appears to be achievable.

In Press: *Journal of Atmospheric and Oceanic Technology.*

Supported by: NSF Grant OCE87-09614; ONR Contracts N00014-89-J-1683, N00014-90-J-1490 and N00014-90-J-1423.

WHOI Contribution No. 8273.

DISCUSSION OF THE NRC REPORT "STATISTICS IN OCEANOGRAPHY"

Anand Gnanadesikan

It is always easy to find flaws in a review paper which attempts to cover the whole of one's field. It is a persistent feature of such papers that they will inevitably omit what someone considers the central issue of the field. While the present report does contain some such omissions, it also raises a great many important issues. The application of a number of these issues to the field of satellite remote sensing is well presented in the report and is, in my opinion, important to the development of the field as a whole. In this discussion, I would like to amplify some of the issues raised by looking at some different examples than those presented in the text. The use of these examples should not be taken as denigrating the importance of satellite-based remote sensing for understanding oceanic dynamics. Rather, I would like to show how some of these issues raised are of broad interest to a range of oceanographers.

Submitted to: *Statistical Science.*

Supported by: ONR Contracts N00014-91-J-1495 and N00014-91-J-1891.

WHOI Contribution No. 8594.

THE IMET (IMPROVED METEOROLOGY) SHIP AND BUOY SYSTEMS

D. S. Hosom, R. A. Weller, R. E. Payne and K. E. Prada

The recently developed IMET (Improved METeorology) system for ships and buoys and the key elements of the program that led to its development are described. The system improves

the ability to measure mean meteorological variables, including wind velocity, barometric pressure, incoming shortwave and longwave radiation, air temperature, sea surface temperature, humidity, and precipitation, from both types of platforms. Extensive laboratory and field tests of a variety of sensors were conducted to investigate and document their stability, accuracy, and reliability. Modular electronics were developed so that each sensor in the system communicated digitally, returning calibrated values to a central data recorder. IMET systems have been deployed on buoys in the Atlantic and Pacific Oceans and are being installed on research vessels. The history of the program, reasons for the choice of the present sensor suite, the design of the sensor modules, a description of the data acquisition system, and examples of data collected with the system are described. A discussion of the areas in which further improvements to the system will be sought is also provided.

In Press: *Journal of Atmospheric and Oceanic Technology.*

Supported by: NSF Grant OCE91-15000.

WHOI Contribution No. 8485.

A COMPARISON OF SOME BAROMETRIC PRESSURE SENSORS

Richard E. Payne

A variety of pressure sensors have been tested in the laboratory for accuracy and long term stability. The Paroscientific 215-AT and the Rosemount 1201F1B were found to be the most accurate, maintaining 0.1 mb accuracy over long periods. These were followed by the Setra 270 with long term accuracy of 0.2 mb and the AIR DB-1A with 0.5 mb in most units tested. The Paroscientific and AIR sensors require the least power and are the most suitable for remote deployments. Results on inexpensive sensors show that some are worthy of consideration if accuracy requirements can be relaxed somewhat.

Submitted to: *Journal of Atmospheric and Oceanic Technology.*

Supported by: NSF Grants OCE87-09614 and OCE91-15000.

WHOI Contribution No. 8358.

OTHER

INVESTIGATION OF FERROELECTRIC EFFECTS IN TWO SULFIDE DEPOSITS

Charles E. Corry

Since 1950 it has been known that makedonite ($PbTi0_3$) is ferroelectric. Laboratory studies by different investigators using various techniques have expanded the number of known ferroelectric ore minerals to about twenty. These include such common ore minerals as bismuthinite (Bi_2S_3), cassiterite ($Sn0_2$), chalcocite (Cu_2S), pyrrhotite ($Fe_{1-x}S$), and stibnite (Sb_2S_3).

Two field investigations of sulfide ore bodies that contain known ferroelectric minerals were undertaken to investigate possible ferroelectric effects in these deposits.

The two deposits, at Mount Emmons (38° 53'N 107° 03'W), Colorado, and Three R Canyon (31° 28'N 110° 46'W) in the Patagonia Mountains, Arizona, demonstrate ferroelectric effects which include directional polarization and apparent resistivity, electrically-excited resonance, and lack of reciprocity. Other observations include history-dependent electrical behavior and inductive effects that are probably related to the presence of ferroelectric minerals.

Submitted to: *Journal of Applied Physics.*

Supported by: Climax Molybdenum - Division of AMAX, Inc.

WHOI Contribution No. 8403.

REPLY TO DISCUSSION OF "GEOLOGY OF THE SOLITARIO" GSA SPECIAL PAPER 250 BY HENRY AND OTHERS

Charles E. Corry

We have had strong disagreements with Henry and others for a number of years. I note with regret that in their present discussion Henry and others have been largely reduced to *argumentum ad hominem.*

We have been accumulating geological, geophysical, geochronological, and geochemical data in the Solitano over nearly three decades and the data from our work is presented in 18 tables, 48 figures, 8 appendices, and 4 maps, as well as 97 pages of text. Where data were available, we presented maps and figures at different map scales and time periods, or in the case of the magnetic data, at different flight elevations. The effects of 3 orogenies and 2 extensional events are documented. Sample locations are described and given in appendices. Known fossils are tabulated

and localities plotted. Various hypotheses are examined and methods described in detail.

Submitted to: *Bulletin of the Geological Society of America.*

WHOI Contribution No. 8455.

A LARAMIDE AGE PUSH-UP BLOCK: THE STRUCTURES AND FORMATION OF THE TERLINGUA-SOLITARIO STRUCTURAL BLOCK, BIG BEND REGION, TEXAS

Charles E. Corry, James B. Stevens and Eugene Herrin

Erdlac (1990) has argued that the Terlingua-Solitario uplift represents a Laramide age "pushup" block. Since we do not find "push-up" block in the geologic glossary we feel that it would have been appropriate to define the term or provide a reference that does define the term. Whatever he may mean by his structural term, we wish to point out a number of difficulties in accepting his thesis that it is a Laramide feature and the result of compression tectonics.

Submitted to: *Bulletin of the Geological Society of America.*

WHOI Contribution No. 8456.

WIND FORCED BIOLOGICAL-PHYSICAL INTERACTIONS ON AN ISOLATED OFFSHORE BANK

Craig V. W. Lewis, Cabell S. Davis and Glen Gawarkiewicz

Large advective losses of bank water during winter due to strong wind forcing are hypothesized to be a significant factor limiting recruitment of spring spawning plankton and subsequent feeding success of larval fish. The plausibility of this "washout hypothesis" is examined using numerical modeling of plankton and physical dynamics on an idealized off-shore bank, approximating conditions on Georges Bank. A semi-spectral primitive equation model (SPEM) is used to study three dimensional wind and density driven circulation. Biological models were used to represent: 1) a single generation of copepods and 2) a simple planktonic food web. Results indicate that the typically high winds during winter (velocity: 24 knots; duration: 20 days) can cause significant replacement of the bank water mass with surrounding waters. This large exchange causes major reductions in zooplankton populations and zooplankton and phytoplankton production over the bank. These alterations in bank trophic structure reduce the energy transfer from primary production to secondary production and may lead to poor recruitment at higher trophic levels.

In Press: *Topical Studies in Oceanography.*

Supported by: NSF Globec 8168901.

WHOI Contribution No. 8578.

FINESCALE PARAMETERIZATIONS OF TURBULENT DISSIPATION

K. Polzin, J. Toole and R. Schmitt

Fine- and microstructure data from a free-fall profiler are analyzed to test models of the relationship between the turbulent dissipation rate (ε) and internal wave dynamics. The data were obtained from several distinct internal wave environments, yielding considerably more range in stratification, wave energy and frequency content than has been previously available.

Observations from the far field of a seamount in a region of negligible large-scale flow were examined to address the issue of the buoyancy scaling of ε. These data exhibited large variations in background stratification with depth and internal wave characteristics undifferentiable from the GM76 (Garrett and Munk, 1975; as modified by Cairns and Williams, 1976) spectrum. The magnitude of ε and its functional dependence upon internal wave energy level (E) and buoyancy frequency (N) was best described by the dynamical model of Henyey *et al.* (1986) ($\varepsilon \sim E^2N^2$). A second dynamical model, McComas and Muller (1981b), predicted an appropriate (E,N) scaling, but overestimated the observed dissipation rates. Two kinematical dissipation parameterizations (Gargett and Holloway (1984) and Munk (1981)) predicted buoyancy scalings of $N^{3/2}$ which were inconsistent with the observed buoyancy scaling.

Data from a warm core ring dominated by strong near-inertial shears, a region of steep topography exhibiting high frequency internal wave characteristics and a mid-ocean regime dominated at large wavelengths by an internal tide were analyzed in order to examine the parameter dependence of ε in wave fields which exhibited non-GM spectral characteristics. The GM based predictions of the dynamical models ($\varepsilon \sim E^2N^2$) exhibited over an order of magnitude scatter with respect to the observed dissipation rates. This variability was associated with variations in the wave field frequency. Application of a frequency based correction to the Henyey *et al.* model (Henyey, 1991) returned dissipation values consistent with observed estimates to within a factor of 4. These results indicate that vertical mixing rates are low for typical GM internal wave

conditions, becoming large only when wave energy levels are elevated. In the deep ocean, internal wave interactions with topographic features are the most promising candidate for achieving strong vertical mixing.

Submitted to: *Journal of Physical Oceanography.*

Supported by: ONR Contracts N00014-89-J-1073 and N00014-92-J-1323.

WHOI Contribution No. 8465.

DOUBLE DIFFUSION IN OCEANOGRAPHY

Raymond W. Schmitt

The modern study of double-diffusive convection began with Melvin Stern's article on "The salt fountain and thermohaline convection" in 1960. In that paper he showed how opposing stratifications of two component species could drive convection if their diffusivities differed. Stommel, *et al.*, (1956) had earlier noted that there was significant potential energy available in the decrease of salinity with depth found in much of the tropical and subtropical ocean. While they suggested that a flow (the salt fountain) would be driven in a thermally conducting pipe, it was Stern who realized that the two order of magnitude difference in heat and salt diffusivities allowed the ocean to form its own pipes which later came to be known as "salt fingers." Stern also identified the potential for the oscillatory instability when cold, fresh water overlies warm, salty water in the 1960 paper, though only in a footnote. Turner and Stommel (1964) demonstrated the "diffusive-convection" process a few years later.

From these beginnings in oceanography over three decades ago, double diffusion has come to be recognized as an important convection process in a wide variety of media, including magmas, metals, and stellar interiors (Turner 1985). However, it is interesting to note that about one hundred years before Stern's paper, W.S. Jevons (1857) reported on the observation of long, narrow convection cells formed when warm, salty water was introduced over cold, fresh water. He correctly attributed the phenomenon to a difference in the diffusivities for heat and salt in a qualitative way. His attempt to apply the results to cloud convection were misguided, and possibly led to their being ignored. Otherwise, it is easy to imagine that Rayleigh or some other scientific giant of the last century could have initiated the theoretical study of double diffusion and we would now have over ten decades of progress, rather than only three!

None the less, it is fitting that the ocean should be the impetus for the discovery of this fundamental convection process. As will be discussed below, the ocean is rather strongly unstable to double-diffusive processes and seems to be profoundly affected by its presence. It is only the recent advances in ocean instrumentation which have enabled us to begin to understand the workings of double-diffusive mixing in the large, under-explored fluid which covers most of the Earth. Given the vital role of mixing in control of ocean heat storage, the thermohaline circulation, climate, carbon dioxide absorption and pollutant dispersal, it is increasingly important that we achieve a more complete understanding of oceanic double diffusion.

In the following (necessarily) brief review, I attempt to summarize our current knowledge of oceanographic double-diffusion for the salt finger, diffusive convection and intrusive instabilities. Due to my own interests, there is a more complete discussion of salt fingers. In addition, I note some of the potential implications for large scale modelling of the ocean thermohaline circulation.

Published in: *Annual Review of Fluid Mechanics,* 26:255–285, 1993.

Supported by: ONR Contract N00014-92-J-1323.

WHOI Contribution No. 8315.

THE DISTRIBUTION OF LANTERNFISH CERATOSCOPELUS MADERENSIS (LOWE 1839) OFF NORTHWEST-AFRICA AND ITS RELATION TO WATER MASSES

Clementine Zelck and Birgit Klein

Adult *Ceratoscopelus maderensis* have a wide vertical range and a prevailing zonal distribution, but represent also a high ranking lanternfish species in the Mauritanian upwelling. The previous concept of a temperature dependent distribution is questioned on base of hydrographic and fish larvae data from a new survey and literature studies. The almost congruent horizontal distributions of adults and larvae can better be described by salinity characteristics in the 1000 m depth layer, the lowermost range of the adults, than by temperature. Adult *C. maderensis* live during daytime in deep water with Mediterranean influence. The southernmost limit coincides with oxygen deficiencies at the respective depth.

Submitted to: *Deep-Sea Research.*

Supported by: Deutsche Forschungsgemeinschaft, SFB 133 Institut für Meereskunde Kiel.

WHOI Contribution No. 8610.

MARINE POLICY CENTER

James M. Broadus III, Director

MARINE POLICY CENTER

CLIMATE CHANGES AND SOCIO-ECONOMIC IMPACTS

Anders Alm, Erik Blommestein, and James M. Broadus

Many of the physical effects of climatic changes in the Gulf of Mexico/Caribbean Sea region will have socio-economic impacts. The presumption is that, for most cases, the net effect will be costly, but this will depend on the facts of each case. For several reasons, prior work has been mostly on the potential impacts of sea-level change, but other climatic changes in the region may have impacts which equal or surpass those. A matrix that relates types of climate-change effects to qualitative impacts on economic sectors is presented. Potential impacts on fisheries, agriculture and forestry, tourism, settlements and structures, the immediate coastal zone, public health, and waste disposal and drainage are discussed. Descriptive and prescriptive issues of public responses are examined, along with attention to techniques and research issues in efforts to estimate socio-economic impacts.

Published in: *Climate Change in the Intra-Americas Sea*, G. Maul, ed. E. Arnold, London, :333-349, 1993.

Supported by: The Pew Charitable Trusts and The National Institute for Global Environmental Change (US Department of Energy).

WHOI Contribution No. 6779.

FLAT ORGANIZATIONS FOR EARTH SCIENCE

Jesse H. Ausubel and John H. Steele

The institutions that made American science famous figure less and less in the leadership and management of American science. Causes for this decline, especially evident in ocean and atmospheric sciences, include large programs that cut across institutions, the volume of federal funds, the scale of scientific instruments and facilities, easier travel and telecommunications, and time horizons of entrepreneurial science. The pattern emerging results not from a deliberate policy of bypassing major institutions and their management, but from radical changes in the structure of scientific activity. Science is matching industry in a trend toward flatter management and functional, rather than geographic organization. Some risks and needs arise with the new balance-or imbalance-of power.

Published in: *Bulletin of the American Meteorological Society*, 74(5):1-6, 1993.

Supported by: Rockefeller University; The Marine Policy Center.

WHOI Contribution No. 8359.

REPORT ON THE MARINE POLICY CENTER OF THE WOODS HOLE OCEANOGRAPHIC INSTITUTION (WHOI), WOODS HOLE, MASSACHUSETTS

James M. Broadus

Policy issues involving the world's oceans and coastal areas arise across a broad range of human endeavors, including progress in science and technology, access to and control of resources, environmental protection, and international and intergovernmental relations. The Marine Policy Center (MPC) at the Woods Hole Oceanographic Institution (WHOI) is one of a relatively small number of research centers in the world dedicated to the application of social scientific and legal scholarship to these issues. To be useful, this research must be based on the best available scientific information. WHOI thus provides an excellent setting for research in the identification and analysis of problems in marine policy. Since its inception in 1971, MPC has hosted the work of nearly 100 resident research fellows and staff. The Center's staff, though small, has gained international stature and recognition. MPC research concentrates on optimizing the management of coastal and marine resources. MPC research priorities focus on four areas of interest: (1) global climate change; (2) ocean conservation; (3) science and technology policy; (4) polar affairs.

Published in: *Ocean Yearbook 10.* E. M. Borgese, N. Ginsburg, and J. R. Morgan, eds. University of Chicago Press, Chicago, :358-364, 1993.

Supported by: The Marine Policy Center.

WHOI Contribution No. 7993.

MARINE POLLUTION GETS INTERNATIONAL ATTENTION

James Broadus, Yoshiaki Kaoru, Sarah Repetto, and Suzanne Demisch

Land-based pollution is the world's most serious marine pollution problem. The problems and opportunities offered by international efforts to control land-based marine pollution are exemplified in three regions of Europe: the Baltic, Mediterranean, and North Seas. Several lessons from a review of these regions are identified and discussed. To secure participation, individual

nations must believe that proposed actions will benefit them directly. States that fail to foresee gains from collective actions have no incentive to respond to the accords. Because self-interest differs from nation to nation and because a key rationale for collective action is to facilitate information sharing and exchange, program effectiveness and efficiency will be enhanced by provisions that help participants exchange their expertise, technology, and other resources. Too little effort has been made to assign costs based on how much a nation contributes to the problem or how much it can afford to pay. Since a program's effectiveness ultimately depends on the commitment of the participating nations, collective, high-level international political intervention can help make a difference.

Published in: *Forum for Applied Research and Public Policy*, 9(1):59-63, 1994.

Supported by: U.S. Environmental Protection Agency.

WHOI Contribution No. 8304.

PROBLEMS IN THE MESO-SCALE INTERPRETATION OF SATELLITE CHLOROPHYLL DATA

E. W. Henderson and J. H. Steele

The satellite data for the North Sea show significant differences from *in situ* measurements when analyzed in terms of variance as a function of spatial scale. It seems likely that various factors in the instrument and in the data processing could produce changes in this variance distribution particularly at small scales (large wave numbers) of the order of 1-10 km. For these reasons, it appears inappropriate to use the satellite data to infer conclusions about plankton dynamics in the meso-scale range without reference to *in situ* data.

Published in: *Continental Shelf Research*, 13(8/9):845-861, 1993.

Supported by: NSF OCE-9123451.

WHOI Contribution No. 7934.

MANGANESE NODULE PRICE TRENDS: DIM PROSPECTS FOR THE COMMERCIALIZATION OF DEEP SEABED MINING

Porter Hoagland

Prospects for the commercialization of deep seabed mining hinge upon projections of future revenues and estimates of costs associated with new technologies. Future revenues will depend upon the behavior of prices for metals that might be recovered from nodules. In this article, we construct a hypothetical grade and recoverability weighted manganese nodule price from the turn of the century forward and examine its behavior over time. Long-term trends and the potential for cycles in the prices of nodule metals are considered. Four techniques are employed to make future predictions about the commercial prospects for deep seabed mining. The most optimistic expected date of commercialization resulting from these predictions is well into the 21st century. Given fixed assumptions about technologies, there are many other reasons for being even more pessimistic about the commercial prospects for deep seabed mining.

Published in: *Resources Policy*, 19(4):287-298, 1993.

Supported by: UN Division for Ocean Affairs and Law of the Sea; Korea Ocean Research and Development Institute; The East-West Center; The Marine Policy Center.

WHOI Contribution No. 8435.

PLANNING VS. REALITY: POLITICAL AND SCIENTIFIC DETERMINANTS OF OUTER CONTINENTAL SHELF LEASE SALES

Porter Hoagland and Scott Farrow

We investigate the political, scientific, and organizational factors affecting a decision about the number of lease sales to be held on OCS lands during the period 1987-1992. Based upon a conceptual model of rent-seeking from the field of public choice, we extend the analysis of Farrow (1991) to investigate more deeply the role of political interest groups in the decision. We examine the determinants of the number of planned (ex ante) and actual (ex post) lease sales. Ex ante, we find evidence to support Farrow's (1991) model of rational-scientific decisionmaking in the selection of the number and location of lease sales. Ex post, we find evidence to support a model of multiparty negotiation in which political interests both for and against OCS leasing influence the selection of lease sales. In addition, we find, ex post, that a measure of environmental sensitivity has no direct influence on the negotiated outcome. We conjecture that rent-seeking behavior exhibited by political interest groups leasing to the imposition of areawide leasing "moratoria" may be socially wasteful. Furthermore, the rational planned procedures for OCS leasing found in U.S. law have only a marginal effect on where and how often leasing occurs, although they may have value in providing information for participants in the negotiation. A case study of OCS decisionmaking is included.

In Press: *The Political Economy of Pollution Control*, Roger Congleton, ed. University of Michigan Press, Ann Arbor.

Supported by: Center for Business and Government, Harvard University; The Marine Policy Center.

WHOI Contribution No. 8570.

TECHNOLOGY TRANSFER AND SCIENTIFIC RELEVANCE

Porter Hoagland and Hauke Kite-Powell

How can scientific research results be disseminated and applied in ways that foster the achievement of national goals, such as economic competitiveness, public health, national security, and environmental protection? This consideration is sometimes referred to broadly as "technology transfer." Within the last decade, much discussion has been generated about the concept, but little attention has been paid to its theoretical underpinnings in economics. In this paper, we take an economic approach to the meaning and implications of technology transfer. We define technology broadly as information (new knowledge) developed as a result of research. The problem of technology transfer is to identify efficient means for knowledge dissemination. Scientific publication has been and continues to be the most important form of technology transfer in oceanography. Public policy that focuses solely on technology *licensing* as an indicator of the relevance of scientific research to national goals may be misdirected if it ignores the benefit of other forms of technology transfer, such as scientific publication. (We also examine the problems faced by a research laboratory in licensing technology.)

In Press: *Oceanography.*

Supported by: ONR N00014-93-I-0028; NOAA NA26AD0156 to the Massachusetts Center for Excellence in Marine and Polymer Sciences.

WHOI Contribution No. 8230.

MULTIMEDIA WASTE DISPOSAL OPTIMIZATION UNDER UNCERTAINTY WITH AN OCEAN OPTION

Di Jin

Many communities face a waste management crisis. An increase in waste generation and decline in available landfill capacity have led to rapid increases in waste management costs. Using sewage sludge management in coastal New York and New Jersey as an example, this paper examines optimal multimedia waste disposal under cost uncertainty. Using expected value-variance analysis, the study looks at the effects on the optimal disposal strategy of uncertainty associated with waste-management cost and the community's risk preferences. The results indicate that, based on available cost data, the optimal strategy of a moderately risk-averse decision maker is to manage sludge through land-based facilities. These results hold over a wide range of risk-aversion parameters and even at low levels of cost uncertainty. Thus, the Ocean Dumping Ban Act of 1988 is consistent with such results.

In Press: *Marine Resource Economics.*

Supported by: Alfred P. Sloan Foundation; The Marine Policy Center.

WHOI Contribution No. 8577.

ENVIRONMENTAL COMPLIANCE AND OPTIMAL OIL AND GAS EXPLOITATION

Di Jin and Thomas A. Grigalunas

This paper examines the impacts of environmental regulations on firms in the oil and gas industry. A model is developed using optimal control theory, which extends the existing models by incorporating the environmental compliance costs into the exploration and production stages. An approach for measuring the cumulative impacts of these regulations on the firm's exploration and production is presented. The results indicate that rising environmental compliance costs lead to reductions in investment and production, and the alteration of investment and production profiles. This implies that fewer resources will be developed and associated economic benefit will decline. Therefore, it is vital for policy makers to consider carefully whether the perceived environmental benefits derived from these regulations justify associated compliance costs.

In Press: *Natural Resource Modeling.*

Supported by: The Marine Policy Center; Rhode Island Agricultural Experiment Station.

WHOI Contribution No. 8599.

MONITORING MARINE RESOURCES: ECOLOGICAL AND POLICY IMPLICATIONS AFFECTING THE SCIENTIFIC COLLECTING AND COMMERCIAL VALUE OF NEW ENGLAND CONCH *(BUSYCON)*

Ilene M. Kaplan and Barbara C. Boyer

This paper examines the socio-economic and ecological trends in the New England conch (the

commercial name for the whelk *Busycon*) fishery and concomitant changes in marine policy regarding the commercial fishing of conch.

Published in: *Biological Bulletin*, 183:379-380, 1992.

WHOI Contribution No. 8529.

DISCRETE-CHOICE CONTINGENT VALUATION OF BEACH RECREATION BENEFITS FOR TOURISTS AND LOCAL RESIDENTS

Yoskiaki Kaoru

Economic studies measuring recreation benefits have not paid much attention to the variation in recreational activities engaged and the resources consumed by individual recreationists during their trips. It is important to make clear distinctions about the heterogeneous aspects of on-site recreational activities and costs incurred by recreationists for uses of specific recreational resources. This paper estimates recreation benefits at a beach on Martha's Vineyard in Massachusetts by a discrete-choice contingent valuation method. Individual recreationists included in the on-site survey were classified into tourists and local residents. These two different groups of recreationists were asked separate sets of questions about their recreation expenditures and willingness to pay for their access to the beach. Individual socioeconomic characteristics and beach quality ratings influenced the beach recreation benefits differently for tourists and local residents. The beach recreation benefits per trip for a tourist were substantially higher than those for a local resident. However, the seasonal beach recreation benefits were found to be very close. On average, the local resident's seasonal benefits were about 80 percent of the tourist's seasonal benefits.

Submitted to: *Environmental and Resource Economics.*

Supported by: The Marine Policy Center.

WHOI Contribution No. 8500.

THE VALUE OF HISTORIC SHIPWRECKS: CONFLICTS AND MANAGEMENT

Yoshiaki Kaoru and Porter Hoagland

Underwater cultural resources, such as historic shipwrecks, recently have emerged as an important class of marine resources. Since World War II, a generalized "demand" for these resources has expanded, and institutions through which the beneficial attributes of historic shipwrecks are provided have increased in number. These factors have exacerbated conflicts among user groups over the resource. As a result, coastal and marine cultural resource managers now face more significant issues relating to resource allocation and distributions of benefits. Because of difficulties in accounting for "nonmarket" benefits, in the past the allocation of historic shipwreck resources may have been unnecessarily costly in terms of lost opportunities. In this article, we develop a conceptual framework for underwater cultural resource management. We characterize historic shipwrecks as "quasi-natural resources," and we argue that methods of estimating nonmarket values in environmental and natural resource management can be applied to improve decision-making in cultural resource management.

In Press: *Coastal Management.*

Supported by: NSF DIR-9114699 and The Marine Policy Center.

WHOI Contribution No. 8384.

USING RANDOM UTILITY MODELS TO ESTIMATE RECREATIONAL VALUE OF ESTUARINE RESOURCES

Yoshiaki Kaoru, V. Kerry Smith, and Jin Long Liu

This paper describes an integrated model using a household production framework to link measures of nonpoint source pollution to fishing quality and a random utility model to describe how that quality influences the decisions of sport fishing parties in the Albemarle-Pamlico estuarine system in North Carolina. The results provide clear support for using a model that evaluates the effects of pollution on the activities and decisions associated with the fishing activity once a trip is taken. Site selection decisions are then conditioned on the anticipated quality of fishing trips at each site. The framework also has the advantage of linking the spatial, technical, and economic information required to evaluate the management plans required for estuaries under the National Estuarine Program.

Submitted to: *The American Journal of Agricultural Economics.*

Supported by: NOAA Sea Grant No. NA86AA-D-SG046; University of North Carolina Sea Grant Program Project Nos. R/MRD-9 and R/MRD-22; The Pew Charitable Trusts; The Marine Policy Center.

WHOI Contribution No. 8533.

ECONOMICS OF STANDARDS, SYSTEM ANALYSIS, AND SEA TRIALS: TOWARD AN ASSESSMENT OF THE PROPOSED IMO PERFORMANCE STANDARD FOR ECDIS

Hauke Kite-Powell

The International Maritime Organization (IMO), with the International Hydrographic Organization (IHO), continues to work toward adoption of a minimum performance standard for ECDIS. Much of the work on the draft standard has been performed by the IMO/IHO Harmonization Group on ECDIS (HGE). HGE published its most recent draft of the standard in September 1992. This paper presents a methodology for assessing the draft standard, using economics, system analysis, and operational data. It sets out alternative formulations of objectives for the standard, discusses how an economic theory of standards and engineering systems analysis can be used together with operational sea trials data to help determine what the content of and IMO performance standard for ECDIS ought to be, and concludes with a brief discussion of how this compares to the draft standard proposed by HGE.

Published in: *ECDIS '93 (Conference Proceedings of the Second Annual Conference and Exposition for Electronic Chart Display and Information Systems.)* 8-9 March 1993, Baltimore. International Hydrographic Bureau and International Maritime Organization, 1993.

Supported by: ONR N00014-90-J4040 to the USGS, sponsors of the US ECDIS Test Bed Project; NOAA NA87-AA-D-M0 037, NA90-AA-D-NC 250 to the Mass. Centers of Excellence; and NOAA NA26-A-D-0-156 to the Mass. Foundation for Excellence in Marine and Polymer Sciences.

WHOI Contribution No. 8320.

ELECTRONIC CHART SYSTEMS IN THE SHIP CONTROL PROCESS: THE ROLE OF OPERATORS AND INSTRUMENTS IN SAFETY OF NAVIGATION

Hauke Kite-Powell

Electronic chart systems are technologically feasible and coming into use aboard civilian and military ships. They have considerable potential for improving the safety and efficiency of navigation by automating position plotting and assisting track-keeping and grounding avoidance. The International Maritime Organization (IMO), with the International Hydrographic Organization (IHO), continues to work toward adoption of a minimum performance standard for electronic charts. The largest obstacle to their widespread use on commercial vessels is the non-availability of digital chart data certified by hydrographic authorities. Drawing on a methodology initially developed to evaluate the proposed IMO standard, this paper describes a system analysis of navigational safety conducted to examine the potential of electronic chart devices for preventing accidents and increasing efficiency. The model describes the process of traditional navigation, centered around the ship operators and their perceptions of the ship's navigational status. The model is used to identify weak links that can compromise safety, and suggests how electronic charts can strengthen the system. The paper concludes by commenting on recent progress in the IMO electronic chart standard setting process and its likely effect on the evolution and adoption of electronic chart technology in the commercial shipping industry.

Published in: *Tenth Ship Control Systems Symposium, Proceedings*, October 1993, National Defense Canada, Ottowa, 5:21-31, 1994.

Supported by: ONR N00014-90-J-4040; U.S. ECDIS Test Bed Project 39598500; NOAA NA87-AA-D-M0 037; NOAA NA90-AA-D-NC 250; NOAA NA26-A-D-0 156.

WHOI Contribution No. 8320A.

PRELIMINARY OPERATIONAL AND USER SURVEY RESULTS FROM U.S. ECDIS TEST BED PROJECT SEA TRIALS

Hauke Kite-Powell

The U.S. ECDIS Test Bed Project is conducting ECDIS sea trials and gathering input from professional mariners who have operational experience with electronic chart systems. The purpose of these trials and interviews is to support and inform the ongoing deliberations within the International Maritime Organization and International Hydrographic Organization on an international performance standard for ECDIS. Primary sources of data are the Test Bed ECDIS, which will record operational usage information during the trials, and questionnaires given to operators. This paper discusses some preliminary results from the trials and surveys conducted to date.

Published in: *ECDIS '93 (Conference Proceedings of the Second Annual Conference and Exposition for Electronic Chart Display and Information Systems.)* 8-9 March, 1993, Baltimore. International Hydrographic Bureau and International Maritime Organization, 1993.

Supported by: US Coast Guard; ONR N00014-90-J-4040; NOAA Grants NA87-AA-D-M0 037 and NA90-AA-D-NC 250 to the Mass. Centers of Excellence Corporation and Grant NA26-A-D-0 156 to the Mass. Foundation for Excellence in Marine and Polymer Sciences.

WHOI Contribution No. 8319.

BOOK REVIEW: *OCEANOGRAPHY IN THE NEXT DECADE*

James C. Kraska

The review summarizes *Oceanography in the Next Decade*, which details the relevance of ocean science to a broad range of national priorities and offers an excellent depiction of the Navy's programs and contributions within the context of ocean science generally. The volume is recommended as a good primer on the direction of U.S. ocean science and its contribution and relevance to U.S. economic, environmental and national security planning.

In Press: *Naval War College Review.*

Supported by: ONR N00014-93-0028 and The John E. Sawyer Endowed Fund.

WHOI Contribution No. 8541.

GATEKEEPER OF THE GULF: THE IRANIAN NAVY AND PERSIAN GULF SECURITY TOWARD THE 21ST CENTURY

James C. Kraska

In the wake of Desert Storm, Iran is emerging as a new threat to Persian Gulf security. This threat is characterized by an expansion of naval capabilities and assertiveness as part of an ambitious program to dominate the waters of the Gulf by the end of this century. First Prize, U.S. Naval Institute International Navies Essay Contest.

Published in: *Naval Institute Proceedings*, 3(March):44-47, 1994.

Supported by: ONR N00014-93-0028 and The John E. Sawyer Endowed Fund.

WHOI Contribution No. 8543.

OCEANOGRAPHIC AND NAVAL DEPLOYMENTS OF EXPENDABLE MARINE INSTRUMENTS UNDER U.S. AND INTERNATIONAL LAW

James C. Kraska

United States government and civilian vessels and aircraft annually deploy tens of thousands of expendable marine instruments into the world's oceans. The instruments may be active only a few minutes or for as long as several years, but once they cease operation, they sink to the floor of the ocean. The devices are essential to collect data about the water column for use in naval operations, oceanographic and scientific research, and commercial ocean industry, and to promote safe navigation. With burgeoning world-wide environmental awareness and tightening of environmental rules, questions naturally arise about the legality of the practice under U.S. and international law. The deployment of expendable marine instruments has been virtually ignored by lawyers in the United States and abroad, but this condition is eroding. This article suggests that the practice is problematic under U.S. environmental law. Perhaps more important, under the international law of the sea, coastal states are beginning to assert jurisdiction over the practice as far as 200 nm from their coastlines. This trend already regulates oceanographic deployments of expendable marine instruments and promises to impinge on naval deployments of the devices as well.

Submitted to: *Columbia Journal of Environmental Law.*

Supported by: ONR N00014-93-0028 and The John E. Sawyer Endowed Fund.

WHOI Contribution No. 8540.

THE US NAVY AND NO CURE, NO PAY SALVAGE LAW

James C. Kraska

Strategy, force structure, and doctrine, dictate how the U.S. will conduct national security operations. Another component of military planning is law. A greater awareness of how to structure and reform the law to meet defense requirements is emerging. One area ripe for reform is U.S. Navy salvage law. The U.S. government does not participate in the international no cure, no pay salvage regime. As a result, the Navy may be unprepared to cope with wartime salvage requirements. This paper analyzes the current architecture of Navy salvage law and suggests that no cure, no pay salvage should be adopted.

Submitted to: *The Naval Law Review.*

Supported by: ONR N00014-93-0028 and The John E. Sawyer Endowed Fund.

WHOI Contribution No. 8338.

THE U.S. NAVY AND THE MARINE POLLUTION CONVENTION

James C. Kraska

In step with society's increasing environmental awareness, navies are striving to become environmentally friendly. The U.S. Navy, for instance, has initiated a program called "Environmentally Sound Ships of the 21st Century," which aims to bring Navy vessels into compliance with tough environmental standards within the next decade, and other maritime powers are following suit. The most comprehensive agreement to control solid waste discharges is MARPOL 73/78. Historically, naval vessels are afforded sovereign immunity from maritime regulations such as MARPOL. This is the case with MARPOL generally, but the Marine Plastic Pollution Research and Control Act, which implements Annex V of the Convention under U.S. law, requires unprecedented full compliance by the Navy. The difficulties of compliance are related to the unique nature of warship operations. Because warships travel worldwide and in remote locations, they do not always have convenient access to port waste management facilities. All warships, but especially submarines, have severe size, weight, and space constraints. In addition, waste treatment processes aboard submarines cannot be allowed to contaminate the carefully controlled artificial atmosphere. The Navy's interim report to Congress indicates that it cannot meet some of the solid waste discharge standards by the implementation deadline, and that others may never be met.

Published in: *American Bar Association National Security Law Report*, 15(9):1-2, 5-6, 1993.

Supported by: ONR N00014-93-0028, The John E. Sawyer Endowed Fund.

WHOI Contribution No. 8542.

DEVELOPMENT OF THE UNITED STATES ELECTRONIC CHART DISPLAY AND INFORMATION SYSTEM (ECDIS)

David J. Scott and Arthur G. Gaines, Jr.

The U.S. Electronic Chart Display and Information System (ECDIS) test-bed project was jointly initiated by the Woods Hole Oceanographic Institution's (WHOI) Marine Policy Center and the Radio Technical Commission for Maritime Services (RTCM). The project, officially begun in 1990, provides a facility for testing the International Maritime Organizations's (IMO) provisional performance standards for Electronic Navigation Chart displays.

The planning phase of the project, completed in July 1991, provided a System Requirements Specification (SRS) based on the IMO standard, including International Hydrographic Organization (IHO) standards and other information as appropriate. The SRS was used as a basis for a System Design Document (SDD) building on Intergraph Corporation commercial graphics hardware and software.

Assembly of an "IMO compliant" ECDIS is the objective of the second phase of the project, which began in September 1991. This phase involves ECDIS software development and hardware integration, with the experimental ECDIS unit scheduled for completion by September 1992. This paper details the design and functionality base line of this testbed platform, and reports on the status of phase II development effort.

Published in: *Proceeding of the U.S. Hydrographic Conference, 25-28 February, 1992, Baltimore, Maryland.*

Supported by: NOAA Grants NA87-AA-D-MO 037 and NA90-AA-D-NC 250 to the Mass. Centers of Excellence Corporation.

WHOI Contribution No. 8284.

AN EXPLORATORY ANALYSIS OF A RECORD OF EL NIÑO EVENTS, 1800-1987

Andrew R. Solow

This paper describes an exploratory analysis of a record of major El Niño events covering the period 1800-1987. This record contains both the years during which the events occurred and a binary indication of their magnitude. The record is modelled as a marked point process in which the times of the events follow a renewal process and the sequence of binary marks follows a stationary first-order Markov chain.

Submitted to: *Journal of the American Statistical Association.*

Supported by: The Marine Policy Center; Office of Global Climate Change; NOAA.

WHOI Contribution No. 8521.

A TEST OF INDEPENDENCE BETWEEN A TIME SERIES AND A MARKOV CHAIN

Andrew R. Solow

This note describes a conditional test of independence of an arbitrary time series and a first-order Markov chain against a mean-shift

alternative. The results of a small simulation study of the performance of the test are presented. An example concerning the relationship between the occurrence of rain and sewage contamination in Boston Harbor is given.

Submitted to: *Technometrics.*

Supported by: The Marine Policy Center.

WHOI Contribution No. 8539.

COMMENT (ON NRC REPORT ON STATISTICS AND PHYSICAL OCEANOGRAPHY)

Andrew R. Solow

By necessity, this report, like the ocean itself, is a good deal broader than it is deep. While the report provides an admirably panoramic view of data-rich areas within the field of physical oceanography, it does seem a little short on statistics. This is unfortunate, because there is no reason to believe that it will be harder to teach statisticians what they need to know about physical oceanography than to teach physical oceanographers what they need to know about sound statistical practice. In particular, the need to think carefully about a *statistical* model for data is often lost on oceanographers (and other scientists) in their search for methods. Methods are, of course, a dime a dozen. The trick lies in understanding when and why they work and when and why they do not.

In Press: *Statistical Science.*

Supported by: The Marine Policy Center.

WHOI Contribution No. 8490.

DETECTING CHANGE IN THE COMPOSITION OF A MULTI-SPECIES COMMUNITY

Andrew R. Solow

This paper describes an approach to extracting a trend from a time series of the composition of a multi-species community. The approach is based on a modification of a method for trend extraction from ordinary multiple time series. Two applications to a Northwest Atlantic ecosystem are described.

Submitted to: *Biometrics.*

Supported by: National Marine Fisheries NFFM2150252867.

WHOI Contribution No. 8410.

INFERRING EXTINCTION IN A DECLINING POPULATION

Andrew R. Solow

This note describes a test for extinction in a declining population based on a record of sightings. The test assumes that, prior to extinction, the sightings follow a Poisson process with decreasing rate function. An application to a sighting record of the black-footed ferret is presented.

Published in: *Journal of Mathematical Biology,* 32:79-82, 1993.

Supported by: The Marine Policy Center.

WHOI Contribution No. 8184.

ON THE ASSOCIATION BETWEEN SNOW ACCUMULATION AND EL NIÑO EVENTS IN THE QUELCCAYA ICE CAP, PERU

Andrew S. Solow

Thompson et al. (1984) identified an association between reduced snow accumulation in a core from the Quelccaya ice cap and the occurrence of El Niño events over the period 1964-1983. An extension of this analysis back to the beginning of the 19th century indicated that there is actually a significant association between *increased* accumulation in the core and El Niño events.

Submitted to: *Climate Change.*

Supported by: The Marine Policy Center.

WHOI Contribution No. 8491.

ON THE USE OF CROSS-CORRELATION IN SEISMOLOGY

Andrew R. Solow

The identification of relationships between seismicity in different regions is commonly based on establishing the statistical significance of the largest absolute value in the cross-correlogram between time series of seismicity. The assessment of significance typically ignores the selection of the largest absolute value in the cross-correlogram and consequently exaggerates significance. In this note, a simple method for correcting the significance level for selection is presented. The method is valid as long as the two series are each serially independent. An example concerning seismicity in Mexico and Kamchatka is presented. In this case, correcting for selection has a dramatic effect.

Submitted to: *Tectonophysics.*

Supported by: The Marine Policy Center.

WHOI Contribution No. 8549.

SATURDAY EFFECTS IN TANKER OIL SPILLS: COMMENT

Andrew R. Solow

Goodstein identified and discussed a "Saturday Effect" in data on the timing of tanker oil spills. This comment describes two ways in which the validity of the statistical analysis used to identify and confirm this effect can be strengthened.

Submitted to: *Journal of Environmental Economy and Management.*

Supported by: The Marine Policy Center.

WHOI Contribution No. 8333.

STATISTICAL METHODS FOR BOUT ANALYSIS

Andrew R. Solow

A common problem in quantitative ethology is the identification of bouts in a sequence of behavioral events. In a typical situation, the intervals between successive events are used to test for the existence of bout structure, fit the distributions of the within-bout and between-bout intervals, and devise a rule for assigning intervals to one of these categories. For conciseness, this process will be referred to as bout analysis. A number of methods have been proposed for bout analysis (e.g., Fagen and Young, 1978; Slater and Lester, 1982; Sibly, et al., 1990). From a statistical point of view, these methods are to some extent *ad hoc*, involving fitting by eye, binding the data arbitrarily, and applying tests based on the normal distribution to non-normal data. The purpose of this note is to describe a more formal statistical approach to bout analysis. In doing so, it is convenient to take the three steps in bout analysis in reverse order. Although this note, like most of the literature, focuses on the case in which there are two kinds of intervals, the extension to the case of more than two kinds of intervals is mentioned at the end.

Submitted to: *Animal Behavior.*

Supported by: The Marine Policy Center.

WHOI Contribution No. 8474.

ESTIMATING THE RATE OF SYNONYMY

Andrew R. Solow, Laurence A. Mound, and Kevin J. Gaston

A species description is said to be synonymized if it is found to be equivalent to an earlier description. Because a proportion of currently unsynonymized descriptions will be synonymized in the future, the observed rate of synonymy underestimates the true rate. A method for estimating the true rate and for providing an approximate confidence interval is described. The method is illustrated by estimating the synonymy rate for descriptions of the insect order Thysanoptera for the period 1900-1993.

Submitted to: *Systematic Biology.*

Supported by: The Marine Policy Center.

WHOI Contribution No. 8467.

ON THE MEASUREMENT OF BIOLOGICAL DIVERSITY

Andrew Solow, Stephen Polasky, and James Broadus

In optimizing strategies aimed at the conservation of biological diversity, it is necessary to compare the consequences of competing strategies for biological diversity. This paper presents a general approach to this problem. An example concerning the conservation of crane species is given.

Published in: *Journal of Environmental Economics and Management*, 24:60-68, 1993.

Supported by: The Pew Charitable Trusts and The Marine Policy Center.

WHOI Contribution No. 7875.

CONDITIONAL SIMULATION AND THE VALUE OF INFORMATION: A BAYESIAN APPROACH

Andrew R. Solow and Samuel J. Ratick

One option in decision making under uncertainty is to reduce uncertainty by acquiring information. The decisionmaker will choose to acquire additional information if its value exceeds its cost. This paper describes the use of nested conditional simulation in implementing a Bayesian assessment of the value of information in an explicitly spatial setting. A simple example is given concerning the management of flood damage.

Published in: *Geostatistics for the Next Century*, Rousso Dimitrakopoulos, ed. Kluwer Academic Publishers, Netherlands, :209-217, 1994.

Supported by: Subcontract to Clark University under NOAA NA26GPO459-01.

WHOI Contribution No. 8364.

COUPLING BETWEEN PHYSICAL AND BIOLOGICAL SCALES

John H. Steele and Eric W. Henderson

Temporal changes in population abundance display a great diversity of patterns. This diversity is acknowledged by reviewers of marine and terrestrial data, but their explanations tend to fall into two categories: internal factors related to population or community structure; and external aspects determined by the environment. The former we associate with terrestrial studies and the latter with marine. In this paper we stress the importance of the characteristic time scales in the dynamics of the populations and their relation to the scales of relevant environmental forces. We suggest that the coupling between these different scales, rather than the nature of the internal or external processes themselves, can provide a partial description, if not an explanation, of the diversity of patterns.

Published in: *Philosophical Transactions of the Royal Society of London, Series B*, 341:361-374, 1994.

Supported by: ONR N00014-92-J-1527.

WHOI Contribution No. 8462.

THE SIGNIFICANCE OF INTERANNUAL VARIABILITY

John H. Steele and Eric W. Henderson

A simple plankton model is used to link interannual variability in mixed layer depth with organic production and fluxes. Application to the 35-year physical data from Bermuda shows a more than threefold variability in annual production and flux. The process model also displays the great dependence of the absolute values on the parameters for zooplankton growth and mortality.

Published in: *Proceedings of the NATO Advanced Research Workshop "Towards a model of biogeochemical ocean processes."* Geoffrey T. Evans and Michael J. R. Fasham, eds. NATO ASI Series. Series I. Proceedings of a Workshop, May 9, 1992, Chateau de Bonas, France. Springer-Verlag, Berlin, Heidelberg, 10:237-260, 1993.

Supported by: ONR N00014-92-J-1527.

WHOI Contribution No. 8250.

COASTAL RESEARCH CENTER

Robert C. Beardsley, Director

COASTAL RESEARCH CENTER

A MODEL FOR THE MEDITERRANEAN SEAS: THE COOPERATIVE MARINE SCIENCE PROGRAM FOR THE BLACK SEA (COMSBLACK)

David G. Aubrey and Frank J. Gable

Marginal seas around the world typically encompass common borders of many littoral countries. Such seas often suffer from not-uniform or absent environmental controls, leading to degradation of that body of water. Attempts to improve the water resources may come after such degradation, but may be hampered by those national boundaries which are encompassed with the sea. Water resource improvement must include both land-based and marine analysis components: whereas land-based sources (river-borne, atmospherically-derived, and distributed) generally are the dominant contributors to degraded water quality and other water problems, clean-up of these land-based sources is long-term and often daunting technologically and economically. Marine science can play a key role here by assessing the health of the sea, determining its assimilative capacity for various pollutants, and hence ranking the susceptibility of that sea to various inputs. Such susceptibility may vary from sea to sea, depending on circulation, natural water chemistry, basin geometry, distribution of sources about the sea, etc. In addition, modern techniques now permit scientists to evaluate the efficacy of various mitigation strategies, prior to their costly implementation. Without such information, clean-up may be ineffective, wasteful of resources, and misdirected. As an example of a response to the need for adequate scientific input at a critical juncture in the life history of one sea, we discuss the Black Sea. Here past social and political conditions have contributed to massive pollution of a nearly-enclosed body of water. Disparate of nonexistent environmental controls, inadequate capability for monitoring, and lack regional coordination have precluded effective management of this regional resource. With changing political climates and international awareness, however, this situation is changing. Among the changes are some notable advances: a regional Convention for the Protection of the Black Sea against Pollution has been negotiated but not signed, UNEP is in the early stages of implementing an Action Plan, and the site is being considered for a Global Environmental Facility (GEF). As these activities are unfolding, scientists and scientific institutions have banded together to provide a cohesive, coordinated look at the health of the Black Sea. Although only one component of the overall international and national plans for effective resource management, the scientific input is critical at this early juncture. A non-governmental organization, name the Cooperative Marine Science Program for the Black Sea (CoMSBlack), has emerged from a year of discussions and planning. This consortium includes leading institutions and scientists from all Black Sea littoral states except Georgia (for now), as well as the U.S. and western Europe. Terms of Reference were established at a meeting in Varna, Bulgaria, in October 1991. CoMSBlack is implementing a detailed scientific plan to investigate and quantify the causes and effects of degradation in the Black Sea, to help resources manager and policy makers implement more effectively the necessary regional management plan for improvement of this resource. CoMSBlack is liaising closely with the various national and international efforts within the Black Sea, providing advice where requested and responding to the needs of these groups. CoMSBlack may be a useful model for other marginal seas. Coordination among scientists is often easier than coordination among littoral countries which may have long histories of social, political, or economic differences. By providing non-governmental coordination efforts such as CoMSBlack, the scientists can hasten the way towards regional management by assuring uniform monitoring, sampling, and scientific analysis throughout the region. This in turn provides the more complex intergovernmental Action Plans or implementation plans with essential scientific input that fosters effective regional integrated management.

Published in: *Symposium Mediterranean Seas 2000.* Norberto F.R. Della Croce, ed. Università di Genova, Instituto Scienze Ambientali Marine, Santa Margherita Ligure, :177-206, 1993.

Supported by: The Andrew W. Mellon Foundation; and the Regional Environmental Center for Central & Eastern Europe (Budapest).

WHOI Contribution No. 7955.

GRADUATE STUDENTS

Abstracts of papers of theses submitted in 1993 by graduate students of the Woods Hole Oceanographic Institution Doctoral Degree Program and the Woods Hole Oceanographic Institution/Massachusetts Institute of Technology Joint Program in Oceanography/ Oceanographic Engineering. Other papers authored or coauthored by graduate students are included in the departmental sections.

AN EXPERIMENTAL STUDY OF AIR ENTRAINMENT BY BREAKING WAVES

Eric Lamarre

Breaking waves charge the surface layer of the ocean with small air bubbles which play an important role in air-sea gas transfer and in underwater acoustics near the ocean surface. This work reports on a series of laboratory and field experiments on the measurements on air entrainment by breaking waves.

The first part of this thesis addresses the measurement of high volumetric concentrations of air (0.3% to 100% void-fraction) found immediately beneath breaking waves. Instrumentation based on the change of electrical impedance of the bubbly mixture with change in void-fraction is developed. Laboratory measurements are conducted in a wave channel and in a large three-dimensional wave basin. Maps of the evolution of the void-fraction distribution in bubble plumes generated by various size breaking waves are presented. Moments of the void-fraction field are shown to scale with the initially enclosed air volume at breaking and the energy dissipated by breaking is found to be expanded in entraining bubbles against their buoyancy. The results reveal that the bubble plumes experience rapid transformations within the first wave period after the onset of breaking. In particular, the plumes loose 95% of the initially entrained air volume during the first wave period. Predictions of the low-frequency resonant oscillations of the bubble plumes from measurements of the void-fraction compare well with acoustic measurements. Measurements near the ocean surface show high void-fractions up to 24% immediately beneath breaking waves. These are several orders of magnitude greater than previously reported time-averaged measurements.

The second part addresses the measurement of very low void-fractions. instrumentation based on the propagation velocity of low-frequency acoustic pulses is developed. Simultaneous measurements of the sound-speed (and thus the void-fraction) at several depths are conducted during two field experiments. Time-series of sound-speed and attenuation show dramatic fluctuations over time periods on the order of minutes or less. These are attributed to the formation of bubble plumes or passage of bubble clouds. Frequent occurrences of sound-speed anomalies greater than 100m/s and attenuation greater than 30dB/m are observed for moderate wind conditions (8m/s). The signals at various depths are highly correlated and mostly coherent at frequencies below 0.05Hz. The time-averaged (20min) sound-speed profile is found to be significantly more pronounced and shallower than previously reported. Simultaneous measurements at several acoustic frequencies show that the sound-speed is non-dispersive below 20kHz for moderate wind conditions. Bubble size distributions are inferred from the sound-speed and attenuation measurements.

Supported by: Funding was provided by The Office of Naval Research and the National Science Foundation through the Massachusetts Institute of Technology.

HYDRODYNAMICS AND MORPHODYNAMICS OF SHALLOW TIDAL CHANNELS AND INTERTIDAL FLATS

Carl Takeo Friedrichs

The Ultimate goal of this study is to relate the hydrodynamics of shallow tidal embayments to patterns of natural evolution and morphologic equilibrium. The specific problems addressed in this thesis are largely motivated by two mechanisms previously identified as major controls on net sediment transport in shallow tidal systems: temporal and spatial asymmetries in maximum bottom shear stress (τ). In the process of investigating these mechanisms, important aspects of basic mass and momentum balances in these systems are also revealed.

A new perturbation scheme is applied to nonlinear propagation in shallow embayments which identifies and quantifies the mechanisms ultimately responsible for temporal asymmetries in τ. This new scheme, which employs a perturbation in time (but not space) is simpler than previous methods, is consistent with available observations, and maintains the fundamental features of "exact" numerical solutions. This approach allows the major geometric properties controlling tidal asymmetry to be combined into a single non-dimensional parameter, γ. Solutions of overtides which determine asymmetry are compact and easily interpreted. For $\gamma > 0$, time varying depth plays a larger role in determining asymmetry than time-varying width, and the rising tide is of shorter duration. For $\gamma > 0$, time varying width plays a larger role, and the falling tide is of shorter duration.

Morphologic implications of the spatial distributions of τ are also investigated. Observations of cross-sectional area along many tidal channels are observed to be consistent with equilibrium models based on a uniform distribution of τ. The critical stress just capable of initiating sediment motion is found to provide a lower bound on τ, and the characteristic value of τ appropriate to individual systems is found to be a function of spring tidal range. Small along-channel

deviations away from uniform τ are associated with along-channel variation in the direction of maximum discharge. Uniform τ is then used to derive equilibrium hypsometries (the distribution of basin area as a function of elevation) for intertidal flats. Domination of τ by either tidal currents or wind waves is found to favor convex or concave hypsometries, respectively, a trend which is consistent with empirical observations. In addition to uniform τ, the effect of shoreline curvature on equilibrium hypsometry is also found to be important.

The investigation of mechanisms which control embayment evolution also reveals important aspects of basic hydrodynamics balances in shallow tidal embayments. A scaling relevant to prismatic channels having strong tidal asymmetries indicates friction often dominates acceleration in the momentum equation. The resulting balance between pressure gradient and friction gives a single time-varying diffusion equation for tidal elevation which only permits tidal amplitude to decay along channel. This result, which is consistent with observations and numerical solutions, diverges from classical co-oscillation. Classical co-oscillation with (weak) friction suggests amplitude should oscillate through nodes and anti-nodes due to the interaction of incident and reflected waves.

Uniform τ is used to justify a new scaling of the continuity equation for exponentially-shaped channels. In tidal channels having a nearly uniform distribution of τ (such as the Delaware, Thames and Tamar), along-channel gradients in velocity are small and discharge gradients in the continuity equation are dominated by gradients in cross-sectional area. With this scaling, the resulting governing equation is a first-order wave equation. The solution is a constant amplitude, forward propagating waveform which is independent of channel length – in contrast to the length sensitive resonance of classical co-oscillation. Amplitude can grow or decay if higher order effects are taken into account, but these effects are due to variations in the rate of channel convergence rather than interactions between incident and reflected waves.

Supported by: Funding was provided by The Office of Naval Research through the American Society of Engineering Education and the National Science Foundation under grant No. OCE91-02429.

LATE CRETACEOUS (MAESTRICHTIAN) CALCAREOUS NANNOPLANKTON BIOGEOGRAPHY WITH EMPHASIS ON EVENTS IMMEDIATELY PRECEDING THE CRETACEOUS/PALEOCENE BOUNDARY

Thomas Wolfgang Ehrendorfer

The Maestrichtian biogeography of calcareous nannoplankton is investigated in order to characterize paleoenvironmental conditions in the marine photic zone during the latest Cretaceous. Different theories explaining the biospheric turnover at the Cretaceous/Paleocene (K/P) boundary have alternatively suggested or denied substantial environmental perturbations during the last ~500 ky of the Cretaceous. The purpose of this study is to determine whether evidence from calcareous nannoplankton supports a gradual (or stepwise O decline of the photic zone environment presaging the K/P boundary.

In order to achieve this goal a detailed quantitative study of the biogeography of calcareous nannoplankton was carried out in three time slices from early and late Maestrichtian. Well preserved material was investigated from five sections: Ocean Drilling Program Site 690 in the Atlantic sector of the Southern Ocean represents the Maestrichian high southern nannoplankton province. Indian Ocean Sites 217 and 761, South Atlantic Site 528 and the land based, epicontinental section from Millers Ferry, Alabama, represent the Maestrichtian mid-/low latitudinal bioprovince. Quantitative counts were performed on settling slides under the light microscope. Occasionally scanning electron microscopy was employed to resolve taxonomic uncertainties.

A pronounced turnover from early to late Maestrichtian occurred in the nannoplankton in high southern latitudes. Numerous taxa (Biscutum boletum, B. coronum, B. dissimilis, B. magnum, Misceomarginatus spp., Monomarginatus spp., Neocrepidolithus watkinsii, Nephrolithus corystus, Octocyclus magnus, Phanulithus obscurus, Psyktosphaera firthii, and Reinhardtites spp.) that are restricted to (or most abundant in) high southern latitudes became extinct in the latest early and earliest late Maestrichtian (between ~72.4 and 70.4 Ma), resulting in a loss of about one third of the early Maestrichtian nannoplankton (corresponding to ~20-25% of the assemblage). It is argued that the extinctions are not a consequence of temperature changes alone. Instead they may be a consequence of increased surface water fertility (and only secondarily due to a temperature decrease).

In addition to the extinctions, about another

third of all taxa present (Biscutum constans, B. notaculum, Biscutum sp. 1, Chiastozygus garrisonii, C. amphipons, Discorhabdus ignotus, Rhombolithion rhombicum, Scapholithus fossilis, Staurolithites laffittei, Watznaueria barnesae, Zygodiscus, compactus, and Z. diplogrammus) disappeared from high southern latitudes during the same time interval (~72.4 and 70.4 Ma) but persisted until the end of the Maestrichtian in lower latitudes. These geographic restrictions are interpreted as a consequence of global cooling. No comparable changes were recorded in mid- and low latitudes in the early Maestrichtian, but this may represent an artifact of sampling.

While previous speculations on the paleoenvionmental preferences of some nannofossil taxa have been confirmed, several commonly accepted interpretations of the biogeographic significance of other taxa are contradicted. Micula staurophora seems to be a warm water indicator and abundance peaks of this species cannot be attributed exclusively to diagenetic effects. The biogeographic evolution of the high latitude taxon Ahmuellerella octoradiata does not correlate with temperature trends suggested from stable isotope studies implying that this taxon is not a cold water indicator. Abundance changes of other high latitude tasa (e.g. Nephrolitus frequens, Cribrosphaerella daniae, Kamptnerius magnificus, and Gartnerago spp.) correlate roughly with temperature changes, but seem to respond only beyond a certain threshold.

No gradual or stepwise extinctions were observed during the last 500 ky of the Maestrichtian. Environmental perturbations as indicated by stable isotope studies (e.g. warming pulse, circulation changes) led to abundance fluctuations of a few taxa, but did not result in any extinctions. This supports previous observations that the extinctions of the calcareous nannoplankton at the K/P boundary were not presaged during the Maestrichtian.

Supported by: Funding was provided by the Education Program and the Ocean Ventures Fund of the Woods Hole Oceanogrpahic Institution with additional grants-in-aid from the American Association of Petroleum Geologists, Paleontological Society/Margaret C. Wray Trust and the Sigma Xi Society.

THE BEHAVIORAL PHYSIOLOGY OF LABROID FISHES

Mary Carla Curran

The family Labridae, or wrasses, is one of the most specious fish families and is exceptional in its wide range of morphological and behavioral diversities. The cunner *Tautogolabrus adspersus* is one of two temperate-dwelling Western North Atlantic representatives of this family, and they are one of the few fishes that remain in New England waters throughout the year. In the winter, the cunner enters a state of "torpor" which has previously been described based solely on behavioral observations. The present study showed that cunner undergo physiological torpor, or hibernation, based on low oxygen consumption rates in winter, contributing to a large Q_{10} value of 8.5. It is thus established as one of the few marine species that is known to hibernate.

Cunner withstood four months of starvation at 4°C. Glycogen, lipid, and protein in the liver decreased during this period, as did the liver/body ratio, but these components did not decrease significantly in the whole-body samples. Since liver components were not exhausted, and body components were not significantly affected, cunner can withstand long periods without eating. Regression analysis predicts that they can live at least 6 months given the rate of decrease of glycogen and lipid reserves, and 9 months based on their protein reserves.

Oxygen consumption rates were monitored continuously over several days to determine diel variations in metabolic rate. The values obtained at night were significantly lower than the daytime values. Cunner did not maintain a diel cycle throughout the year; the length of this cycle varied from approximately 24 hours during warm temperatures to approximately 48 hours at temperatures generally below 8°C. Metabolic rates were more variable at warmer temperatures, which is in agreement with the expected increase in spontaneous activity.

Two tropical labroids, the wrasse *Thalassoma bifasciatum* and the parrotfish *Scarus iserti*, also had significantly higher oxygen consumption rates during the day than at night. Both hibernation and sleep are thought to be energy conserving mechanisms in fishes. The ability of labrids to sleep may have predisposed them to becoming established in temperate waters by surviving cold temperatures through hibernation.

Supported by: Funding was provided by the Ocean Ventures Fund, the Mobile Co. through the Coastal Research Center of Woods Hole Oceanographic Institution and the NOAA National Sea Grant College Program Office, Dept., of Commerce, under Grant No. NA86-AA-D-SG090, Sea Grant Project Nos. R/A-26-PD and R/B-106-PD.

CHLOROPHYLL DIAGENESIS IN THE WATER COLUMN AND SEDIMENTS OF THE BLACK SEA

Linda L. King

This thesis examines the degradation pathways of chlorophyll in the Black Sea water column and sediments. Measurements are made of total chlorophyll in sediment traps from two locations and depths in the water column, and at two locations in surface sediments. Individual chlorophyll degradation products are also identified. This data is used to construct a mass balance of chlorophyll production and sedimentation showing the major pathways for chlorophyll loss and the ultimate sedimentary sinks. The distribution of chlorophyll degradation products is also analyzed down core and related to environmental changes in the Black Sea.

Several new sinks for chlorophyll degradation products are identified. Steryl esters of pyropheophorbide-*a* are identified in sediment trap and sediment samples. It is thought that these compounds are formed during grazing. In sediment traps it is found that the distribution of the sterols esterified to pyropheophorbide-*a* change with season and that the sterols esterified are related to the distribution of sterols synthesized by the phytoplankton living in the photic zone at the time of production. Analysis of pyropheophorbide-*a* steryl esters in sediments shows the distribution of sterols to be quantitatively and qualitatively more similar to the distribution of free sterols in sediment traps than in sediments. The esterification of the sterols to pyropheophorbide-*a* apparently prevents the preferential removal of 4-desmethylsterols relative to 4-methylsterols during degradation of the sterol esters.

Chlorophyll degradation products which are incorporated into high molecular weight material and material which is only accessible with strong acid are also identified. The chlorophyll degradation products incorporated into these structures represent only a few percent of the total structure. In the high molecular weight material, only phorbins derived from chlorophyll-a are identified, where as in the acid extractable material, porphyrins are also identified. In surface sediments, the acid extractable chlorophyll degradations products and the solvent extractable macromolecular chlorophyll degradation products each comprise approximately 30% of total sedimentary chlorophyll degradation products. The acid extractable chlorophyll degradation products are identified in sediment trap samples, and evidence is presented for the occurrence of the solvent extractable macromolecular chlorophyll degradation products in sediment trap samples.

Using data from sediment traps, sediments, and the literature, a mass balance of chlorophyll flux, degradation, and accumulation in the Black Sea is presented. In the photic zone, chlorophyll degradation products are either destroyed by photo-oxidation and grazing, or they are transported into the anoxic water column in large, rapidly sinking particles. Once the chlorophyll degradation products have reached the anoxic water column, they survive to be deposited in the underlying sediments. As a comparison, 25 times more total organic carbon reaches the anoxic water column than does total phorbin, but 75% of total organic carbon which reaches the anoxic water column is degraded, either in the anoxic water column or in the very surface sediments. Though a larger percentage of total organic carbon passes out of the photic zone, the phorbin macrocycle appears to be more stable under anoxic conditions than is total organic carbon. The chlorophyll which can be detected below the chemocline of the Black Sea in the form of chlorophyll degradation products will survive to be deposited in surface sediments. Once in sediments, chlorophyll degradation products are found in four different reservoirs: phorbin steryl esters, free phorbins, solvent extractable macromolecular chlorophyll degradation products, esters, free phorbins, solvent extractable macromolecular chlorophyll degradation products, and acid extractable chlorophyll degradation products. Evidence for the occurrence of porphyrins in surface Black Sea sediments is also presented.

The distribution of chlorophyll degradation products in Unit I Black Sea sediments varies greatly with sediment depth. The concentration of total phorbin generally increases with increasing burial depth, but the concentrations of the individual chlorophyll degradation products vary in a manner which is both dissimilar to total phorbin and to each other. No parent/daughter relationships for the chlorophyll degradation products are indicated by the data. The distribution of sterols esterified to pyropheophorbide-a changes with sediment depth with the largest qualitative changes occuring in strata where the total phorbin concentration shows the largest quantitative changes. It is suggested that the variations seen in the esterified sterols are related to changes in the phytoplankton community over time. From the presented data, it is also suggested that total phorbin concentration, normalized to total organic carbon, in Black Sea Unit I sediments is related to paleoprimary production.

Several conclusions are drawn from the work presented in this thesis. There is approximately 3 times more chlorophyll-derived phorbin in Black Sea sediments than can be accounted for when considering only individual pheopigments, and

therefore the sedimentary degradation of chlorophyll is much more complex than previously thought. In the anoxic sediments of the Black Sea, the total phorbin distribution can be accounted for with organically extractable high molecular weight degradation products, pyropheophorbide steryl esters, pheopigments, and acid extractable chlorophyll degradation products. The sterol distribution in the pyropheophorbide steryl esters may preserve the sterol distribution in surface waters as synthesized by the phytoplankton, and pyropheophorbide steryl esters are preserved in sediments over the long term.

Supported by: Funding was provided by the National Science Foundation and the Woods Hole Oceanographic Institution's Ocean Ventures Fund.

MARINE MICROBIAL PRODUCTION OF DIMETHYLSULFIDE FROM DISSOLVED DIMETHYLSULFONIOPROPIONATE

Kathleen M. Ledyard

Dimethylsulfide (DMS) plays a central role in the transfer of sulfur from the ocean to the atmosphere, and ultimately to land. The most abundant volatile organosulfur compound in seawater, DMS is believed to account for the bulk of the sea-to-air biogenic sulfur flux. DMS has also been implicated as the major precursor of submicron-sized sulfate aerosol over the ocean. This aerosol acts as an effective site for cloud droplet condensation, suggesting a possibly important role for DMS in marine cloud formation. In the ocean, the precursor of DMS is presumed to be the zwitterionic sulfonium compound dimethylsulfoniopropionate (DMSP), a common osmoticum in certain classes of marine algae. While some algae can cleave DMSP intracellularly to form DMS, correlation of DMS concentrations with indicators of algal productivity on a local scale is poor.

This thesis focuses on an alternative pathway of DMS formation: microbial cleavage of dissolved (extracellular) DMSP. In laboratory studies, bacteria able to cleave DMSP to form DMS were isolated from seawater by a DMSP enrichment technique, and the kinetics of DMSP uptake and DMS production were examined closely in pure cultures of a bacterial isolate from the Sargasso Sea. The isolate cloud grow with both DMSP and acrylic acid, one of the products of DMSP cleavage, as the sole source of carbon and energy, and the enzyme catalyzing DMSP cleavage appeared to be induced by both of these compounds. Kinetic parameters were estimated for DMSP uptake and cleavage by whole cells. Comparison of the 16S rRNA sequence of this isolate with that of known eubacteria showed that it was most closely related to *Erythrobacter longus*, an aerobic, bacteriochlorophyll-containing member of the α proteobacteria.

DMS production from dissolved DMSP, along with microbial DMSP and DMS removal, was investigated in seawater incubation experiments with the goal of establishing turnover times for DMSP and DMS. These were determined to be on the order of days in both coastal (Vineyard Sound) and oligotrophic (Sargasso Sea) seawater. Loss of DMSP from the dissolved phase always occurred more rapidly than production of DMS; on average, microbial removal processes turned DMSP over on timescales of less than a day. This suggests that processes which do not result in DMS production, such as demethylation, may be important sinks for DMSP. Kinetic parameters for DMSP uptake and DMS production varied, possibly as a function of season. However, more data are needed to assess the seasonal dependence of this process.

These results imply that microbial production of DMS from dissolved DMSP is likely to be a quantitatively significant mode of DMS formation in both coastal and oligotrophic marine environments. Timescales of DMS turnover with respect to this process are comparable to published estimates of DMS turnover times due to biological consumption, indicating that coupling between these two microbially-mediated processes may constitute an important control on oceanic DMS levels.

Supported by: Funding was provided by the NASA Graduate Student Researchers Program, NASA, the National Science Foundation and the Ocean Ventures Fund.

ANALYSIS OF TOXIC AND NON-TOXIC *ALEXANDRIUM* (DINOPHYCEAE) SPECIES USING RIBOSOMAL RNA GENE SEQUENCES

Christopher Alan Scholin

Sequences of small subunit (Ss) and large subunit (Ls) ribosomal RNA genes (rDNA) from the marine dinoflagellates Alexandrium tamarense, A. catenella, A. fundyense, A. affine, A. minutum, A. lusitanicum and A. andersoni were compared to assess the organisms' relationships. Cultures represent isolates from North America, Western Europe, Thailand, Japan, Australia and the ballast water of several cargo vessels, and include both toxic and non-toxic strains. An emphasis was placed on the A. tamarense/catenella/fundyense "species complex," a group of morphotypically-similar organisms found in many regions of the world.

Two distinct SsrRNA genes, termed the "A gene" and the "B gene," were found in a toxic A. fundyense isolated from eastern North America. The B gene is considered to be a pseudogene. A restriction fragment length polymorphism (RFLP) assay developed to detect the A and B genes revealed five distinct groups of Alexandrium isolates. Three subdivide the A. tamarense/catenella/fundyense complex, but do not correlate with morphospecies designations. The two remaining groups are associated with cultures that clearly differ morphologically from the A. tamarense/catenella/fundyense group: the fourth group consists of A. affine isolates, and the fifth group is represented by A. minutum, A. lusitanicum and A. andersoni. The B gene was only found in A. tamarense/catenella/fundyense, but not in all members of this species complex. The B gene is not uniformly distributed among global populations of Alexandrium. All A. tamarense/catenella/fundyense isolates from North America harbor this gene, but it has also been found in some A. tamarense from scattered locations in Japan, as well as in A. tamarense from the ballast water of one cargo vessel which was on a defined run from Japan to Australia. The B gene may be endemic to North American populations of A. tamarense/catenella/fundyense. It is possible that in the recent past North American A. tamarense were introduced to Japanese waters, and cysts of these organisms have been transported from Japan to Australia.

A subset of isolates examined using the RFLP assay were also compared by cloning and sequencing a fragment of their LsrDNA. Eight major classes of LsrDNA sequences, termed "ribotypes," were identified. Five ribotypes subdivide members of the A. tamarense/catenella/fundyense complex; all isolates containing the B gene cluster as one ribotype. The three remaining ribotypes are typified by: 1)A. affine; 2)A. minutum and A. lusitanicum; and 3)A. andersoni. LsrDNAs from A. minutum and A. lusitanicum are indistinguishable. A. minutum/lusitanicum/andersoni may represent another Alexandrium species comples, analogous to the A. tamarense/catenella/fundyense group. An organisms' ability to produce toxin appears to be correlated with its LsrDNA phylogenetic lineage. Ribotypes ascribed by the LsrDNA sequences are in complete agreement with, and offer a finer-scale resolution of, groups defined by SsrDNA restriction patterns. The SsrDNA RFLP groups and LsrDNA ribotypes are useful species-and population-specific markers.

Alexandrium tamarense/catenella/fundyense exist as genetically-distinct "strains" (populations), not three genetically-distinct species: representatives collected from the same geographic region appear the most similar, regardless of morphotype, whereas those from geographically-separated populations are more divergent even when the same morphospecies are compared. Contrary to this general patter, A. tamarense/catenella from Japan were found to be exceptionally heterogeneous. Ballast water samples show that viable cysts (resting spores) or toxigenic A. tamarense/catenella are being discharged into Australian ports from multiple, genetically-distinct source populations.

The rDNA sequences were also used to test theories accounting for the evolution and global dispersal of A. tamarense/catenella/fundyense. Results suggest a monophyletic radiation of these organisms from a common ancestor that included, or gave rise to, multiple morphotypes. Populations appear to have diverged as a result of vicariance (geographic isolation). The co-occurrence of genetically-distinct strains of these organisms is an indication of dispersal. An example of this is seen in Japan where an introduction of North American A. tamarense appears likely. Determining the timing of dispersal events is problematic if based strictly on rDNA sequence similarities, since these molecules undergo change on a scale of millions of years.

Supported by: Funding was provided by the Ocean Ventures Fund and the National Science Foundation through Grant No. OCE89-11226.

VORTEX-INDUCED FORCES ON OSCILLATING BLUFF CYLINDERS

Ramnarayan Gopalkrishnan

Vortex-induced forces and consequent vibration of long cylindrical structures are important for a large number of engineering applications, while the complexity of the underlying physical mechanisms is such that this is one of the canonical problems of fluid mechanics. In the case of a marine tubular exposed to a shear flow, the situation is particularly difficult since the vortex shedding force varies in frequency and magnitude along the length of the structure, causing the response at any point to be amplitude-modulated in space and time.

In this thesis, the focus is on the measurement, via forced-oscillation experiments, of the vortex-induced lift and drag forces acting on circular cylinders undergoing sinusoidal and amplitude-modulated oscillations. Basic concepts on vortex formation and vortex-induced vibrations, a review of the existing literature, and details of the experimental apparatus and data processing methods are all introduced early in the thesis. A comprehensive program of stationary and sinusoidal oscillation tests is presented. Several

novel properties are described, among them the role of the lift force phase angle in causing the amplitude-limited nature of VIV, and use of the lift force "excitation region" in contrast with the often-quoted but quite different lift force "lock-in region". Next, a comprehensive data error analysis, and a simple VIV prediction scheme are described. New data on amplitude-modulated oscillations are presented, with an analysis of behavior of the fluid forces in response to beating excitation. Finally, the concept of control of the mean wake velocity profile via the control of the major vortical features is explored, with the possible applications being the reduction of the in-line wake velocity and the alteration of the wake signature. The thesis concludes with the principal findings of this research as well as suggestions for future work.

Supported by: Funding was provided by the National Science Foundation, the Office of Naval Technology, the Sea Grant Program and the office of Naval Research.

COSMOGENIC ^{32}P AND ^{33}P IN THE ATMOSPHERE AND OLIGOTROPHIC OCEAN AND APPLICATIONS TO THE STUDY OF PHOSPHORUS CYCLING

Nathalie Waser

Cosmic-ray produced ^{32}P ($t_{1/2}$=14.28 days) and ^{33}P ($t_{1/2}$=25.3 days) are powerful tracers of upper ocean P cycling, when coupled with time-series estimates of the atmospheric sources. The cycle of cosmogenic ^{32}P and ^{33}P in the atmosphere and euphotic zone of the ocean was investigated in the Sargasso Sea. A method was developed for the determination of the low-level beta activities of both nuclides in rainwater and marine particulate matter. The fallout rates of ^{32}P and ^{33}P by precipitation were determined over a period of 12 months at a marine site, at Bermuda, coinciding with measurements of the activities and activity ratio $^{33}P/^{32}P$ in suspended particulate matter and plankton tows at the Bermuda Atlantic Time-series Study (BATS) station (31°50′N, 64°10′W). The *in situ* production rates of ^{32}P and ^{33}P in the upper ocean were estimated by measuring the activities of ^{32}P and ^{33}P produced in Cl, K and S targets exposed to cosmic rays at Woods Hole, on Mount Washington, and on l'Aiguille du Midi. Fallout by precipitation was found to be the major source of radiophosphorus to the ocean; *in situ* production in the upper ocean was found to account for 5% for ^{32}P and 1% for ^{33}P of the wet deposition rates. Knowledge of all the sources of radiophosphorus to the Sargasso Sea allowed the cycling of ^{32}P and ^{33}P in suspended particulate matter and macrozooplankton to be studied. The study was based on a new approach consisting of the determination of the activity ration $^{33}P/^{32}P$ in the different pools of phosphorus. The activity ratios $^{33}P/^{32}P$ in suspended particulate matter and plankton tows ranged from 1.0 to 5.0 and were either equal to or higher than the activity ratio in rainwater. The monthly activity ratio in rain was remarkably constant and on average 0.96. The increase in the ratio in plankton relative to rain can be interpreted as aging of the phosphorus in that pool or in the pool from which it is derived. This is because of differential radioactive decay rates of ^{32}P and ^{33}P. The activity ratio was higher in particle collections dominated by higher levels in the ocean food web. The residence time of P in macrozooplankton was estimated to range from 40 to 60 days. A grazing rate of macrozooplankton of 0.024 day $^{-1}$ was determined, allowing the determination of a grazing flux of 110 mg C/m^2/d and a flux of particulate carbon due to defecation of zooplankton of 30 mg C/m^2/d.

Supported by: Funding was provided by the National Science Foundation under Grant Nos. OCE-9022284, OCE-8817836 and the Department of Energy Grant DE-FG02-88ER60681, the Ocean Ventures Fund of the Woods Hole Oceanographic Institution and Scurlock Funds of Mr. Arch Scurlock to the Massachusetts Institute of Technology and Woods Hole Oceanographic Institution Joint Program.

ACOUSTIC TOMOGRAPHY IN THE STRAITS OF FLORIDA

David Brian Chester

Variability of the Florida Current has been monitored via acoustic tomography. A reciprocal tomography experiment was conducted in the eastern half of the Florida Straits during mid October and November, 1983. A triangular array of transceivers, with leg separations of approximately 45 kilometers, was deployed at 27°N. The presence of a surface mixed layer in the region allowed for the ducted propagation of acoustic energy in the surface layer. A deeper layer was sampled by an unresolved group of refracted, bottom reflected ray arrivals. Incorporating the complete set of arrivals, we are able to obtain depth dependent estimates of the temperature field, current velocity, and relative vorticity. The oceanography of the region has been shown to be dominated by the lateral shifting of the surface and subsurface core of the Florida Current. The influx of westward flowing water through the Northwest Providence Channel at 26°N also appears as a large scale signal in the eastern Florida Straits. Low frequency fluctuations of

temperature, current velocity, and vorticity occur at periods ranging from several days to nearly two weeks, and are intimately related to meandering of the Florida Current System.

Supported by: Funding was provided by the Massachusetts Institute of Technology.

STRUCTURAL CHARACTERIZATION AND BACTERIAL DEGRADATION OF MARINE CARBOHYDRATES

Carol Arnosti

The goal of this thesis was to develop and apply an integrated chemical and microbial approach to study the effects of chemical structure on the rates and patterns of carbohydrate degradation by anaerobic marine bacteria.

Polysaccharides produced by five species of marine plankton, *Dunaliella tertiolecta, Emiliania huxleyi, Stephanopixis palmeri,* a *Phaeocystis* sp., and *Synechococcus* WH7335, were surveyed using one- and two-dimensional nuclear magnetic resonance spectroscopy (NMR). Two carbohydrates from *Synechococcus* Wh7335 were characterized in detail. *Synechoccus* produced an $\alpha(1,4)$ glucose polysaccharide with $\alpha(1,6)$ branches, which probably functions as an energy reserve. The nominal molecular weight of the polysaccharide was ~5000 daltons. Large quantities of a glycerol-polysaccharide, which was tentatively identified as a teichoic acid similar in structure to teichoic acids found in cell walls of gram-positive bacteria, were also produced by *Synechococcus* WH7335. This is the first report of teichoic acids in cyanobacteria.

Enrichment of bacteria from anoxic marine sediments on specific carbohydrates yielded reproducible model systems with which to study the degradation of chemically well-defined substrates. Headspace gases (Co_2, H_2, CH_4, H_2S) were monitored by gas chromatography, and carbohydrate substrates and intermediates were separated and quantified via gel-permeation chromatography and high-pressure liquid chromatography. The transfer of carbon from substrates through to end products was followed quantitatively. Nuclear magnetic resonance spectroscopy was used to check for selective structural alterations (such as preferential cleavage of specific linkage types or positions) of the substrates.

A series of enrichment experiments showed that mixed cultures of marine bacteria distinguish even between small, very closely-related substrates which do not require extracellular hydrolysis prior to uptake. A galactose-$\beta(1,3)$-arabinose dimer was degraded at half the rate of seven other similar disaccharides and three larger oligosaccharides. A further series of degradation experiments with polysaccharides (pullulan, laminarin) showed that they are degraded by bacteria at virtually the same rate as structurally related substrates in the molecular weight range of 300-600 daltons. Degradation of the branched glucan and the teichoic acid-type polysaccharide from *Synechococcus* WH7335 was also very rapid.

The time-course of bacterial hydrolysis of pullulan was examined with gel permeation chromatography and NMR to provide the first molecular-level evidence in marine systems of the bacterial extracellular transformation of high molecular weight organic matter to lower molecular weight organic matter. NMR spectra provided evidence that the pullulan was hydrolyzed by pullulanase, an endo-acting extracellular enzyme which preferentially hydrolyzes $\alpha(1,6)$ linkages. This is the first experimental evidence of pullulanase activity among marine mesophilic bacteria.

The culture results suggest that enzymatic hydrolysis of macromolecular carbohydrates to transportable pieces is not the slow step in bacterial degradation of at least some types of polysaccharides. The results from the oligosaccharide experiments suggest that certain heteropolysaccharides may not be degraded as quickly. Chemical structure can be more important than molecular weight in determining degradation rates of carbohydrates. Varying rates of organic polymer degradation in anoxic sediments may be largely determined by the sensitivity of bacterial enzymatic and transport systems to structural features.

Supported by: Funding was provided by the Ocean Ventures Fund, the Woods Hole Oceanographic Institution, the Department of Energy (DE-FG0292ER61428).

ANALYSIS OF MODAL EVOLUTION CAUSED BY A WEAKLY RANGE-DEPENDENT SEABED IN SHALLOW WATER AND ITS APPLICATION TO INVERSION FOR GEOACOUSTIC PROPERTIES

Kazuhiko Ohta

In a shallow water ocean environment, the range-dependent variation of the geoacoustic properties of the seabed is one of the crucial factors affecting sound propagation. Since the local modes of propagation depend on the spatial changes in the bottom sediments, the local eigenvalues of these modes are useful as tools for examining the range dependence of the sediment properties. In order to extract the local eigenvalues from measurements of the pressure field in a

laterally inhomogeneous waveguide, the zero-order asymptotic Hankel transform with a short sliding window is utilized. The local peak positions in the output spectra differ from the local eigenvalues due to both the range variation of the local modes and the interference of adjacent modes. The departure due to the former factor is evaluated analytically by using the stationary phase method. In order to reduce the error induced by the latter factor, mode filtering is utilized by incorporating data from a fixed vertical array of receivers.

The use of the above zero-order Hankel transform in a three-dimensionally varying waveguide results in an underestimate of the local eigenvalues due to the effect of horizontal refraction. Thus a general asymptotic Hankel transform with a 2-D sliding window is used to correct for the underestimated amount. By expanding the latter transform with respect to the azimuthal angle, it can also be shown that the first term in the Taylor series corresponds to the former transform; the rest of the terms account for the value difference between the underestimated and actual local eigenvalues.

In order to obtain the spatial variation of the sediment properties from the range-dependent variation of the extracted local eigenvalues, the analytical relationship between these two variations is derived by using a perturbation method in a horizontally varying, multi-layered bottom model. Upon use of the n^2-linear profile in each layer, the relationship can be obtained in closed form. As a result, the range variation of the local eigenvalues may be separated into terms that depend on each geoacoustic parameter. Based on this relation, an inversion method for determining the range-dependent geoacoustic parameters is developed.

The methods developed in this thesis are applied to simulated pressure field data as well as experimental field data. It is shown that the evolution with range of the local modes as well as the range-dependent geoacoustic properties can be successfully estimated.

Supported by: Funding was provided by the Japan Defense Agency and the Woods Hole Oceanographic Institution.

DESIGN OF A CONTROLLABLE PITCH UNDERWATER THRUSTER SYSTEM

Robert W. Keefe

Control systems for underwater vehicles have reached the level of sophistication where they are limited by the dynamic performance of the thrust actuators. Standard fixed-pitch propellers have been shown to have very poor dynamic characteristics, particularly at low thrust levels. The dynamic response of a fixed-pitch propeller is dependent upon highly non-linear transients encountered while the shaft speed approaches its steady-state value. This thesis proposes the use of a controllable pitch propeller system to address this problem. A controllable pitch propeller varies the amount of thrust produced by varying the pitch angle of the blades at a constant shaft speed. The bandwidth of this type of thrust actuator would be dependent primarily on the speed at which the pitch angle of the blades are changed. A variable pitch propeller system suitable for retrofit into an ROV is designed and built. The system is designed for maximal pitch angle bandwidth with low actuator power consumption.

Supported by: Funding was provided by the United States Navy.

AMBIENT NOISE AND SURFACE WAVE DISSIPATION IN THE OCEAN

Francis C. Felizardo

There is a growing consensus that the sound generated by breaking waves is responsible for much of the ambient noise level in the ocean. While numerous field measurements have shown a strong correlation between the ambient noise spectrum level (N) in the range 100 Hz to 25 kHz and wind speed in the ocean, very little have been done to establish a comparable correlation between the ambient noise spectrum level and surface wave field parameters. The difficulty in establishing this relationship is remarkable given that the frequency and intensity of wave breaking are dependent on the characteristics of the wave field.

In Fall 1991, an experiment was conducted from the research platform Flip 130 kilometers off the coast of Oregon, where the ambient noise between 2.5 and 25 kHz, the wind speed, and the sea surface elevation using wire wave gauges were measured.

The correlation between N and the root mean square wave amplitude a was found to be poor but could be improved if the swell was filtered out from the wave elevation time series. The influence of swell on the value of A was disproportionate to the level of ambient noise since its characteristics were not directly due to the local wind-wave conditions. Observations of the dependence of the high frequency wind waves and the directional wave spectrum under turning winds suggested that the high frequency wave components responded more quickly to changes in the wind speed and wind direction than the energy-containing frequencies.

The ambient noise level also correlated well with the root mean square wave slopes s. This is consistent with previous laboratory measurements which showed that the steepness of a packet of

waves correlates with the strength of wave breaking and with characteristics of breaking waves such as loss of momentum flux, dissipation, initial volume of air entrained, mixing, and sound generation.

Comparisons of surface wave dissipation estimates using field measurements and models developed by Phillips (1985) and Hasselmann (1974) show that although the two models have very different forms, they give values that are comparable in magnitude. The relationship between the ambient noise level and log of dissipation give correlation coefficients (0.93-0.95) that are comparable to those between ambient noise and wind speed. The mean square acoustic pressure was shown to vary with the dissipation, with $p^2 \propto D^{0.6-0.8}$. The results suggest that measurements of ambient sound may prove to be useful in inferring surface wave dissipation.

Supported by: Funding was provided by the Massachusetts Institute of Technology.

THE IMPORTANCE OF FINE-SCALE FLOW PROCESSES AND FOOD AVAILABILITY IN THE MAINTENANCE OF SOFT-SEDIMENT COMMUNITIES

Paul V.R. Snelgrove

Although the association between soft-sediment invertebrates and a specific sediment type has been documented for many habitats, most studies have been correlative and have failed to convincingly demonstrate any single mechanism to explain this association. Sediment type has generally been characterized by grain size, however, many other potential causal factors correlate with grain size, including organic content, microbial content, stability, food supply, and larval supply. One hypothesis for animal-sediment associations is that settling larvae are transported as passive particles and are sorted into different sedimentary habitats much like sediment grains.

To test the hypothesis that near-bed hydrodynamics may modify larval settlement, field and flume experiments were conducted where larval settlement was compared between microdepositional environments (small depressions) and non-trapping environments (flush treatments). Depressions have been observed to trap passive particles, and these experiments were therefore designed to test whether settling larvae would be trapped in depressions like passive particles. Flume flow simulations were carried out with the polychaete *Capitella* sp. I and the bivalve *Mulinia lateralis*. Experiments with flush and depression sediment treatments were conducted in the absence of the potentially confounding effects of suspended sediment and organic matter and therefore offered a highly controlled, explicit test of passive hydrodynamic deposition of larvae in depressions. Although larvae of both species were generally able to actively select a high-organic sediment over a low-organic alternative with a comparable grain size, elevated densities of both species were observed in depressions for a given sediment treatment. Thus, both species appeared to be vulnerable to hydrodynamic trapping. *M. lateralis* larvae, however, often made a "poor choice" by settling in high numbers in depressions containing the low-organic sediment while *Capitella* sp. I larvae were generally able to "escape" from depressions if the sediment was unsuitable. In field experiments carried out at Station R in Buzzards Bay, Massachusetts, significantly higher densities of *Mediomastus ambiseta* juveniles, spionid polychaeta juveniles, bivalves, gastropod larvae, and nemerteans were observed in depressions compared with flush treatments over 5 relatively short experimental periods (3 or 4 days each) during the summer of 1990. Of the abundant taxa, only *Capitella* spp. was not significantly more abundant in depressions compared with flush treatments, although numbers tended to be higher in depressions. Experiments were conducted over a short time period to minimize potential biological interactions between taxa and reduce the likelihood that organic material accumulate in depressions and provide a cue for settling larvae. Thus, higher numbers in depressions suggest that larvae were passively entrained. These flume and field experiments suggest that near-bed hydrodynamics may modify settlement at some scales, and that both active and passive processes may operate in determining larval distributions in shallow-water, muddy habitats.

In deep-sea ecosystems, the role of near-bed hydrodynamics is also of interest because of the potential role that larval settlement in organic patches may play in maintaining the immense species diversity characteristics of many deep-sea ecosystems. To try to understand the role of organic patches in deep-sea communities, several investigators have used colonization trays containing sediments that have been treated in different ways. These experiments have been criticized in the past because the sediment surface in the trays was elevated above the bottom and may therefore have interfered with natural boundary layer flow. Flume simulations of flow over these circulation trays revealed serious flow artifacts generated by the trays, and that flow across the sediment surface of the trays was characterized by turbulent eddies, accelerated velocities and boundary layer thickening. These sorts of flow characteristics would not be expected over natural sediments, and an alternative colonization tray was designed to eliminate these artifacts.

To test the hypothesis that different types of food patches would result in different types of larval response, and determine how near-bed hydrodynamics may influence larval settlement, flush colonization trays filled with prefrozen sediment were deployed in tandem with artificial depressions south of St. Croix, U.S.V.I. at 900 m depth. Colonization trays and artificial depressions were either unenriched or enriched with *Thalassiosira* sp. and *Sargassum* sp. two types of algae chosen to mimic natural food patches on the sea floor. Unexpectedly high densities of organisms colonized trays after only 23 days. The *Thalassiosira* trays were colonized by high densities of a relatively low diversity, opportunistic fauna, *Sargassum* trays were colonized by lower densities of a higher diversity fauna, and unenriched trays were colonized by very low numbers of a very diverse fauna. All tray faunas were markedly different in composition from the natural, ambient fauna. These findings suggest that different patch types did, indeed, result in a specialized faunal response to each of the "patch" types. Depressions on the sea floor provide a natural mechanism for food patch formation because passive particles such as detritus and algae tend to be entrained in the depressions. To determine whether dominant colonizers would be entrained in depressions like passive particles or could differentiate between depression "patch" types in a flow environment that might be expected to make active selection more difficult, artificial depressions were unenriched or enriched with *Sargassum* sp. or *Thalassiosira* sp. Total densities of organisms and densities of the most abundant species were substantially lower in artificial depressions than in trays. Densities in *Thalassiosira* depressions were lower than in *Sargassum* depressions and densities in unenriched depressions were extremely low, suggesting that dominant colonizers were not passively entrained in depressions and that colonization was specialized and highly active for these taxa. A different fauna was also observed in natural depressions compared with flush sediments, suggesting that natural depressions do contribute to species coexistence. Long-term tray deployments designed to test whether different faunas would be present in "patches" of different ages indicated that time may also play an important part in a deep-sea patch mosaic.

Supported by: Funding was provided by the National Science Foundation OCE-88-12651, NOAA:NA88AA-H-URO20, ONR:N00014-89-J-1637.

EXCHANGES BETWEEN HEMISPHERES AND GYRES: A DIRECT APPROACH TO THE MEAN CIRCULATION OF THE EQUATORIAL PACIFIC

Susan Elizabeth Wijffels

An extensive set of new high-quality hydrographic data is assembled in order to determine the mean circulation in the equatorial Pacific, and thus the pathways for cross-equatorial and cross-gyre exchange. Making up the core of the data set are two onetime transpacific zonal sections nominally at 10°N and 14°S. Supplementing these are repeat surveys of the equatorial currents along the 165°E meridian with direct shear measurements, and repeat surveys of the western boundary current at 8°N including direct velocity measurements. The repeat survey data are crucial for obtaining a good estimate of the mean conditions in the face of strong annual and interannual variability of the near-equatorial flow field. A comparison with historical XBT and hydrographic data shows that the interior thermocline transports in the one-time sections are fortuitously representative of the mean conditions.

A detailed study of the water mass distribution along the sections is the basis for choosing reference levels for the thermal wind shear in an initial guess circulation field. Using an inverse model, the initial guess circulation is adjusted such that volume, heat and salt are conserved in a set of subthermocline layers (σ_Θ >26.7). Cross-isopycnal diffusion and advection are explicitly accounted for in the inverse model, and the diapycnal diffusivity is constrained to be positive, though its value is allowed to vary with depth and location. Net mass conservation constraints are applied to the enclosed volumes of the North Pacific and eastern Pacific, and essentially require that the Ekman divergence be equal to the geostrophic convergence. The Ekman fluxes as estimated from wind-stress climatologies are an important element of the mass budget, and yet are subject to large uncertainties. The model is therefore given the freedom to determine the Ekman fluxes within the range of error of the wind-stresses.

The circulation of the coldest waters (Θ <1.2°C) is dominated by the northward flow of Lower Circumpolar Water (LCPW) in a system of narrow western boundary currents. A net transport of 12.1 Sv of LCPW flows across 14°S, 9.6 Sv of which flows into the North Pacific across 10°N. The bulk of the LCPW flux across the equator appears to occur in the denser part of the western boundary current which follows topography directly across the equator. Dissipation in the boundary layer can thus modify

the potential vorticity of the fluid and allow it to cross the equator.l The circulation of the upper part of the LCPW is dominated by a strong westward jet at the equator which is supplied both by upwelling from below and the recirculation of modified LCPW from the North Pacific.

At mid-depth ($4.0 > \Theta > 1.2°C$) high silica and low oxygen concentrations mark the North Pacific Deep Water (NPDW) which is present in both the North and South Pacific Oceans. Across both 10°N and 14°S, a net of 11 Sv of NPDW flows southward, returning the northward mass flux associated with the LCPW. In contrast to the LCPW, narrow western boundary currents are not present in this layer, and it is not clear how the deep water flows across the equator. Strong zonal jets on and about the equator may be important in allowing mass to cross the equator by increasing the time available for the cross-equatorial diffusion of potential vorticity to act on a fluid parcel.

At intermediate depths equatorward advection is suggested by the presence of intermediate water salinity minima formed in the subpolar latitudes: Antarctic Intermediate Water dominates the 4 to 8°C classes south of the equator, while North Pacific Intermediate Water occupies this range north of the equator. Determination of the mean circulation of the intermediate waters is, however, confounded by the large eddies that dominate the geostrophic transport stream function along the onetime zonal sections.

The equatorial thermocline is occupied by waters of subtropical origin: the shallow salinity minimum waters and saline Central Water from both the North and South Pacific Ocean. The equator marks the location of a front between northern and southern subtropical gyre waters, except in the lower thermocline where water from the South Pacific subtropical gyre penetrates to about 4°N to feed the Northern Subsurface Countercurrent at 165°E. All of the equatorward flowing thermocline waters are entrained in the eastward equatorial currents which in turn feed the upwelling system in the eastern Pacific. The upwelled waters largely supply the South Equatorial Current in the eastern Pacific, accounting for its large transport compared to that predicted by Sverdrup dynamics. Northward flow across the equator of the upwelled waters in the thermocline or surface layer in the western Pacific is necessary to supply the Ekman flux into the North Pacific.

The analysis indicates that the Pacific Ocean does not convert a large amount of abyssal water to thermocline water, as required by several theories of the global thermohaline circulation. In contrast to the Atlantic Ocean, the thermocline circulation in the Pacific appears decoupled from the abyssal overturning, with little upwelling of abyssal waters occurring in either the North Pacific or the equatorial Pacific. The leakage of Pacific water into the Indian Ocean is deduced to be essentially zero, though an error analysis allows a range of 0-8 x $10^6 m^3 s^{-1}$.

Supported by: Funding was provided by NASA Global Change Fellowship.

ACOUSTIC TRAVEL TIME PERTURBATIONS DUE TO AN INTERNAL TIDE AND INTERNAL WAVE FIELD IN THE BARENTS SEA

Douglas Scott Ray

Travel time perturbations of adiabatic normal modes due to an internal tide and internal mode field in the Barents Sea are examined. A formalism for the travel time perturbation due to a change in sound speed is presented. Internal tide and internal wave amplitude spectra are calculated from Brancker temperature loggers which were deployed on moorings in the Barents Sea during the August 1992 Barents Sea Polar Front Experiment. In particular, the first three internal wave mode amplitudes are estimated from the four Brancker temperature loggers on the southwest mooring of the array. Modal perturbations in acoustic pulse travel time and the travel time covariance are calculated and compared for consistency to a simple ray model. These perturbations are small for the modal arrivals that the vertical acoustic array which was deployed is expected to resolve. The third internal wave mode has the largest impact on the acoustic arrivals, per unit amplitude, but the first internal wave mode dominates the scattering due to having a much larger amplitude overall.

Supported by: Funding was provided by the United States Navy.

ORIENTATION DEPENDENCE OF THE ACOUSTIC BACKSCATTER FOR ELONGATED ZOOPLANKTON

Matthew Lloyd Johnson

The width of the main lobe of the acoustic backscatter directivity pattern of decapod shrimp (*Palaemonetes vulgaris*) is examined versus acoustic frequency. Using the distorted wave Born approximation (DWBA) and the geometry of a prolate spheroid, and analytic formula for the backscatter cross section as a function of orientation angle is derived. A directivity pattern is determined from the analytic formula and the width of the main lobe (beamwidth) is computed. The relationship between beamwidth and acoustic

frequency is presented in plots of beamwidth versus ka and L/λ. The model is adapted to experimental limitations of animal motion, discrete sampling and observed side lobe levels. The backscatter directivity patterns of live decapod shrimp, determined experimentally at frequencies between 72 and 525 kHz, are presented. A non-monotonic relationship between beamwidth and frequency is illustrated in this study. This relationship is in contrast to the monotonic relationship exhibited when sound scatters off of an impenetrable flat plate. Reasonable agreement is found between the theoretically predicted beamwidths and most experimental data, where the beamwidth was more-or-less oscillatory about a mean value of 19°. The structure can at least be partly explained by scattering theory.

Supported by: Funding was provided by the United States Navy.

FORWARD SCATTERING OF A PULSED CONTINUOUS WAVE SIGNAL THROUGH LAMINAR AND TURBULENT THERMAL PLUMES

Stephen Gerard Bowen

The results of an experiment examining the forward propagation of an acoustic signal through a buoyant plume are discussed. Two distinct testing sights were used. One made use of a small fresh water tank in NUWC to provide a controlled plume. The other used a larger salt water tank at WHOI to create a more realistic oceanic model. Using the Born and Rytov approximations, an estimation of the effects of the laminar plume on the propagated signal are shown. As the plume moves from laminar to turbulent, the scintillation index and the Fourier transform of the magnitude square response provide insight into the nature of the transition. Finally, from the turbulent response a model for the scattering function is developed.

Supported by: Funding was provided by the United States Navy.

DISPERSION OF FINE PARTICLES BY WAVE-INDUCED MASS TRANSPORT

Carole A. Womeldorf

We begin with the linearized irrotational theory describing the diffraction of an incoming plane wave by a vertical cylinder. From the free-surface motion, we describe the boundary-layer flow field U_{oi} near that cylinder. The flow field is then used to calculate the modified convective velocities U_i and symmetric dispersivities D_{ij}.

Through our calculations we have demonstrated convective flow reversal for both large and very small cylinders. In addition we have characterized four regions of waves and transport about the large cylinder relating to the different characteristics of each region: reflected region, scattered region, plane wave region, and sharp-edged shadow region. Our understanding of the transport velocities and dispersivities allows us to speculate qualitatively on the transport of fine particles near a round island in a diffracted wave field.

Supported by: Funding was provided by the National Science Fellow Creative Award.

TIME-DEPENDENT ASSIMILATION OF CTD DATA TO AN OPEN OCEAN ROSSBY WAVE MODEL

James Reginald Gunson

For two CTD surveys taken two months apart during the 1981 Ocean Tomography experiment southwest of Bermuda, a time-dependent ocean state is estimated that evolves from the first to the second survey. The mesoscale motions are modelled by quasi-geostrophic dynamics, and the ocean model state is represented by freely propagating Rossby waves in the 1st and 2nd baroclinic modes whose time-dependent amplitudes are fit to the data at the two survey times. First the linear dispersion relation is used to evolve the waves in time, then the weak nonlinear interactions between the waves are incorporated into the model. The wave-wave interactions enable the waves in the barotropic mode to enter into the model state evolution as an unknown control variable. Three techniques from optimal control theory are developed and applied to this problem: the Kalman filter/smoother, the adjoint method and dynamic programming. These methods allow the barotropic component of the flow, which is indeterminate from the CTD data, to be estimated.

Supported by: Funding was provided by the Massachusetts Institute of Technology.

PASSIVE LOCALIZATION OF UNDERWATER ACOUSTIC BEACONS

Dennis Michael Wojcik

This thesis examines the use of a single, omnidirectional hydrophone as a receiving sensor to passively localize an acoustic beacon. The

localization problem is presented as a constrained, nonlinear parameter estimation problem, and Lagrange multipliers are introduced to solve for the maximum likelihood estimate of the acoustic beacon's position. An iterative algorithm is developed using range difference measurements to solve for the maximum likelihood estimate of a stationary acoustic beacon's position. This algorithm is then extended to include linear, constant velocity motion of the acoustic beacon. Finally, design specifications for a receiver to implement the maximum likelihood estimation algorithms are developed.

To test the maximum likelihood estimate algorithms, Monte Carlo simulations are conducted. Results from six representative scenarios are presented. Test results show that as the number of range differences used increases, or the distance that the observer travels between received beacon signals increases, the accuracy of the estimated position improves. Also, test show that accuracy of the estimated beacon position is directly related to the accuracy in which the observer's position is measured. To test the receiver's design specifications, a prototype receiver is built using commonly available components. It is then shown that the prototype receiver meets or exceeds the design specifications.

Supported by: Funding was provided by the United States Navy.

THE DYNAMIC ROLE OF RIDGES IN A β-PLANE CHANNEL TOWARDS UNDERSTANDING THE DYNAMICS OF LARGE SCALE CIRCULATION IN THE SOUTHERN OCEAN

Liping Wang

In the thesis, the dynamic role of bottom topography in a β-plane channel is systematically studied in both linear homogeneous and stratified layer models in the presence of either wind stress (Chapters 2, 3, 4, and 6) or buoyancy forcing (Chapter 5). In these studies, the structure of the geostrophic contour plays a fundamental role, and the role of bottom topography is locked at from two different angles. It is shown that blocking all the geostrophic contours leads to two different physical processes in which bottom topographic form drag is generated (Chapters 2, 3, and 4) and enables geostrophic flow in a β-plane channel to support a net cross-channel volume transport (Chapters 5 and 6). It is demonstrated that by blocking all the geostrophic contours in the presence of a sufficiently high ridge, the dynamics of both source-sink and wind driven circulations in a β-plane is similar to that in a closed basin.

First, wind-driven circulation in the inviscid limit is discussed in a linear barotropic channel model in the presence of a bottom ridge. There is a critical height of the ridge, above which all geostrophic contours in the channel are blocked. In the subcritical case, the Sverdrupian balance does not apply and there is no solution in the inviscid limit. In the supercritical case, however, the Sverdrupian balance applies. The form drag is generated through two different physical processes: the through-channel recirculating flow and the Sverdrupian gyre flow. These processes are fundamentally different from the nonlinear Rossby wave drag generation. In this linear model, the presence of a supercritical high ridge is essential in the inviscid limit. With this form drag generation determined, an explicit form for the zonal transport in the channel is obtained, which shows what model parameters determine the through-channel transport. In addition, the model demonstrates that most of the potential vorticity dissipation occurs at the northern boundary where the ridge intersects.

The result from the homogeneous channel model in Chapter 2 is then extended to a model whose geometry consists of a zonal channel and two partial meridional barries along each boundary at the same longitude. Both the model transport and especially the model circulation are significantly affected by the presence of the two meridional barriers. The presence of the northern barrier always leads to a decrease in the transport. The presence of the southern barrier, however, increases the transport for a narrow ridge. The northern barrier only has a localized influence on the circulation pattern, while the southern barrier has a global influence in the channel.

Then a multi-layer Q-G model is constructed by assuming that potential vorticity in all subsurface layers is homogenized. The circulation is made up of baroclinic and the barotropic part. The barotropic part is same as that in a corresponding barotropic model, and is solely determined by the wind stress, while the baroclinic part is not directly related to the wind stress. It is determined by the potential vorticity homogenization and lateral boundary conditions. The presence of the stratification does not affect the bottom topographic form drag generation. The interfacial form drag is generated by the stationary eddies. Corresponding to the circulation structure, the zonal through-channel transport associated with the barotropic circulation is determined by the wind stress and bottom topography. The other part associated with the baroclinic circulation, however, is not directly related to the wind stress and it is determined by the background stratification.

Based upon the discussion on the geostrophic contour, a simple barotropic model of abyssal

circulation in a circumpolar ocean basin is constructed. The presence of a supercritically high ridge is both necessary and sufficient for geostrophic flow in a β-plane channel to support a net cross-channel volume flux. In the presence of a sufficiently high ridge, the classical Stommel & Arons theory applies here, but with significant modifications. The major novelty is that a through-channel recirculation is generated. Both its strength and direction depend critically upon the model parameters. Then, a schematic picture of the abyssal circulation in a rather idealized Southern Ocean is obtained. The most significant feature is the narrow current along the northern boundary of the circumpolar basin, which feeds the deep western boundary currents of the Indian Ocean and Pacific Ocean and connects all the oceanic basins in the Southern Ocean.

Finally, the question of how the northward surface Ekman transport out of the circumpolar ocean is returned is discussed in a two-layer model with an infinitesimally thin surface Ekman layer on top of a homogeneous layer of water in a rather idealized Southern Ocean basin. First, the case with a single subtropical ocean basin is discussed. In the case with a sufficiently high ridge connecting the Antarctic and the meridional barrier, an explicit solution is found. The surface Ekman layer sucks water from the lower layer in the circumpolar basin. This same amount of water flows northward as the surface Ekman drift. It downwells in the subtropical gyre, and is carried to the western boundary layer. From there, the same amount of water flows southward as a western boundary current across the inter-gyre boundary between the circumpolar ocean and the subtropical gyre along the west coast to the southern boundary of the meridional barrier. Then, the same amount of water is carried southward and feeds the water loss to the surface Ekman layer due to the Ekman sucking in the interior circumpolar ocean. The case with multiple subtropical ocean basin such as the Southern Ocean is also discussed. It is demonstrated that the surface Ekman drift drives a strong inter-basin water mass exchange.

A TOMOGRAPHIC OCEAN SOUND SPEED PROFILE FROM A LONG VERTICAL ACOUSTIC ARRAY

James Murwanthanje Njeru

An average sound speed profile over a 1000 km section of the northeast Pacific ocean is obtained using Ocean Acoustic Tomography, from data acquired during the 1987 *SVLA* experiment on a long (900 m) 120 hydrophone vertical acoustic array.

In particular, we pulse compress the received signal with a phase-only matched filter. The signal, centered at 80 Hz, is phase-modulated by a maximal length sequence. A fast m-sequence cross-correlation algorithm based on the Hadamard transform is used. In addition, wide band Doppler correction and coherent averaging of repetitions of the signal are performed.

The tomographic inversion is initialized from a range averaged climatological profile. Multipaths are identified from ray theory. The identified arrivals are inverted for a range-independent sound speed profile change estimate. Estimates of source and array position error are also obtained. For the limited data set used, the sound speed change estimate is found to be insignificant, and a significant instrument position estimate is obtained.

DEEPLY-TOWED UNDERWATER VEHICLE SYSTEMS: A VERIFIED ANALYTICAL PROCEDURE FOR CREATING PARAMETERIZED DYNAMIC MODELS

Franz S. Hover

The dynamics of deeply-towed cable/vehicle systems are governed by nonlinear partial differential equations and as a result, trajectory control is generally difficult using the available techniques. This work examines the possibility of utilizing parametric dynamic models in differential equation form, to present a far more tractable controls problem. A learning-model method for generating accurate approximations of this type is used, and the identification process is unique in that an analytically-based model provides the primary data sets, allowing for *a priori* characterization of system responses without using any real data. The performances of the parametric forms are then *verified* through comparison of model output against actual sea data obtained during recent cruises in the Caribbean and Mediterranean Seas. The respective merits and limitations of several different model structures are discussed, with respect to both pure performance and identification efficiency.

Supported by: Funding was provided by ONR:N00014-86-C-0038, N00014-89-D-0255, NSF:OCE-8511431.

TURBULENT MIXING IN STRATIFIED FLUIDS - LAYER FORMATION AND ENERGETICS

Young-Gyu Park

A turbulent mixing experiment was conducted to observe the dynamics and the energetics of layer

formation along with the region of layer formation in the Reynolds number (Re) and the overall Richardson number (Ri_o) space. A salt stratified fluid was mixed uniformly throughout its depth with a vertical rod that moved horizontally at a constant speed. The evolution of density was measured with a conductivity probe.

As the instability theory of Phillips (1972) and Posmentier (1977) shows, an initially uniform density profile turns into a series of steps when Ri_o is larger than a critical value Ri_c, which forms a stability boundary. For fixed Re, as Ri_o decreases to Ri_c, the steps get weaker; the density difference across the interface and the difference of density gradient between layers and interfaces become small. Ri_c increases as Re increases with a functional relation $log\ Ri_c \approx Re/900$. The steps evolve over time, with small steps forming first, and larger steps appearing later through merging and decay of the interfaces. After some time the interior seems to reach an equilibrium state and the evolution of the interior steps stops. The length scale of the equilibrium step, l_s, is a linear function of U/N_i, where U is the speed of the rod and N_i is the buoyancy frequency of the initial profile. The functional relationship is $l_s = 2.6U/N_i + 1.0cm$. For $Ri_o < Ri_c$, the mixing efficiency, R_f, monotonically decreases to the end of a run. However, for $Ri_o > Ri_c$, the evolution of R_f is closely related to the evolution of the density field. R_f changes rapidly during the initiation of the steps. For $Ri_o, > Ri_c$, R_f increases initially, while for $Ri_o \geq Ri_c$, R_f decreases initially. When the interior reaches an equilibrium state, R_f becomes uniform. Posmentier (1977) theorized that when steps reach an equilibrium state, a density flux is independent of the density gradient. The present experiments show a uniform density flux in the layered interior irrespective of the density structure, and this strongly supports the theory of Posmentier. The density flux generated in the bottom boundary mixed layer goes through the interior all the way to the top boundary mixed layer without changing the interior density structure. Thus, turbulence can transport scaler properties further than the characteristic length scale of active eddies without changing a density structure. When the fluid becomes two mixed layers, the relation between R_f and Ri_l was found for $Ri_l > 1$. Here, Ri_l is the local Richardson number based on the thickness of the interface. R_f does decrease as Ri_l increases, which is the most crucial assumption of the instability theory.

ASSIMILATION OF ALTIMETER DATA IN A QUASI-GEOSTROPHIC MODEL OF THE GULF STREAM SYSTEM: A DYNAMICAL PERSPECTIVE

Antonietta Capotondi

The dynamical aspects involved in the assimilation of altimeter data in a numerical ocean model have been investigated. The model used for this study is a quasi-geostrophic model of the Gulf Stream region. The data that have been assimilated are maps of sea surface height which have been obtained as the superposition of sea surface height variability deduced from the Geosat altimeter measurements and a mean field constructed from historical hydrographic data. The method used for assimilating the data is the nudging technique. Nudging has been implemented in such a way as to achieve a high degree of convergence of the surface model field toward the observations.

We have analyzed the mechanisms of the model adjustment, and the final statistical equilibrium characteristics of the model simulation when the surface data are assimilated. Since the surface data are the superposition of a mean component and an eddy component, in order to understand the relative role of these two components in determining the characteristics of the final statistical steady state, we have considered two different experiments: in the first experiment only the climatological mean field is assimilated, while in the second experiment the total surface streamfunction field (mean + eddies) has been used.

We have found that the mean component of the surface data determines, to a large extent, the structure of the flow field in the subsurface layers, while the eddy field, as well as the inflow/outflow conditions at the open boundaries, affect its intensity. In particular, if surface eddies are not assimilated only a weak flow develops in the two deeper model layers where no inflow/outflow is prescribed at the boundaries.

Comparisons of the assimilation results with available in situ observations show a considerable improvement in the degree of realism of the climatological model behavior, with respect to the model in which no data are assimilated. In particular, the possibility of building into the model more realistic eddy characteristics, through the assimilation of the surface eddy field, proves very successful in driving components of the mean model circulation that are in good agreement with the available observations.

Supported by: Funding was provided by the Massachusetts Institute of Technology.

THE ISOTOPE GEOCHEMISTRY OF ABYSSAL PERIDOTITES AND RELATED ROCKS

Jonathan E. Snow

This dissertation studies several aspects of the formation of the Earth's oceanic mantle and crust, using a variety of geologic techniques, principally major elements, radiogenic isotopes and trace elements, but including petrography, mineral chemistry, x-ray diffraction, seafloor geomorphology, and analysis of the tectonics of fracture zones. The first chapter is an introduction to the problems to be addressed in this work. The second chapter examines the composition of basalts erupted near the Atlantis II Fracture Zone on the Southwest Indian Ridge. Trends in major element compositions of those basalts can be related directly to the nearby presence of the fracture zone. The effects of mantle composition and crustal level lateral transport of magma in the rift system can be ruled out by the analysis of isotopes and the geomorphology of the fracture zone floor. This is the best demonstration to date of a transform fault effect on basalt compositions. In trying to quantify putative transform fault effects documented at other fracture zones, no systematic correlation of transform offset age with mantle temperature change can be found, suggesting that mantle composition and lateral transport phenomena play a larger than expected role in the evolution of those areas.

The third chapter relates to oceanic mantle rocks as they are altered at or near the Earth's surface. The major elements which make up abyssal peridotites are extensively redistributed by the alteration they have undergone. Mg is shown to be extracted from the peridotites, and a variety of trace elements added. This elemental redistribution is taken as evidence for extensive Mg transport by circulating waters. Since the solubility of Mg-bearing minerals in hydrothermal solutions is quite limited, much lower temperatures and much higher water/rock ratios are required to explain the major element compositions of the peridotites than had previously been assumed.

The behavior of the Nd, Sr and Os isotopic systems during seafloor alteration was also studied. The isotope systematics of these rocks strongly support the hypothesis of high water/rock ratios in the formation of serpentinized abyssal peridotites. Nonetheless, Nd and Sr reside in a phase which is resistant to alteration (clinopyroxene) and the concentration of Os is high relative to that of seawater, so that it too appears resistant to alteration. Primary mantle isotopic signatures may be obtained from abyssal peridotites by careful analysis, even of extremely weathered rocks.

Radiogenic strontium in excess of what could be introduced by seawater contamination or *in situ* radiogenic growth in a reasonable period of time was also found. These observations confirm earlier work which had been discredited for many years. The only plausible mechanism for the formation of this "orphan" ^{87}Sr is that it is introduced as part of a sedimentary component which infiltrates the rock during metamorphism and/or weathering. The ^{87}Sr may be contained by or sorbed onto extremely fine clay particulates, or colloidal suspensions, as opposed to the dissolved ionic Sr which is normally thought of as characterizing the Sr isotopic composition of seawater. The high water/rock ratios required by the bulk isotopic analysis, as well as the pervasive elemental redistribution arguing for extensive near-surface weathering at high water/rock ratios strongly support this hypothesis. Given pervasive percolation of water throughout the samples, sufficient radiogenic, sediment-derived strontium may be drawn deep into the crust in the course of its weathering to cause such high $^{87}Sr/^{86}Sr$ ratios.

The fourth chapter deals exclusively with primary mantle isotopic information from abyssal peridotites. This is the first study which has attempted to relate the Os isotopic system in the oceanic mantle to other isotopic systems and to trace elements. It is possible, with some extreme assumptions, to model the range of Os isotopes in the oceanic mantle alone in a standard model of formation of the depleted mantle by extraction of the crust. The additional constraints provided by the study of Nd isotopes in depleted mantle rocks from the oceans show that partial melt extraction and the formation of a depleted reservoir alone are not sufficient to account for the range of both Nd and Os isotopes in the Earth's mantle. Possible mechanisms for the decoupling of the Os and Nd isotopic systems include elemental fractionation via the porous flow of basalt through the mantle, mantle metasomatism, recycling of a subducted component in the mantle and core formation. The core extraction model is pursued in some detail. Such core extraction models can account for the distributions and isotopic compositions of compatible and incompatible trace elements in the Earth's mantle, but they are highly non-unique, and thus difficult to test.

Supported by: Funding was provided by a National Science Foundation Graduate Fellowship, and by the Ocean Ventures Fund of the Woods Hole Oceanographic Institution.

Index

Adachi, M. B-1
Agrawal, Yogesh C. AOPE-12,14
Alm, Anders MPC-1
Altabet, Mark A. MCG-1,2,11
Amaral, L. A. B-10
Anderson, Donald M. B-1,8,16,17
Arimoto, Richard MCG-9
Arnosti, Carol JP-8
Arthur, M. A. GG-1
Aubrey, David G. GG-9,11,12,17,31,33;CRC-1
Austin, J. A., Jr. GG-18
Ausubel, Jesse H. MPC-1

Bacon, Michael P. MCG-9
Baggeroer, Arthur B. AOPE-2
Barth, G. A. GG-15
Beardsley, Robert C. PO-17,18,19,23
Bellingham, James G. AOPE-17
Bemis, Karen G. GG-9
Benfield, Mark AOPE-18
Benner, Ronald MCG-15
Bennett, Lenore MCG-15
Bercovici, David GG-15
Berteaux, H. GG-26
Besiktepe, S. GG-33
Bird, Robert T. GG-20
Black, Dianne E. B-4
Blommestein, Erik MPC-1
Blough, Neil V. MCG-1,4,14
Bocconcelli, Alessandro AOPE-10;GG-26
Bock, Erik J. AOPE-11,13
Bogdanov, Y. A. MCG-12
Bolmer, S. GG-26
Bothner, Michael H. MCG-3
Bowen, Stephen Gerard JP-13
Bower, Amy S. PO-1
Bowin, Carl GG-16
Bowles, W. MCG-15
Bowlin, James B. AOPE-17
Boyd, Janice AOPE-1,5
Boyer, Barbara C. MPC-3
Boyle, Edward GG-32
Bradley, Albert M. AOPE-4,11
Brady, David AOPE-6,17
Brewer, Peter G. MCG-13
Brink, K. H. PO-17
Broadus, James M. MPC-1,9
Brooks, Benjamin A. GG-21
Brooks, James M. MCG-6
Brown, Holly S. GG-24
Brown, W. S. PO-9
Bryan, Wilfred B. GG-10,13,38
Bryden, Harry L. PO-1,13
Buesseler, Ken O. MCG-10,13
Buhl, Peter GG-19
Bulgakov, S. N. PO-2

Burns, Kathryn A. B-2
Butman, Cheryl Ann AOPE-14;B-18

Cacchione, David A. AOPE-18;PO-17
Callahan, Sean M. B-3
Candela, Julio PO-1,2,17
Cann, Johnson R. GG-14
Capotondi, Antonietta JP-16
Carlson, Craig A. MCG-15
Carneiro, Nelson PO-17
Caron, David A. B-2,3,10
Carter, Patricia GG-22
Carter, S. J. GG-2
Cartlidge, J. E. GG-38
Caruso, Michael PO-21
Casey, John F. GG-10
Castro, Belmiro PO-17
Caswell, Hal B-7,11
Cathles, Lawrence M., III MCG-5
Catipovic, Josko A. AOPE-4,5,6,7,9,17
Chapman, David C. PO-18,20
Chave, Alan D. AOPE-12;GG-16,21,24
Chen, Changsheng PO-18,19
Chen, Y. John GG-22
Chester, David Brian JP-7
Chin, Michael B-16
Chiu, Ching-sang AOPE-2
Christeson, G. L. GG-17
Chu, Dezhang AOPE-14,18
Church, Thomas M. MCG-9
Churchill, James H. PO-19,20
Cohen, G. J. GG-1,7
Coles, Victoria J. PO-3
Colman, S. M. GG-1,2,7
Colodner, Debra GG-32
Corda, David B-14
Corfield, R. M. GG-38
Cornillon, Peter C. PO-20
Cornuelle, Bruce D. AOPE-1,5
Corry, Charles E. PO-25,26
Cowen, Robert K. PO-20
Cretin, J. GG-26
Curran, Mary Carla JP-3
Currie, L. A. GG-4
Curry, W. B. GG-34
Curtin, Thomas B. AOPE-17

Dacey, John W. H. B-6,9
Daher, Mary Ann B-20
Davis, Cabell S. B-4
Davis, Cabell S. PO-26
Dean, W. E. GG-1
DeLong, Edward F. B-9,10
Demisch, Suzanne MPC-1
Dennett, Mark R. B-3
Detrick, Robert S. GG-10,19

Deuser, W. G. MCG-13,15
Dever, E. P. PO-20
Diaconu, V. GG-33
Dick, Henry J. B. GG-9
Dickey, T. D. PO-3,24
Dickneider, Trudy A. MCG-4
Dieu, Julie J. GG-38
DiPerna, Daniel T. AOPE-15
Doherty, Kenneth W. B-20
Donelan, M. A. AOPE-7,14
Dragos, Paul PO-20
Drake, D. E. AOPE-18
Drennan, W. M. AOPE-7,14
DuBois, D. L. GG-23
Duda, Timothy F. AOPE-1,5,17
Dunlap, Paul V. B-3

Eastwood, Robert L. AOPE-18
Ebert, James R. GG-14
Edmond, John GG-32
Edson, J. B. AOPE-4
Edwards, Christopher A. PO-3
Eglinton, Lorraine Buxton MCG-5,6,7
Eglinton, Timothy I. MCG-4
Ehrendorfer, Thomas Wolfgang JP-2
Ehrhardt, Manfred G. B-2
Elder, K. L. GG-6
Eliet, Pierre P. GG-9
Elskus, Adria E. B-4
Esser, B. K. GG-32
Etchemendy, Steven AOPE-17
Etourmy, N. GG-26
Ewing, J. I. GG-23

Fabre, A. GG-26
Fairall, C. W. AOPE-4
Farrington, John W. MCG-3
Farrow, Scott MPC-2
Felizardo, Francis C. JP-9
Filloux, J. H. AOPE-12
Fink, Mark J. B-23
Firing, Eric PO-13
Fitzwater, Steve E. MCG-15
Flagg, C. N. AOPE-7
Flierl, Glenn R. B-4
Forester, R. M. GG-1
Foster, D. S. GG-1
Francois, Roger MCG-2,9,11
Friedrichs, Carl Takeo GG-11,31;JP-1
Friedrichs, Marjorie A. M. PO-4
Frisk, George V. AOPE-8
Fry, Brian GG-5;MCG-2
Frye, Daniel AOPE-10
Fryer, G. J. GG-17

Gable, Frank J. CRC-1
Gaetani, Glenn A. GG-38
Gagnon, A. R. GG-4,5,6
Gaines, Arthur G., Jr. MPC-7
Gallo, David G. GG-24
Gangemi, P. GG-1
Garwan, M. A. GG-5
Gaston, Kevin J. MPC-9
Gawarkiewicz, Glen PO-18,20,21,26
George, Joseph B-20
Geyer, W. Rockwell AOPE-3;B-14;PO-17
Giese, Graham S. GG-11,12
Gille, Sarah T. PO-5
Gillis, Kathryn M. MCG-7,8
Glenn, Scott M. PO-20
Glover, David M. MCG-13
Glover, Edward B-5
Gnanadesikan, Anand PO-24
Goehringer, Dale D. B-6
Goericke, Ralf MCG-2
Goldsborough, R. GG-26
Gooch, Jay W. B-4
Goodman, Louis AOPE-14
Gopalkrishnan, Ramnarayan AOPE-14;JP-6
Gould, M. GG-26
Gouriou, Yves PO-5
Goyet, Catherine MCG-13
Granata, T. PO-3
Grassle, J. Frederick B-18,19
Green, Sarah A. MCG-1,4,14
Greene, Charles H. B-22
Grigalunas, Thomas A. MPC-3
Grosenbaugh, M. A. AOPE-1,17
Gross, T. F. AOPE-3
Grove, Timothy L. GG-38
Guiral,.J. Escartin GG-17
Gunson, James Reginald JP-13
Gurvich, E. G. MCG-12
Gust, G. MCG-15

Hacker, S. B-11
Hahn, Mark E. B-4,5,10,19,22
Hall, Melinda M. PO-4,6
Haney, J. Christopher PO-21
Hannington, Mark D. MCG-8,12
Hanzawa, Satoshi B-6
Hara, Tetsu AOPE-11,13
Harbison, G. R. B-11
Harding, Alistair J. GG-19
Hare, Jonathan A. PO-20
Hart, Michael W. B-5
Hart, Stanley R. GG-8,9,11,18,38
Hauri, Erik H. GG-38
Hay, B. J. GG-1
Heggie, D. T. GG-35
Helfrich, Karl R. B-9;PO-13,14
Helz, R. T. GG-15
Henderson, Eric W. MPC-2,10
Herrin, Eugene PO-26
Herzog, Michel B-17
Hickey, Barbara M. AOPE-3
Hildebrand, John A. AOPE-1,5
Hill, Richard W. B-6
Hinton, David E. B-23
Hoagland, Porter MPC-2,3,4
Hoaki, Toshihiro B-6,8

Hobart, Edward AOPE-10
Hodges, K. V. GG-13
Hodgkiss, William S., Jr. AOPE-1,5
Hogg, Nelson G. PO-6
Holbrook, W. Steven GG-18,22
Honjo, S. GG-38
Hosom, D. S. PO-24
Hover, Franz S. JP-15
Howald, Terrance B-6
Howe, Bruce M. AOPE-1,5
Howell, C. T. AOPE-1
Howes, Brian L. B-2,6,7,12,13,20,21,22
Huang, He AOPE-12
Huang, K. GG-6
Huang, Rui Xin PO-12,14
Hufford, G. PO-9
Humphris, Susan E. GG-10;MCG-8
Hunt, John M. MCG-5
Hutton, D. L. GG-1,5,6
Hwang, P. A. AOPE-14

Ichiro, Tayasu B-7
Irish, James D. AOPE-12;PO-17
Ishida, Y. B-1
Ito, Garrett T. GG-19
Ivanov, L. GG-33;MCG-13

Jacobson, Dean M. B-8
Jannasch, Holger W. B-6,8
Jaroslow, Gary E. GG-11
Jebb, Matthew B-15
Jenkins, William J. PO-6
Jiang, Min AOPE-9
Jin, Di MPC-3
Jin, Guoliang AOPE-6
Johnson, Carl G. MCG-3
Johnson, H. Paul GG-28
Johnson, Matthew Lloyd JP-12
Johnson, R. MCG-15
Jones, A. G. GG-24
Jones, Glenn A. GG-1,2,3,4,5,6,7,8,24
Joyce, Terrence M. PO-6

Kahma, K. K. AOPE-14
Kaoru, Yoshiaki MPC-1,4
Kaplan, Ilene M. MPC-3
Katsaros, K. B. AOPE-7
Kayen, R. W. AOPE-18
Keefe, Robert W. JP-9
Keigwin, Lloyd D. GG-1,4,35,36
Keller, William C. AOPE-8, 9
Kelley, Deborah S. MCG-7,8
Kelly, Kathryn A. PO-7,8
Kennicutt, Mahlon C. MCG-6
Kent, Graham M. GG-19
Kery, S. GG-26
Kessel, E. D. GG-6
Key, R. M. GG-5
Kim, Stacy L. B-9
Kimura, Ryuji PO-15
Kinder, Thomas H. PO-1
Kineke, Gail C. AOPE-3,10,13,18
King, Geoffrey C. P. GG-20
King, J. W. GG-1
King, Linda L. JP-4
Kitaigorodskii, S. A. AOPE-14
Kite-Powell, Hauke MPC-3,5
Klein, Birgit PO-27
Kleinrock, Martin C. GG-15,20,21,30
Klinedinst, D. B. GG-4
Klitgord, Kim D. GG-24
Klouda, G. A. GG-4
Knox, Robert B-23
Kodama, M. B-1
Koelsch, D. E. GG-26
Kogan, M. G. GG-23
Korotaev, G. K. PO-2
Korytko, Peter J. B-10
Kraska, James C. MPC-6,7
Kravtsov, Yu A. AOPE-16
Kremer, P. B-11
Krishfield, R. GG-38
Krupp, David A. B-6
Kuptsov, V. M. GG-2
Kurtz, R. D. GG-24
Kyle, Philip R. GG-8

LaCasce, J. H. PO-17
Lalou, Claude MCG-8
Lamarre, Eric JP-1
Lambertsen, Richard AOPE-1
Landing, William M. MCG-14
Langdon, C. PO-3
Lanzerotti, L. J. GG-21
Lashkari, Khosrow AOPE-2
Laurent, J. GG-26
Law, Clifford S. AOPE-1
Ledwell, James R. AOPE-1,3
Ledyard, Kathleen M. B-9;JP-5
Lehman, Scott J. GG-36
Lentz, Steven J. PO-17,20,21,22,23
Lessard, Evelyn J. B-3
Lewis, Brent L. MCG-14
Lewis, Craig V. W. PO-26
Liberatore, Stephen AOPE-10
Lim, E. L. B-10
Limeburner, Richard PO-9,17,18,19,23
Lin, Jian GG-15,19,20,22,24,26,29,30
Lindstrom-Seppa, Pirjo B-10
Litherland, A. E. GG-5
Little, Sarah A. GG-22
Liu, James T. GG-12
Liu, Jin Long MPC-4
Liu, Li MCG-5
Liu, Z. PO-15
Livingston, H. D. MCG-13
Lizarralde, Daniel GG-22
Lockhart, W. Lyle B-22
Lohmann, G. P. GG-33,34
Lohmann, K. C. GG-34
Lozano, Carlos J. PO-2

Lozier, M. Susan PO-1,7
Ludwig, K. R. GG-13
Lynch, James F. AOPE-6,12,15,16
Lyzenga, David AOPE-13

Maclennan, C. G. GG-21
Madin, Laurence P. B-5,11,20
Madsen, N. AOPE-7
Makris, J. GG-18
Maley, Carlo C. B-11
Manov, D. V. PO-24
Mao, Shaozhi MCG-5
Marra, J. PO-3
Marra, M. AOPE-9
Marshall, John C. PO-16
Martin, Linda AOPE-18
Martini, Marinna AOPE-11
Martinsen, Robert J. AOPE-11
Marty, Gary D. B-23
Maruyama, Tadashi B-6
Mastumoto, G. I. B-11
McCartney, Michael S. PO-3,4,7,11
McCorkle, Daniel C. GG-35
McGowan, John A. B-23
McMurtry, Gary M. GG-32
McNichol, A. P. GG-1,4,5,6
Mcnutt, M. K. GG-23
McSherry, Thomas M. GG-9
Medford, L. V. GG-21
Mercer, James A. AOPE-1,5
Michaels, A. F. MCG-15
Mikhalevsky, Peter AOPE-2
Miknis, Fran MCG-7
Miller, Charles B. B-23
Miller, James H. AOPE-2
Miller, Richard L. B-5
Millham, Newton P. B-12,13
Milliman, John D. GG-39
Moeller, H. H. AOPE-12
Moore, J. G. GG-13
Moore, Michael J. B-13
Moore, Mike I. PO-13
Moran, David D. B-23
Moran, S. Bradley MCG-10
Morawitz, W. M. L. AOPE-15
Morrison, Archie T., III AOPE-10,11
Mound, Laurence A. MPC-9
Moxnes, S. AOPE-1
Mukai, Hiroshi B-7
Mullineaux, Lauren S. B-9,14
Mutter, John C. GG-19
Myers, Mark S. B-13

Nadeau, M-J GG-5
Nakanishi, T. GG-38
Neff, E. D. GG-1
Njeru, James Murwanthanje JP-15
Norris, R. D. GG-38
Nowlin, Worth D., Jr. PO-13

Ogata, T. B-1
Oguz, T. GG-33
Oh, J. GG-18
Ohta, Kazuhiko JP-8
Oldale, Robert N. GG-7,14
Olmez, Ilhan AOPE-16
Olson, Donald B. PO-3
Omnes, G. GG-26
Oppo, Delia W. GG-34,36
Orcutt, John A. GG-19
Osborne, E. A. GG-1,5,6
Owens, W. Brechner AOPE-15;PO-7

Park, Young-Gyu JP-15
Pascual, Mercedes B-14
Pawlowicz, Richard AOPE-6,15
Payne, Richard E. PO-24,25
Peal, Kenneth R. AOPE-8;GG-26
Pedlosky, Joseph PO-3,15,16
Peltzer, Edward T. MCG-15
Petersen, Sven MCG-8
Petitt, Robert A., Jr. AOPE-8, 9,12
Petrecca, R. F. B-19
Pickart, Robert S. PO-7,8
Pilskaln, C. H. MCG-2
Pink, Francis X. AOPE-16
Plant, William J. AOPE-8, 9
Plueddemann, A. PO-3
Poland, Alan B-5
Polasky, Stephen MPC-9
Polzin, K. PO-26
Prada, K. E. PO-24
Pratt, Larry PO-16
Preisig, James C. AOPE-2,8
Price, James PO-10
Proakis, John G. AOPE-4,5,7,9
Pruell, Richard J. B-4
Purdy, G. M. GG-10,17,18,23,24

Qiu, Bo PO-8,14

Rajan, Subramaniam D. AOPE-8
Ralph, Elise A. PO-16
Raman, C. V. MCG-8
Rankin, Kelly L. B-14
Rao, T. S. S. B-14
Ratick, Samuel J. MPC-9
Ravizza, Greg GG-31,32
Ray, Douglas Scott JP-12
Reguera, B. B-1
Reiter, Edmund C. GG-18
Repeta, Daniel J. MCG-2
Repetto, Sarah MPC-1
Reynolds, R. L. GG-1
Richardson, Phillip L. PO-9,10
Rimski-Korsakov, N. A. MCG-12
Romanov, A. MCG-13
Rome, Lawrence C. B-14
Rona, Peter A. GG-28;MCG-8,11,12
Ronquille, Velma B-20
Rudnick, Daniel L. PO-9
Ruppel, C. GG-13,23

Ruttenberg, K. C. MCG-3

Séguin, F. H. GG-6
Sachs, Julian GG-32
Sagalevitch, A. M. MCG-12
Sako, Y. B-1
Sawyer, D. GG-18
Sayres, C. H. GG-21
Scanlon, Lori AOPE-18
Scheltema, Amélie H. B-15
Scheltema, Rudolf S. B-15,16
Schmitt, Raymond W. PO-26,27
Schneider, David A. GG-23
Schneider, R. J. GG-4,6,7
Scholin, Christopher Alan B-16,17;JP-5
Schouten, Hans GG-24,28
Schultz, A. GG-24
Schumacher, Dietmar MCG-6
Scott, David J. MPC-7
Seewald, Jeffrey S. MCG-6,7,10
Sempere, Jean-Christophe GG-24,30
Seyfried, William E., Jr. MCG-10
Shafer, Deborah K. MCG-13
Shanks, Wayne C., III MCG-10
Sharp, Jonathan H. MCG-15
Shaw, Peter R. GG-25,26
Sherwood, Christopher R. AOPE-12
Shigesada, Nanako B-7
Shimizu, Nobu GG-38
Sholkovitz, Edward R. MCG-9,14
Siegel, D. A. PO-24
Smethie, William M., Jr. PO-3
Smith, Deborah K. GG-14,9,22
Smith, J. Torquil GG-16,18
Smith, V. Kerry MPC-4
Smolowitz, Roxanna B-23
Snelgrove, Paul V. R. B-17,18,19;JP-10
Snow, Jonathan E. GG-9;JP-18
Soares, Ivan D. PO-23
Sogin, Mitchell B-17
Solow, Andrew R. MPC-7,8,9
Spall, Michael A. PO-9,10,16
Speer, Paul E. GG-11
Spindel, Robert C. AOPE-1,5
Stanley, Amy B-20
Stanton, Timothy K. AOPE-14,15,18
Stauble, Donald K. GG-12
Steele, John H. MPC-1,2,10
Stegeman, John J. B-4,5,10,19,22,23
Stein, Ross S. GG-20
Steinhart, J. S. GG-18
Stephen, Ralph A. GG-26,27
Sternberg, R. W. AOPE-10,18
Stevens, James B. PO-26
Stewart, W. K. AOPE-9
Stocker, Thomas F. GG-36
Stoffa, P. L. GG-18
Stojanovic, Milica AOPE-4,5,79
Straley, Janice AOPE-1
Stramska, M. PO-3

Sutton, George H. GG-29
Sutton, P. J. AOPE-15
Swank, Doug B-14
Sweetkind, D. S. GG-1
Swift, Stephen A. GG-26,27

Takada, Hideshige MCG-3
Takizawae, T. GG-38
Talley, Lynne D. PO-11
Tate, G. B. AOPE-18
Taylor, Craig D. B-2,20
Teal, John M. B-7
Tebeau, Christopher M. B-20
Terray, Eugene A. AOPE-3,7,8, 9,14
Thompson, Geoffrey GG-10;MCG-7,8,11,12
Tivey, Margaret K. MCG-8
Tivey, Maurice A. GG-27,28
Toole, John M. PO-5,10,26
Trehu, Anne GG-29
Triantafyllou, M. S. AOPE-17
Tripp, Bruce W. MCG-3
Trowbridge, J. H. AOPE-13,17
Tsuchiya, Mizuki PO-11
Tucholke, Brian E. GG-11,29
Tucker, W. B., III GG-38
Tupas, Luis M. MCG-15
Turekian, Karl GG-32
Turpening, R. GG-26

Uchupi, Elazar GG-14
Ulrich, Nathan AOPE-1
Unluata, U. GG-33

Veeh, H. H. GG-35
Verkouteren, R. M. GG-4
Vodacek, Anthony MCG-4
von der Heydt, Keith AOPE-2
von Reden, K. F. GG-1,4,6,7
Voytek, Mary B-3

Walden, Barrie AOPE-11
Wang, Liping JP-14;PO-12
Warren, Bruce A. PO-10,13
Waser, Nathalie JP-7
Watkins, William A. B-20
Watson, Anrew J. AOPE-1
Watts, D. Randolph PO-7
Webb, Doug AOPE-17
Weidman, Christopher R. GG-7,8,14
Weller, Robert A. PO-3,9,24
Wetzel, Laura Reiser GG-30
Wheatcroft, Robert A. AOPE-16
Whelan, Jean K. MCG-4,5,6,7
Whitcomb, Louis L. AOPE-3
White, David S. B-21,22
White, R. S. GG-10
White, Renee D. B-22
Whitehead, J. A. PO-2,15
Whitworth, Thomas, III PO-13
Wiebe, Peter H. AOPE-14,18;B-22,23
Wiedmer, Michael B-23

Wiens, Douglas A. GG-30
Wijffels, Susan Elizabeth JP-11;PO-13
Wilcock, W. S. D. GG-17
Williams, Albert J., 3rd AOPE-3,11,14
Williams, Richard G. PO-16
Wirsen, Carl O. B-6,8
Wojcik, Dennis Michael JP-13
Womeldorf, Carole A. JP-13
Worcester, Peter F. AOPE-1,5,6,15
Wright, Daniel G. GG-36

Yoder, J. PO-3
Yoerger, Dana R. AOPE-3,4,10,11,12

Zani, C. GG-26
Zelck, Clementine PO-27
Zepp, Richard G. MCG-1
Zervas, Christopher E. GG-30
Zhao, X-L. GG-5
Zvonar, Zoran AOPE-6

DOCUMENT LIBRARY

Distribution List for Technical Report Exchange – May 5, 1994

University of California, San Diego
SIO Library 0175C (TRC)
9500 Gilman Drive
La Jolla, CA 92093-0175

Hancock Library of Biology & Oceanography
Alan Hancock Laboratory
University of Southern California
University Park
Los Angeles, CA 90089-0371

Gifts & Exchanges
Library
Bedford Institute of Oceanography
P.O. Box 1006
Dartmouth, NS, B2Y 4A2, CANADA

Commander
International Ice Patrol
1082 Shennecossett Road
Groton, CT 06340-6095

NOAA/EDIS Miami Library Center
4301 Rickenbacker Causeway
Miami, FL 33149

Library
Skidaway Institute of Oceanography
10 Ocean Science Circle
Savannah, GA 31411

Institute of Geophysics
University of Hawaii
Library Room 252
2525 Correa Road
Honolulu, HI 96822

Marine Resources Information Center
Building E38-320
MIT
Cambridge, MA 02139

Library
Lamont-Doherty Geological Observatory
Columbia University
Palisades, NY 10964

Library
Serials Department
Oregon State University
Corvallis, OR 97331

Pell Marine Science Library
University of Rhode Island
Narragansett Bay Campus
Narragansett, RI 02882

Working Collection
Texas A&M University
Dept. of Oceanography
College Station, TX 77843

Fisheries-Oceanography Library
151 Oceanography Teaching Bldg.
University of Washington
Seattle, WA 98195

Library
R.S.M.A.S.
University of Miami
4600 Rickenbacker Causeway
Miami, FL 33149

Maury Oceanographic Library
Naval Oceanographic Office
Building 1003 South
1002 Balch Blvd.
Stennis Space Center, MS 39522-5001

Library
Institute of Ocean Sciences
P.O. Box 6000
Sidney, B.C. V8L 4B2
CANADA

Library
Institute of Oceanographic Sciences
Deacon Laboratory
Wormley, Godalming
Surrey GU8 5UB
UNITED KINGDOM

The Librarian
CSIRO Marine Laboratories
G.P.O. Box 1538
Hobart, Tasmania
AUSTRALIA 7001

Library
Proudman Oceanographic Laboratory
Bidston Observatory
Birkenhead
Merseyside L43 7 RA
UNITED KINGDOM

IFREMER
Centre de Brest
Service Documentation - Publications
BP 70 29280 PLOUZANE
FRANCE

50272-101

REPORT DOCUMENTATION PAGE	1. REPORT NO. WHOI-93-05	2.	3. Recipient's Accession No.

4. Title and Subtitle

Abstracts of Manuscripts Submitted in 1993 for Publication

5. Report Date March, 1994

6.

7. Author(s)

Editor: Alora Paul

8. Performing Organization Rept. No. WHOI 94-05

9. Performing Organization Name and Address

The Woods Hole Oceanographic Institution
Woods Hole, Massachusetts 02543

10. Project/Task/Work Unit No.

11. Contract(C) or Grant(G) No.

(C)

(G)

12. Sponsoring Organization Name and Address

13. Type of Report & Period Covered

Technical Report

14.

15. Supplementary Notes

This report should be cited as: Woods Hole Oceanog. Inst. Tech. Rept., WHOI-94-05.

16. Abstract (Limit: 200 words)

This volume contains the abstracts of manuscripts submitted for publication during calendar year 1993 by the staff and students of the Woods Hole Oceanographic Institution. We identify the journal of those manuscripts which are in press or have been published. The volume is intended to be informative, but not a bibliography.

The abstracts are listed by title in the Table of Contents and are grouped into one of our five departments, Marine Policy Center, Coastal Research Center, or the student category. An author index is presented in the back to facilitate locating specific papers.

17. Document Analysis a. Descriptors

1. abstracts
2. oceanography
3. ocean engineering

b. Identifiers/Open-Ended Terms

c. COSATI Field/Group

18. Availability Statement

Approved for publication; distribution unlimited.

19. Security Class (This Report) UNCLASSIFIED

20. Security Class (This Page)

21. No. of Pages 220

22. Price

(See ANSI-Z39.18) *See Instructions on Reverse*

OPTIONAL FORM 272 (4-77)
(Formerly NTIS-35)
Department of Commerce